research report

Higher Capacity Cold-Formed Steel Sheathed and Framed Shear Walls for Mid-Rise Buildings: Part 2

RESEARCH REPORT RP17-6

July 2018

American Iron and Steel Institute

DISCLAIMER

The material contained herein has been developed by researchers based on their research findings and is for general information only. The information in it should not be used without first securing competent advice with respect to its suitability for any given application. The publication of the information is not intended as a representation or warranty on the part of the American Iron and Steel Institute or of any other person named herein, that the information is suitable for any general or particular use or of freedom from infringement of any patent or patents. Anyone making use of the information assumes all liability arising from such use.

Copyright 2018 American Iron and Steel Institute

HIGHER CAPACITY COLD-FORMED STEEL SHEATHED AND FRAMED SHEAR WALLS FOR MID-RISE BUILDINGS: PART 2

By

Vincent BRIERE

Project Supervisor: Colin Rogers

Department of Civil Engineering and Applied Mechanics

McGill University, Montréal, Québec, Canada

August 2017

Research Report

© Vincent Brière, 2017

ABSTRACT

Despite the increase in the use of cold-formed steel (CFS) in mid-rise construction, the North American cold-formed steel standards AISI S400 and S240 do not provide a standard design procedure for CFS sheathed and framed shear walls for use in such constructions. The main objective of this research was to develop a design procedure for CFS sheathed and framed shear walls to achieve higher strength and ductility and to resist the larger forces expected in mid-rise construction. The design procedure is proposed for inclusion in the AISI S400 and S240 standards.

Full-scale experiments have been performed using a shear wall testing frame at McGill University, where a total of 31 specimens were tested monotonically and / or cyclically. These specimens were constructed with thicker sheathing and framing members not currently available for design, using two innovative building configurations (double-sheathed and centre-sheathed) to eliminate the effects of eccentric sheathing placement and take full advantage of bearing failure in the sheathing.

The specimens were built with varying construction parameters (material thickness, screw size and screw spacing) and the test data was analysed using the Equivalent Energy Elastic-Plastic (EEEP) method. The configuration using a single concentric sheathing placement (centre-sheathed configuration) reached shear strengths nearly four times higher than what is listed in the current standards. Further, the walls' ductility was substantially improved (up to 8% drift), giving this design a strong potential to be used in mid-rise construction.

A preliminary design method was introduced for this configuration, taking into consideration the different behaviour from these shear walls. A preliminary Limit States Design procedure for Canada (LSD) and the USA and Mexico (LRFD) was determined based on the test results. Resistance factors, ϕ, and overstrength values were also provided. The "test-based" ductility-related and overstrength-related seismic force modification factors for Canada (R_d and R_o) obtained the values of 2.8 and 1.5. This promising centre-sheathed configuration requires further research in order to advance towards a definitive design method for the use of CFS framed and sheathed shear walls in mid-rise construction.

RÉSUMÉ

Malgré une utilisation plus importante de l'acier formé à froid dans les constructions de mi-hauteur (jusque 5 niveaux), les normes Nord-Américaines pour l'acier formé à froid AISI S400 et S240 ne proposent pas de procédure de dimensionnement standard pour les murs de refend présentant un cadre et un parement en acier formé à froid, dans le cadre d'une utilisation pour de telles constructions. L'objectif principal de cette recherche était de développer une procédure de dimensionnement pour ces murs de refend en particulier, dans le but d'atteindre des niveaux de résistance et de ductilité plus importants et résister ainsi aux forces plus élevées attendues dans des constructions de mi-hauteur. La procédure de dimensionnement sera proposée à l'avenir dans le but d'être incluse dans les normes AISI S400 et S240.

Des expériences grandeur nature ont été réalisées en utilisant le cadre d'essai pour murs de refend de l'Université de McGill où 31 spécimens ont été testés de manière monotonique et cyclique. Ces spécimens ont été construits en utilisant des parements et éléments de cadre présentant des épaisseurs plus importantes que celles présentement proposées pour leur dimensionnement, au travers de deux configurations de construction innovantes (parement double et parement central) afin d'éliminer les effets dus au placement excentré du parement et tirer au maximum avantage de sa rupture ductile.

Les spécimens ont été construits selon des paramètres de construction variables (épaisseurs des matériaux, taille et espacement des vis auto-perforantes) et les résultats expérimentaux ont été analysés avec la méthode d'équivalence de l'énergie élasto-plastique (EEEP). La configuration utilisant un parement central a atteint des résistances aux efforts de cisaillement environ quatre fois supérieures à celles proposées dans les normes actuelles. De plus, la ductilité des murs fut considérablement améliorée (déplacement latéral relatif à l'étage jusque 8%), procurant un fort potentiel à cette configuration concernant son utilisation dans des constructions de mi-hauteur.

Une méthode de conception préliminaire a été initiée pour cette configuration, prenant en considération le comportement différent de ces murs de refend. Une procédure préliminaire de calcul aux états limites pour le Canada (LSD) et pour les Etats-Unis et le Mexique (LRFD) a été établit en se basant sur les résultats expérimentaux. Les facteurs de résistance, ϕ, ainsi que les

valeurs de sur-résistance ont aussi été pourvus. Les valeurs de 2.8 et 1.5 ont été obtenues pour les facteurs de modification de force sismique liés à la ductilité et à la sur-résistance applicables au Canada, R_d et R_o respectivement. Le caractère prometteur de la configuration utilisant un parement central pousse à engager une recherche plus approfondie à ce sujet, dans le but de progresser vers une méthode de conception définitive pour l'utilisation des murs de refend utilisant un cadre et un parement en acier formé à froid dans les constructions de mi-hauteur.

ACKNOWLEDGEMENTS

This research was made possible thanks to the financial support from the American Iron and Steel Institute (AISI), the Canadian Sheet Steel Building Institute (CSSBI) and the Natural Sciences and Engineering Research Council of Canada (NSERC). A special thank you is also extended to Bailey Metal Products Ltd., Simpson Strong-Tie Company Inc., Ontario Tools & Fasteners Ltd., UCAN Fastening Products and Arcelor Mittal for the materials and tools that were provided.

TABLE OF CONTENTS

Abstract ..... **i**

Résumé ..... **ii**

Acknowledgements ..... **iv**

Table of Contents ..... **v**

List of Tables ..... **viii**

List of Figures ..... **x**

Chapter 1 – Introduction and Literature Review **1**

1.1 General Overview 1

1.2 Problem Statement 2

1.3 Research Objectives 3

1.4 Scope of Study 4

1.5 Literature Review 5

1.5.1 Studies on Cold-Formed Steel Shear Walls with Steel Sheet Sheathing 5

1.5.2 Current Cold-Formed Steel Design Standards 14

1.5.3 Summary 17

Chapter 2 – Description of the Experimental Program **18**

2.1 Introduction 18

2.2 Selection of a New Configuration Based on Previous Experimental Programs 18

2.2.1 Lessons from the past 18

2.2.2 Predictions and numerical model 22

2.2.3 Observations related to the use of the Effective Strip Method 33

2.3 Description of the Shear Wall Test Apparatus 35

2.4 Cold-Formed Steel Sheathed Shear Walls Testing Program 37

2.5 Description of the Wall Fabrication and Test Setup 39

2.5.1 Double-sheathed configuration 39

2.5.2 Centre-sheathed configuration 44
2.6 Instrumentation and Data Acquisition 53
2.7 Testing Protocols 54
2.7.1 Monotonic protocol 54
2.7.2 Cyclic protocols 55

Chapter 3 – Test Results and Observations 60

3.1 Introduction 60
3.2 Observations of the Different Failure Modes 60
3.2.1 Connection Failures 61
3.2.2 Sheathing Failures 65
3.2.3 Framing Failures 68
3.3 Proceedings for the Analysis of the Test Results 75
3.4 Test Results 80
3.5 Comparison of the Influence of Protocols, Configurations and Building Parameters 83
3.5.1 Influence of Protocols 83
3.5.2 Influence of the Configuration: double-sheathed vs. centre-sheathed 86
3.5.3 Influence of the Shear Wall Building Parameters 88
3.5.4 Comparison with previous configurations 95
3.6 Material Characterization Coupon Tests 97

Chapter 4 – Interpretation of the Test Results - Discussion 100

4.1 Introduction 100
4.2 Equivalent Energy Elastic Plastic (EEEP) Method (Canada) 100
4.3 Preliminary Modified Effective Strip Method for the Centre-Sheathed Configuration 109
4.4 Development of a Limit States Design Procedure 114
4.4.1 Calibration of the Resistance Factor 115
4.4.2 Factor of Safety 123
4.4.3 Capacity Based Design 128
4.4.4 Calibration of Seismic Design Parameters for Canada 134
4.4.5 The Use of R-Values in the Future 142

Chapter 5 – Conclusions and Future Research 144

5.1 Conclusions 144

5.1.1 Double-sheathed configuration 144

5.1.2 Centre-sheathed configuration 146

5.2 Future Research 149

References 151

Appendix A. Details for Test Configurations 155

Appendix B. Fabrication of the Specimens – Drawings and Details 165

Appendix C. Numerical Model and Sample Results of the Numerical Analysis 176

Appendix D. Effective Strip Method by Yanagi and Yu *(2014)* – Calculation Details 181

Appendix E. Test Observation Sheets 187

Appendix F. Complete Test Results 220

Appendix G. Analysis of the Test Results 229

LIST OF TABLES

Table 1.1 Nominal shear resistance for seismic and other in-plane loads for shear walls with steel sheet sheathing on one side of wall (Table E2.3.1 from AISI S400 *(2015)*) 16
Table 2.1. Sheathed shear wall test program: list of shear wall configurations..... 38
Table 3.1 Test Results Summary (Metric) – Monotonic Tests..... 82
Table 3.2 Test Results Summary (Metric) – Positive Cycles of Cyclic Tests..... 82
Table 3.3 Test Results Summary (Metric) – Negative Cycles of Cyclic Tests 82
Table 3.4 Summary of Material Properties (Metric) 99
Table 4.1 Design Properties Summary (Metric) – Monotonic Shear Wall Tests 108
Table 4.2 Design Properties Summary (Metric) – Positive Cycles of Cyclic Shear Wall Tests 108
Table 4.3 Design Properties Summary (Metric) – Negative Cycles of Cyclic Shear Wall Tests108
Table 4.4 Comparison of prediction methods for centre-sheathed configuration 111
Table 4.5 Strengths ratios from positive and negative ranges of cycles..... 112
Table 4.6 Centre-sheathed configuration tests considered as successfully completed..... 114
Table 4.7 Statistical Data for the Determination of Resistance Factor (AISI S100 *(2016)*) 116
Table 4.8 Ratios of test-to-predicted values for double-sheathed configuration (LSD)..... 118
Table 4.9 Ratios of test-to-predicted values for centre-sheathed configuration 120
Table 4.10 Summary of the resistance factor calibration for different types of components..... 122
Table 4.11 Averages of the resistance factors with respect to the design analysis..... 122
Table 4.12 Factor of safety for double-sheathed specimens - Monotonic tests..... 125
Table 4.13 Factor of safety for centre-sheathed specimens - Monotonic test 125
Table 4.14 Factor of safety for double-sheathed specimens - Cyclic tests..... 126
Table 4.15 Factor of safety for centre-sheathed specimens - Cyclic tests..... 127
Table 4.16 Overstrength design values for double-sheathed specimens – Monotonic tests..... 131
Table 4.17 Overstrength design values for centre-sheathed specimens – Monotonic test 131
Table 4.18 Overstrength design values for double-sheathed specimens – Cyclic tests..... 132
Table 4.19 Overstrength design values for centre-sheathed specimens – Cyclic tests..... 132
Table 4.20 Ductility and R_d values for monotonic tests..... 136
Table 4.21 Average ductility and R_d values for cyclic tests 136
Table 4.22 Ductility and R_d values for cyclic tests – Negative range of cycles 137

Table 4.24 Ductility and R_d considering the walls tested with asymmetric protocol 137
Table 4.23 Ductility and R_d values for cyclic tests – Positive range of cycles 137
Table 4.25 Yield displacement and stiffness for double-sheathed design – Positive cycles 139
Table 4.26 Yield displacement and stiffness for centre-sheathed design – Positive cycles 139
Table 4.27 Overstrength-related force modification factor, R_o, for both configurations..... 142

LIST OF FIGURES

Figure 1.1 Cold-formed steel used as structural members and cladding for a house using CFS shear walls as SFRS (photo courtesy of J. Ellis, Simpson Strong-Tie Co. Inc.) 2
Figure 1.2 Shear wall presenting special detailing: blocking at mid-height (Yu and Chen *(2009)*) 8
Figure 1.3 Bridging for shear walls: a. positions of bridging members (Ong-Tone *(2009)*) and b. flexural buckling of bridging used for chord studs (Balh *(2010)*) 9
Figure 1.4 Blocking members for shear walls: a. connection on field stud, b. connection on chord stud and c. position of the blocking members (DaBreo *(2012)*) 11
Figure 1.5 Gravity load system (DaBreo *(2012)*) 11
Figure 1.6 Shake table test setup for double-storey cold-formed steel shear walls: a. side elevation and b. end elevation 13
Figure 2.1. Damage due to eccentric sheathing placement: a. torsional forces on chord stud, and b. out-of-plane forces on centre stud due to shear buckling of the sheathing (Rizk *(2017)*) 20
Figure 2.2. Double-sheathed configuration (front sheathing partially removed in drawing) 21
Figure 2.3. Regular centre-sheathed configuration (sheathing transparent in drawing) 22
Figure 2.4 Typical CFS shear wall for the Effective Strip Method by Yanagi and Yu *(2014)* 24
Figure 2.5 Shear force applied and equivalent tension force in the sheathing by Yanagi and Yu *(2014)* 25
Figure 2.6 Sheathing-to-framing fastener connection layout and maximum width of the effective strip by Yanagi and Yu *(2014)* 26
Figure 2.7 From experimental specimen to numerical model: a. screws located within the tension field, b. equivalent strips attributed to the screw connections and c. equivalent frame elements for the numerical model in SAP2000 29
Figure 2.8 Numerical model in SAP2000 of specimen W28: a. shear flow applied to the top horizontal member and b. deformed shape of the model after analysis 32
Figure 2.9. Forces in members of specimen W28 from SAP2000 structural analysis: a. shear forces, b. bending moments and c. axial forces 32
Figure 2.10 Evolution of the Effective Strip Method: a. initial strip method, b. second estimate based on observations and c. final estimate of the tension field width 35

Figure 2.11 Test frame and a shear wall test specimen 36
Figure 2.12 Complete shear wall test setup 36
Figure 2.13 Double-sheathed configuration: assembly of the framing members, a. chords studs, field stud and tracks, and b. fastening of first sheathing panel 41
Figure 2.14 Double-sheathed configuration: a. specimen fastened to the frame and b. installation of the second sheathing panel 42
Figure 2.15 Double-sheathed configuration: specimen ready to be tested 42
Figure 2.16 Double-sheathed configuration: detailing of the sheathing's screw pattern in the corner (hidden parts in blue) 43
Figure 2.17 Double-sheathed configuration: associated cross-sections 43
Figure 2.18 Connection between horizontal framing and chord stud using clip angles 46
Figure 2.19 Transmission of vertical forces from horizontal framing member to chord studs: a. through contact between the track and chord studs / centre stud and b. through clip angle connections 47
Figure 2.20 Top holdown with nine extra holes outside the centreline of the shear wall 48
Figure 2.21 Original centre-sheathed configuration: detailing of the sheathing's screw pattern in the corner (hidden parts in blue) 49
Figure 2.22 Original centre-sheathed configuration: associated cross-sections 49
Figure 2.23 Final centre-sheathed configuration: cross-section of a chord stud and its reinforcement 51
Figure 2.24 Final centre-sheathed configuration: stiffeners added in the corners 51
Figure 2.25 Final centre-sheathed configuration: Holdowns fastened prior to completion of the chord stud's reinforcement 52
Figure 2.26 Final centre-sheathed configuration: a. before completion of reinforcement and b. after completion: specimen ready to be tested 52
Figure 2.27 Test setup: LVDTs at the bottom corners and string potentiometer in top right corner 53
Figure 2.28 Actuator (on the left) and the load cell (in circle) 54
Figure 2.29 Pattern of the CUREE Reversed Cyclic Protocol for a given specimen: primary cycles in red, trailing cycles in green. 57
Figure 2.30 Key values for the determination of the CUREE cycles for a given wall 57

Figure 2.31 CUREE Reversed Cyclic Protocol and test results for test W29-C 58
Figure 2.32 Asymmetric cyclic protocol to capture the degradation in strength and high ductility of the wall specimens built with the centre-sheathed configuration..... 59
Figure 3.1 Steel bearing damage in sheathing from double-sheathed configuration..... 61
Figure 3.2 Steel bearing damage in sheathing from centre-sheathed configuration..... 61
Figure 3.3 Tear-out of the sheathing from two screws 62
Figure 3.4 Pull-through sheathing failure: a. right before happening and b. just after..... 63
Figure 3.5 Shear failure of screws: shear capacity conserved on all the layers (in green) and capacity lost on the top layer (in red)..... 64
Figure 3.6 Shear flow running in built-up chord member subjected to bending 65
Figure 3.7 Tension (red) and compression (blue) fields in a deformed rectangular shape..... 66
Figure 3.8 Shear buckling of sheathing during monotonic tests: a. double-sheathed wall and b. centre-sheathed wall..... 66
Figure 3.9 Damage after cyclic test: a. two directions of shear buckling and b. one of the holes that appeared at intersections 67
Figure 3.10 Frame damages in chord studs: a. elastic local buckling and b. web of the stud slightly pulled out by the holdown during the test..... 69
Figure 3.11 Damage in chord studs of specimen W18-M: a. axial compression load and bending moment interaction failure in the vertical chord studs and b. local damage of the chord stud flanges due to contact with the horizontal framing members at corners..... 70
Figure 3.12 Damage in chord stud of specimen W16-MR: a. general view of the damaged specimen, b. local buckling of the chord stud's flange and lip at mid-height and c. local buckling of the chord stud's web at the base 71
Figure 3.13 Specimen W25-CR after cyclic test: a. framing members in good condition and b. damage confined to the sheathing and its connections (bearing damage). 72
Figure 3.14 Built-up chord studs split due to out-of-plane forces caused by shear buckling of the sheathing 72
Figure 3.15 Failing chord studs: a. complete built-up chord stud failing on W18-M, b. local buckling of the flange and lip of the outer part of the built-up member on W16-MR and c. local buckling of the webs and flanges of the inner parts of the built-up member..... 73

Figure 3.16 Failed chord studs: a. flange at the top of the chord stud failed during test due to contact with horizontal framing member and b. good condition of the flange at top of the chord stud when using stiffeners 74
Figure 3.17 Damaged holdowns on the strongest specimens, using the highest degree of reinforcement (R3) 75
Figure 3.18 Force vs. deformation results plotted for W18-M (monotonic test) 76
Figure 3.19 Force vs. deformation results plotted for W26-CR3 (asymmetric cyclic test) 77
Figure 3.20 Backbone curves and associated energy “dissipated” (in red and blue) by W30-C differentiating the positive and negative displacements or the CUREE reversed cyclic protocol 78
Figure 3.21 Backbone curve and associated energy “dissipated” (in blue) by W26-CR3 during the asymmetric cyclic protocol 78
Figure 3.22 Energy dissipated (in green) during the execution of a complete intermediate primary cycle of a cyclic test 79
Figure 3.23 Graphic representation of the parameters included in test results 81
Figure 3.24 Monotonic and cyclic force vs. deformation behaviour of double-sheathed configuration specimens 85
Figure 3.25 Monotonic and cyclic behaviours of centre-sheathed configuration specimens 85
Figure 3.26 Specimens W15-CR3 and W15B-CR3 tested with two different protocols 86
Figure 3.27 Force vs. deformation test results (backbone curves) from the two shear wall configurations constructed using nominally comparable components 88
Figure 3.28 Test results from the two shear wall configurations using different sheathing thicknesses 89
Figure 3.29 Test results from the two shear wall configurations using different sheathing screw spacing 91
Figure 3.30 Test results from the two shear wall configurations using different screw diameter 92
Figure 3.31 Centre-sheathed configuration monotonic test results showing behaviour of specimens with different chord stud reinforcement schemes (None & R) 93
Figure 3.32 Centre-sheathed configuration monotonic test results showing behaviour of shear wall specimens with different reinforcement schemes (MR, MR2 & MR3) 95
Figure 4.1 Equivalent Energy Elastic-Plastic (EEEP) bilinear model 101
Figure 4.2 EEEP model and definition of $\Delta_{u(EEEP)}$ for case 1 102

Figure 4.3 EEEP model and definition of $\Delta_{u(EEEP)}$ for case 2 102
Figure 4.4 Parameters defining the EEEP curve 104
Figure 4.5 EEEP curve for the monotonic test W29-M 107
Figure 4.6 EEEP curves for the cyclic test W29-C 107
Figure 4.7 Bearing strength and screws participating for a centre-sheathed configuration specimen 110
Figure 4.8 Definition of the factor of safety for double-sheathed specimens related to ultimate and factored resistances for LSD (using EEEP analysis method) and LRFD 123
Figure 4.9 Representation of the overstrength for a double-sheathed specimen 129
Figure 4.10 Ultimate and design overstrength for the centre-sheathed configuration 130
Figure 4.11 Inelastic deformations resulting in a similar R_d value for double-sheathed and centre-sheathed walls 140

CHAPTER 1 – INTRODUCTION AND LITERATURE REVIEW

1.1 General Overview

Focusing on residential and commercial buildings, cold-formed steel has been used in low to mid-rise constructions. It has become an economical alternative, especially in regions such as Hawaii where cold-formed steel has become the standard material for homes *(Hawaii Steel Alliance, 2016)*. Cold-formed steel is very durable; it can be shipped in coils and then roll formed on site or in an industrial facility near to the construction site, resulting in a cost-effective shipping and fabrication process. In addition, with non-combustible properties and recyclability, cold-formed steel has been increasingly used as cladding, decking, and diaphragms but more importantly as structural framing for buildings (Figure 1.1).

In earthquake prone areas, seismic force-resisting systems (SFRS) have to be included in the design of the buildings. Cold-formed steel shear walls can be used as a SFRS. CFS framing with gypsum panels and wood structural panels as sheathing were an early development for shear wall construction. More recently, cold-formed steel sheathing has been used to replace the wood panels. Recent studies (e.g. Yu et al. *(2007)*, Yu & Chen *(2009)*, Balh et al. *(2014)*, Shamim et al. *(2013)*) have provided information and guidelines for the design of cold-formed steel sheathed and framed shear walls, which have made their way into the AISI S400 North American Standard for Seismic Design of Cold-formed Steel Structural Systems *(2015)*.

As a relatively new lateral load carrying system, cold-formed steel sheathed and framed shear walls require further studies to advance and optimize their design so that their full potential can be realized.

Figure 1.1 Cold-formed steel used as structural members and cladding for a house using CFS shear walls as SFRS (photo courtesy of J. Ellis, Simpson Strong-Tie Co. Inc.)

1.2 Problem Statement

The American Iron and Steel Institute (AISI) in the USA, the Canadian Standards Association (CSA) in Canada and the Camara Nacional de la Industria del Hierro y del Acero (CANACERO) in Mexico joined efforts to develop design specifications applicable throughout North America. The standards resulting (e.g. AISI S100 *(2016)* and S400 *(2015)*) were adapted to each country, varying the terminology and the procedures when design and building code requirements are different.

The most recent version of the North American Standard for Seismic Design of Cold-Formed Steel Structural Systems AISI S400 *(2015)* contains a design procedure for cold-formed steel shear walls with steel sheet sheathing. This is in addition to procedures for shear walls sheathed with wood structural panels and walls using strap braces. The AISI S400 Standard was developed using the former AISI S213 Standard *(2007)* as a model. The design information for CFS shear walls is presented in tabular format in Section E2 Table E2.3-1 of the AISI S400 Standard *(2015)*, whereby the results of wall configurations subjected to testing were used to establish the nominal design

values. The maximum listed nominal shear resistance reaches 2085 lb/ft (30.4 kN/m) for the USA and Mexico, while 23.3 kN/m (1603 lb/ft) is the upper limit for Canada. Further, an analytical design method for steel sheathed shear walls (Effective Strip Method) was developed by Yanagi and Yu *(2014)* based on the assumption that a partial width of the steel sheet sheathing will participate in providing lateral strength to the shear wall by means of a tension field. This method was included in Section E2.3.1.1.1 of AISI S400 *(2015)*; however, it is only permitted to be used in the USA and Mexico, restricting the design of these systems in Canada to the design method using tabulated values based on previous laboratory based studies. Whether the analytical method or Table E2.3-1 are used, they are limited to certain variations of the parameters (e.g. screw spacing, material thicknesses, etc.), within the range of existing CFS framed shear wall test data, restricting the freedom of design for the cold-formed steel shear walls with steel sheet sheathing. Consequently, the nominal shear strength of cold-formed steel shear walls with steel sheet sheathing is limited, preventing the use of these shear walls in mid-rise construction where design loads are anticipated to be greater, especially in high seismic zones.

1.3 Research Objectives

This research project has four main objectives related to the design of higher strength and more ductile steel sheathed shear walls:

- Determine innovative configurations for shear walls capable of achieving higher strength and higher ductility than shear walls currently listed in the AISI S400 Standard *(2015)*;

- Test full-scale specimens of innovative configurations of cold-formed steel shear walls using thicker framing and thicker sheathing not currently listed in the AISI S400 Standard *(2015)*;

- Propose a design method to predict the nominal shear strengths of these innovative configurations for cold-formed steel shear walls with steel sheet sheathing.

- Determine design related factors for use in Canada, in the USA and in Mexico.

1.4 Scope of Study

All shear wall specimens presented a 2:1 aspect ratio, with dimensions of 2438 × 1219 mm (8’ × 4’), built using two different configurations; the double-sheathed configuration, using one steel sheet on each face of the shear wall, and the centre-sheathed configuration using a single steel sheet at the centreline of the wall. These two configurations were built using various parameters; varying framing and sheathing thicknesses, sheathing screw spacing and screw sizes. Overall, 15 shear walls were tested by the author (8 using the double-sheathed configuration and 7 using the centre-sheathed configuration) for a total of 31 shear walls (16 and 15 respectively) tested throughout this experimental program, subjected to monotonic and CUREE cyclic protocols. The remaining 16 shear walls are presented in Santos *(2017).* The framing thicknesses used were 1.73 mm (0.068”) and 2.46 mm (0.097”), whereas the sheathing thicknesses were 2 × 0.36 mm (2 × 0.014”), 2 × 0.47 mm (2 × 0.019”), 0.84 mm (0.033”) and 1.09 mm (0.043”). The sheathing screw spacing used were 50 mm (2”), 100 mm (4”) and 150 mm (6”), with #10 and #12 screws. Due to the exploratory nature of the experimental program, the selection of the shear wall parameters to be tested had to be modified during the laboratory phase of the research to accommodate for the design issues encountered while testing the innovative configurations. Thus, a limited range of varying parameters was tested.

During the experimental program, an iterative design approach was used for the centre-sheathed configuration specimens; the member sizes were modified throughout the program, resulting in an evolving centre-sheathed configuration from one test to the next.

Analysis of data was performed using the Equivalent Energy Elastic Plastic (EEEP) method (Park *(1989)*; Foliente *(1996)*). A new preliminary design method was defined for the centre-sheathed configuration, taking into consideration the specific behaviour of these shear walls. Design related factors were determined; the resistance factors, ϕ, for limit states design in Canada (LSD), in the USA and Mexico (LRFD), the recommended factors of safety as well as test-based seismic force modification factors, R_d and R_o for Canada.

The material used for this experimental program was submitted to coupon testing in order to determine and confirm the thicknesses and mechanical properties of each member.

1.5 Literature Review

Studies of cold-formed steel framed shear walls have been carried out on specimens constructed using different sheathing materials to provide for lateral in-plane strength and stiffness. These materials were plywood, OSB, gypsum, cement board, cold-formed steel straps or cold-formed steel sheet sheathing. Most recently, walls sheathed with thin steel sheet have been the subject of further investigation, which has resulted in design methods being integrated into the cold-formed steel standards. As the present experimental program is also with regards to cold-formed steel shear walls sheathed with steel sheet, the literature review presented herein concentrates on the related past research.

1.5.1 Studies on Cold-Formed Steel Shear Walls with Steel Sheet Sheathing

Several research projects have been carried out throughout the past decades with regards to cold-formed steel framed and sheathed shear walls. A summary of these projects is presented in this section.

1.5.1.1 The beginnings of cold-formed steel shear wall using steel sheet sheathing

The cold-formed steel framed and sheathed shear walls presently found in AISI S400 follow the same main construction details that existed when this type of lateral system was first investigated. Although it is possible to use sheathing on both faces, shear walls are mostly built using sheathing on one face of the wall, and fastened to the built-up chord studs using self-drilling screws. The chord studs are made of two C-sections fastened back-to-back using the necessary amount of screws at a regular spacing. Holdowns are installed inside the chord studs to resist the overturning forces. The report published by Serrette et al. *(1997)* is complementary to the 1996 test program (Serrette *(1996)*) that provided shear wall design values for CFS steel framing assemblies sheathed with plywood, oriented strand board (OSB) and gypsum wallboard (GWB). In addition to the limitations in terms of material used, the framing thickness was also limited to 0.84 mm thick (0.033”). Serrette et al. *(1997)* carried out a follow-up shear wall test program, the purpose of which was to clarify some of the values provided by the 1996 study, but more importantly to offer

a wider range of design options. To this end, they included flat strap X-braced walls and steel sheathed walls (0.46 mm (0.018”) and 0.69 mm (0.027”) thick steel sheets), high aspect ratio walls and framing thicknesses of 1.09 mm (0.043”) and 1.37 mm (0.054”). For both laboratory test programs, the shear wall specimens were subjected to monotonic and cyclic lateral loading protocols.

These studies showed the failure of steel sheathed wall assemblies resulted from a combination of bearing damage at screw fastener locations and pullout of these screws from the chord studs. In addition, Serrette et al. showed that reducing the screw spacing and/or increasing the thickness of the sheathing led to local buckling in the chord stud, due to the development of a higher shear resistance from the wall, and the associated larger forces on the framing members. It also showed the impact of the thickness of the wall members and the size of the screws on the constructability of the wall; small screws with thick sheathing required predrilling in the chord studs/sheathing. These results were then integrated into the North American Standard for Cold-Formed Steel Framing – Lateral Design AISI S213 *(2004)* as design provisions specifically for the range of steel sheet sheathing thickness tested by Serrette *(1997)* (i.e. 0.46 mm (0.018”) and 0.69 mm (0.027”)).

1.5.1.2 Continuing studies on cold-formed steel shear walls using steel sheet sheathing

The promising ductility from the steel sheet sheathing was an incentive to complete further research using more variations of the construction parameters. These variations are numerous; screw spacing, thickness of the framing, thickness of the sheathing, or aspect ratio of the wall. Providing more test results would allow for additional wall construction details / combinations in the lateral standard, offering more possibilities to design engineers when integrating CFS shear walls in their structures.

Yu et al. *(2007)* provided nominal shear strengths for wind and seismic loads obtained from the monotonic and cyclic tests conducted on 0.69 mm (0.027”), 0.76 mm (0.030”) and 0.84 mm (0.033”) steel sheet sheathed shear walls, with varying aspect ratios (2:1 and 4:1) and screw spacing (from 150 mm (6”) to 50 mm (2”)). Overall, 66 shear wall tests were conducted; 33 were tested using a monotonic protocol conforming to the Standard Practice for Static Load Test for Shear Resistance of Framed Walls for Buildings ASTM E564 *(2006)* and 33 others were tested

using the CUREE (Consortium of Universities for Research in Earthquake Engineering) reversed-cyclic protocol (Krawinkler *et al (2001)*, ASTM E2126 *(2011)*). In addition, this report was used to evaluate the deflection equation provided in AISI S213. A staggered screw pattern fastening the sheathing to the flanges of both the C-sections composing each built-up chord stud was investigated. This fastener pattern moderately improved the shear strength of the wall and reduced the distortion of the chord stud flanges. The shear strength reduction factor for high aspect ratio walls (comprised between 2:1 and 4:1) found in AISI S213 was confirmed. This research project highlighted the effect the framing thickness had on the shear capacity of the wall; it was described that thicker framing may greatly improve the shear strength of the steel sheet sheathed shear walls. The testing methods, building parameters used and the tests results are summarized in Yu *(2010)*. This research project also exhibited discrepancies with previous works by Serrette *(1997)* and Ellis *(2007)* regarding the 0.69 mm (0.027") thick sheet sheathed shear walls, revealing than the previous works provided non-conservative shear resistance values. Tests on the shear walls constructed with other sheathing thickness by Serrette *(1997)* (i.e. 0.46 mm (0.018")) were realised by Yu and Chen *(2009)*, and revealed inconsistent discrepancies (monotonic and cyclic tests provided opposite discrepancies), requiring further investigation to verify the published values.

The second phase of this research program by Yu and Chen *(2009)* comprised special detailing for twenty-three 8'×6' (2438 × 1829 mm) shear walls with 50 mm (2") screw spacing, using blocking and strapping at mid-height of the specimens (Figure 1.2), as well as the staggered pattern for sheathing screws as per Yu et al. *(2007)*. The idea behind it was to limit the distortion of the chord studs and to increase the nominal shear strength and ductility of 8'×6' (2438 × 1829 mm) shear walls using 0.84 mm (0.033") and 1.09 mm (0.043") thick framing with a sheathing thickness up to 0.84 mm (0.033"). However, it also showed that special detailing was not necessary to have satisfactory performance of 8'×6' (2438 × 1829 mm) shear walls using 0.84 mm (0.033") thick sheathing and 1.37 mm (0.054") thick framing. In addition, this phase determined that the shear strength reduction factor for shear walls with high aspect ratio (mentioned hereinbefore) was conservative, pushing for research to further investigate this aspect. This phase is summarized in Yu and Chen *(2011)*.

Figure 1.2 Shear wall presenting special detailing: blocking at mid-height (Yu and Chen *(2009)*)

A total of 54 cold-formed steel shear walls with steel sheet sheathing built with 18 different sets of parameters were tested during the summer 2008 in the structural laboratory of the Department of Civil Engineering and Applied Mechanics at McGill University (Ong-Tone *(2009)*; Balh *(2010)*). The shear walls were built using similar sheathing and framing thicknesses to the previous studies by Serrette *(1997)*, Yu et al. *(2007)* and Yu and Chen *(2009)*. Thicknesses of 0.46 mm (0.018”) and 0.76 mm (0.030”) were used for the sheathing and thicknesses of 0.84 mm (0.033”), 1.09 mm (0.043”) and 1.37 mm (0.054”) were used to build the framing members. Height-to-width aspect ratios varied between 4:1 (2438 × 610 mm (8’ × 2’)) and 1:1 (2438 × 2438 mm (8’ × 8’)), when the smallest aspect ratio that had been tested for steel sheathed shear wall at that moment was 2:1. The walls were tested using monotonic and CUREE reversed cyclic protocols also used by Yu et al. *(2007)* and Yu and Chen *(2009)*. These tests showed consistency in the results for all

configurations, demonstrating the same failure modes observed in previous studies. The decrease in screw spacing was directly related to the increase in shear strength, as well as the increase of the thickness of the sheathing.

Bridging was also used to reduce the distortion damage in the chord studs due to the presence of the sheathing on one face of the wall, creating torsional forces on the chord studs through eccentric loading. The bridging was installed at each quarter height of the wall (Figure 1.3a), stiffening the wall and increasing its shear resistance. Although reduced damage and higher capacities were observed, it was concluded that the bridging members were too slender to have a real impact on the resistance since they buckled during the tests (Figure 1.3b). Blocking between stud members was also tested; the walls constructed as such showed a better behaviour in terms of improved buckling resistance of the blocking at large displacements and provided the wall with a higher shear resistance. However, the overall ductility of the shear wall (lateral drift) was affected, resulting in a lower energy dissipation than the specimens using bridging members.

a. b.

Figure 1.3 Bridging for shear walls: a. positions of bridging members (Ong-Tone *(2009)*) and b. flexural buckling of bridging used for chord studs (Balh *(2010)*)

The investigation of shear walls with aspect ratios of 4:1 showed that the walls were prevented from developing their shear resistance at a consistent drift (compared to 1:1 and 2:1 aspect ratios

wall), due to the increased flexibility of the assembly. Ultimately, Balh *(2010)* proposed a resistance factor $\phi = 0.70$ to be used in the relevant design standards, an overstrength factor of 1.4 and values of 2.5 and 1.7 for test-based seismic force modification factors R_d and R_o respectively, as well as a maximum drift limit of 2%. The results are summarized in Balh et al. *(2014)*. These *R*-values could not be validated when checked according to the Federal Emergency Management Agency (FEMA) P695 standard methodology *(2009)*, where the adjusted collapse margin ratio (ACMR) could not meet the minimum requirements. The *R*-values were then revised, recommending a R_d value of 2.0 and a R_o value of 1.3, as well as a height limit of 15 m (49.2'), corresponding to a five-storey building.

DaBreo *(2012)* investigated the performances of cold-formed steel shear walls with steel sheet sheathing built with blocking members between the studs (Figure 1.4), similar to bridging but using stockier members to avoid the flexural buckling failure mode. In addition, the shear wall specimens were tested under combined gravity and lateral loading, using a gravity load system as per Figure 1.5. Hikita and Rogers (2006) had already tested wood sheathed / CFS framed shear walls under gravity loads but the force applied by this system presented a horizontal component when submitting the wall to lateral displacements. This new testing system was intended to avoid this drawback. The gravity load had a magnitude of 10 kN/m (685 lb/ft), a value consistent with the previous research on combined gravity and lateral loads applied to shear walls. The experimental program is summarized in DaBreo et al. *(2014)*.

This program comprised 14 specimens of a single aspect ratio of 2:1 (2438 × 1219 mm (8' × 4')) exhibiting 8 different sets of parameters; sheathing thicknesses of 0.46 mm (0.018") and 0.76 mm (0.030"), framing thicknesses of 1.09 mm (0.043") and 1.37 mm (0.054") and sheathing fastener spacing of 50, 75, 100 and 150 mm (2", 4", 6", 8"), similarly to the previous research programs.

a. b. c.

Figure 1.4 Blocking members for shear walls: a. connection on field stud, b. connection on chord stud and c. position of the blocking members (DaBreo *(2012)*)

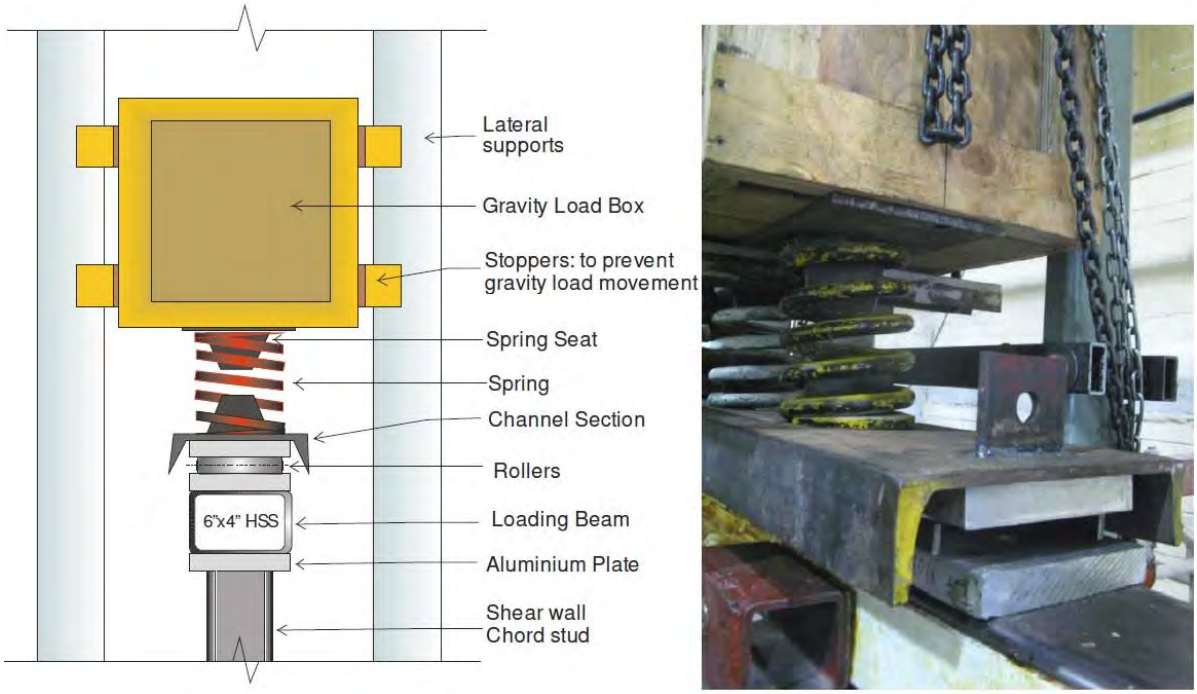

Figure 1.5 Gravity load system (DaBreo *(2012)*)

DaBreo's research confirmed the influence of the building parameters on the shear strength of the wall; reducing the screw spacing increases the shear strength of the wall, increasing the thickness of the sheathing increases the shear strength of the wall as well. In addition, it showed that the

walls using blocking members had nominal shear strength between 1.37 and 1.80 times higher than the same specimen built without blocking members. There was no consistent effect on the elastic stiffness, but the tests revealed a general decrease in the walls' ductility when blocking was installed, similarly to that observed by Balh *(2010)*. Overall, the vertical loading capacity of the chord studs was not compromise throughout the tests.

DaBreo recommended a similar resistance factor $\phi = 0.7$ and test-based seismic force modification factors R_d and R_o, with values of 2.0 and 1.3 respectively. However, these test-based factors could not be validated following the FEMA P695, achieving an ACMR of 1.5 when 1.56 was the value required by FEMA.

In order to include seismic design provisions for this kind of SFRS in the National Building Code of Canada (NBCC) and the AISI S213 Standard (replaced in 2015 by the AISI S400), further tests were conducted by Shamim *(2012)* on the École Polytechnique de Montreal structural laboratory shake table (Figure 1.6), using full-scale single- and double-storey cold-formed steel shear walls with steel sheet sheathing; each wall segment having a 2:1 aspect ratio. The blocking investigated by Balh *(2010)* and DaBreo *(2012)* was installed on these shear walls. The dynamic test program included impact tests, harmonic forced vibration tests and ground motion tests representative of the seismic hazard in Quebec and Vancouver, Canada (Shamim et al. *(2013)*). Overall, ten specimens were tested; 5 single-storey and 5 double-storey shear walls. The single-storey specimens were all built with 1.09 mm (0.043") thick framing members with sheathing thicknesses of 0.46 mm (0.018") and 0.76 mm (0.030"). The same sheathing thicknesses were used for the double-storey walls but using thicknesses of 1.09 mm (0.043"), 1.37 mm (0.054") and 1.73 mm (0.068"). Numerical modeling was also realized in the OpenSees software for two-, four- and five-storey buildings located in Halifax (low seismic activity), Montreal (medium seismic activity) and Vancouver (high seismic activity) (Shamim and Rogers *(2013)*).

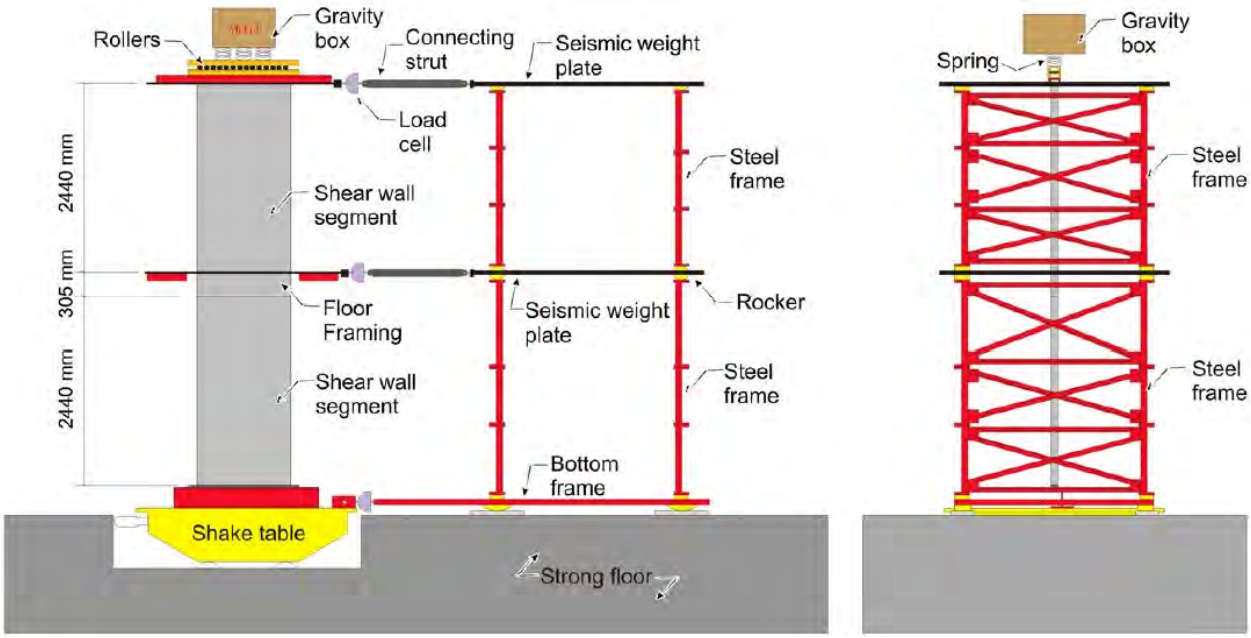

a. b.

Figure 1.6 Shake table test setup for double-storey cold-formed steel shear walls: a. side elevation and b. end elevation

A few specimens showed the same kind of damage observed in previous research, including the torsional damages due to the in-plane forces within the tension field acting on the chord studs' flange at fastener locations. But again, the framing members remained generally without significant damage. The gain in shear resistance due to the use of the blocking at quarter height of the wall was confirmed with these tests. Generally, the behaviour did not differ from that exhibited by the cold-formed steel shear walls with steel sheet sheathing tested monotonically and cyclically by Ong-Tone *(2009)*, Balh *(2010)* and DaBreo *(2012)*, summarized in DaBreo et al. *(2014)*.

The numerical modelling using OpenSees, described in Shamim and Rogers *(2013)*, included two phases where the non-linear models were calibrated differently. Phase 1 comprised non-linear models calibrated using the test data from shear walls tested using reversed-cyclic protocols. The second phase comprised more advanced models calibrated using the data from the dynamic shake table tests presented hereinabove. The shear wall models accounted for the influence of the construction details and the P-delta effect. Overall, the building models subjected to non-linear time history dynamic analysis using a ground motion record similar to the spectral shape assumed

in design for Vancouver proved to be satisfying and indicated that the response would be reasonable for further research and future analyses.

Shamim and Rogers *(2015)* provided seismic design provisions that were to be included in the new AISI S400 Standard *(2015)*, replacing the former AISI S213 Standard, based on the previous works using the displacement-based testing and dynamic testing, the dynamic numerical models developed in OpenSees and the dynamic response time history analyses previously depicted. The design method was shown to be appropriate and the seismic force modification factors R_d and R_o were set once again to 2.0 and 1.3 respectively.

1.5.2 Current Cold-Formed Steel Design Standards

Some of the cold-formed steel design standards have been unified for Canada, the USA and Mexico. They provide shared specifications for cold-formed steel structures that can slightly vary from one country to the other. For example, the common proceedings when designing a cold-formed steel structure in Canada involve the National Building Code of Canada (NBCC) *(NRCC, 2015)* referring to the Canadian Standards Association (CSA) S136 *(2012)* Specification for Cold-Formed Steel Design (same as AISI S100), which ultimately refers to the American Iron and Steel Institute (AISI) S400 Standard *(2015)*.

Seismic design provisions for cold-formed steel shear walls sheathed with steel sheet were provided for use in the USA and Mexico in AISI S213 *(2007)* until the release of the AISI S400 Standard *(2015)*, the North American Standard for Seismic Design of Cold-Formed Steel Structural Systems, which then included provisions for such walls for use in Canada. These provisions are based on numerous research programs involving monotonic and cyclic testing, as well as shake table tests, the development of non-linear dynamic numerical models and a building performance assessment according to the FEMA P695 methodology (Canadian design method).

The design methods provided by the AISI S400 Standard differ in terms of the nominal shear strength since the USA and Mexico were based on the ultimate strength measured during tests, whereas the Canadian values were determined following an approach that considers the yield strength of the specimens. Although they provide different values, these design methods have

much in common since they are comprised of tabulated values (Table 1.1) that limit the choice of building parameters one can use when designing shear walls. Indeed, the tabulated values originate from the same set of shear wall test data, mainly obtained from studies carried out at the University of North Texas by Yu et al. *(2007)* and Yu and Chen *(2009)*, and reported in Yu *(2010)* and Yu and Chen *(2011)*, as well as at McGill University by Ong-Tone *(2009)*, Balh *(2010)* and DaBreo *(2012)*, summaries by DaBreo et al. *(2014)* and Balh et al. *(2014)*. These tables define the perimeter within which the shear walls can be designed; i.e. material thicknesses and strength, aspect ratios, screw spacing and screw size, and the use of blocking (Table 1.1).

Yanagi and Yu *(2014)* introduced a new method for the design of cold-formed steel shear walls with steel sheet sheathing called the Effective Strip Method, which was adopted by the AISI S400 Standard. This method allowed for the prediction of the nominal shear resistance of a specimen based on the building parameters used to build the shear wall. The nominal shear resistance predicted by this method corresponds to the ultimate shear resistance of the specimen concerned, hence the limitations for the use of this method in the USA and Mexico only. The main concept behind this method is that the shear resistance is provided by a delimited portion of the sheathing: the effective strip. This portion of the sheathing is of variable width, depending on the building parameters of the wall being designed (e.g. material strengths, edge distance, nominal screw diameter, etc.). It was calibrated using most of the data for cold-formed steel shear walls with steel sheet sheathing gathered until then (i.e. Serrette et al. *(1996)* and Serrette *(2002)*, Balh *(2010)*, Yu *(2010)* and Yu and Chen *(2011)*). As the calibration was made using experimental investigations, the Effective Strip Method can only be used within the range of construction parameters delimited by these tests. One can design a shear wall specimen using a set of building parameters that had never been realised before using this method, to the condition that these parameters be included within the limits set for the method.

Table 1.1 Nominal shear resistance for seismic and other in-plane loads for shear walls with steel sheet sheathing on one side of wall (Table E2.3.1 from AISI S400 *(2015)*)

U.S. and Mexico (lb/ft)								
Assembly Description	Max. Aspect Ratio (h:w)	Fastener Spacing at Panel Edges[2] (in.)				Stud Blocking Required	Designation Thickness[5] of Stud, Track and Stud Blocking (mils)	Minimum Sheathing Screw Size
		6	4	3	2			
0.018" steel sheet	2:1	390	-	-	-	No	33 (min.)	8
0.027" steel sheet	2:1[3]	-	1000	1085	1170	No	43 (min.)	8
	2:1[3]	647	710	778	845	No	33 (min.)	8
0.030" steel sheet	2:1[3]	910	1015	1040	1070	No	43 (min.)	8
	2:1[3]	-	-	-	1355	Yes	43 (min.)	10
0.033" steel sheet	2:1[3]	1055	1170	1235	1305	No	43 (min.)	8
	2:1[3]	-	-	-	1505	Yes	43 (min.)	10
	2:1[3]	-	-	-	1870	No	54 (min.)	8
	2:1[3]	-	-	-	2085	Yes	54 (min.)	10
Canada **(kN/m)**								
Assembly Description	Max. Aspect Ratio (h:w)	Fastener Spacing at Panel Edges[2] (mm)				Stud Blocking Required	Designation Thickness[5] of Stud, Track and Stud Blocking (mils)	Required Sheathing Screw Size
		150	100	75	50			
0.46 mm steel sheet	2:1	4.1	---	---	---	No	33 (min)	8
0.46 mm steel sheet	2:1	4.5	6.0	6.8	7.5	No	43 (min)	8
0.68 mm steel sheet	2:1	6.5	7.2	7.9	8.7	No	33 (min)	8
0.76 mm steel sheet	4:1	8.9	10.6	11.6	12.5	No	43 (min)	8
0.84 mm steel sheet	4:1	10.7	12.0	13.0	14.0	No	43 (min)	8
0.46 mm steel sheet	2:1	7.4	9.7	11.6	13.5	Yes	43 (min)	8
0.76 mm steel sheet	2:1	11.7	14.3	---	---	Yes	43 (min)	8
0.76 mm steel sheet	2:1	---	---	19.9	23.3	Yes	54 (min)	8

1. F or SI: 1" = 25.4 mm, 1 ft = 0.305 m, 1 lb = 4.45 N. For U.S. Customary Units: 1 mm = 0.0394", 1 m = 3.28 ft, 1 N = 0.225 lb
2. See Section E2.4.1.1 for installation requirements for screws in the field of the panel.
3. See Section E2.3.1.1 for *shear wall* height to length aspect ratios (h:w) greater than 2:1, but not exceeding 4:1.
4. See Section E2.3.1.1.2 and Section E2.3.1.1.3 for requirements for sheathing applied to both sides of wall.
5. Only where *Designation Thickness* is specified as a (min) is substitution with a thicker member permitted.

1.5.3 Summary

Numerous research projects have already been conducted on cold-formed steel framed shear walls with steel sheet sheathing using various building parameters. Nevertheless, the building configurations of these walls remained relatively the same, limiting the progress in terms of maximum shear resistance and ductility. Besides, the design of these walls is restricted to the configurations and building parameters listed in the construction codes where corresponding tabulated values are provided for the USA and Mexico, as well as for Canada since 2015.

Studies on the subject have continuously been realized in order to extend the design space from within these shear walls can be selected. The use of framing reinforcement such as bridging or blocking has been investigated to improve the behaviour of the shear walls facing higher forces while using thicker sheathing and framing material. Despite the fact that these frame blocking members could facilitate reaching higher shear strength in the walls, the ductility of the shear walls was negatively impacted. The similar damage patterns observed in shear wall test specimens throughout many past laboratory studies have illustrated the need for a new framing configuration in order to achieve higher shear resistance, with an efficient ductile behaviour.

The test program described in Chapters 2 through 4 of this report was shaped based on the previous research projects, creating new configurations to address the weaknesses observed for the regular building configurations for cold-formed steel framed shear walls.

CHAPTER 2 – DESCRIPTION OF THE EXPERIMENTAL PROGRAM

2.1 Introduction

Experimental programs are necessary when it comes to assessing the performance of a member or a system; they provide experimental data allowing the calibration of numerical models or methods to better foresee the behaviour of a given specimen in a specific application.

This chapter presents the experimental program carried out to describe the behaviour of cold-formed steel sheathed shear walls using innovative configurations. The progression towards these configurations will first be described, followed by a presentation of the testing program. Then a detailed description of the materials and methods used to build the specimens will be presented before closing this chapter with the presentation of the different loading protocols used throughout the experimental program.

2.2 Selection of a New Configuration Based on Previous Experimental Programs

As depicted in the preceding chapter, several research projects regarding cold-formed steel shear walls have been carried out in the past, including a few using cold-formed steel sheathing on a cold-formed steel frame. Although they have behaved well, improved building configurations are needed in order to achieve better strength and ductility. The last experimental program on cold-formed steel shear walls that would be the closest to that described herein in terms of building parameters and material used was carried out at McGill University by Rizk *(2017)*. The design of the new shear walls had to take into consideration the shortcomings, in terms of performance under loading, of Rizk's shear walls in order to minimize their effect on the ductility and the resistance of the specimens.

2.2.1 Lessons from the past

The experimental program previously carried out by Rizk *(2017)*, using a cold-formed steel frame and a cold-formed steel sheathing on a single face of the wall, showed an overall good resistance

and ductility. However, the existing eccentricity caused by the placement of the sheathing imposed too much torque on the chord studs (Figure 2.1a), limiting the screw spacing or the thickness of the sheathing that could be used. The use of a thicker sheathing and/or smaller screw spacing would not have been possible. The resulting increase in resistance would have caused greater forces transmitted by the sheathing through screw connections, thus amplifying the torque in the chord studs and increasing the potential for their failure. Indeed, frame damage must be limited; most of the strength and ductility should be derived from the screw/sheathing interfaces.

Therefore, minimizing the eccentricity caused by the sheathing being placed on one side of a wall became the first main objective for the new configuration. Besides bringing high torsional forces to the chord studs, the sheathing placement imposed out-of-plane forces, caused by its shear buckling, to be applied on one face only, pushing the centre stud out-of-plane and thus reducing its contribution to sustain gravity loads that could be applied on the shear wall (Figure 2.1b). In addition to eliminating these failure modes, minimizing the eccentricity would allow for the removal of the requirement for the frame blocking, as used in Rizk's research, and would provide for higher forces since a thicker sheathing could be used with the same screw spacing.

Another phenomenon that took place in Rizk's tests using reversed cyclic protocols was that the bearing deformations at the screw/sheathing interface gradually increased in the corners of the wall (where the tension field is located) while going through higher and higher chord rotations. As the bearing slots at these screw/sheathing interfaces enlarged, the sheathing pulled over the heads of the screws due to the out-of-plane forces caused by shear buckling of the sheathing and the cyclic displacements that were applied. This tremendously affected the residual strength and the ductility of the wall, since most of the connections located in the sheathing tension field did not contribute after this behaviour had commenced. For that reason, it was also necessary to find a way to keep the sheathing working in bearing with the screws for the highest number of load / displacement cycles possible.

a. b.

Figure 2.1. Damage due to eccentric sheathing placement: a. torsional forces on chord stud, and b. out-of-plane forces on centre stud due to shear buckling of the sheathing (Rizk *(2017)*)

Two different configurations were considered, both presenting no eccentric loading on the stud framing; and one of the two providing for improved screw bearing contact:

- The first configuration was composed of two pieces of sheathing; one on each face of the shear wall (Figure 2.2). Given the symmetry of this configuration, no eccentric loading would be applied on the chord studs, therefore allowing for a higher shear resistance since the chord studs would in principle not experience torque and hence would not become damaged if designed for the in-plane moment and axial forces.

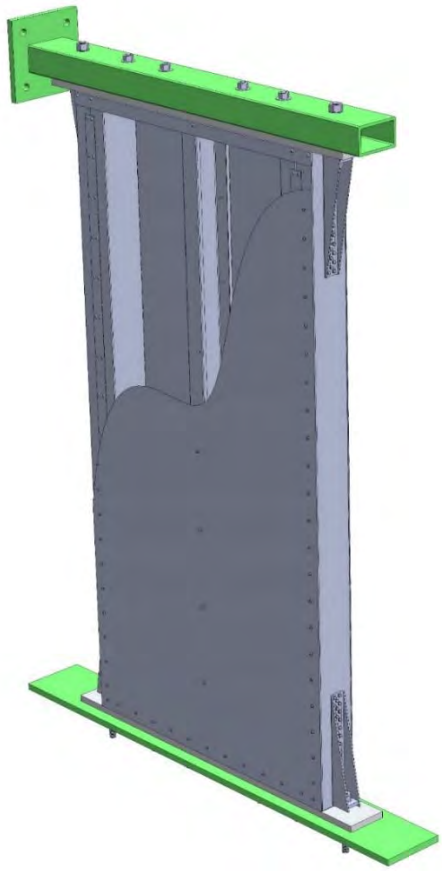

Figure 2.2. Double-sheathed configuration (front sheathing partially removed in drawing)

- The second configuration comprised a single piece of sheathing placed along the mid-line of the wall. This steel sheet was sandwiched by built-up vertical studs on each face of the sheathing and horizontal members located at the base and top of the wall (Figure 2.3). The concept was to have symmetric loading on the framing members and to confine the sheathing such that it could not disengage from the screws. The central stud was excluded from this configuration since the out-of-plane forces due to shear buckling of the sheathing would damage it. Consequently, the top horizontal member is required to act as a beam transferring any point loads originating from upper floor or roof framing members into the chord studs.

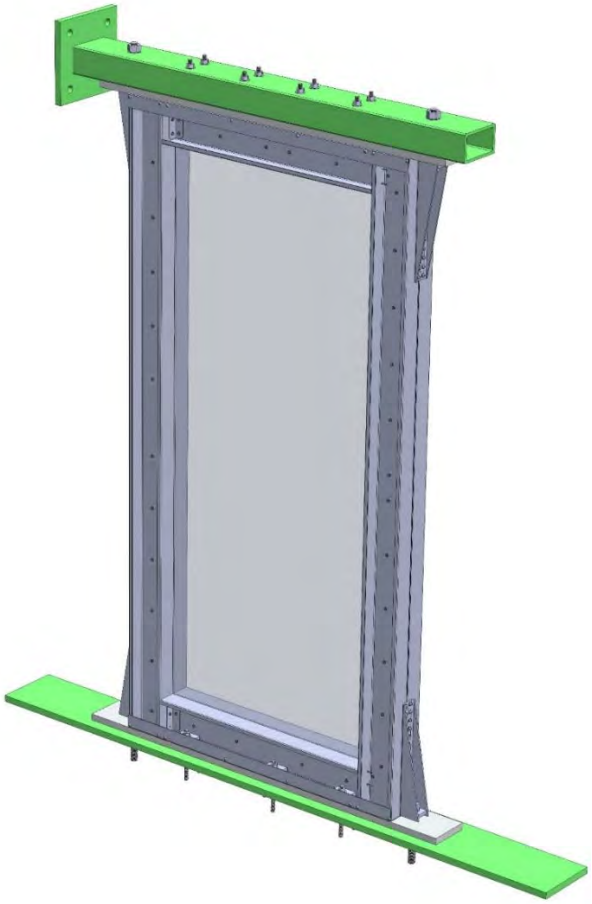

Figure 2.3. Regular centre-sheathed configuration (sheathing transparent in drawing)

2.2.2 Predictions and numerical model

Once the conceptual configurations were chosen, numerical analysis had to be carried out in order to determine the specific member sizes. Indeed, the higher resistance expected from the sheathing placement and screw size / pattern would impose higher forces in the studs; therefore, members of greater resistance were required. Furthermore, given the extent of the anticipated tension field force, it was necessary to consider combined axial and flexural loading on these framing members.

Since the two proposed configurations had never been previously tested, it was necessary to rely on existing design methods, valid for standard cold-formed steel shear walls, to predict the forces expected in the framing members. The Effective Strip Method presented by Yanagi and Yu *(2014)*, which also is found in AISI S400 *(AISI, 2015)*, was developed for walls such as those presented in

Rizk *(2017)*. The method assumes that lateral forces applied to the wall are carried by a partial width of the sheathing, also called the tension field. It had been calibrated using the experimental data of 70 monotonic and 72 cyclic full-scale tests of cold-formed steel sheathed shear walls from Yu *(2010)*, Yu and Chen *(2011)* and Balh *(2010)*. These tests covered different wall building parameters having single-sided sheathing, using various framing thickness, sheathing thickness, fastener spacing and wall aspect ratio, all varying within specified ranges. The Effective Strip Method is currently available for designers in the AISI S400 Standard but its application is only permitted in the United States and Mexico.

An adaptation of this method, using strips to represent the tension field of the wall, was used to develop a SAP2000 model in order to perform the structural analysis of the test specimens. Although the new construction details and wall parameters are different from those for which this method had been developed, the Effective Strip Method was used in its original form to predict the strength and member forces of the first walls included in the research program described herein.

2.2.2.1 The Effective Strip Method for CFS sheathed shear walls

This Effective Strip Method consists of determining the width of the tension field as well as the force that develops in the wall sheathing under lateral loading. This information is based on the parameters of the wall, which comprises the thicknesses of the framing members and sheathing as well as their tensile strengths, the spacing of the sheathing fasteners and their capacity, and the aspect ratio of the wall. This analytical model was developed for cold-formed steel framed shear walls sheathed with cold-formed steel sheathing in order to predict their nominal strength. The Effective Strip Method is an alternative to full-scale shear wall tests to determine the strength of a specific cold-formed steel sheathed shear wall. Thus, the intent is to allow engineers to determine the shear resistance for wall exhibiting building parameters that have not been tested. Although the parameters of the walls may vary, their construction should remain similar to the walls listed in the AISI S400 provisions as described below and as illustrated in Figure 2.4:

- The sheathing is fastened on one face of the frame only, using self-drilling screws all around the boundary elements (tracks at top and bottom and chord studs on the sides). Fasteners are also used to connect the sheathing to the field stud (or interior stud) running at mid-width of the specimen.
- Chord studs are built-up members made of two studs fastened back-to-back. The sheathing is fastened to the flanges located on the outside of the frame.
- Holdown anchors are attached to the chord studs at top and bottom in order to resist overturning forces.

When a lateral load is applied at the top of the shear wall, it is transferred diagonally through the tension field. This tension force finds its equilibrium through the shear capacity of the fasteners as shown in Figure 2.5.

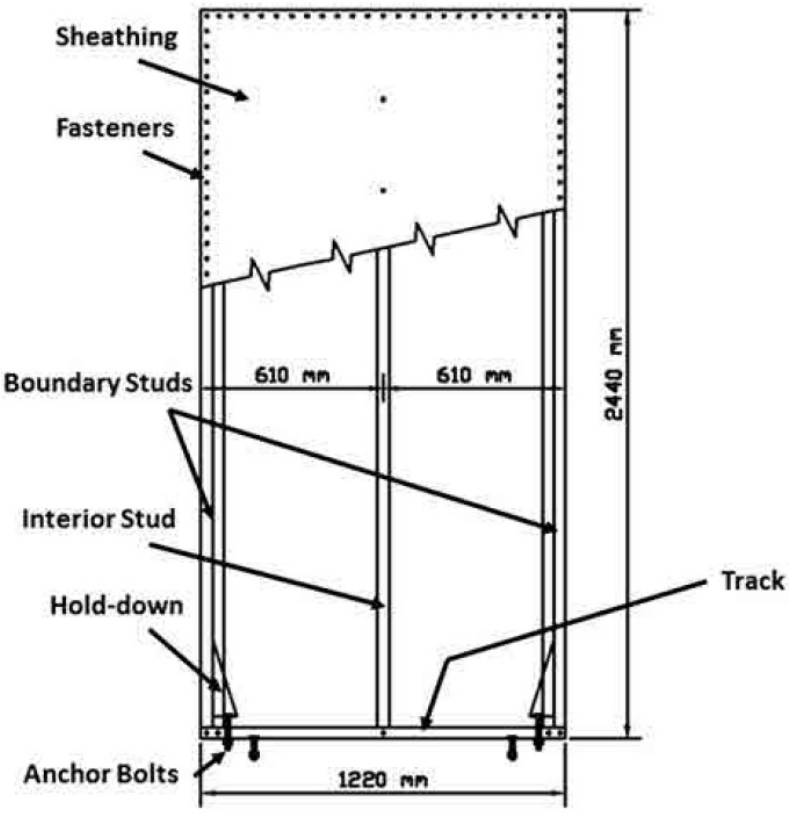

Figure 2.4 Typical CFS shear wall for the Effective Strip Method by Yanagi and Yu *(2014)*

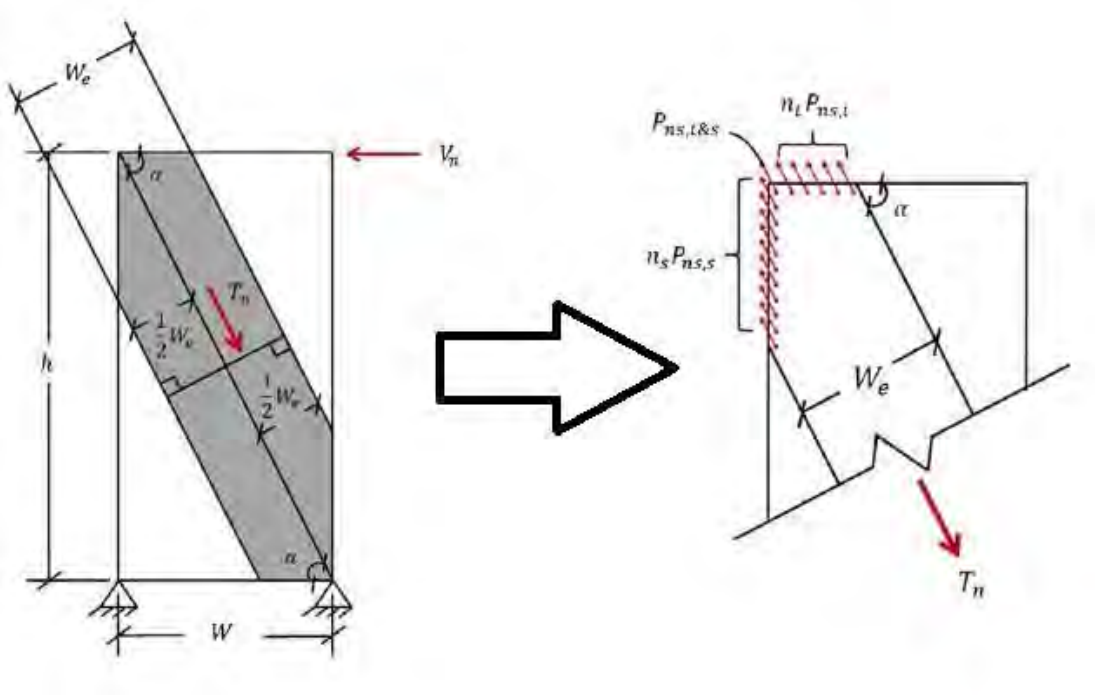

Figure 2.5 Shear force applied and equivalent tension force in the sheathing by Yanagi and Yu *(2014)*

Knowing the spacing of the fasteners, their shear capacity (provided by the manufacturer), the thicknesses of the elements composing the wall and the strengths of the material used, λ and ρ can be defined using Equation 2.3 and 2.2, respectively. Equation 2.1 provides the effective strip (tension field) width (W_e) of the steel sheet sheathing.

$$W_e = \begin{cases} W_{max}, & if\ \lambda \leq 0.0819 \\ \rho W_{max}, & if\ \lambda > 0.0819 \end{cases} \quad \text{Eq. 2.1}$$

$$\rho = \frac{1-0.55(\lambda-0.08)^{0.12}}{\lambda^{0.12}} \quad \text{Eq. 2.2}$$

$$\lambda = 1.736\frac{\alpha_1\alpha_2}{\beta_1\beta_2\beta_3^2 a} \quad \text{Eq. 2.3}$$

Where W_{max} = maximum width of effective strip as illustrated in Figure 2.6, $W_{max} = W/\sin(\alpha)$. The coefficients $\alpha_1, \alpha_2, \beta_1, \beta_2, \beta_3$ and a depend on the tensile strength of the sheathing, the tensile strength of the framing, the thickness of the sheathing, the thickness of the framing, the spacing of the fasteners on the panel edges and the aspect ratio of the wall, respectively.

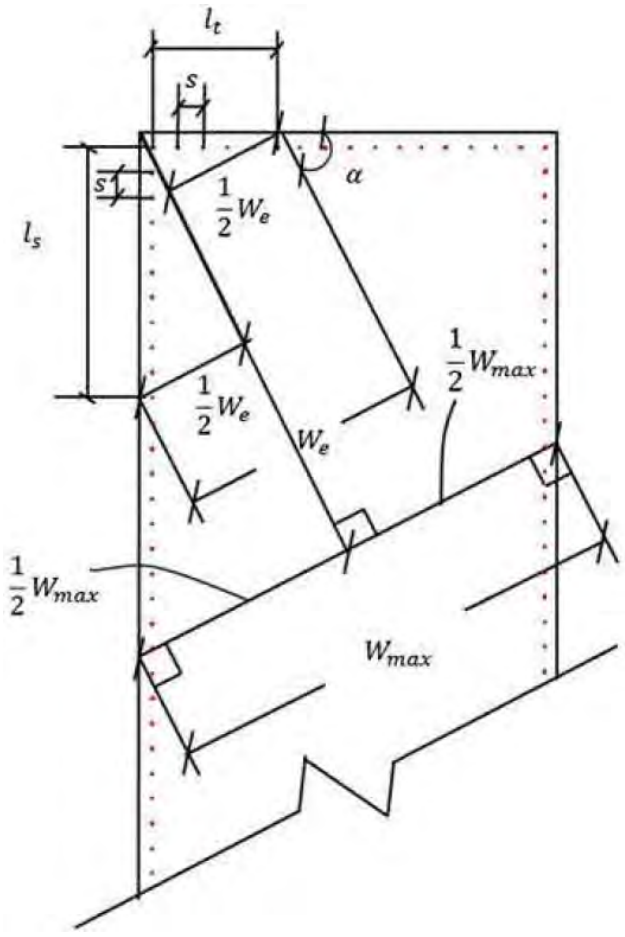

Figure 2.6 Sheathing-to-framing fastener connection layout and maximum width of the effective strip by Yanagi and Yu *(2014)*

Ultimately, the design shear for a specific wall using this method is given by:

$$V_n = min\left[\left(\frac{W_e}{2s\sin\alpha}P_{ns,t} + \frac{W_e}{2s\cos\alpha}P_{ns,s} + P_{ns,t\&s}\right) \times \cos\alpha\,, W_e t F_y \cos\alpha\right] \quad \text{Eq. 2.4}$$

Where P_{ns} represents an individual screw connection's capacity for tilting and bearing at the tracks ($P_{ns,t}$), the studs ($P_{ns,s}$), as well as in the corner of the wall ($P_{ns,t\&s}$) (Figure 2.5). P_{ns} is taken as the smallest value between the shear strength of the screw provided by the manufacturer and the shear strength of the screw limited by tilting and bearing determined as per section J4.3.1 of AISI S100 *(AISI, 2016)*.

This nominal shear strength as calculated using the Effective Strip Method is important since it is the input shear flow for the numerical model that was used to determine the forces in the framing

members of the test walls (Section 2.2.2.2). The section sizes were chosen based on these member forces. Further details and sample calculations using the Effective Strip Method can be found in Appendix C.

It is important to understand the scope of application of this method, which is based on the calibration approach that was used by Yanagi and Yu. As specified earlier, the various parameters for the configurations used for calibration are defined within specified ranges:

- Framing thickness: from 0.84 mm (0.033”) to 1.37 mm (0.054”);
- Sheathing thickness: from 0.46 mm (0.018”) to 0.84 mm (0.033”);
- Fastener spacing: from 51 mm (2”) to 152 mm (6”);
- Wall aspect ratio: from 1:1 to 4:1;
- Sheathing screws are to be minimum No. 8;
- Yield stress of the sheathing shall not exceed 345 MPa (50 ksi).

As a result, the AISI S400 Standard currently permits the use of this method only for walls with parameters fitting the specified ranges used for the calibration. Further, it is applicable to determine the ultimate shear resistance of a shear wall, which is used for design in the US and Mexico. However, it does not provide the shear resistance value as determined per the Equivalent Energy Elastic Plastic (EEEP) method of data analysis. The EEEP method was used to develop the tabulated shear resistance values in AISI S400 for shear wall design in Canada.

2.2.2.2 Numerical model in SAP2000

In order to incorporate the Effective Strip Method into a numerical model, adaptations had to be made. As the nominal shear strength applied to the wall is transferred to the tension field through the multiple sheathing screw connections located within this same tension field, it appeared logical to divide the latter into several strips of which the number, and therefore the width, was defined based on the screw spacing of the corresponding specimen. Thus, each strip of sheathing acted independently from the other and could easily be modelled in SAP2000 (Figure 2.7).

Consequently, the model is composed of the frame as well as the strips accounting for the material located within the tension field. In order to represent the few screw connections between the different framing members, the modeled framing elements are all pin connected to each other and the bottom corners are simply supported (Figure 2.7c.). The number of strips used is based on the number of sheathing connections on the chord stud, located within the tension field (Figure 2.7a.). As the wall aspect ratio was 2:1, the horizontal edges of the walls contain fewer screws located inside the tension field. To this end, the spacing of the joints on the horizontal edges of the numerical model was divided by two to account for the 2:1 aspect ratio of the wall and to match the joints located on the chord stud with the regular screw spacing of the specimen (Figure 2.7b. and c.).Thus, for *n* chord stud sheathing screws located within the tension field, equations 2.5 to 2.7 were obtained:

$$n_s = 2n + 1 \qquad \text{Eq. 2.5}$$

$$w_s = {W_e}/{n_s} \qquad \text{Eq. 2.6}$$

$$A_s = w_s t_{sh} \qquad \text{Eq. 2.7}$$

where,

n_s = Number of strips for the numerical model;

w_s = Width of a strip for the numerical model;

W_e = Width of the tension field (as per Equation 2.1);

A_s = Cross-sectional area of a strip;

t_{sh} = Thickness of the sheathing panel.

The strips are pin connected at both their extremities in the numerical model (Figure 2.7c).

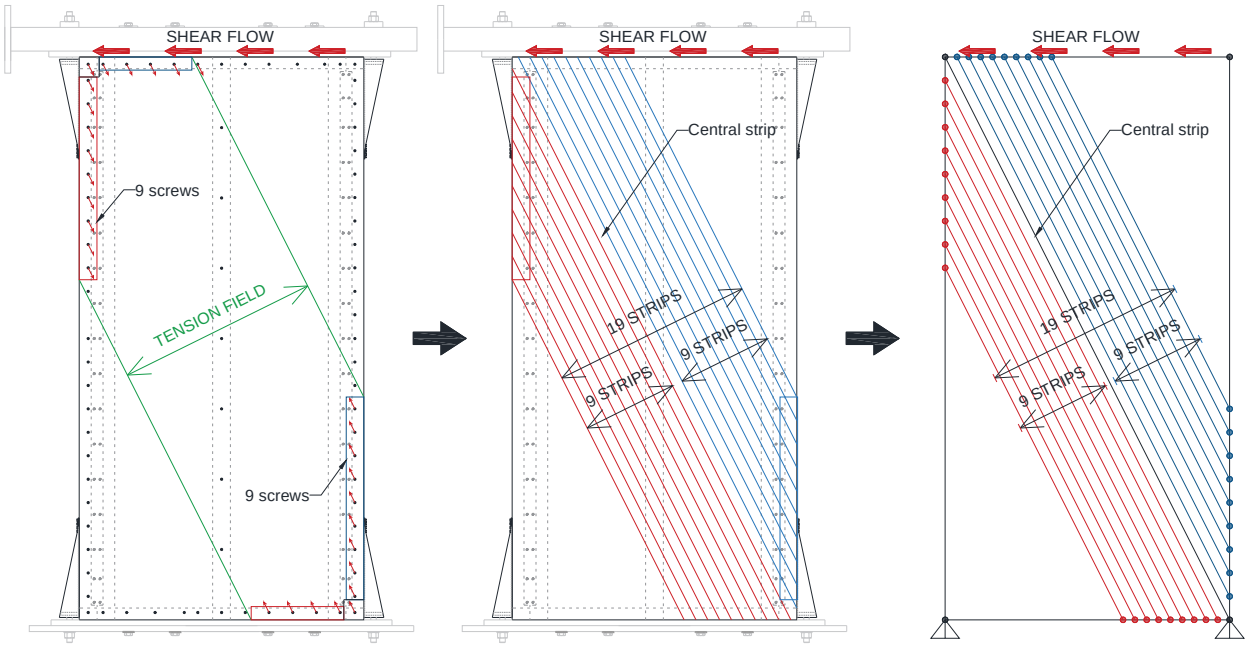

a. b. c.

Figure 2.7 From experimental specimen to numerical model: a. screws located within the tension field, b. equivalent strips attributed to the screw connections and c. equivalent frame elements for the numerical model in SAP2000

Once modelled, section properties needed to be attributed to the corresponding frame elements in the model. The sections were created in SAP2000, using the cold-formed steel sections available in the software, if they corresponded to those being considered for the wall in question. When the sections were not included in the software, a regular section was selected and modification factors were applied to define the section. Thus, creating the built-up section on CFS Software made it possible to find the section properties (gross properties) of the built-up section (Moment of inertias and Area) and set the modification factors on SAP2000 in order to transform the regular section into a built-up section with its corresponding properties. The strips were defined as flat elements using the Section Designer of SAP2000 in order to create custom elements according to the dimensions found when defining the number of strips for the given tension field width and the thickness of the sheathing (Equations 2.5, 2.6 and 2.7).

A load case corresponding to the shear flow applied at the top of the test wall was created in SAP2000, selecting a non-linear analysis type and taking into consideration the P-Delta effect for the geometric non-linearity parameters. A frame distributed load corresponding to the shear strength of the wall found with Equation 2.4 was eventually applied to the top track of the frame with respect to its long axis (horizontal axis). This load was then assigned to the shear flow load case, and the analysis was run for the model (Figure 2.8 shows the model before analysis and its deformed shape after analysis). The analysis provided the forces on the chord studs (Figure 2.9), values that were then used in comparison with the AISI S100 (CSA S136 *(CSA, 2012)*) predicted factored resistance using the CFS Software "Member check", after inputting the length of the member, its support conditions as well as the forces it was withstanding.

Selecting the 2012 NAS – Canada (LSD) specification in the software, the "Member check" consisted of evaluating two load combinations from the CSA S136 Standard: combined bending and shear (Equation 2.8) as well as combined compressive axial load and bending (Equations 2.9 and 2.10), following the LSD method. The chord stud was considered adequate if the interaction equations were satisfied.

$$\sqrt{\left(\frac{M_f}{\phi_b M_{nxo}}\right)^2 + \left(\frac{V_f}{\phi_v V_n}\right)^2} \leq 1.0 \qquad \text{Eq. 2.8}$$

$$\frac{P_f}{\phi_c P_n} + \frac{C_{mx} M_{fx}}{\phi_b M_{nx} \alpha_x} + \frac{C_{my} M_{fy}}{\phi_b M_{ny} \alpha_y} \leq 1.0 \qquad \text{Eq. 2.9}$$

$$\frac{P_f}{\phi_c P_{no}} + \frac{M_{fx}}{\phi_b M_{nx}} + \frac{M_{fy}}{\phi_b M_{ny}} \leq 1.0 \qquad \text{Eq. 2.10}$$

where,

$M_f =$ Required flexural strength;

$M_{nxo} =$ Nominal flexural strength about centroidal x-axis;

$V_f =$ Required shear strength;

$V_n =$ Nominal shear strength;

$\phi_b =$ Resistance factor for flexural strength ($\phi_b = 0.90$);

$\phi_v =$ Resistance factor for shear strength ($\phi_v = 0.80$);

ϕ_c = Resistance factor for compressive strength ($\phi_c = 0.80$);

P_f = Required compressive axial strength;

P_n = Nominal axial strength;

P_{no} = Nominal axial strength (determined with $F_n = F_y$);

M_{fx}, M_{fy} = Required flexural strength with respect to centroidal axes;

M_{nx}, M_{ny} = Nominal flexural strength about centroidal axes;

C_{mx}, C_{my} = 1.0, unrestrained members considered (conservative);

$\frac{1}{\alpha_x}, \frac{1}{\alpha_y}$ = Magnification factors (Eq. C5.2.2-4, -5, -6, -7 of CSA S136 *(CSA, 2012)*);

V_f, P_f, M_{fx} and M_{fy}, were the input values for the "Member check" procedure in the CFS Software. Further details and sample results of the member design are presented in Appendix C.

This method was applied for the centre-sheathed and double-sheathed configurations going from smaller to bigger sections until eventually finding the one that would, according to the analysis and design resistance calculations, be strong enough to keep the chord studs from failing (built-up members to be described in Section 2.5).

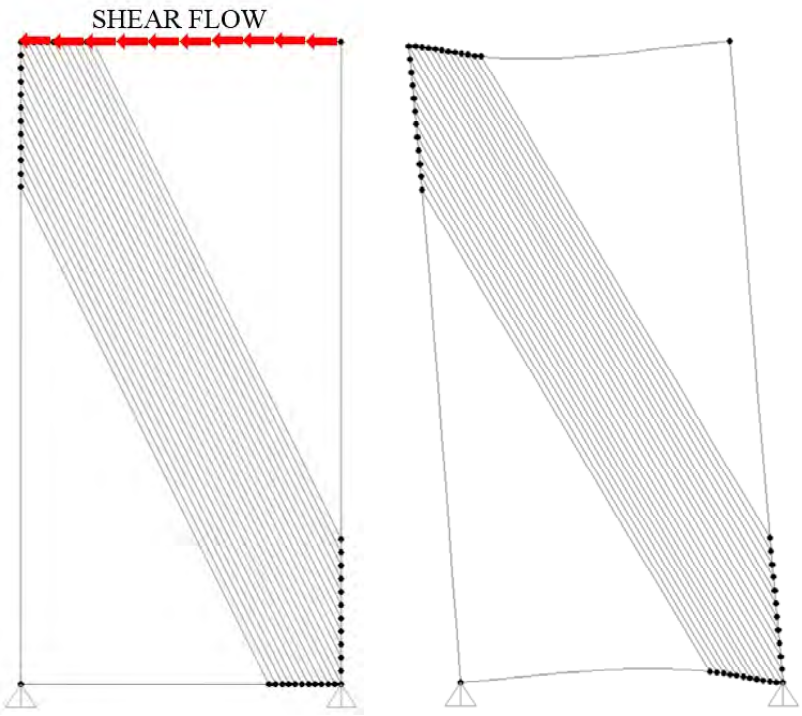

a. b.

Figure 2.8 Numerical model in SAP2000 of specimen W28: a. shear flow applied to the top horizontal member and b. deformed shape of the model after analysis

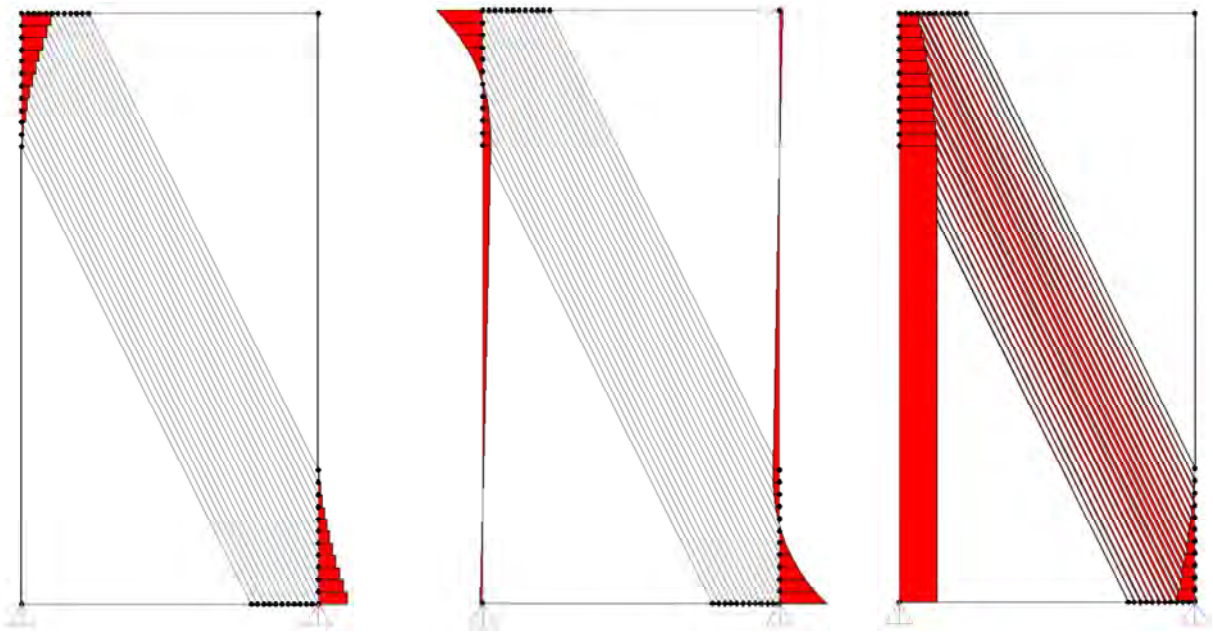

a. b. c.

Figure 2.9. Forces in members of specimen W28 from SAP2000 structural analysis: a. shear forces, b. bending moments and c. axial forces

2.2.3 Observations related to the use of the Effective Strip Method

The behaviour exhibited by the specimens built with the centre-sheathed configuration differed from that observed for the standard cold-formed steel-sheathed shear walls and the double-sheathed shear walls tested beforehand. The resistance achieved in the first centre-sheathed test (W17-M) was much higher than anticipated, which caused the frame members to fail before reaching the maximum potential of the sheathing (details provided in Chapters 3 and 4). The Effective Strip Method as provided in AISI S400 was found to be not adequate for the centre-sheathed configuration. That is, it under predicted the width of and the force in the tension field for these walls, which were composed of much stiffer framing members compared with the walls used by Yanagi and Yu *(2014)* in the calibration process. Hence, the chord studs of the centre-sheathed walls needed to be reinforced due to the greater forces. Since it was impossible to predict accurately the resistance of the walls using the existing Effective Strip Method, another approach needed to be found to determine the expected forces for the next centre-sheathed wall building parameters to be tested.

The first approach consisted of taking the maximum horizontal force measured during the previous test as the input value for the shear flow in SAP2000 to be applied on a wall with the same building parameters. Thus, higher forces on the chord studs were determined, which could be designed accordingly. Reinforced chord studs resulted from this analysis and were installed on the next specimen to be tested, using the same parameters in terms of sheathing thicknesses and screw spacing. However, when testing this new specimen using reinforced chord studs, higher forces were again reached, causing the frame to fail again, prior to maximising the capacity of the sheathing and its connections.

The second approach was based on the observations of the sheathing damage after a test; the tension field was measured to be wider than that predicted using the Effective Strip Method for the same building parameters. Therefore, it was decided to set the width of the tension field based on these observations, counting the screw connections where steel bearing was observed on the sheathing to define a new tension field width to use in the SAP2000 model (Figure 2.10). This led to another level of reinforcement, allowing for greater lateral force to be reached, thus higher forces in the chord studs.

Although this force was taken into account in the design of the chord studs, it still was lower than that possible when the chord studs remained essentially elastic and the sheathing's resistance was maximised. The subsequent post-test observations of the sheathing showed that nearly all the screws going through the sheathing participated in carrying load since steel bearing failure could be observed at all fastener locations (Figure 2.10 shows the evolution in terms of width of the tension field).

A final chord stud design was carried out assuming the full width of the sheathing participated in carrying forces and using the cold-formed steel bolt bearing strength for an inside sheet of a double shear connection from Section J3.3.1 of AISI S100 *(AISI, 2016)* as the screw fastener's nominal bearing capacity (Equation 2.11). The sheathing being confined within two outer studs, the connection was closer in terms of behaviour to this double shear bolt connection than to the regular two-ply screw connection used in the original method. Note, this double shear bolt connection considered the sheathing as the only possible failing element of the connection system. However, given the size of the screws used and the greater thickness of the framing members, the shear capacity limited by tilting and bearing of the screws (Equation 2.12), determined as per Section J4.3.1 of AISI S100 *(AISI, 2016)*, was found to provide a lower resistance. The use of the double shear bolt connection bearing resistance for the screw connections in the centre-sheathed wall allowed for an increase of 48% in the nominal capacity compared with what would normally be used in design.

$$P_{nb} = Cm_f dt_{sh} F_{ush} \qquad \text{Eq. 2.11}$$

$$P_{nv} = 2.7 t_{sh} d F_{ush} \qquad \text{Eq. 2.12}$$

where,

$C = 3.0$ (ratio of fastener diameter to member thickness for the case where $d/t_{sh} < 10$);

$m_f = 1.33$ (inside sheet of double shear connection using standard holes);

$d =$ Nominal screw diameter;

$t_{sh} =$ Thickness of the sheathing panel;

$F_{ush} =$ Tensile strength of the sheathing panel.

This final wall configuration is that described in Section 2.5.2. The drawings and photographs of the different levels of reinforcement for the centre-sheathed specimens are presented in Appendix B.

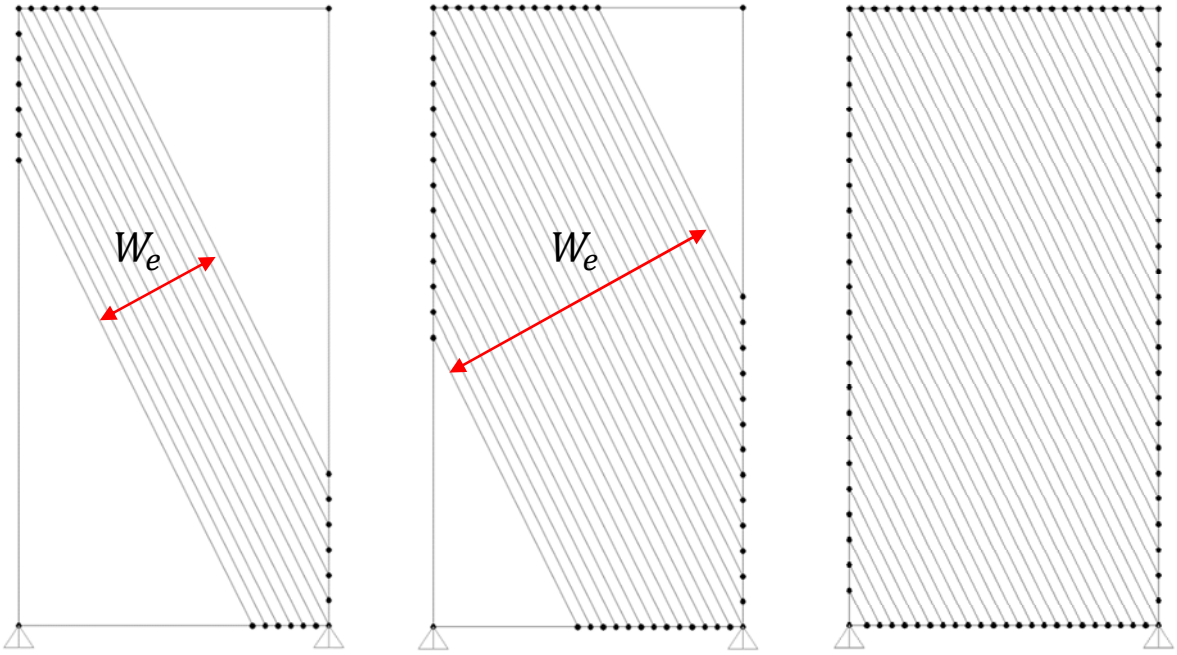

a. b. c.

Figure 2.10 Evolution of the Effective Strip Method: a. initial strip method, b. second estimate based on observations and c. final estimate of the tension field width

2.3 Description of the Shear Wall Test Apparatus

The self-reacting test apparatus (Figure 2.11) used to realize all the CFS framed shear wall experimental programs at McGill University is composed of a 250 kN MTS 244 Series hydraulic actuator for dynamic loading with a stroke length of 10” (254.0 mm). The 250 kN load cell is an MTS 661 Series High Capacity Force Transducer specifically designed for cyclic and monotonic testing applications. The loads are transferred to the wall through a loading beam built using a 25.4 mm-thick (1”) 304.8×304.8 mm (12”×12”) steel plate welded to a 10 mm-thick (0.4”) 152.4×101.6 mm (6”×4”) steel HSS (see photographs in Appendix B). The braces are used as lateral supports for the wall in order to keep the displacements in the plane of the wall. They are made of pairs of HSS (one in front, one in the back) attached at top and bottom of the frame. Two of those braces were utilized to keep the wall straight during the tests using Teflon elements meant to slide on

each side of the loading beam. All the details regarding the properties of the test frame and its design can be found in Zhao *(2002)*. Figure 2.12 shows the shear wall test setup with specimen installed.

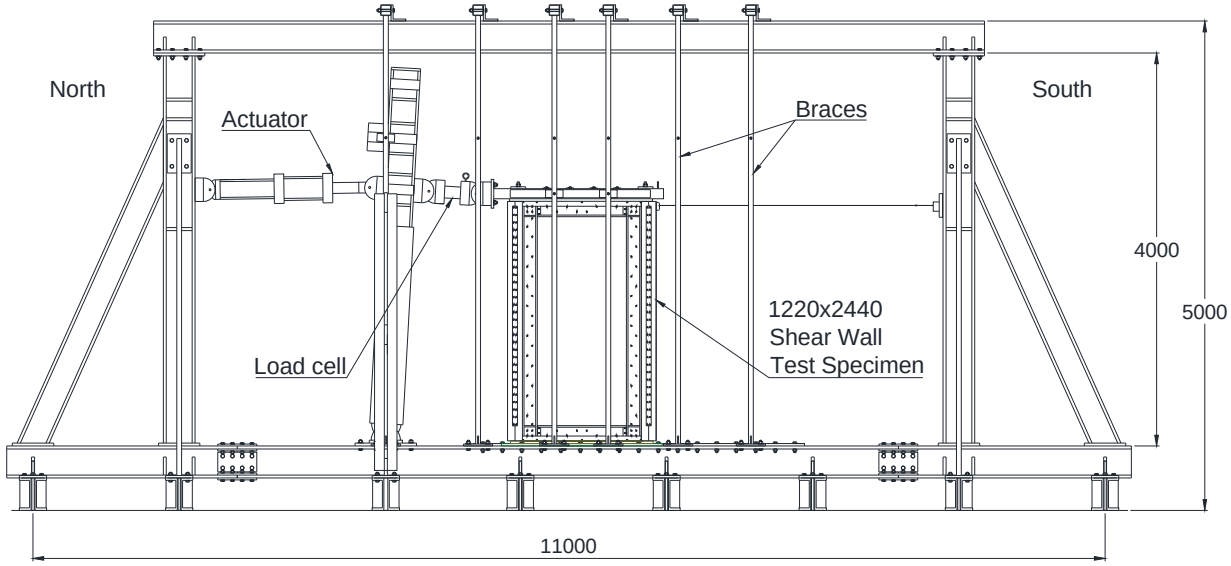

Figure 2.11 Test frame and a shear wall test specimen

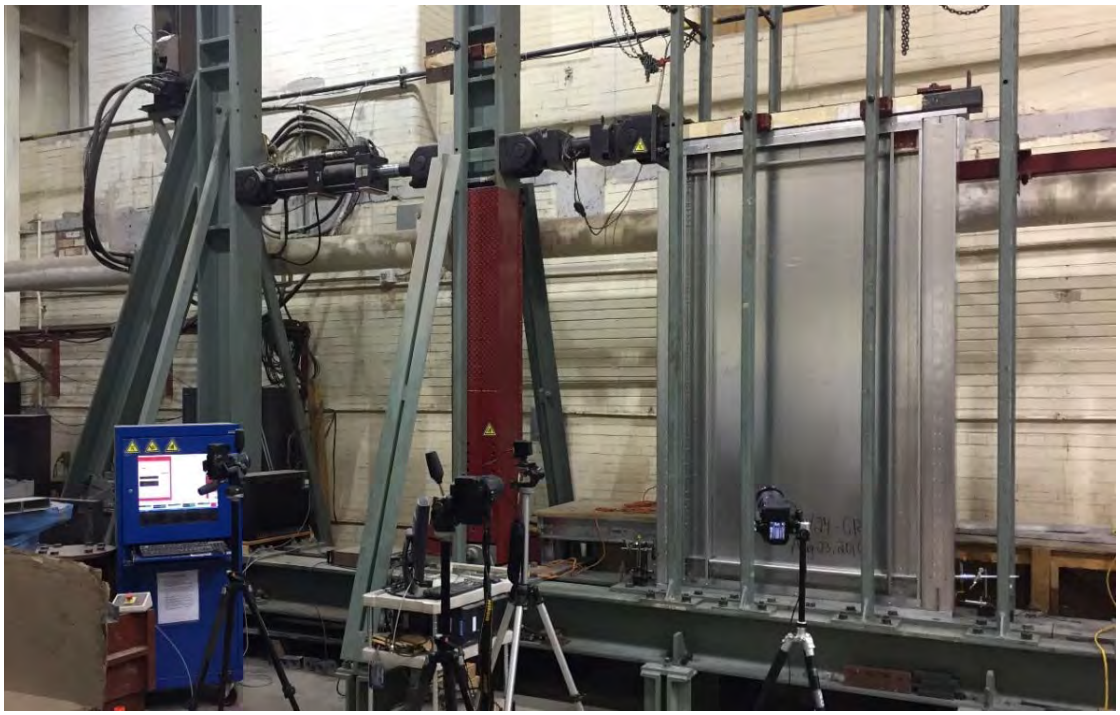

Figure 2.12 Complete shear wall test setup

2.4 Cold-Formed Steel Sheathed Shear Walls Testing Program

As presented in Section 2.2.1, two distinct wall configurations were tested during this experimental program, which were both of the same general construction: i.e. cold-formed steel sheathing screw connected to a cold-formed steel frame. Each configuration was tested using several building parameters, presented in Table 2.1, where the thickness of the sheathing, the spacing as well as the size of the screw connections would vary. Two different frame thicknesses were used for the double-sheathed walls, whereas only the thickest framing sections were used for the centre-sheathed specimens. Although the specimens using the double-sheathed configuration behaved as expected, this was not the case for the specimens using the centre-sheathed configuration. Indeed, different chord stud reinforcement schemes had to be introduced in order to prevent the failure of the framing as the test program progressed from one wall to the next. The reinforcement schemes are represented by _R, _R2 and _R3 in the last column of Table 2.1, _R being the first reinforcement scheme and _R3 the last, which was found to be adequate. Four reversed cyclic tests (W15B-CR3, W23B-CR3, W25-CR3 and W26-CR3) have been carried out with an asymmetric protocol (described in Section 2.7.2) allowing for the capture of the post-peak behaviour of these specific wall configurations. The aspect ratio was the same for all the specimens tested in this program; a width-to-height ratio of 1:2, i.e. 1220×2440 mm (4'×8') specimens, excluding the additional chord stud reinforcement. This report presents half of the specimens tested ([3] in Table 2.1), while the other half is presented in Santos *(2017)*. A detailed description of all the wall parameters tested for this report can be found in Appendix A.

Table 2.1. Sheathed shear wall test program: list of shear wall configurations

Test ID	Sheathing thickness mm (in)	Framing thickness mm (in)	Sheathing screw size (#)	Fastener spacing mm (in)	Type of test[1]
Double-Sheathed Wall Configuration					
W19[4]	2 × 0.36 (0.014)	1.73 (0.068)	10	50 (2)	M & C
W20[4]	2 × 0.36 (0.014)	1.73 (0.068)	10	100 (4)	M & C
W21[4]	2 × 0.36 (0.014)	2.46 (0.097)	10	50 (2)	M & C
W22[4]	2 × 0.36 (0.014)	2.46 (0.097)	10	100 (4)	M & C
W28[3]	2 × 0.47 (0.019)	2.46 (0.097)	10	50 (2)	M & C
W29[3]	2 × 0.47 (0.019)	2.46 (0.097)	10	100 (4)	M & C
W30[3]	2 × 0.47 (0.019)	2.46 (0.097)	12	50 (2)	M & C
W31[3]	2 × 0.47 (0.019)	2.46 (0.097)	12	100 (4)	M & C
Centre-Sheathed Wall Configuration					
W15[4]	0.84 (0.033)	2.46 (0.097)	10	50 (2)	MR3 & CR3
W16[4]	0.84 (0.033)	2.46 (0.097)	10	50 (2)	MR & MR2
W17[4]	0.84 (0.033)	2.46 (0.097)	10	150 (6)	M & C
W18[3]	0.84 (0.033)	2.46 (0.097)	10	100 (4)	M, MR & CR
W23[3]	1.09 (0.043)	2.46 (0.097)	12	100 (4)	CR3
W24[3]	1.09 (0.043)	2.46 (0.097)	12	150 (6)	CR3
W25[2,4]	0.84 (0.033)	2.46 (0.097)	10	100 (4)	CR3
W26[2,3]	1.09 (0.043)	2.46 (0.097)	10	100 (4)	CR3
W15B[2,4]	0.84 (0.033)	2.46 (0.097)	10	50 (2)	CR3
W23B[2,3]	1.09 (0.043)	2.46 (0.097)	12	100 (4)	CR3

[1] M: Monotonic; C: Cyclic; _R, _R2 and _R3: Different frame reinforcement scheme
[2] Asymmetric cyclic test to reach a higher maximum chord rotation
[3] Specimens tested by the author
[4] Specimens tested by Santos *(2017)*

2.5 Description of the Wall Fabrication and Test Setup

As the two general wall configurations were constructed of different materials and different erection methods, they will be presented separately. This section will provide a succinct description of the material and the construction process for both of the configurations.

2.5.1 Double-sheathed configuration

2.5.1.1 Materials

The double-sheathed specimens were composed from a combination of the following:

- Studs: 1.73 mm (0.068”) and 2.46 mm (0.097”) nominal thickness cold-formed steel studs of 345 MPa (50 ksi) strength (ASTM A653 Grade 50 (340)). Nominal dimensions of a single stud are 152.4 mm (6”) web, 76.2 mm (3”) flanges and 15.9 mm (5/8”) lip. The chord studs are built-up members obtained by attaching two single studs facing each other using screw connected cold-formed steel strips as the joint. A simple stud is used as a centre stud (or field stud) (Figure 2.1a).

- Strips: 1.09 mm (0.043”) nominal thickness cold-formed steel strips of 345 MPa (50 ksi) strength (ASTM A653 Grade 50 (340)). 50.8 mm (2”) wide strips connecting the flanges on each side of the built-up chord studs using two No.10 screws (spaced 25.4 mm (1”)) with a 152.4 mm (6”) screw spacing all along the chord stud.

- Tracks: 1.73 mm (0.068”) and 2.46 mm (0.097”) nominal thickness cold-formed steel top and bottom tracks of 345 MPa (50 ksi) strength (ASTM A653 Grade 50 (340)). Nominal dimensions of a single track are 155.0 mm (6.11”) or 156.0 mm (6.15”) web respectively with 50.8 mm (2”) flanges.

- Sheathing: 0.36 mm (0.014”) and 0.47 mm (0.019”) base metal thickness cold-formed steel sheathing of 230 MPa (33 ksi) strength (ASTM A653 Grade 33 (230)). Two sheets of the same thickness are used per specimen, one on each face of the wall.

- Connectors: Simpson Strong-Tie S/HD15S holdowns, attached on the exterior side of the chord studs, two at the top and two at the bottom, with a 10 mm spacing with the top (resp. bottom) of the wall. 33 #14 self-drilling hex-head screws are used to attach each holdown to the wall and a 25.4 mm (1") ASTM A193-B7 threaded rod with ASTM A194-2H nuts and washers to connect each holdown to the test frame.

- Shear connectors: 19.1mm (3/4") ASTM F3125 grade A325 bolts with 152.4x101.6 mm (6"×4") 1" steel plate in the inside of the tracks, to resist the vertical forces caused by the tension field action and to avoid bearing damage to the track members.

- Fasteners: #10 wafer head self-drilling screws for the built-up chord studs and to connect the tracks to the studs. #10 or #12 (depending on the building parameters) pan-head self-drilling screws to attach the sheathing to the frame.

2.5.1.2 Fabrication of the specimens and test setup

To create a built-up box section, two single studs were assembled face-to-face using cold-formed steel strips screw connected along the studs' flanges. Holdowns were installed 10 mm inside the length of the chord in order to avoid contact with the base during high chord rotations. The tracks were drilled prior to their installation to receive four 19.1 mm-diameter (3/4") F3125 grade A325 bolts, then connected to the studs. The rectangular shape of the wall specimen being built was confirmed by measurement of the corner-to-corner diagonals. A field stud was installed at mid-width of the wall (Figure 2.13a). All these connections were realized using #10 self-drilling wafer head screws since the sheathing was placed over top of these fasteners. A sheathing panel was, at that stage, installed on one face of the wall (Figure 2.13b) using #10 or #12 pan head screws (depending on the building parameters of the wall) following the pattern previously marked corresponding to the fastener spacing schedule from Table 2.1. The sheathing screws were placed 38 mm (1-1/2") from the edges of the sheathing. The cold-formed steel sheathing panels were 1220×2440 mm (4'×8') in size, and covered the entire front or back surface of the wall specimen.

Once a sheathing panel had been installed on one side, the wall was placed in the test frame, and then attached to the loading beam and test frame with the shear anchor bolts (Figure 2.14a). After

the wall was anchored into position through proper torqueing of the bolts, the sheathing panel on the other side of the wall was installed (Figure 2.14b). As a last stage for the assembly of a test wall, the anchor rods for the holdowns were installed. Figure 2.15 shows a specimen completely fastened and equipped, ready to be tested. Figures 2.16 and 2.17 show details of the corner of a wall as well as the corresponding cross sections. The complete construction details, including cross-sections and elevation views, can be found in Appendices A and B.

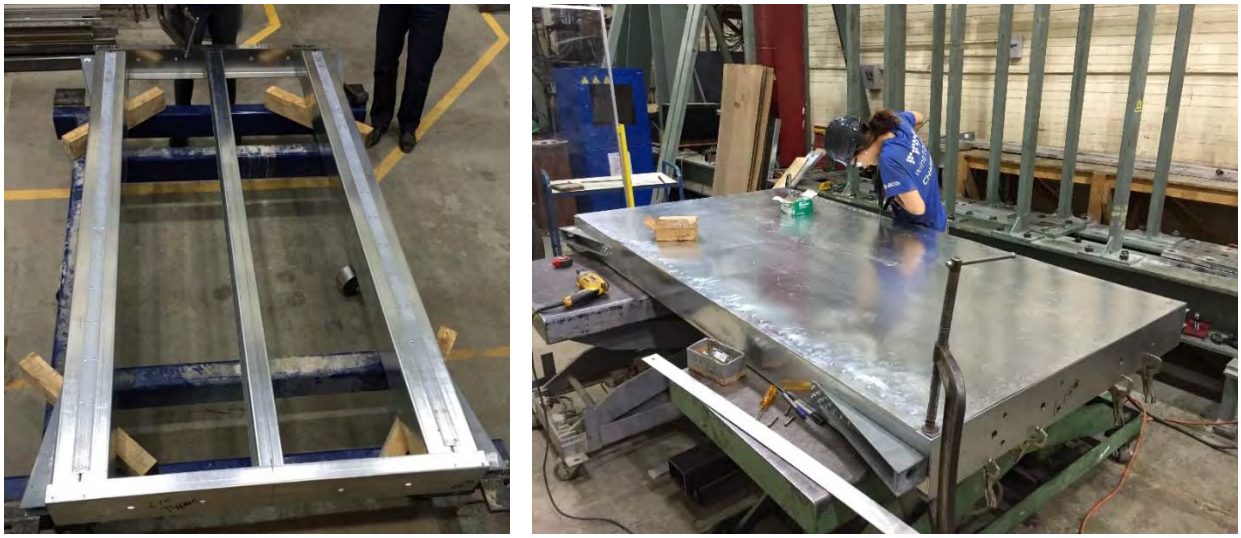

a. b.

Figure 2.13 Double-sheathed configuration: assembly of the framing members, a. chords studs, field stud and tracks, and b. fastening of first sheathing panel

a. b.

Figure 2.14 Double-sheathed configuration: a. specimen fastened to the frame and b. installation of the second sheathing panel

Figure 2.15 Double-sheathed configuration: specimen ready to be tested

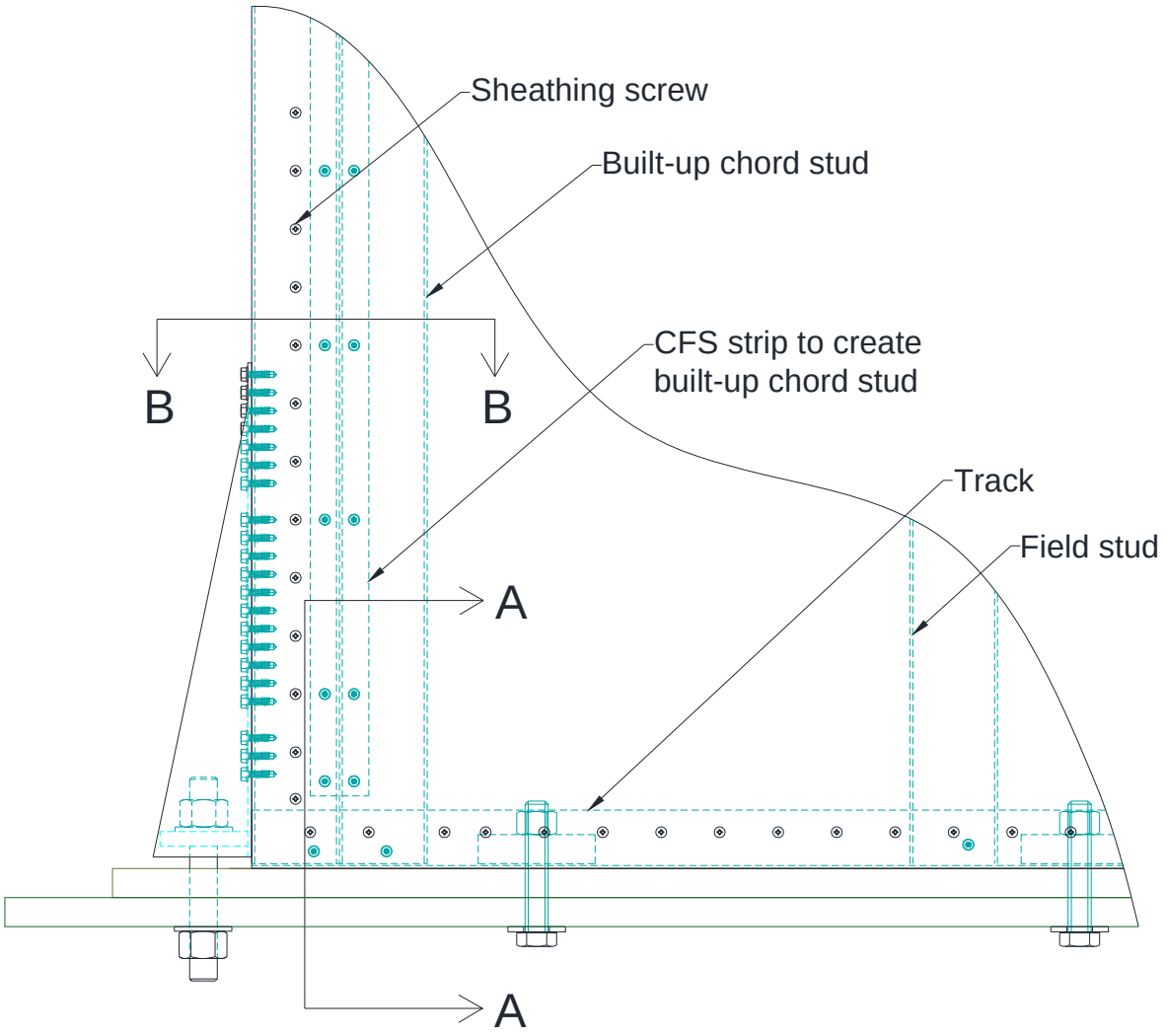

Figure 2.16 Double-sheathed configuration: detailing of the sheathing's screw pattern in the corner (hidden parts in blue)

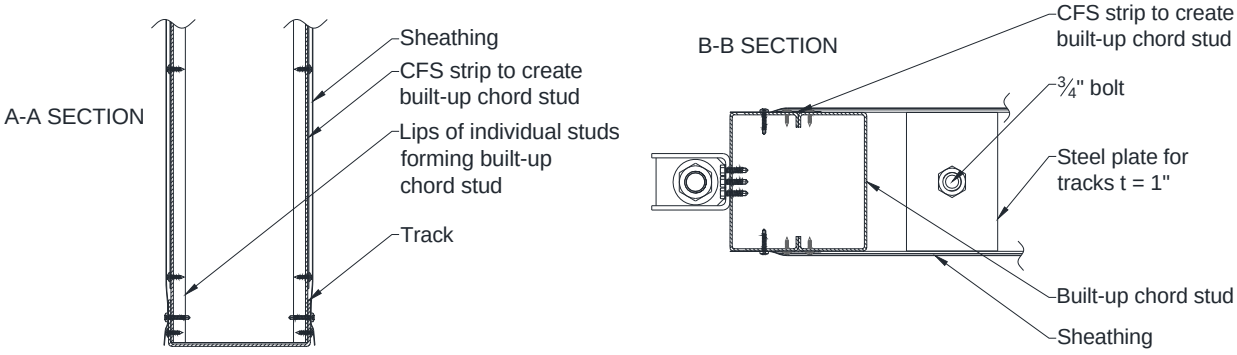

Figure 2.17 Double-sheathed configuration: associated cross-sections

2.5.2 Centre-sheathed configuration

2.5.2.1 Materials

The centre-sheathed specimens were composed from a combination of the following:

- Studs: 2.46 mm (0.097”) nominal thickness and 345 MPa-strength (50 ksi) cold-formed steel studs (ASTM A653 Grade 50 (340)). Nominal dimensions of a single stud are 152.4 mm (6”) web, 76.2 mm (3”) flanges and 15.9 mm (5/8”) lip. The studs are attached back-to-back, “sandwiching” the sheathing, thus creating a built-up member including the sheathing panel. Horizontal pieces at top and bottom of the walls are the same size as the stud members and installed following the same method.

- Tracks: 2.46 mm (0.097”) nominal thickness and 345 MPa (50 ksi) strength cold-formed steel top and bottom tracks (ASTM A653 Grade 50 (340)). Nominal dimensions of a single track are 156.0 mm (6.15”) web and 50.8 mm (2”) flanges.

- Chord Stud Reinforcement: 2.46 mm (0.097”) nominal thickness and 345 MPa (50 ksi) strength cold-formed steel studs (ASTM A653 Grade 50 (340)). Nominal dimensions of a single reinforcing stud are 152.4 mm (6”) web, 76.2 mm (3”) flanges and 15.9 mm (5/8”) lip. Several reinforcement schemes were tested as the test program progressed (see Sections 2.2.3 and 2.5.2.2). Ultimately, the reinforcement scheme found to be adequate for centre-sheathed configuration is a box reinforcement created by attaching two studs facing each other and attached with two screw connected strips linking the flanges of the two studs (built-up member similar to the double-sheathed configuration chord stud members) (Figure 2.22).

- Strips: 1.73 mm (0.068”) nominal thickness cold-formed steel strips of 345 MPa (50 ksi) strength (ASTM A653 Grade 50 (340)). 50.8 mm (2”) wide strips connecting the flanges on each side of the built-up chord stud reinforcement using two No.10 screws (spaced 25.4 mm (1”)) with a 76.2 mm (3”) screw spacing all along the chord stud.

- Sheathing: 0.84 mm (0.033”) and 1.09 mm (0.043”) nominal thickness cold-formed steel sheathing of 230 MPa (33 ksi) strength (ASTM A653 Grade 33 (230)). The sheathing becomes part of the built-up chord studs when building the specimen.

- Stiffeners: 1.73 mm (0.068”) nominal thickness and 345 MPa (50 ksi) strength cold-formed steel pieces 146 mm (5-3/4”) long (ASTM A653 Grade 50 (340)). Nominal dimensions of a stiffener are 152.4 mm (6”) web, 50.8 mm (2”) flanges and 15.9 mm (5/8”) lip.

- Connectors: Simpson Strong-Tie S/HD15S holdown connectors, attached on the interior side of the box reinforcement, two at the top and four at the bottom (when required), with a 10 mm spacing with the top (resp. bottom) of the wall. 33 #14 self-drilling hex-head screws are used to attach each holdown to the wall and a 25.4 mm (1”) ASTM A193-B7 threaded rod with ASTM A194-2H nuts and washers to connect each holdown to the test frame.

- Shear connectors: 12.7 mm (1/2”) ASTM F3125 grade A325 bolts with 76.2x63.5 mm (3”×2-1/2”) 3/4” steel plate inside the horizontal studs.

- Fasteners: #10 or #12 hex-head self-drilling screws to attach the built-up chord studs sandwiching the sheathing. The box reinforcements are attached to the chord studs using #12 hex-head self-drilling screws with two screws every 76.2 mm (3”).

2.5.2.2 Fabrication of the specimens and test setup

The original configuration is composed of built-up chord studs made of two C-shape studs sandwiching the long edges of the sheathing, fully integrating the latter into the built-up member since the sheathing fasteners were the connectors used to create the built-up chord studs. Built-up horizontal framing members similar to the built-up chord studs are used at the top and bottom of the wall in order to sandwich the sheathing around its perimeter. The framing members are placed inside the sheathing’s perimeter, held in position using clamps along their length, to minimize the gap between the sheathing and the studs after creating the built-up member. The studs are marked

on one side following a staggered pattern (see framing members in Figure 2.20) defined in advance and corresponding to the fastener spacing schedule (Table 2.1). This staggered pattern is necessary since these screws fastened the sheathing and also connected the members of the built-up chord stud. The same method is used for the horizontal pieces at top and bottom of the specimen to insure the sheathing is confined between framing members on all of its edges.

The idea of using centre studs was abandoned since their positioning on each side of the sheathing would have caused them to bend globally due to the out-of-plane forces caused by the shear buckling of the sheathing. Besides, as the sheathing was fastened to the horizontal framing members and no longer to the tracks, it was necessary to find a mechanism to transfer the vertical forces through the chord studs. Therefore, connecting the horizontal framing members to the chord studs allowed for them to act as beams transferring the vertical forces from the sheathing or the potential gravity loads to the chord studs, thus taking over from the centre stud's purpose (Figure 2.19). Clip angles are used to make that connection, at the top and bottom of both faces of the specimens, using the corresponding sheathing's screw size (as per Table 2.1) since these fasteners also connect the sheathing to the frame (Figure 2.18). These horizontal framing members have one flange pre-drilled since the shear anchors will be placed through both the track and the horizontal framing members.

Figure 2.18 Connection between horizontal framing and chord stud using clip angles

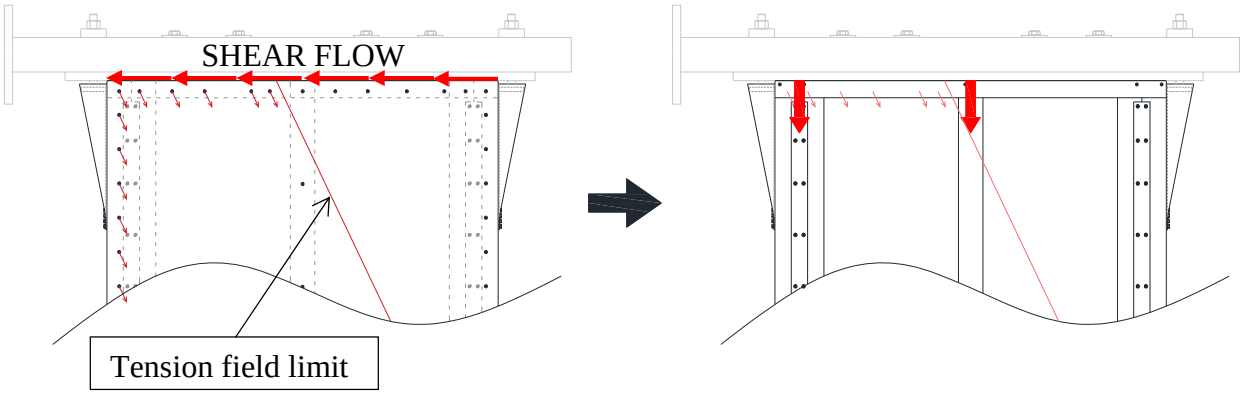

a. Double-sheathed configuration

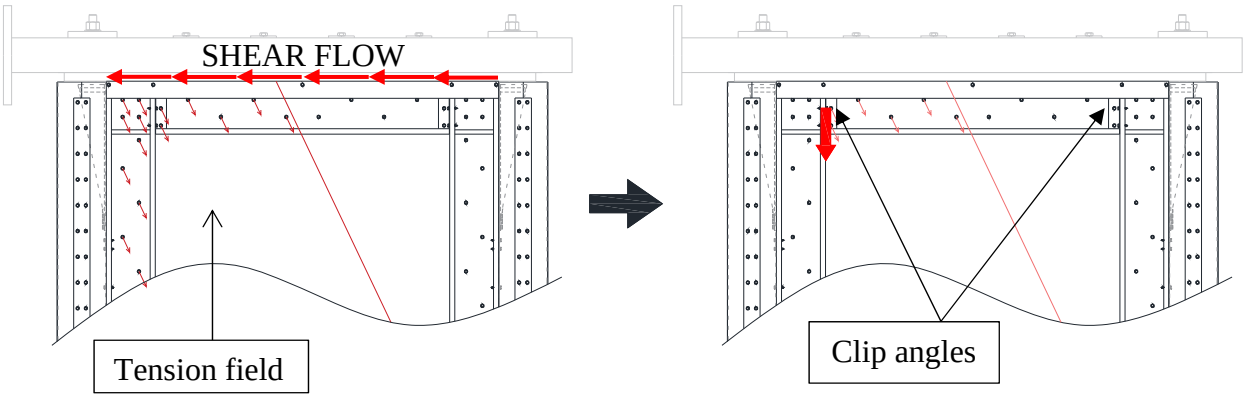

b. Final centre-sheathed configuration

Figure 2.19 Transmission of vertical forces from horizontal framing member to chord studs: a. through contact between the track and chord studs / centre stud and b. through clip angle connections

The holdowns, installed at top and bottom of the wall, required 33 #14 self-drilling screws each. In the original wall configuration the holdowns are installed at the centre section of the wall; thus, their centreline coincided with the sheathing panel. Consequently, the pre-drilled holes on the centreline of the holdowns could not be used; new holes needed to be drilled in the holdowns where space was available. By following this approach all 33 screws could be installed (Figure 2.20).

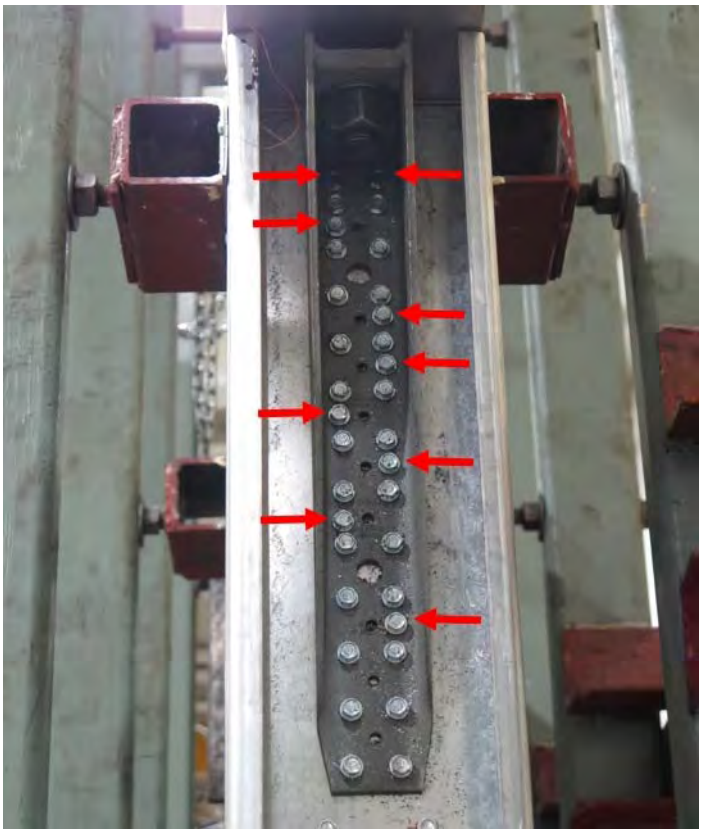

Figure 2.20 Top holdown with nine extra holes outside the centreline of the shear wall

The tracks are installed using 10 #10 self-drilling screws per track (5 per flange), connecting the flanges of the tracks to the lips of the chord studs and horizontal pieces. The tracks are pre-drilled according to a different pattern for the top and the bottom, matching the horizontal framing members' pre-drilled holes. They will both receive 12.7 mm (1/2") diameter bolts, 8 at the top where the shear flow will be applied and 6 at the bottom. The specimen is then placed in the test frame and fastened (shear anchors then holdowns). Figures 2.21 and 2.22 show the cross-sections of the chord studs and horizontal framing members (respectively) sandwiching the sheathing.

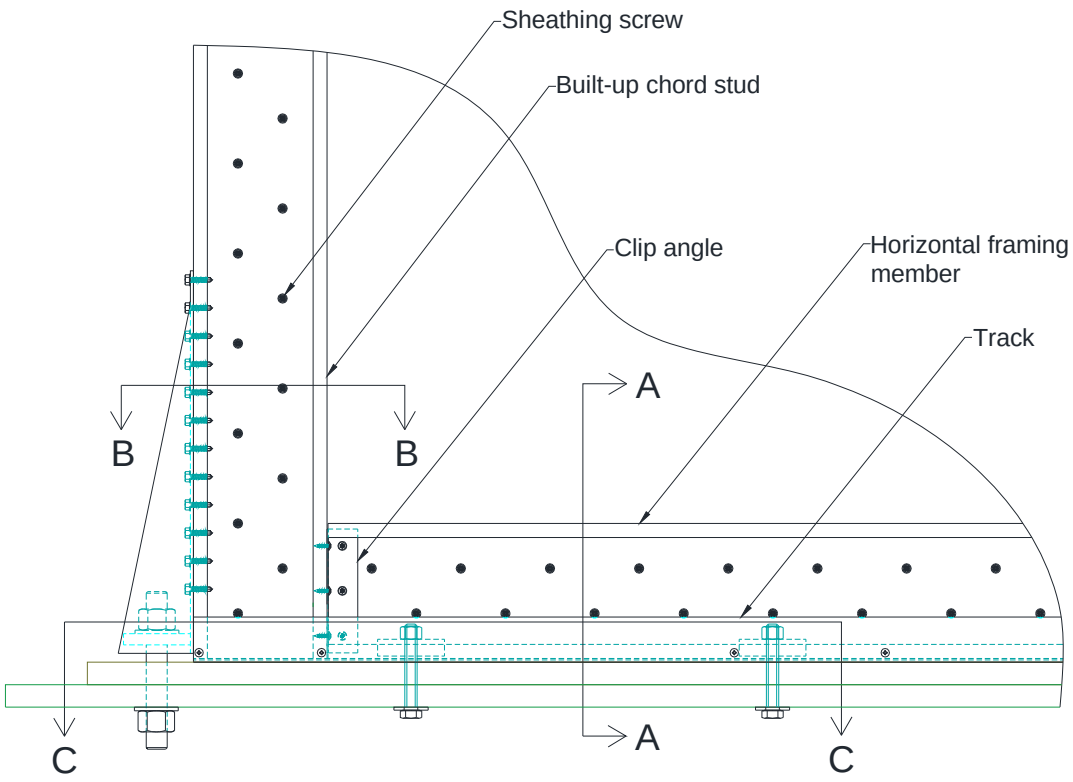

Figure 2.21 Original centre-sheathed configuration: detailing of the sheathing's screw pattern in the corner (hidden parts in blue)

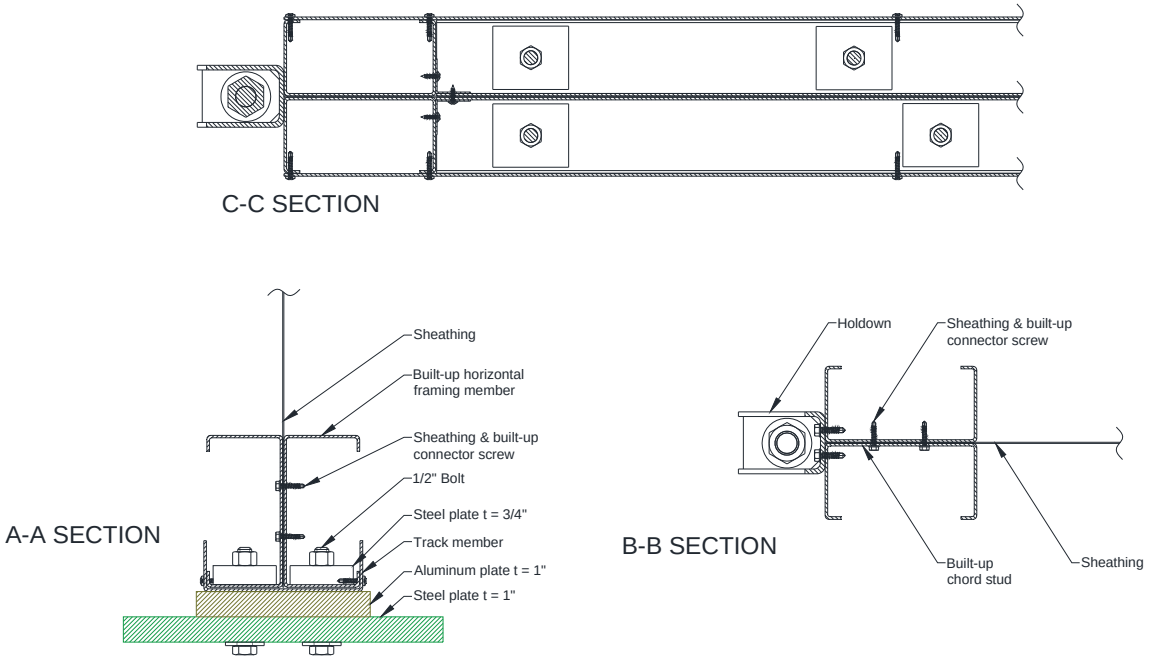

Figure 2.22 Original centre-sheathed configuration: associated cross-sections

The originally constructed centre-sheathed shear wall demonstrated a higher strength than expected, leading to failure of the chord studs. Hence, the original configuration had to be revised, by adding reinforcement to the chord studs. Specific details of the various reinforcement schemes are provided in Section 2.2.3. The construction procedure of the walls had to be modified for the various reinforcement schemes. Appendix A and B contain the details of the final centre-sheathed wall configuration, as well as the evolution of the reinforcement schemes. The final configuration for the reinforced chord studs is composed of a built-up box section, similar to that used for the double-sheathed configuration, attached on the outside of the original chord studs (Figure 2.23).

Since the holdowns were to be attached inside the box reinforcement, each chord stud had to be shifted 2.5 mm inside to accommodate for the extra layer of steel under the holdowns and make them align with the anchor rod holes in the test frame. After putting the corresponding marks on the sheathing, the studs were held in position using clamps and the same construction procedure as for the original configuration was followed for all the framing members. Stiffeners were then needed inside the chord studs at their top and bottom since the horizontal pieces will tend to deform the flanges of the chord studs during the tests at high chord rotations. They were installed on each face of the specimen using four screws identical to the those used for the chord studs and horizontal pieces (i.e. #10 or #12 depending on the test building parameters) since they were going through the sheathing as well (Figures 2.23 and 2.24). The first part of the reinforcement box section could then be installed on the outside of the long edge of the wall using #12 hex head self-drilling screws. Those screws were not installed on the whole length of the reinforcement since the holdowns would be placed at top and bottom of the chord studs, inside the box reinforcement (Figure 2.26a.). Therefore, a pair of screws was placed every 3” (76 mm) along the space between the top and bottom holdowns. Once this part of the reinforcement was fastened, the holdowns were attached to the specimen. Two holdowns, placed side-by-side, were installed at the bottom of the chord studs (Figures 2.23, 2.25a. and 2.26a.) to accommodate for the increased uplift forces; a single holdown was placed at the top of each chord stud as per the original wall configuration (Figures 2.25b. and 2.26a.). The tracks were installed according to the original configuration’s procedure.

The wall was then placed in the test frame and fastened (shear anchors then holdowns (Figure 2.24)). The final step was the completion of the box reinforcement, adding another stud facing the part of the reinforcement already installed, and attached to the latter using the same method as for

the double-sheathed configuration (cold-formed steel strips screw connected to both studs' flanges as per Figure 2.22). However, as the forces reached for this centre-sheathed configuration were significantly higher than for the previous one, it was decided to use two screws every 3" (76 mm) along the length of the whole strip to accommodate for the high shear flow that would run within the connections of the built-up member. Figure 2.25b. shows a specimen built according to the final configuration ready to be tested. All the details including cross-sections and elevation views can be found in Appendices A and B.

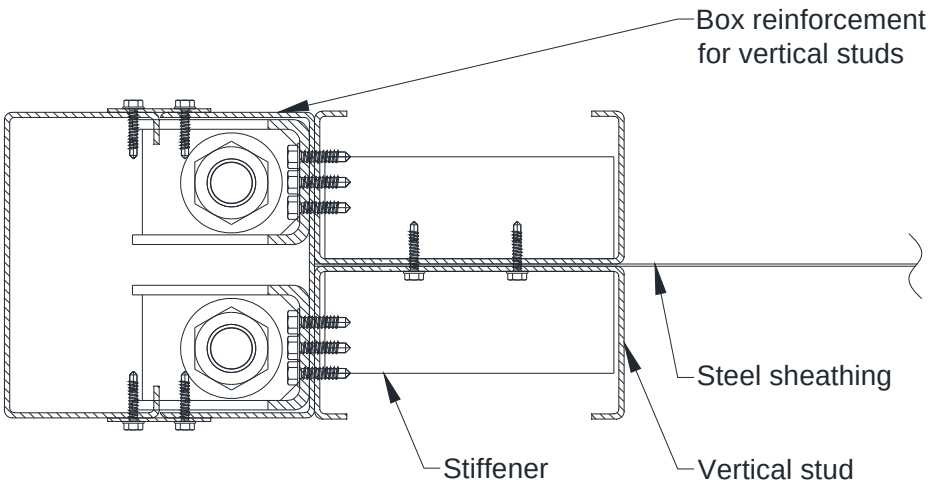

Figure 2.23 Final centre-sheathed configuration: cross-section of a chord stud and its reinforcement

Figure 2.24 Final centre-sheathed configuration: stiffeners added in the corners

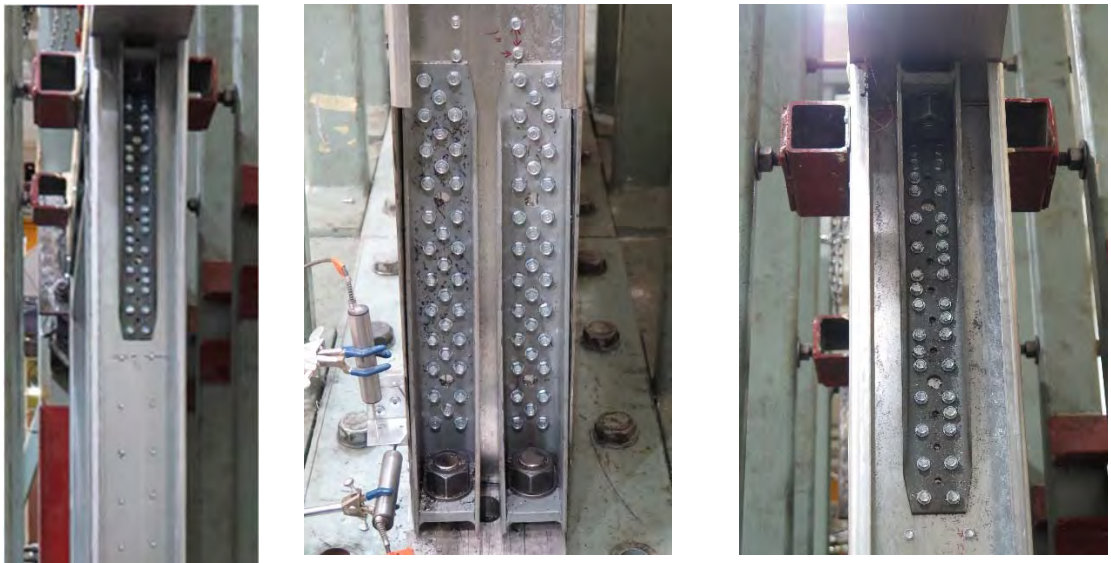

a. Bottom south holdowns b. Top south holdown

Figure 2.25 Final centre-sheathed configuration: Holdowns fastened prior to completion of the chord stud's reinforcement

a. b.

Figure 2.26 Final centre-sheathed configuration: a. before completion of reinforcement and b. after completion: specimen ready to be tested

2.6 Instrumentation and Data Acquisition

Several devices were used in order to monitor the tests and to acquire the data regarding the displacements and forces withstood by the wall during the test. Linear variable differential transformers (LVDTs) were used at the bases of the two chord studs so that their lateral slip and uplift movement could be monitored (Figure 2.27). A string potentiometer was attached at the top corner of each wall specimen to measure the in-plane displacement (Figure 2.27). The actuator's internal LVDT was also monitored. The shear force applied at the top of the wall was recorded through the load cell (Figure 2.28). The measurement instruments were connected to Vishay Model 5100B scanners that were used to record data at 2 scans/s for the monotonic tests, 100 scans/s for the symmetric cyclic tests and 25 scans/s for the asymmetric cyclic tests, using the Vishay System 5000 StrainSmart software.

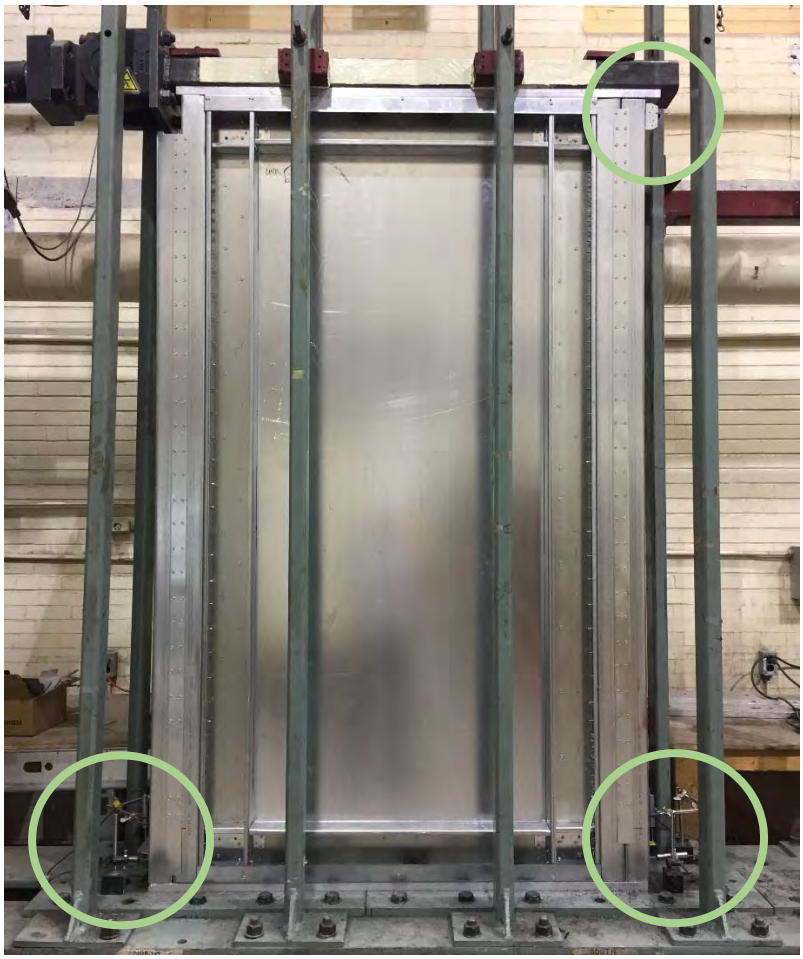

Figure 2.27 Test setup: LVDTs at the bottom corners and string potentiometer in top right corner

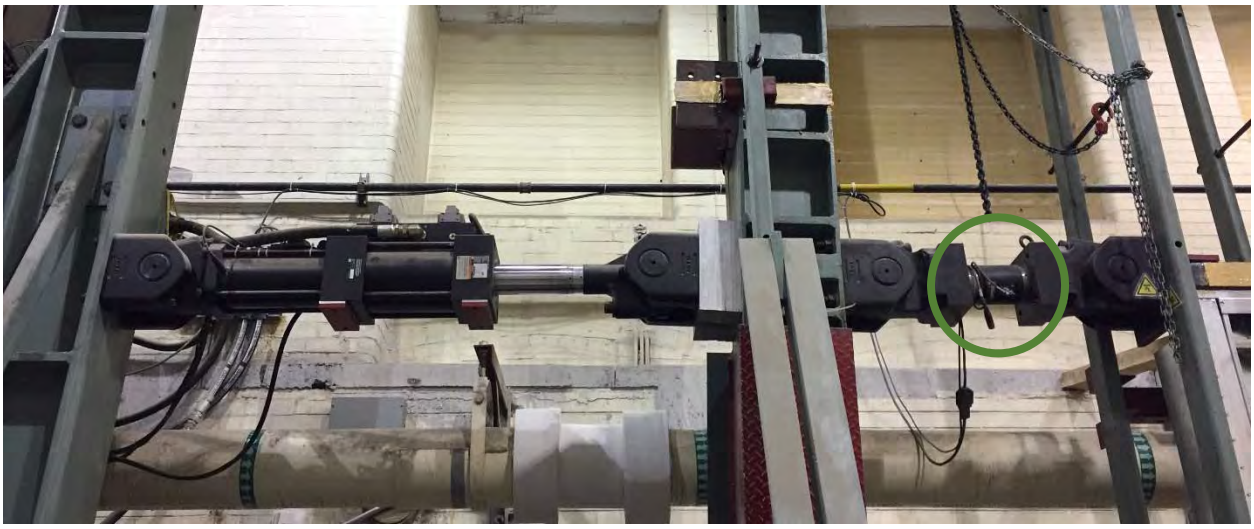

Figure 2.28 Actuator (on the left) and the load cell (in circle)

2.7 Testing Protocols

The specimens were tested using three different protocols: monotonic, symmetric cyclic and asymmetric cyclic. The monotonic protocol was important in order to create the symmetric cyclic protocol for each wall. The symmetric cyclic protocol selected for the experiments was the CUREE (Consortium of Universities for Research in Earthquake Engineering) reversed cyclic protocol (Krawinkler et al. *(2001)*, ASTM E2126 *(2011)*). However, due to the increased ductility of the specimens built following the centre-sheathed configuration, only the cyclic protocol was performed on some specimens (see explanation hereinafter). In addition, the very last specimens were tested under an asymmetric protocol to capture the degradation in strength at large shear deformations.

2.7.1 Monotonic protocol

The monotonic testing protocol consisted of a single direction lateral displacement applied at the top of the wall at a constant rate of 5.0 mm/min (~ 0.2” /min), to represent a static lateral loading such as wind loading for example. For this protocol, a given specimen was tested until its strength dropped under 50% of its ultimate strength (defined during the test), or just before the maximum stroke of the actuator was reached (125 mm (5”)). Since the test frame accommodated for both cyclic and monotonic protocols, the protocol would start at zero displacement (i.e. the specimen is

not subjected to any load), approximately at the centre position of the actuator; that is, the 250 mm (10”) stroke would give approximately ±125 mm around the zero position of the wall.

2.7.2 Cyclic protocols

The CUREE reversed cyclic protocol for Ordinary Ground Motions (Basic Loading History) is a widely used standard for the testing of many recent CFS framed shear wall research programs. Its main objective is to evaluate capacity level seismic performance of components subjected to ordinary ground motions with a probability of exceedance of 10% in 50 years. It is characterized by a specific pattern that consists of primary and trailing cycles (Figure 2.29). The amplitude of the primary cycles increases throughout the test; each of these cycles is followed by 6, then 3 and eventually 2 trailing cycles, whose amplitude is 75% of the preceding primary cycle (Figure 2.29 and 2.31).

The amplitude of each cycle depends on the results of the monotonic test realized with a wall of the same nominal building parameters. In order to define the CUREE protocol cycles for a given specimen, it is important to locate (from the results of the monotonic test) the point where the load drops to 80% of the ultimate load after reaching the latter (80% F_u post-peak). The displacement at that point is called the monotonic deformation capacity (Δ_m) (Figure 2.30).

The reference deformation (Δ) is the maximum deformation (displacement, chord rotation, etc.) the specimen is expected to sustain; it is computed as follows:

$$\Delta = \gamma \Delta_m \qquad \text{Eq 2.13}$$

Where γ is a reduction factor accounting for the differences between monotonic and cyclic testing; the damage occurs and accumulates in a different way leading to earlier deterioration in strength when submitted to cyclic loading. According to Krawinkler et al. *(2001)* the suggested value for their Woodframe project at that time was $\gamma = 0.6$. This same value has been used in all the previous tests realized on cold-formed steel shear walls at McGill University (e.g. Branston *(2004)*, Balh *(2010)*, Rizk *(2017)*). A unique frequency of 0.25 Hz was set for all the cycles of the symmetric

cyclic protocol. Figure 2.31 shows the CUREE Reversed Cyclic Protocol used for specimen W29-C as well as the measured force vs. deformation results.

This method needed adjustment when testing the specimens using the centre-sheathed configuration; when reinforced adequately, the applied shear load did not drop to 80% of the ultimate load given the stroke of the actuator; it was therefore impossible to obtain a value for Δ_m following the test results. This case has been encountered in Rizk *(2017)*, where it was decided to set Δ = 60 mm. This value was based on the 2.5 % inelastic storey-drift limit criterion for seismic design of the ASCE/SEI 7 *(ASCE, 2016)* and the NBCC *(NRCC, 2015)*. As this value remained constant for each of the wall configurations, the CUREE Reversed Cyclic Protocols were the same for all the specimens built with the centre-sheathed configuration. Since a monotonic test result was not needed to establish the cyclic protocol, many of the centre-sheathed walls were tested solely under a cyclic protocol.

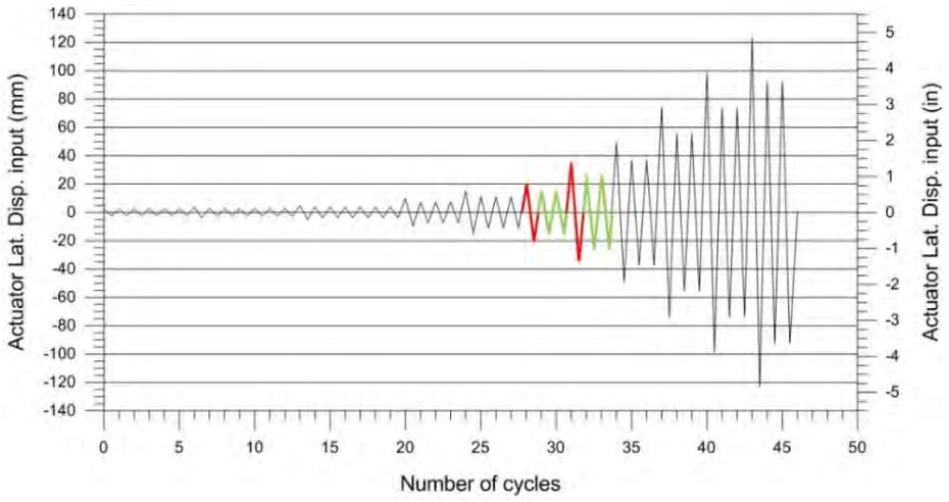

Figure 2.29 Pattern of the CUREE Reversed Cyclic Protocol for a given specimen: primary cycles in red, trailing cycles in green.

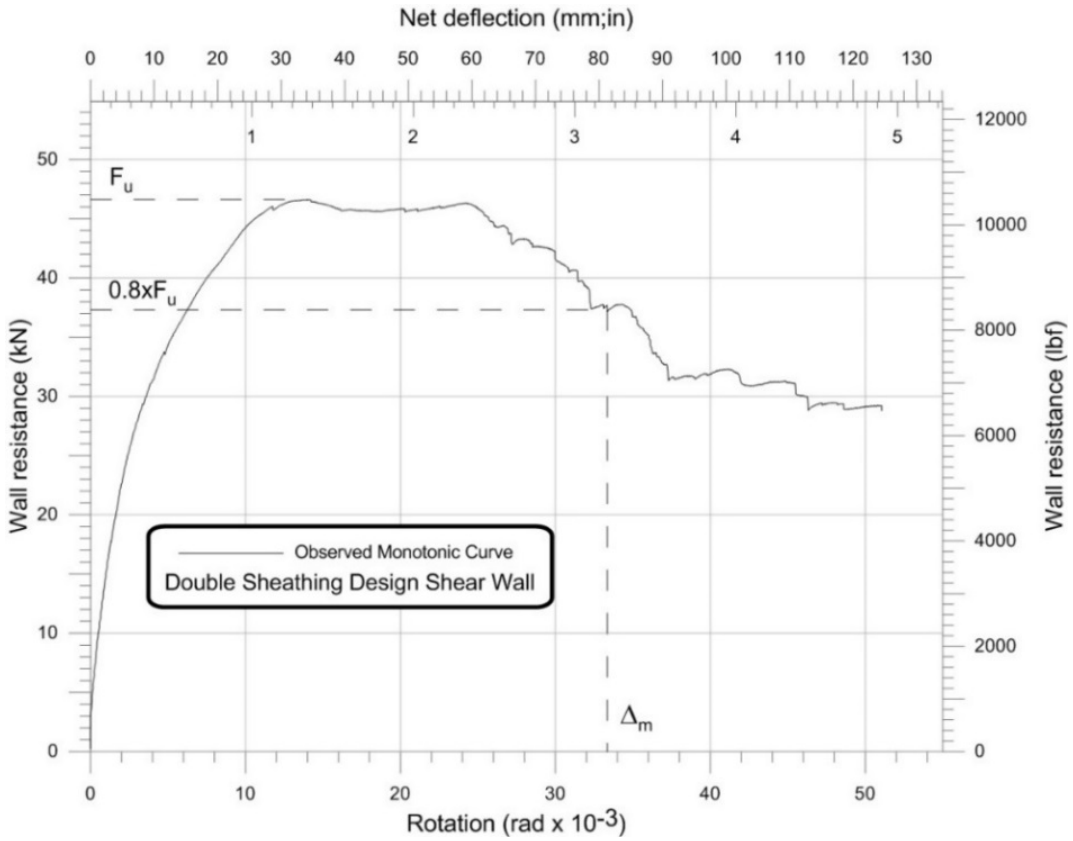

Figure 2.30 Key values for the determination of the CUREE cycles for a given wall

S_u = 46.629 kN

$\Delta_{0.8\ Su\ post\text{-}peak} = \Delta_m$ = 81.337 mm

$\Delta = 0.6*\Delta_m$ = 48.802 mm

Displacement (*Δ)	Actuator Input (mm)	Number of cycles	Cycle Type
0.05	2.466	6	Initiation
0.075	3.698	1	Primary
0.056	2.761	6	Trailing
0.1	4.931	1	Primary
0.075	3.698	6	Trailing
0.2	9.862	1	Primary
0.15	7.397	3	Trailing
0.3	14.793	1	Primary
0.225	11.095	3	Trailing
0.4	19.724	1	Primary
0.3	14.793	2	Trailing
0.7	34.518	1	Primary
0.525	25.888	2	Trailing
1	49.311	1	Primary
0.75	36.983	2	Trailing
1.5	73.966	1	Primary
1.125	55.475	2	Trailing
2	98.622	1	Primary
1.5	73.966	2	Trailing
2.5	123.277	1	Primary
1.875	92.458	2	Trailing

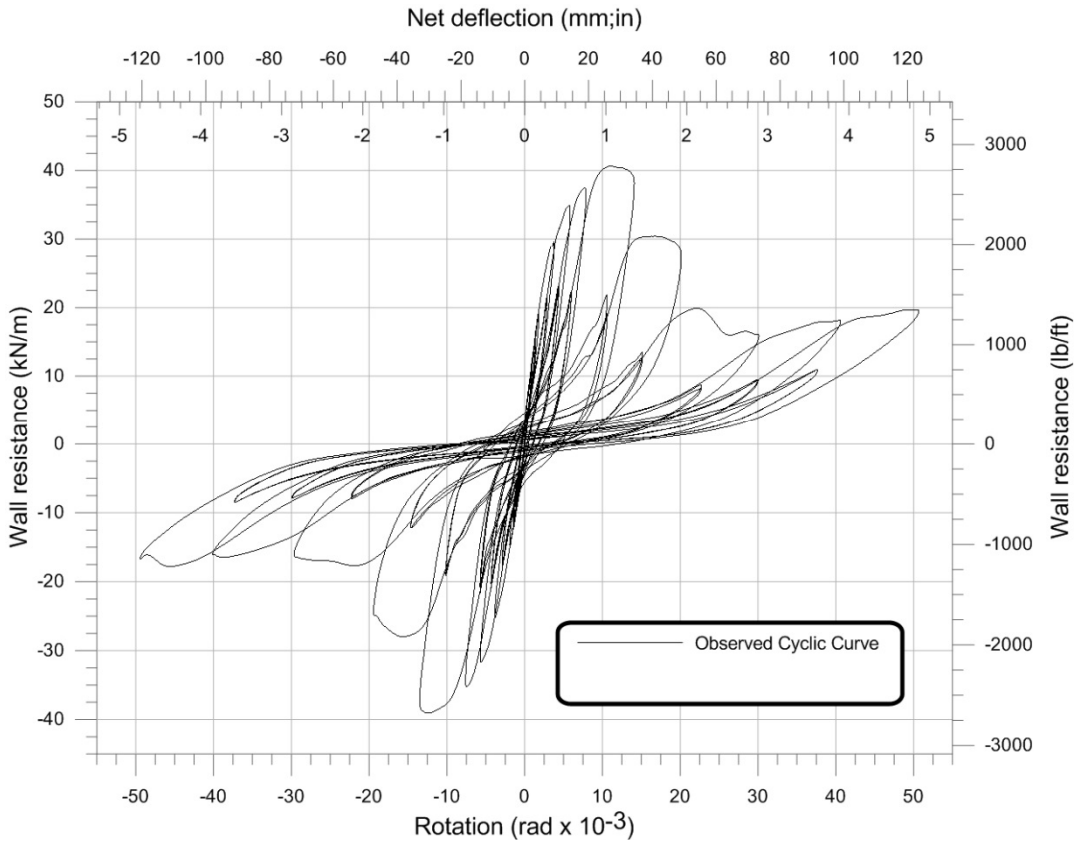

Figure 2.31 CUREE Reversed Cyclic Protocol and test results for test W29-C

The last four shear wall specimens (W15B, W23B, W25 & W26) were submitted to a different cyclic protocol since the ultimate resistance was not reached within the 125 mm displacement provided by the actuator in the symmetric cyclic testing protocol. In order to reach higher chord rotations, the wall was installed 100 mm further from the actuator in the test frame, which only allowed for the application of an asymmetric cyclic protocol. The negative cycles were limited to 5 mm (-5 mm) allowing the positive cycles to reach up to 220 mm (Figure 2.32). The frequency needed to be adjusted for this protocol, especially for the last cycles since the high forces applied and the relatively long distance covered by the actuator between a negative and a positive cycle nearly covered the whole available stroke of the actuator; that led to the use of a frequency of 0.05 Hz for the first cycles and 0.025 Hz for the largest ones to ensure the actuator reached the full amplitude of the cycles in the protocol.

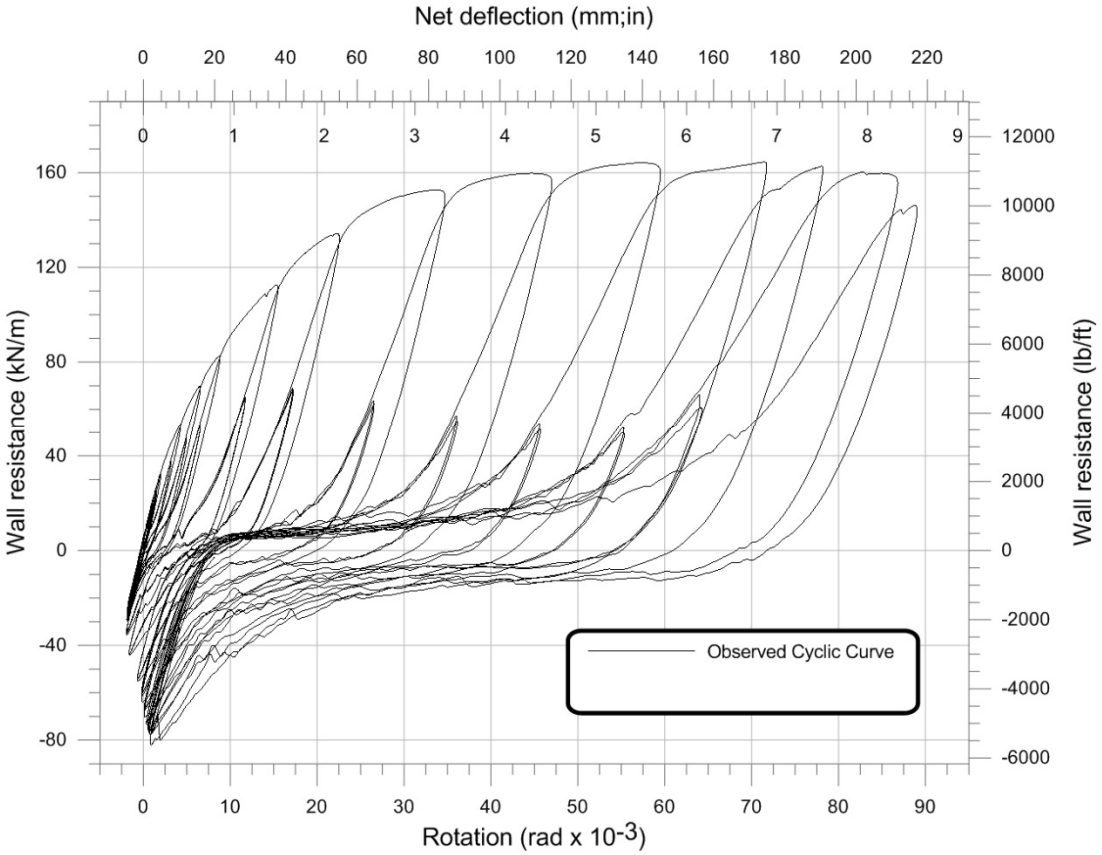

Figure 2.32 Asymmetric cyclic protocol to capture the degradation in strength and high ductility of the wall specimens built with the centre-sheathed configuration

CHAPTER 3 – TEST RESULTS AND OBSERVATIONS

3.1 Introduction

In this chapter are presented the results from the shear wall experimental program described in the Chapter 2, as well as the method with which the data analysis was conducted. It contains four main points:

- The observations of the failure modes; where are presented all the different failure modes observed during these tests (for the connections, the sheathing and the framing members);
- The proceedings of the data analysis; where are detailed the different steps followed to shape the test results in order to use and compare them;
- The test results and the comparison between specimens to describe the influences each building parameter or the configuration can bring to a specimen;
- The coupon tests and the associated results; where the material used for the entire program was subjected to tension tests in order to assess its mechanical properties.

3.2 Observations of the Different Failure Modes

The shear walls comprising the experimental program exhibited several behaviours; some were expected because they were previously revealed in similar experimental programs, but new ones appeared related to the new shear wall configurations. The elastic shear buckling of the sheathing was observed as soon as a displacement at the top of the wall was applied. This behaviour happens because of the compression field that develops in the sheathing. In combination with this, a tension field was also seen in the opposite direction in the sheathing. These behaviours were also observed in previous experimental programs of cold-formed steel sheathed shear walls (e.g. Balh *(2010)*, Yu *(2010)* and Rizk *(2017)*) due to the thin steel sheathing characteristic of these shear walls. Once reaching greater displacements, damage appeared in the sheathing at the connection locations, and sometimes affected the fasteners themselves. At that point, the shear buckling of the sheathing had become inelastic. Large lateral displacements associated with high forces damaged the frame in some cases; these damages are unwanted; hence, the related configurations were corrected to

accommodate for the higher strength experienced by the wall to avoid frame damage at these stages (reinforcement schemes explained in Section 2.2.3). This section describes all the aforementioned modes of failure and expands on the different types of connection failures observed during tests. Appendix E provides the test observation sheets for the shear wall specimens.

3.2.1 Connection Failures

Connection failures exist under several forms and are related to the resistance of the fastened materials, as well as their thicknesses. In the case of the frame-to-sheathing connections, as the differential thickness is important (sheathing has a maximum thickness of 1.09 mm (0.043") whereas framing has a minimum thickness of 1.73 mm (0.068") and is 2.46 mm thick (0.097") for 27 of the 31 specimens tested), damage concentrated in the sheathing at the fastener locations. During this experimental program, this mainly started with steel bearing failure (SB) when the aspect of the frame changed due to the lateral displacement applied at the top of the wall, stressing the rectangular piece of sheathing at its corners in the long diagonal (in the direction of the force applied). Past a certain resistance, the screw gradually progressed through the sheathing (Figure 3.1 and Figure 3.2) creating typical bearing damage to the latter.

Figure 3.1 Steel bearing damage in sheathing from double-sheathed configuration

Figure 3.2 Steel bearing damage in sheathing from centre-sheathed configuration

Steel bearing damage was intensified as the lateral displacements applied at the top of the wall were increased, creating long "tear-shaped" holes where, when the sheathing did not pull over the head of the screw. This led to tear-out sheathing failure (TO) for the screws located nearby the edges of the sheathing (Figure 3.3).

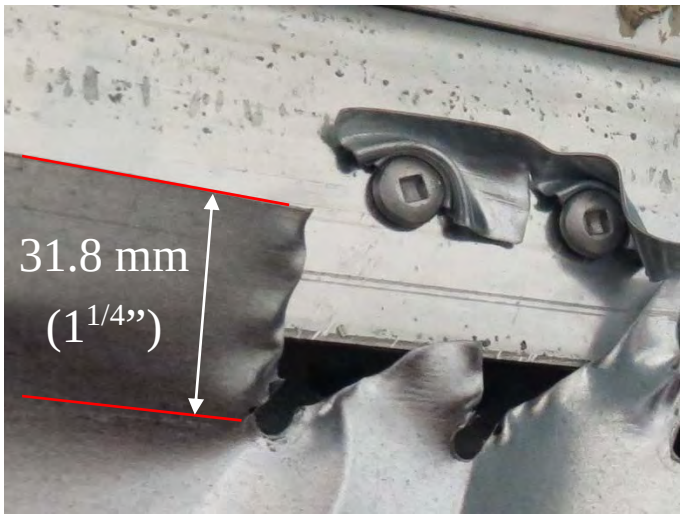

Figure 3.3 Tear-out of the sheathing from two screws

Another failure observed was the pull-through sheathing failure (PT), characterized by the screw breaking through the sheathing. This was observed for the specimens built with the double-sheathed configuration only. For the centre-sheathed configuration, the sheathing could not become detached from the screws as it was confined between the studs forming the built-up framing member. While experiencing bearing damage through repeated cycles of the double-sheathed walls, the screw heads were able to penetrate through the sheathing. However, this is not a pure pull-through sheathing failure since this was mostly due to accumulated bearing damage after repeated loading cycles, in combination with the out-of-plane force applied to the connection because of the shear buckling of the sheathing. Pure PT failures were observed in the early stage of the tests on the field studs; this was due to a relatively large screw spacing of 304.8 mm (1') and the fact that the fasteners were located in the middle of the compression field experiencing out-of-plane deformations due to shear buckling. Figure 3.4 shows a screw located in the compression field experiencing pull-through failure with little steel bearing damage; the out-of-plane forces from the shear buckling of the sheathing alone resulted in failure in this example.

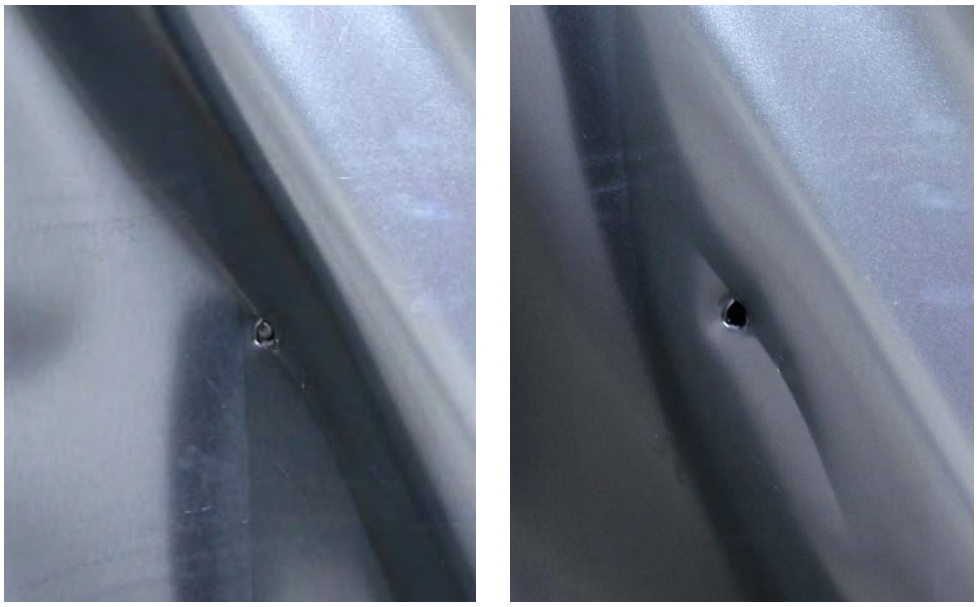

a. b.

Figure 3.4 Pull-through sheathing failure: a. right before happening and b. just after

Shear failures of screws were observed for the centre-sheathed configuration specimens exclusively where, in addition of significantly higher shear forces being applied, the three or five layers of steel the screws had to go through imposed higher shear demands on the screws. The fracture usually happened just below the head of the screw; therefore the shear transfer effect on the first steel layer was lost, but usually remained effective (in terms of shear resistance) for the other layers (Figure 3.5).

Figure 3.5 Shear failure of screws: shear capacity conserved on all the layers (in green) and capacity lost on the top layer (in red)

The last connection related failure did not concern the sheathing itself but the built-up box members used as chord studs or reinforcement; the shear flow created within the built-up member imposed a tilting of the screws connecting the strap to the frame member (see details in Figures 2.16 and 2.17). When the spacing of these screws was large (152.4 mm (6")) tilting of the fasteners could be observed (Figure 3.6). This failure mode was facilitated due to the screws penetrating through only two layers of steel. In tests W23-CR3 the tilting failure mode was avoided by shortening the distance between the screws to 76.2 mm (3"), which reduced the shear force each one of them would receive.

Figure 3.6 Shear flow running in built-up chord member subjected to bending

3.2.2 Sheathing Failures

Two types of failure were observed for the sheathing. The first one was the out-of-plane shear buckling of the sheathing, observed during every test. When deforming a rectangle into a parallelogram, the diagonals of the latter change in length. The analogy applies to the shear walls; as the top of the wall was being displaced in one direction, one diagonal of the parallelogram became longer and experienced tension forces whereas the other one became shorter and thus experienced compression (Figure 3.7). Hence the tension field developing in the long diagonal and the compression field in the short one. As per any member subjected to compression forces, it will end up buckling around its weak axis. The part of the sheathing subjected to compression acts the same way; as it has a strong and a weak axis, it buckled around its weak axis, generating the characteristic waves that define the shear buckling (Figure 3.8). These waves developed in the normal direction of the plane created by the sheathing panel, hence the out-of-plane forces created. Both configurations (double-sheathed and centre-sheathed) were impacted by this failure mode during monotonic and cyclic tests (Figure 3.8).

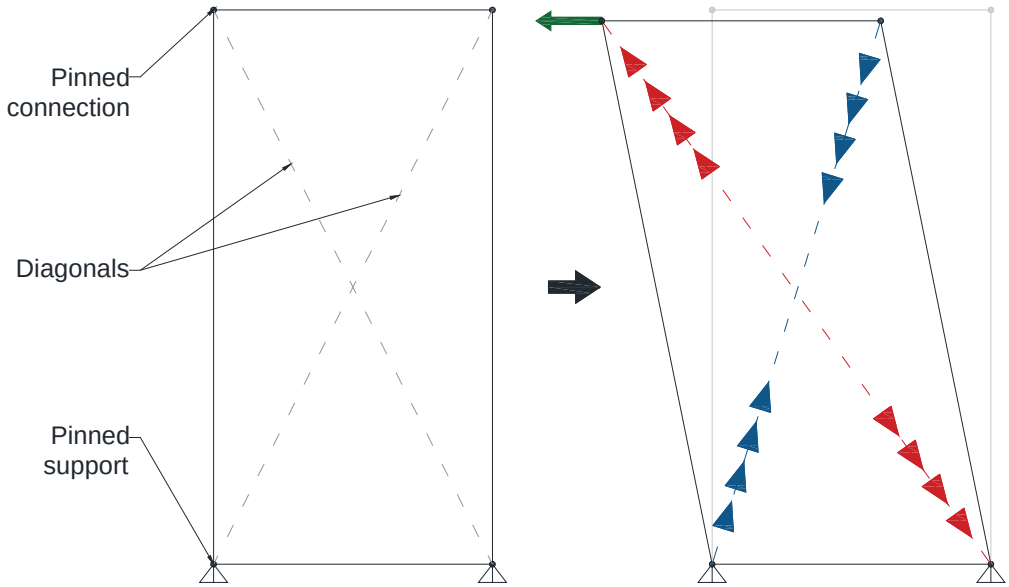

Figure 3.7 Tension (red) and compression (blue) fields in a deformed rectangular shape

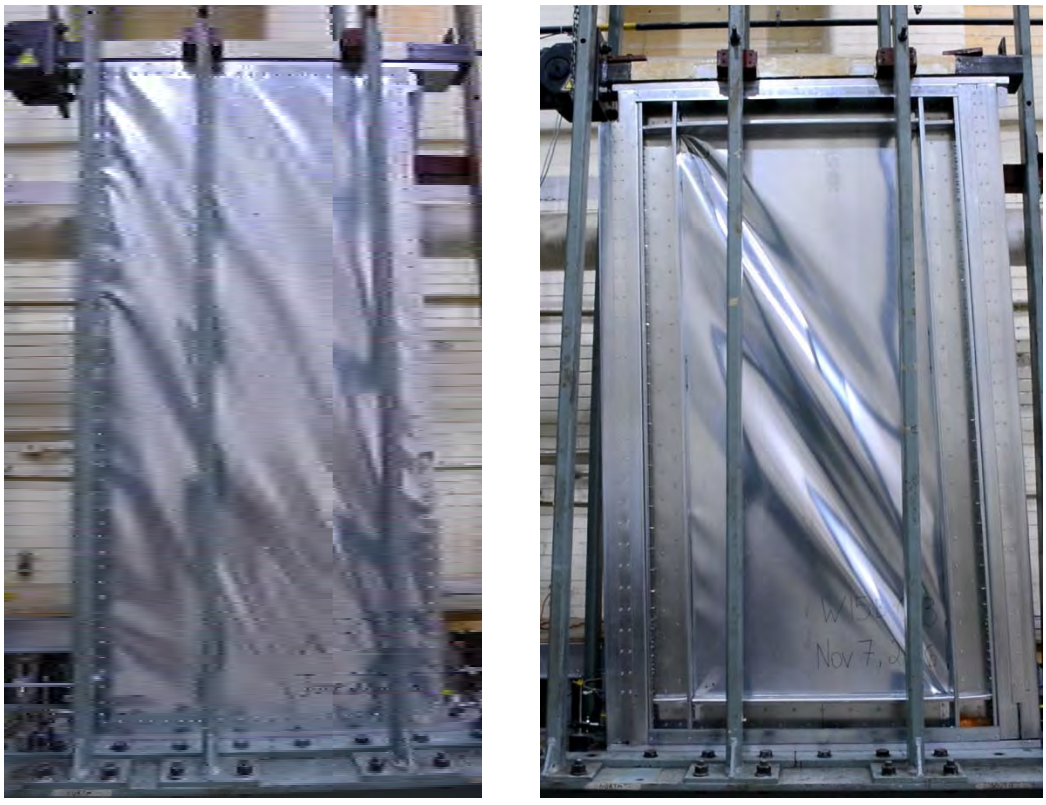

a. b.

Figure 3.8 Shear buckling of sheathing during monotonic tests: a. double-sheathed wall and b. centre-sheathed wall

The other sheathing failure mode was observed during the cyclic tests and happened only when reaching very high drift (about 8%). The alternating cycles resulted in alternating direction of the inelastic shear buckling and tension field. The characteristic waves of the shear buckling are amplified when reaching high drift at the top of the wall and the repetitions of negative and positive cycles (although not reaching a high negative drift) resulted in the creation of holes in the sheathing due to plastic strain accumulation where the inelastic wave deformations from negative and positive cycles crossed (Figure 3.9). This kind of failure happened exclusively for centre-sheathed configuration; in fact, the two pieces of sheathing in the double-sheathed configuration lost their connection with the frame too early in the loading protocol to expect to go through such intense damage.

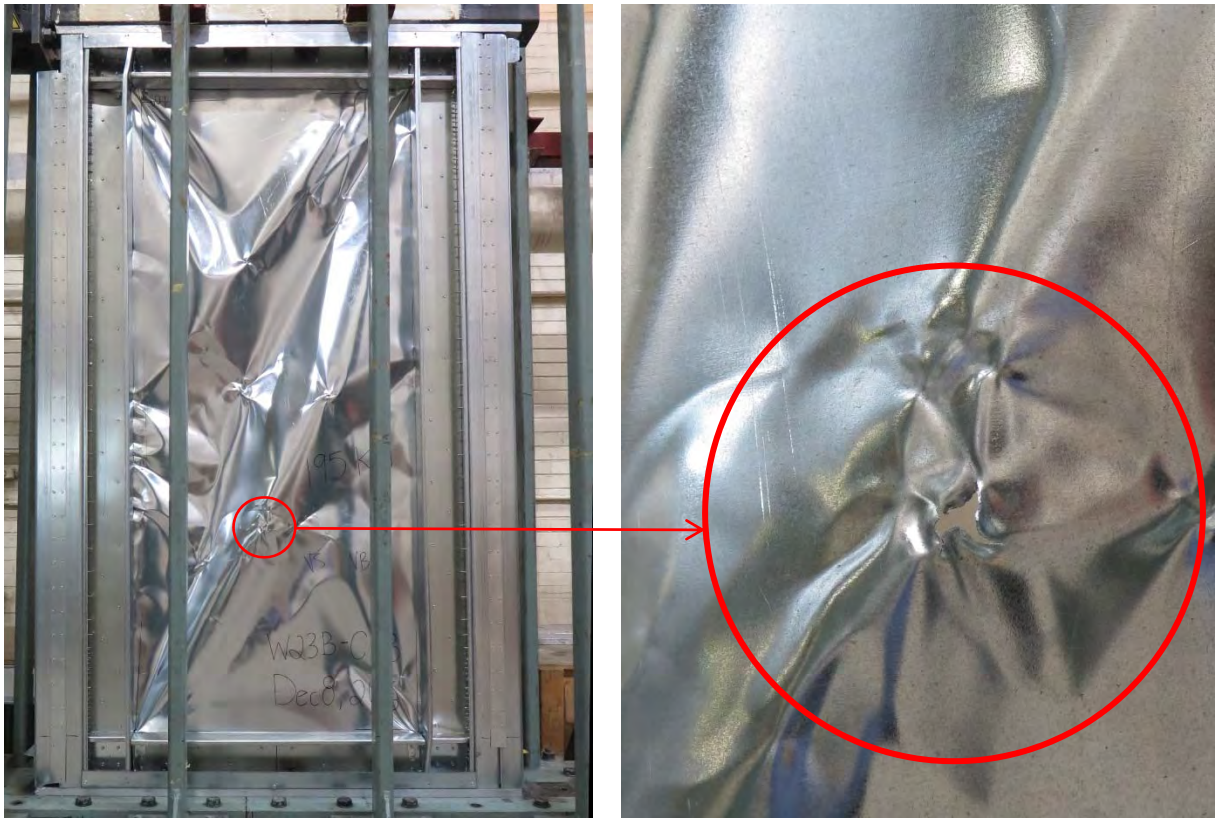

a. b.

Figure 3.9 Damage after cyclic test: a. two directions of shear buckling and b. one of the holes that appeared at intersections

3.2.3 Framing Failures

In order to achieve higher strength and ductility, one of the main objectives of the test program was to minimize the eccentricity of the sheathing placement through use of either the double-sheathed or centre-sheathed configurations. By constructing the walls in this fashion it was possible to avoid the distortion of the framing studs as observed by Balh *(2010)* and Rizk *(2017)*. The two wall configurations included in this study program do not present any eccentricity; consequently, no distortion damages were observed on the chord studs. However, the increased ultimate shear resistance of these wall specimens brought to light other failure modes of the framing studs, if these members were not designed for the corresponding axial force and moment.

3.2.3.1 Double-sheathed configuration

This configuration was the least impacted by framing damage and failures; the chord studs could have been re-used for other tests in most of the cases since their physical properties were barely altered during the tests. The main damage observed on the framing studs was the elastic local buckling of the chord studs' webs (Figure 3.10a) toward the end of the monotonic tests and the web of the studs being pulled out by the holdowns at the corners of the wall (Figure 3.10b). It was also observed that the infill plates used in the tracks for the shear anchors were very efficient at preventing the track from becoming distorted; these tracks showed no damage, which was not the case for the walls tested by Rizk *(2017)*.

a. b.

Figure 3.10 Frame damages in chord studs: a. elastic local buckling and b. web of the stud slightly pulled out by the holdown during the test

3.2.3.2 Centre-sheathed configuration

This configuration was susceptible to chord stud damage when the member forces used in their design were below those actually reached during testing. In fact, the damage of the chord studs for this configuration led the way through different schemes of reinforcement of the chord studs as explained in Section 2.2.3. The first significant damage concerned the initial configuration (W18), whose chord studs were not reinforced (details of each specimen with its building parameters are provided in Appendix A). The high shear forces brought through the sheathing resulted in an axial load and moment combination exceeding the unreinforced chord stud's capacity. Therefore, the latter failed due to the interaction of axial compression load and bending moment (Figure 3.11a.). In addition, damage was observed locally on the flanges of the vertical studs at the corners due to the contact with the horizontal framing members (Figure 3.11b.).

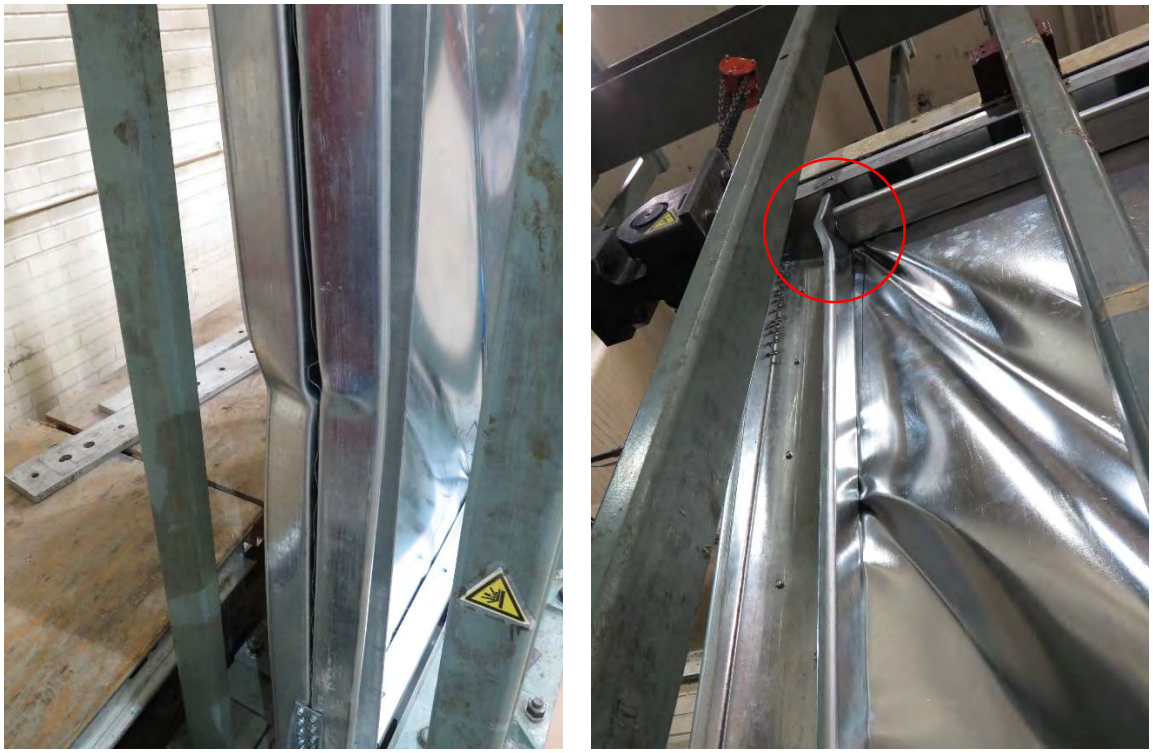

a. b.

Figure 3.11 Damage in chord studs of specimen W18-M: a. axial compression load and bending moment interaction failure in the vertical chord studs and b. local damage of the chord stud flanges due to contact with the horizontal framing members at corners

The damage at the wall corners was reduced considerably by adding stiffeners inside the ends of the chord studs (Figure 2.24). Reinforcement was also added along the length of the chord studs in order to better sustain the bending moment and axial load combination. However, as explained in Chapter 2, more reinforcement brought higher shear strength to the walls, which resulted in larger forces in the chord studs. When those forces became too high, the reinforced chord studs failed in the same fashion as the unreinforced studs (i.e. combined axial compression forces and bending moment) as shown in Figure 3.12, thus needing additional reinforcement. The design of the last reinforcement scheme (all test specimens using “R3”at the end of their identification code, e.g., W15-MR3 or W24-CR3) considered all the sheathing screws to contribute to the shear resistance of the wall, and hence the chosen reinforced chord studs provided enough resistance to sustain the bending moment and axial load combination. The framing members were still in a good condition after the test (Figure 3.13a), whereas the sheathing and its connections became damaged (Figure 3.13b), which is the intent for the seismic design of these shear walls.

a. b. c.

Figure 3.12 Damage in chord stud of specimen W16-MR: a. general view of the damaged specimen, b. local buckling of the chord stud's flange and lip at mid-height and c. local buckling of the chord stud's web at the base

Another type of frame failure was the splitting of the built-up chord member (Figure 3.14), which incorporated the sheathing. One of the characteristics of shear buckling of the sheathing is that a force normal to the wall is developed where the ripples (buckles) in the sheathing contact the frame. It was observed for the specimen with a large sheathing screw spacing (150 mm) that the out-of-plane forces created by these ripples were high enough to separate the individual C-sections that confine the sheathing (Figure 3.14). This resulted in the chord stud assembly not acting as a built-up section, but rather as individual C-sections. A closer sheathing screw spacing and the installation of chord stud reinforcement was necessary to avoid this failure mode.

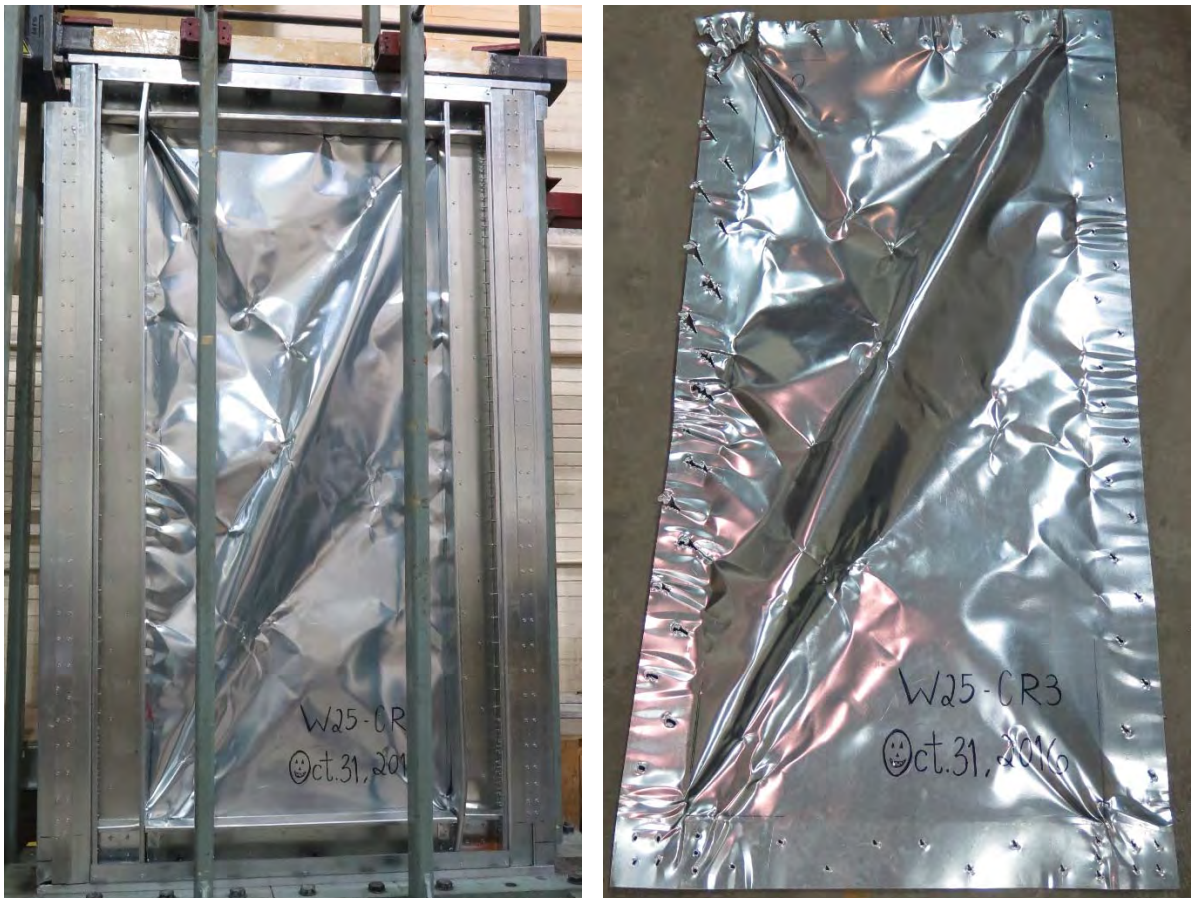

a. b.

Figure 3.13 Specimen W25-CR after cyclic test: a. framing members in good condition and b. damage confined to the sheathing and its connections (bearing damage).

Figure 3.14 Built-up chord studs split due to out-of-plane forces caused by shear buckling of the sheathing

Ultimately, these framing failures, depicted in Figure 3.15, could be avoided by correcting the design and detailing of the frame (e.g. the specimen presented in Figure 3.13a). The damage of the chord stud's flange due to the contact with the horizontal framing was minimised by using stiffeners installed at the extremities of the chord studs (Figure 3.16). Eventually the splitting of the built-up chord stud was corrected using a maximum sheathing fastener's spacing of 101.6 mm (4"). Keeping the minimum fastener spacing's to 50.8 mm (2") limits the ultimate shear strength of the wall, therefore limiting the forces brought in the chord studs and thus limiting the extent of damage in the chord studs.

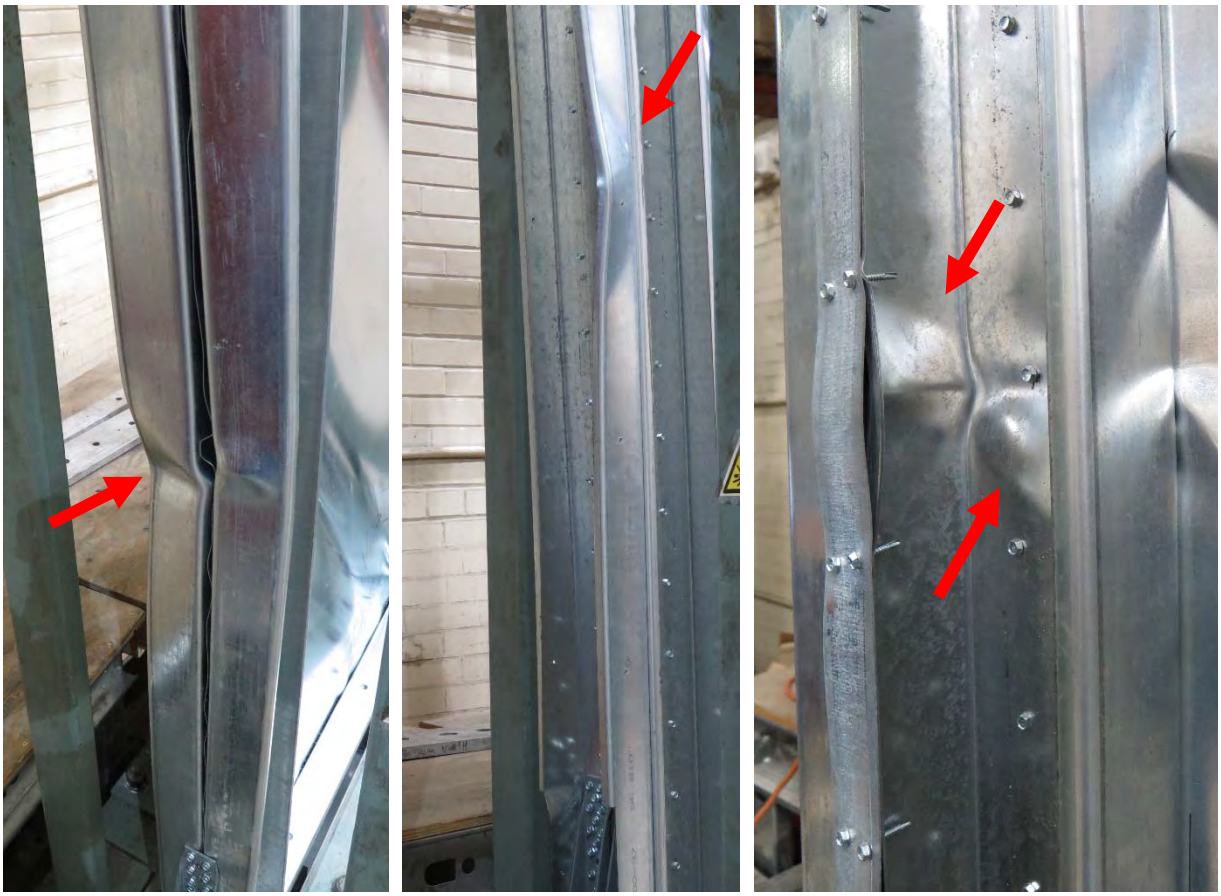

a. b. c.

Figure 3.15 Failing chord studs: a. complete built-up chord stud failing on W18-M, b. local buckling of the flange and lip of the outer part of the built-up member on W16-MR and c. local buckling of the webs and flanges of the inner parts of the built-up member

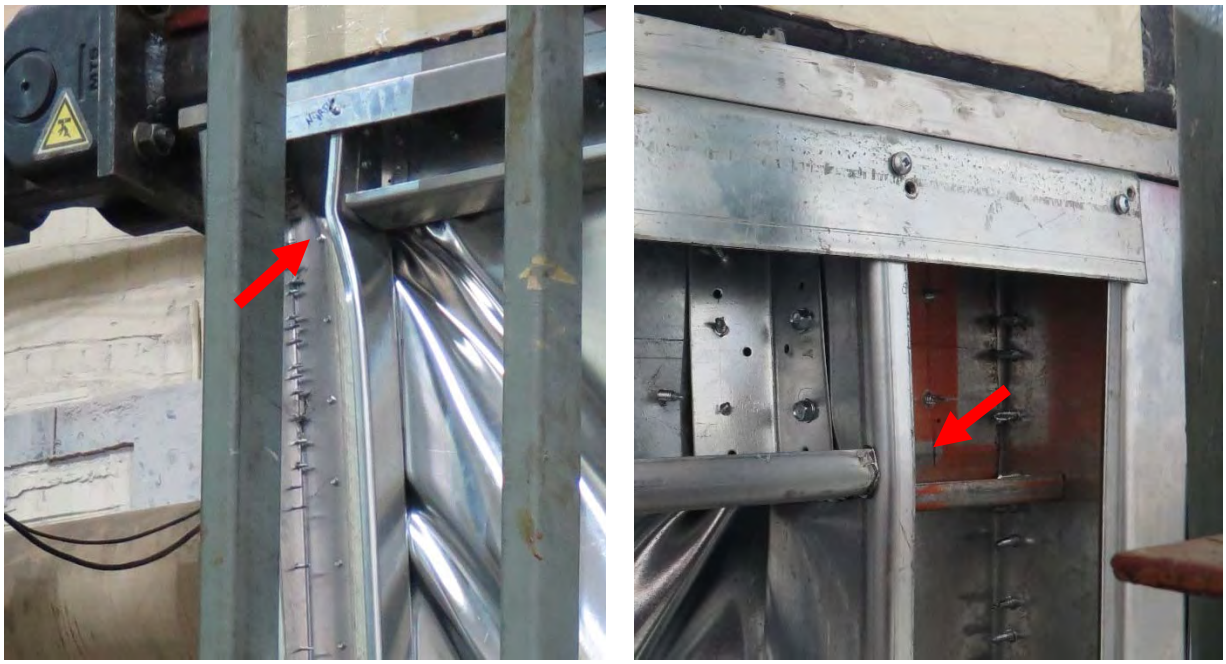

a. b.

Figure 3.16 Failed chord studs: a. flange at the top of the chord stud failed during test due to contact with horizontal framing member and b. good condition of the flange at top of the chord stud when using stiffeners

As the shear capacity of the centre-sheathed walls was increased due to changes in the construction of the framing members (reinforcement schemes), the holdowns were subjected to higher uplift forces, especially at the base of the wall. The high forces led to damage of the holdowns when their nominal tension load, as reported in Connectors for Cold-Formed Steel construction C-CFS-15 *(Simpson Strong-Tie Company Inc. (2015))*, was exceeded; i.e. bent bottom plate and shear failure of screws. Although this failure mode was addressed by adding two holdowns at each side of the base of the walls, the strongest walls experienced minor bending damage to the bottom plate (Figure 3.17) because the uplift forces experienced by the walls reached the nominal tension load of the holdowns.

Damage to the track members was not observed because the sheathing was not directly connected to these members. The horizontal framing, which confined the sheathing at top and bottom of the walls, withstood the loads regardless the building parameters the specimen was built with, without undergoing any particular damage (Figure 3.13a).

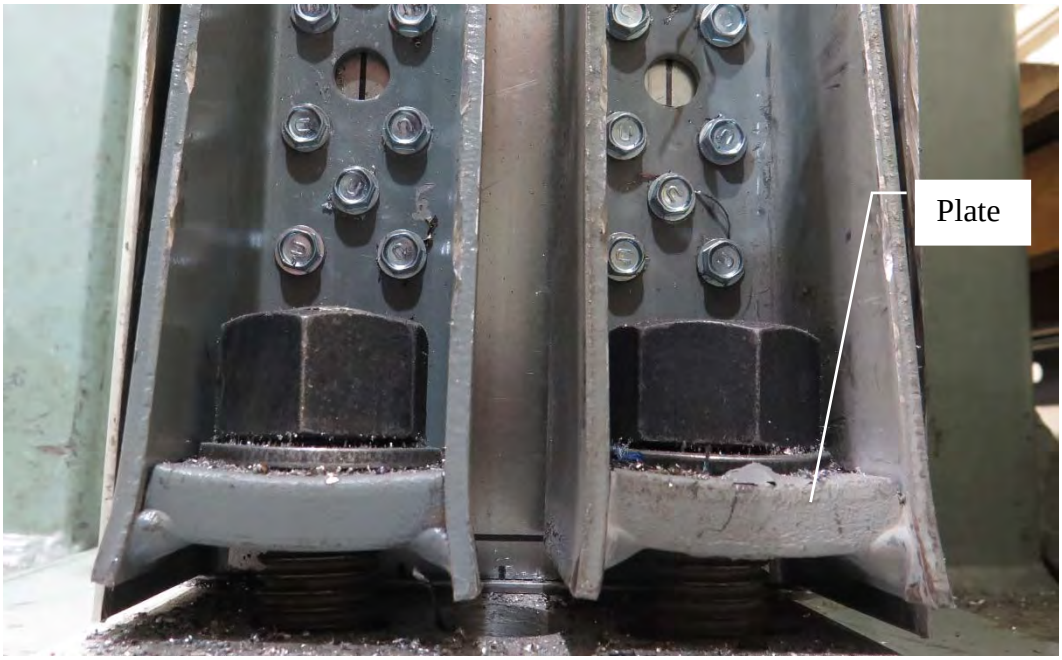

Figure 3.17 Damaged holdowns on the strongest specimens, using the highest degree of reinforcement (R3)

3.3 Proceedings for the Analysis of the Test Results

The analysis of the measured results started with the collection of the important data for each wall from the complete matrix of test specimens. They were:

- The displacement at the top of the wall, Δ_{top};
- The force recorded by the load cell to achieve the requested displacements, F_{act}.

From these were obtained the rotation of the wall (Equation 3.1) as well as the shear flow applied at the top of the wall (Equation 3.2):

$$\theta = \frac{\Delta_{top}}{h} \quad \text{Eq. 3.1}$$

$$S_{top} = \frac{F_{act}}{w} \quad \text{Eq. 3.2}$$

where,

θ = Rotation of the wall (radians);

Δ_{top} = Lateral displacement measured at the top of the wall (mm);

h = Height of the wall (mm);

S_{top} = Shear flow applied at the top of the wall (kN/m);

F_{act} = Shear force applied at the top of the wall (kN);

w = Width of the wall (m).

Figures 3.18 and 3.19 show the representation of these parameters used as a force-deformation relationship for monotonic and cyclic tests.

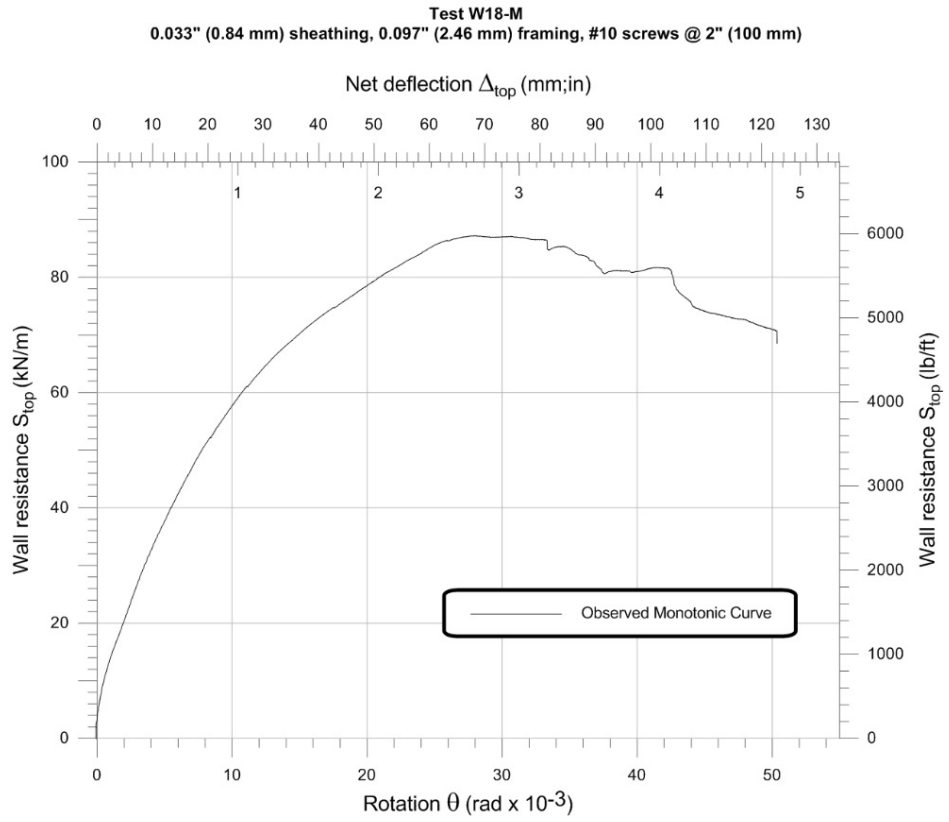

Figure 3.18 Force vs. deformation results plotted for W18-M (monotonic test)

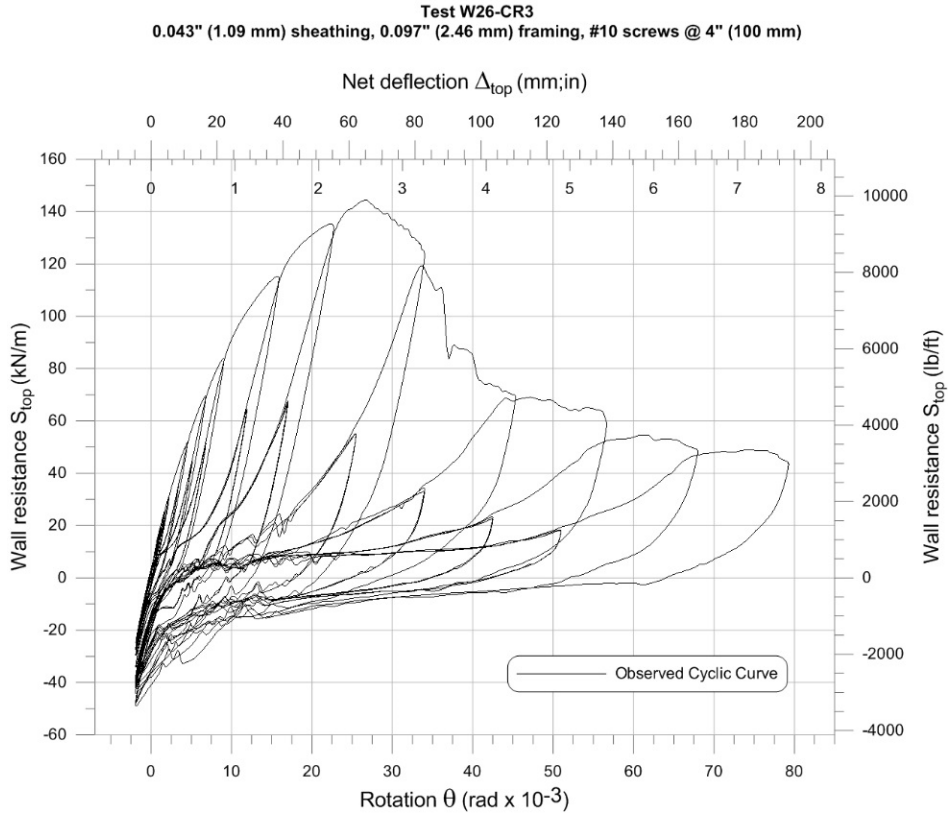

Figure 3.19 Force vs. deformation results plotted for W26-CR3 (asymmetric cyclic test)

The data analysis procedure varied whether it was for a monotonic or a cyclic shear wall test. The parameters needed for the analysis (such as the displacement and resistance of the specimen at the ultimate load or at 80% of the ultimate load post-peak for instance) required the use of a backbone curve (envelope) encompassing the cyclic excursions (Figures 3.20 and 3.21). This curve was produced using the extreme points of all the primary cycles observed during a test. A script had been created in MATLAB in order to use the data from the test to create the associated backbone curve, fitting all the cycles. Once created, this backbone curve can be utilized, as would a monotonic curve, to obtain the necessary performance metrics. The CUREE reversed cyclic protocol for Ordinary Ground Motions (Basic Loading History) and the modified asymmetric cyclic protocol (Section 2.7.2) applied to the shear wall specimens produced separate backbone curves for a nominally identical set of building parameters; examples are shown in Figures 3.20 and 3.21.

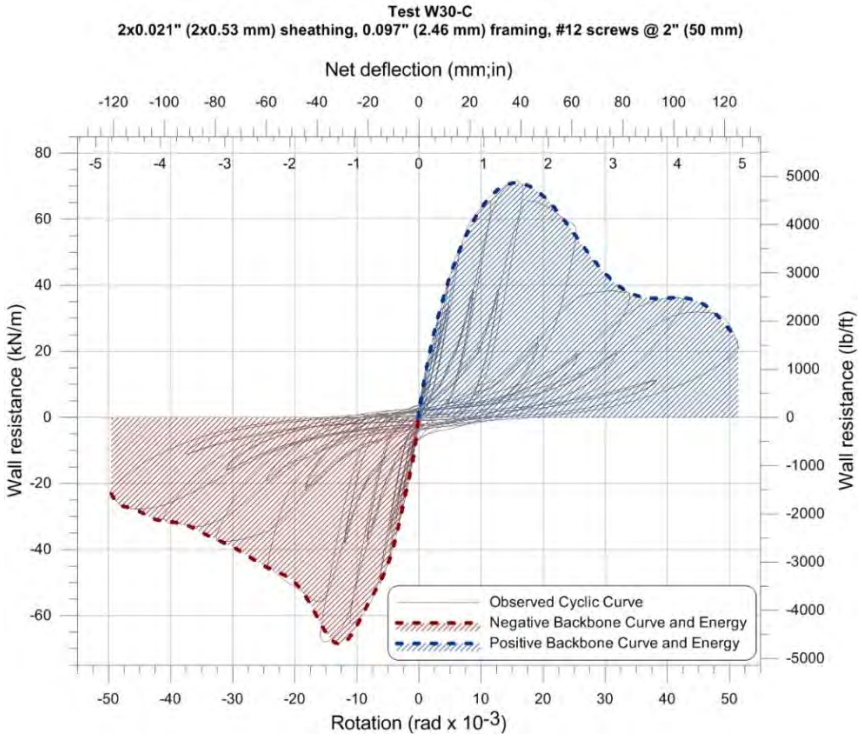

Figure 3.20 Backbone curves and associated energy "dissipated" (in red and blue) by W30-C differentiating the positive and negative displacements or the CUREE reversed cyclic protocol

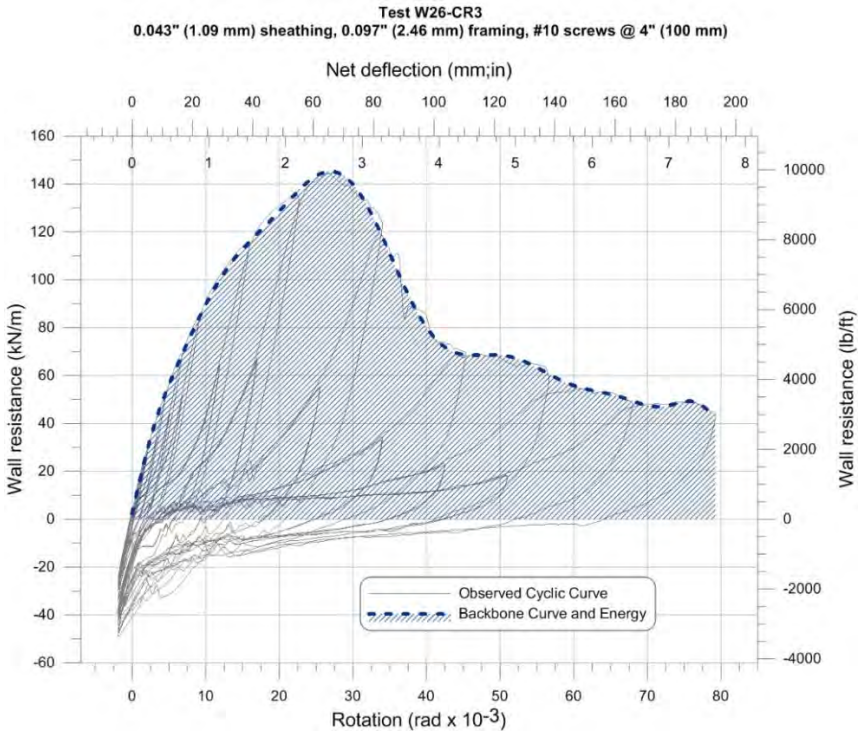

Figure 3.21 Backbone curve and associated energy "dissipated" (in blue) by W26-CR3 during the asymmetric cyclic protocol

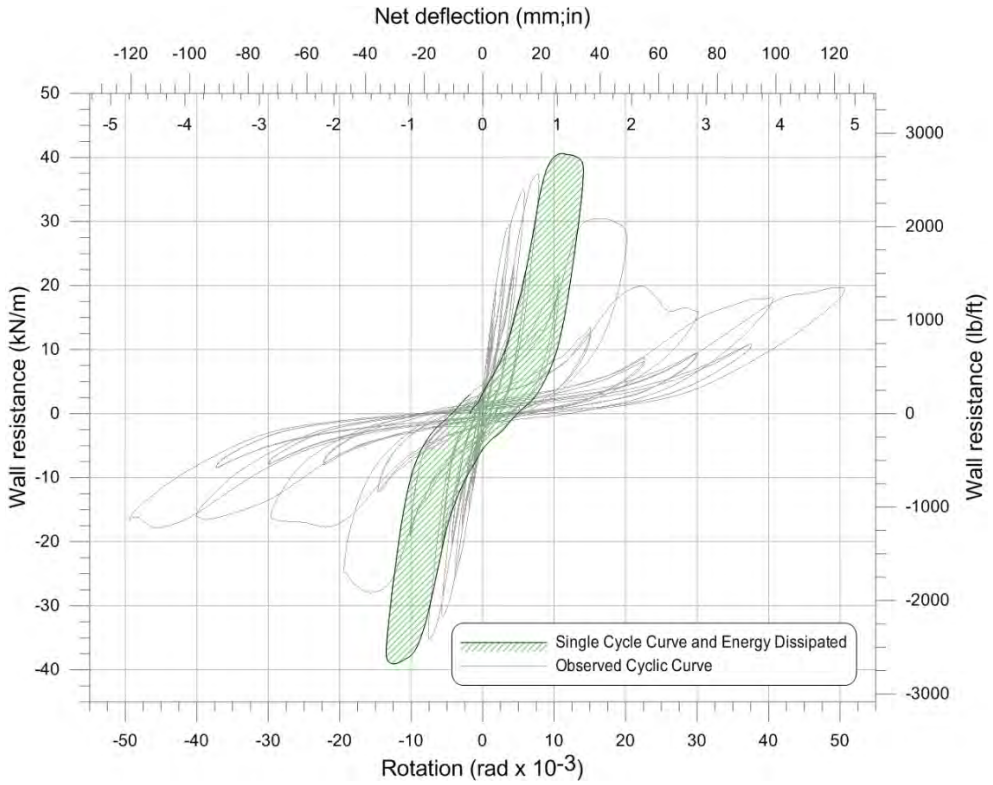

Figure 3.22 Energy dissipated (in green) during the execution of a complete intermediate primary cycle of a cyclic test

Another parameter was obtained from the test results: the energy dissipated by the wall under monotonic and cyclic loading. This energy is represented by the area under the force-deformation monotonic curve. It was calculated using a trapezoidal numerical integration formula in MATLAB using all the points forming the monotonic curve, thus reducing to the minimum the discrepancy between the exact area and the one computed through the formula. As cyclic tests consist of many positive and negative cycles, the total cumulative energy dissipation, E_{TOT}, computed for these tests is represented by the sum of the areas comprised within the force-deformation curve of each cycle (Figure 3.22 shows the energy dissipated during one complete cycle). This total energy was computed using an incremental approach according with Equations 3.3 and 3.4:

$$E_i = \frac{F_i + F_{i-1}}{2} \times \left(\Delta_{top,i} - \Delta_{top,i-1}\right) \quad \text{Eq. 3.3}$$

$$E_{TOT} = \sum E_i \quad \text{Eq. 3.4}$$

where,

E_i = Energy cumulated during increment between points *(i-1)* and *i*;

F_i = Shear force at point *i*;

$\Delta_{top,i}$ = Corresponding displacement at the top of the wall;

E_{TOT} = Total cumulative energy dissipation.

Thus, the total cumulative energy is computed using the complete set of data coming from the cyclic tests, without differentiating the energies cumulated during a positive or a negative displacement. Conversely, the energy "dissipated" by the backbone curves, E_{BB+} and E_{BB-}, are represented by the area under the corresponding backbone curve and differentiates the energies with respect to positive and negative displacements (Figure 3.20).

3.4 Test Results

The results are composed of different parameters taken at specific stages of the test. These stages are defined at: the ultimate wall resistance, S_u, the wall resistance at 80% of S_u post-peak, $S_{0.8u}$, and the wall resistance at 40% of S_u pre-peak, $S_{0.4u}$. The results are represented by the deflection and the rotation parameters taken at these three specific stages and are, respectively: Δ_u, $\Delta_{0.8u}$ and $\Delta_{0.4u}$ for the deflection and θ_u, $\theta_{0.8u}$ and $\theta_{0.8u}$ for the rotation of the wall. In addition, the total cumulative energy dissipated by a specimen in the course of the entire test (monotonic or cyclic as per Section 3.3) is taken as E_{TOT}. These parameters are all graphically represented for a monotonic test in Figure 3.23. For the cyclic test, they are separated into positive and negative values, presented as follows: S_{u+}, $S_{0.8u+}$, $S_{0.4u+}$, S_{u-}, $S_{0.8u-}$ and $S_{0.4u-}$ for the different stages, Δ_{u+}, $\Delta_{0.8u+}$, $\Delta_{0.4u+}$, Δ_{u-}, $\Delta_{0.8u-}$ and $\Delta_{0.4u-}$ for the deflection parameters, θ_{u+}, $\theta_{0.8u+}$, $\theta_{0.4u+}$, θ_{u-}, $\theta_{0.8u-}$ and $\theta_{0.4u-}$ for the rotation parameters.

It is important to note that the results for the asymmetric cyclic tests do not contain parameters regarding negative cycles since, as explained in Section 2.7.2, the deflection was limited in the negative range to allow a larger positive deflection in order to capture strength degradation in the centre-sheathed configuration specimens. The results of the monotonic and cyclic tests for all the specimens tested by the author are listed in Tables 3.1, 3.2 and 3.3. The energies under the positive

and negative backbone curves, E_{BB+} and E_{BB-}, are also presented in these tables. Appendix F provides the results for all the specimens tested in this experimental program, in metric and imperial units.

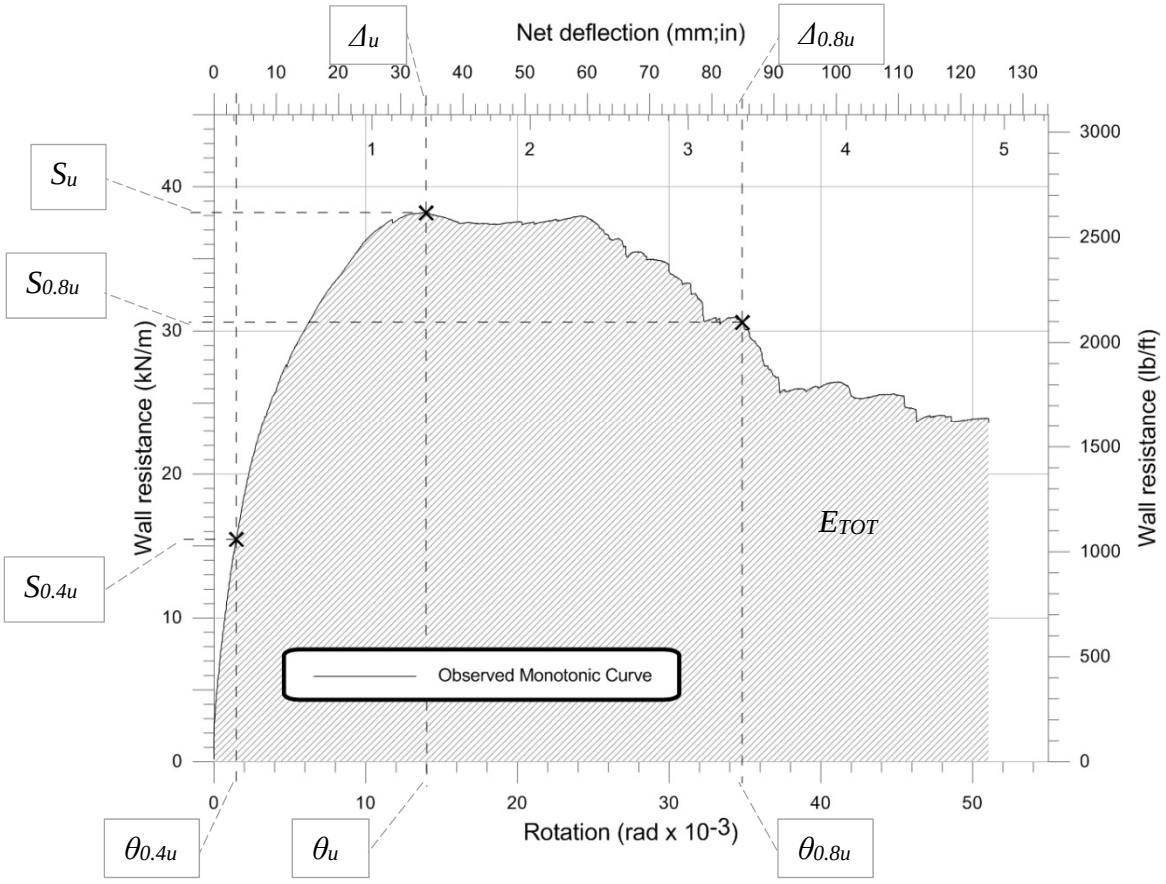

Figure 3.23 Graphic representation of the parameters included in test results

Table 3.1 Test Results Summary (Metric) – Monotonic Tests

Test ID	Ultimate Resistance S_u (kN/m)	Displacement at S_u Δ_u (mm)	Displacement at $0.4S_u$ $\Delta_{0.4u}$ (mm)	Displacement at $0.8S_u$ $\Delta_{0.8u}$ (mm)	Rotation at S_u θ_u (rad.10^{-3})	Rotation at $0.4S_u$ $\theta_{0.4u}$ (rad.10^{-3})	Rotation at $0.8S_u$ $\theta_{0.8u}$ (rad.10^{-3})	Total Energy Dissipated E_{TOT} (J)
Double-Sheathed Wall Configuration								
W28-M	60.99	31.71	5.41	61.82	13.01	2.22	25.35	6463
W29-M	38.22	34.29	3.51	85.01	14.06	1.44	34.86	4674
W30-M	65.42	38.99	7.16	68.70	15.99	2.94	28.17	7248
W31-M	39.29	29.94	3.21	76.18	12.28	1.32	31.24	4783
Centre-Sheathed Wall Configuration								
W18-M	87.22	68.22	10.81	100.0	27.98	4.43	41.02	10481
W18-MR	92.65	87.28	10.83	99.99	35.79	4.44	41.01	11211

Table 3.2 Test Results Summary (Metric) – Positive Cycles of Cyclic Tests

Test ID	Ultimate Resistance S_{u+} (kN/m)	Displacement at S_u Δ_{u+} (mm)	Displacement at $0.4S_u$ $\Delta_{0.4u+}$ (mm)	Displacement at $0.8S_u$ $\Delta_{0.8u+}$ (mm)	Rotation at S_u θ_{u+} (rad.10^{-3})	Rotation at $0.4S_u$ $\theta_{0.4u+}$ (rad.10^{-3})	Rotation at $0.8S_u$ $\theta_{0.8u+}$ (rad.10^{-3})	Total Energy Dissipated E_{TOT} (J)	Backbone Energy E_{BB+} (J)
Double-Sheathed Wall Configuration									
W28-C	61.40	29.54	5.48	50.50	12.12	2.25	20.71	18482	5415
W29-C	40.80	25.71	3.48	40.44	10.55	1.43	16.58	12611	3569
W30-C	70.96	38.20	6.84	59.82	15.66	2.81	24.53	24628	7109
W31-C	45.65	31.86	3.86	48.40	13.07	1.58	19.85	14282	3987
Centre-Sheathed Wall Configuration									
W18-CR	94.75	89.03	13.03	100.0	36.51	5.34	41.01	64012	11079
W23-CR3	162.5	120.4	15.14	100.0	49.40	6.21	41.01	48419	18288
W23B-CR3[1]	158.6	121.6	13.99	100.0	49.87	5.74	41.01	98377	30306
W24-CR3	135.3	81.20	13.50	100.0	33.30	5.54	41.01	76112	14510
W26-CR3[1]	145.3	65.73	12.87	83.53	26.96	5.28	34.25	61059	19176

[1] Asymmetric cyclic test to reach a higher maximum chord rotation

Table 3.3 Test Results Summary (Metric) – Negative Cycles of Cyclic Tests

Test ID	Ultimate Resistance S_{u-} (kN/m)	Displacement at S_u Δ_{u-} (mm)	Displacement at $0.4S_u$ $\Delta_{0.4u-}$ (mm)	Displacement at $0.8S_u$ $\Delta_{0.8u-}$ (mm)	Rotation at S_u θ_{u-} (rad.10^{-3})	Rotation at $0.4S_u$ $\theta_{0.4u-}$ (rad.10^{-3})	Rotation at $0.8S_u$ $\theta_{0.8u-}$ (rad.10^{-3})	Total Energy Dissipated E_{TOT} (J)	Backbone Energy E_{BB-} (J)
Double-Sheathed Wall Configuration									
W28-C	-62.14	-26.43	-6.03	-38.05	-10.84	-2.47	-15.61	18482	4833
W29-C	-39.86	-24.30	-4.90	-37.19	-9.97	-2.01	-15.25	12611	3239
W30-C	-68.59	-31.21	-6.45	-43.97	-12.80	-2.65	-18.03	24628	6203
W31-C	-44.42	-26.53	-3.86	-44.18	-10.88	-1.58	-18.12	14282	3750
Centre-Sheathed Wall Configuration									
W18-CR	-89.91	-70.72	-12.72	-100.1	-29.00	-5.22	-41.03	64012	9775
W23-CR3[1]	-131.8	-50.32	-11.13	-50.32	-20.64	-4.56	-20.64	48419	5074
W24-CR3	-127.5	-77.97	-11.91	-100.0	-31.97	-4.88	-41.01	76112	13367

[1] Protocol stopped during test; negative cycles not completed. Maximum negative displacement reached is 50 mm (1.97")

Note: Appendix F contains Tables 3.1 to 3.3 with results in imperial units.

3.5 Comparison of the Influence of Protocols, Configurations and Building Parameters

The testing of two different shear wall configurations allowed for their comparison in this experimental program. Considering that the objective of this study was to find a way to achieve greater strength and ductility, the building parameters of the shear walls influenced their overall behaviour. Thus, the configuration itself made a great impact on the behaviour of the specimens. In addition, the different parameters (thicknesses, screw spacing and screw size) also impacted the behaviour of the specimens. This section presents the main differences in shear wall response to load observed throughout the experimental program, as well as a brief comparison with the specimens tested by Rizk *(2017)*, which adhered to the configuration currently available in the AISI S400 Standard. Appendix F provides a summary of all the results from monotonic and cyclic tests for both shear wall configurations.

3.5.1 Influence of Protocols

As some centre-sheathed configuration specimens were only tested under a cyclic protocol, data coming from the cyclic tests were used when available, in order to compare specimens more easily. For double-sheathed configuration specimens, monotonic and cyclic tests exhibited differences in terms of behaviour when comparing their respective curves (Figure 3.24). The specimens built with the same parameters all showed a higher ultimate shear resistance but a quicker strength degradation throughout the cyclic tests. The test observations of these specimens showed the screw connections pulled through the sheathing when the tear-shape holes generated by extensive steel bearing damage at the fastener locations appeared on the sheathing. The subsequent alternative positive and negative displacement cycles allowed for the screws to escape through these holes, resulting in a quick loss of strength. This phenomenon did not happen in monotonic tests because wall specimen was being pulled in a single direction, causing bearing damage in that same direction, and therefore avoiding the possibility of the sheathing pulling over the screw head when the applied displacement was reversed.

The sheathing, being confined in built-up frame members for the centre-sheathed configuration specimens, was restrained in place, and therefore the monotonic and cyclic behaviour were

relatively similar (Figure 3.25). However, as for the double-sheathed configuration specimens, the configuration showed a higher ultimate shear strength during the cyclic test.

The cyclic test results for the double-sheathed configuration specimens produced positive and negative backbone curves showing a similar behaviour. Nonetheless, the negative cycles showed ultimate strengths slightly inferior to the positive cycles (Tables 3.2 and 3.3). The cyclic protocol started with a positive lateral displacement, therefore a full cycle always started with a positive displacement, leading to damage in the sheathing. Thus, the subsequent negative cycles were applied to a wall with a sheathing already suffering from damage, hence the slightly inferior shear resistance.

The use of two different cyclic protocols (Section 2.7.2) for the centre-sheathed configuration specimens (W15-CR3 and W23-CR3 tested with CUREE reversed cyclic protocol, W15B-CR3 and W23B-CR3 tested with the asymmetric cyclic protocol) did not modify their behaviour. Figure 3.26 shows the same nominal wall building parameters tested with both protocols. Given the similarity of the cyclic curves in the positive cycles, the two backbone curves could be superimposed for the common range of motion.

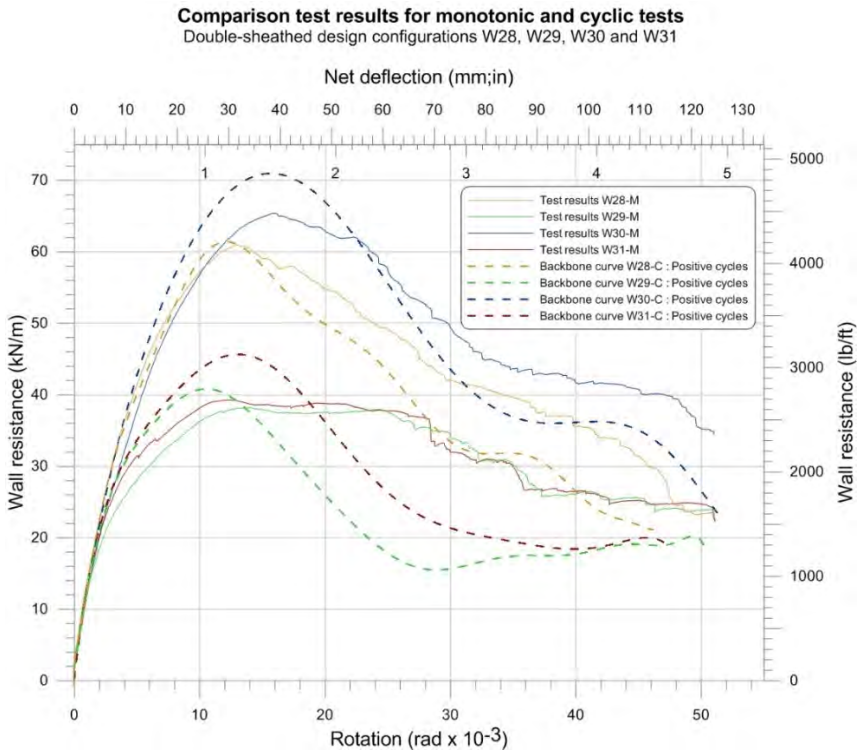

Figure 3.24 Monotonic and cyclic force vs. deformation behaviour of double-sheathed configuration specimens

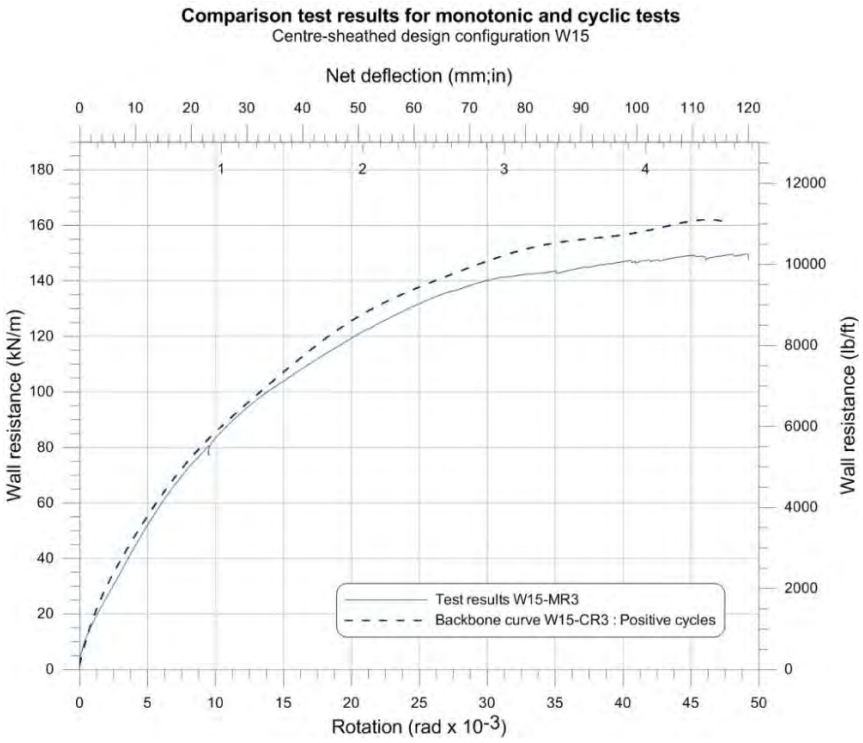

Figure 3.25 Monotonic and cyclic behaviours of centre-sheathed configuration specimens

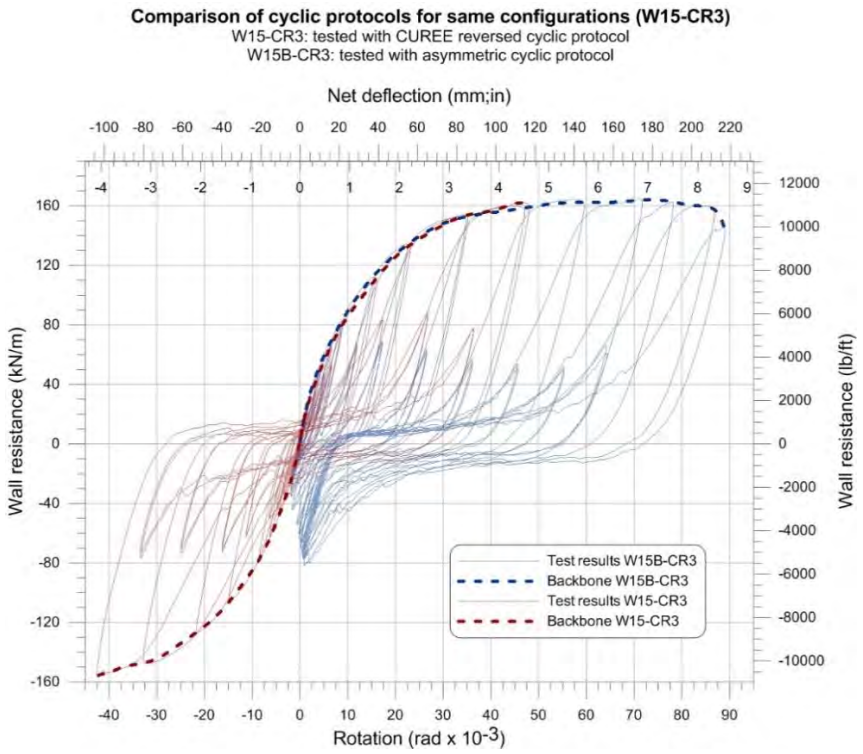

Figure 3.26 Specimens W15-CR3 and W15B-CR3 tested with two different protocols

3.5.2 Influence of the Configuration: double-sheathed vs. centre-sheathed

The greatest impact made on the behaviour of the specimens came from their configuration itself. Figure 3.27 compares the force vs. deformation backbone curves of two specimens (W31-C & W23B-CR3) presenting the same parameters: framing thickness of 2.46 mm (0.097”), No. 12 sheathing screws with a 100 mm (4”) spacing, sheathing thickness of 1.09 mm (0.043”) for the centre-sheathed configuration and 2×0.47 = 0.94 mm (0.037”) for the double-sheathed configuration. Although the sheathing from the centre-sheathed configuration was 16% thicker than the combined thicknesses of the two sheathing panels used for the double-sheathed configuration walls, they were directly compared to one another in terms of performance using thick sheathing. When comparing a centre-sheathed configuration specimen tested under asymmetric cyclic protocol with a specimen tested under the CUREE reversed cyclic protocol, only the positive cycles were considered for the latter.

The centre-sheathed configuration specimen W23B-CR3 showed a maximum shear resistance of 158.6 kN/m (10866 lb/ft), 3.47 times higher than that from the wall with corresponding building

parameters using a double-sheathed configuration (45.65 kN/m (3128 lb/ft)). The ultimate shear resistance was reached at a lateral displacement of 120 mm (4.72”) for the centre-sheathed configuration (drift of 4.9%) whereas it was reached at 30 mm (1.18”) for the double-sheathed wall (drift of 1.2%). The ductility of the centre-sheathed configuration specimen was substantially higher; when the double-sheathed configuration specimen reached its maximum shear strength (at the onset of strength degradation), the centre-sheathed configuration specimen was still acting relatively elastically, resisting 107 kN/m (7330 lb/ft) at the same lateral displacement. The double-sheathed specimen had lost 50% of its shear strength at a lateral displacement of 68 mm (2.68”, drift 2.8%) whereas the centre-sheathed configuration was still gaining resistance, reaching 145 kN/m (9935 lb/ft). The latter had lost 50% of its shear strength once reaching a lateral displacement of 185 mm (7.28”, storey drift 7.6%).

The strongest specimen (W15B-CR3) behaved even better, reaching a maximum shear resistance of 165.7 kN/m (11352 lb/ft) at a lateral displacement of 160 mm (6.3”) (drift of 6.6%) and experiencing an onset of strength degradation after reaching a lateral displacement of 180 mm (7.1”) (drift of 7.4%). This specimen is fully presented in Santos *(2017)*.

The substantial difference in terms of strength and ductility exhibited between the two configurations was related to the fact that one confines the sheathing all around its perimeter, whereas the other did not. The double-sheathed configuration tests showed a majority of screws pulling through the sheathing after high bearing damage, completely losing their contribution to the shear strength of the specimen. Besides, the larger edge spacing of the centre-sheathed configuration (50.8 mm (2”) vs. 9.5 mm (3/8”) for the double-sheathed configuration) most certainly had an impact on the extent of bearing damages the sheathing can undergo.

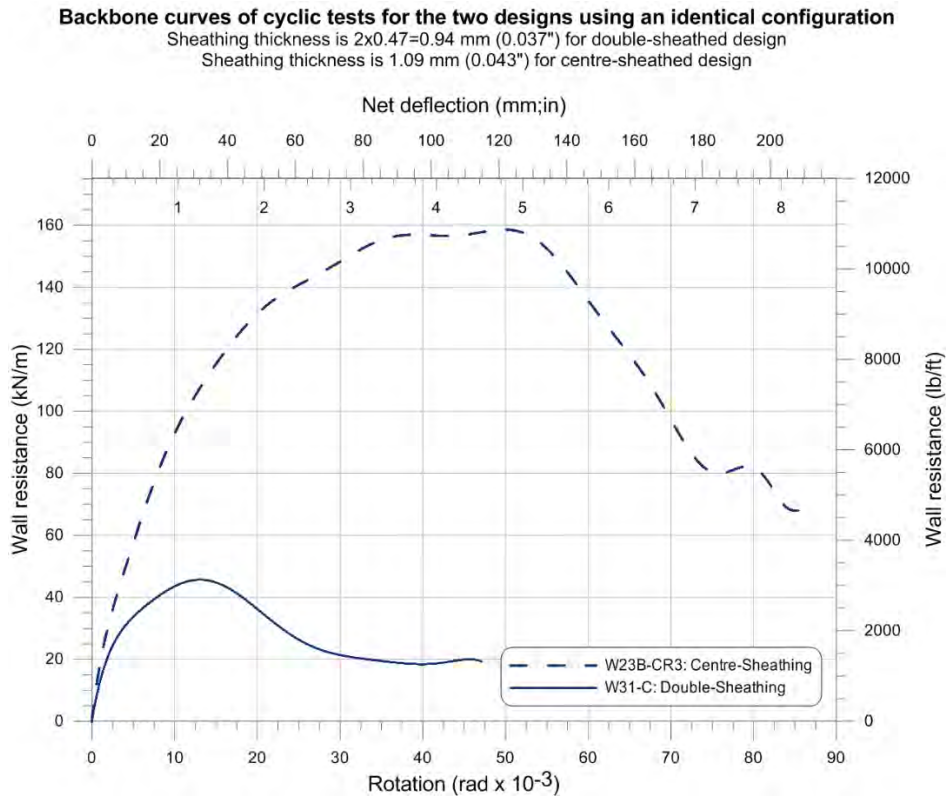

Figure 3.27 Force vs. deformation test results (backbone curves) from the two shear wall configurations constructed using nominally comparable components

3.5.3 Influence of the Shear Wall Building Parameters

Both shear wall configurations were tested using different building parameters, varying the sheathing thickness, screw spacing or screw size. While not modifying the general behaviour of the specimens, each parameter had an influence on the ultimate shear strength and the level of strength degradation the specimen underwent during the test. This section compares the specific behaviours related to the variation of these parameters.

Although the specimens tested by the author present the same framing thickness, two different framing thicknesses were used during this experimental program. The influence of the framing thickness on the shear strength and the ductility of a specimen is explained in Santos *(2017)*. Selected results from Santos *(2017)* are used in this chapter for specific comparison purposes.

3.5.3.1 Influence of the sheathing thickness

The use of a thicker sheathing member resulted in an increase of the ultimate shear strength of the specimen. Figure 3.28 compares specimens using different sheathing thicknesses for both configurations. The parameters in this comparison are nominally identical (except for the sheathing thickness) for specimens built with the same configuration. As the major part of the shear resistance comes from the bearing strength of the sheathing screw connections, the increase of the sheathing thickness resulted in a higher shear strength; indeed, the bearing strength for each connection is directly related to the thickness of the material fastened (see *Nominal capacity of individual fastener* in the Effective Strip Method detailed in Appendix D).

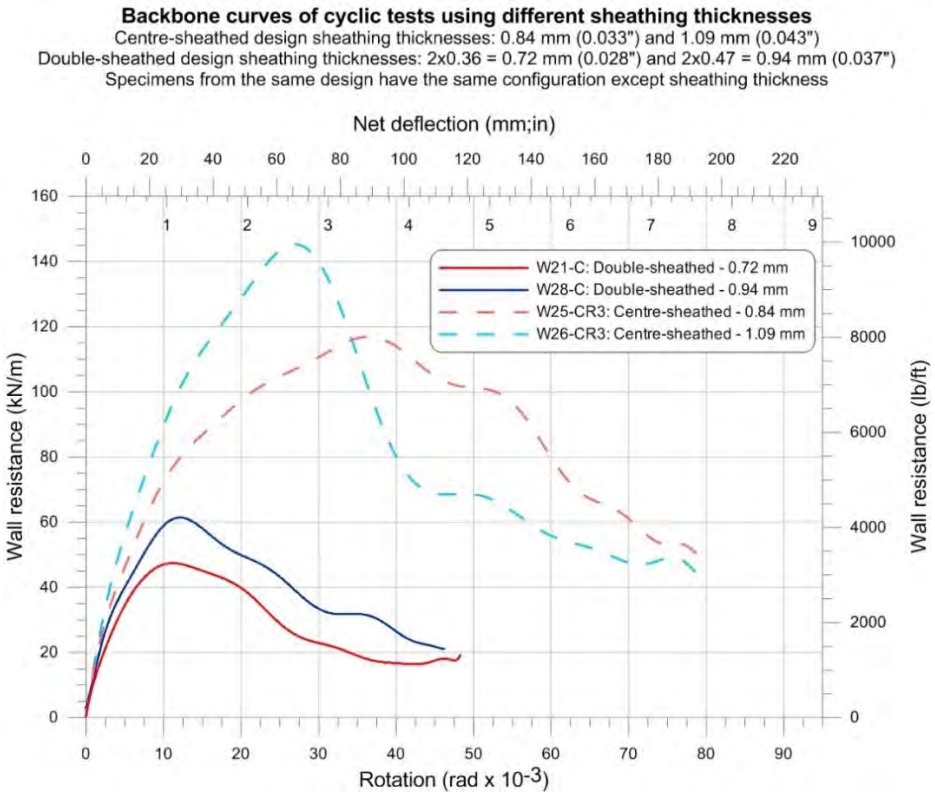

Figure 3.28 Test results from the two shear wall configurations using different sheathing thicknesses

3.5.3.2 Influence of the sheathing screw spacing

The screw spacing had an impact on both configurations; reducing the screw spacing increased the ultimate shear resistance of the specimens (Figure 3.29). For the double-sheathed configuration, specimens W30-C and W31-C presented a different screw spacing as their unique difference: 50.8 mm (2") for the W30-C and 101.6 mm (4") for the W31-C. In the same way, centre-sheathed configuration specimens W23-CR3 and W24-CR3 had a screw spacing of 101.6 mm (4") and 152.4 mm (6") respectively. The sheathing screws are the essential elements used for transferring the nominal shear force applied at the top of the wall through the sheathing; therefore reducing the sheathing screw spacing (i.e. increasing the number of sheathing screws) resulted in an increase of the ultimate strength and the ductility of the specimens, regardless of the configuration. However, the ductility increment is even greater for the centre-sheathed configuration, where the confined sheathing was able to undergo extensive bearing damage at each fastener location. Reducing the screw spacing gave this centre-sheathed specimen a greater ability to deform in the inelastic range without undergoing force degradation (within the range of lateral displacement allowed by the actuator (± 125 mm (± 5)).

In addition for the centre-sheathed configuration, the larger screw spacing pattern (152.4 mm (6")) did not provide enough strength to avoid the built-up chord stud to split (Section 3.2.3.2 and Figure 3.14), therefore failing the latter. This explains the difference in terms of ductile behaviour between the two centre-sheathed specimens: the strength degradation observed for W24-CR3 after a 80 mm (3.15") lateral displacement applied at the top of the wall, did not occur for W23-CR3 where the smaller screw spacing of 101.6 mm (4") provided enough resistance to keep the built-up chord studs together throughout the test.

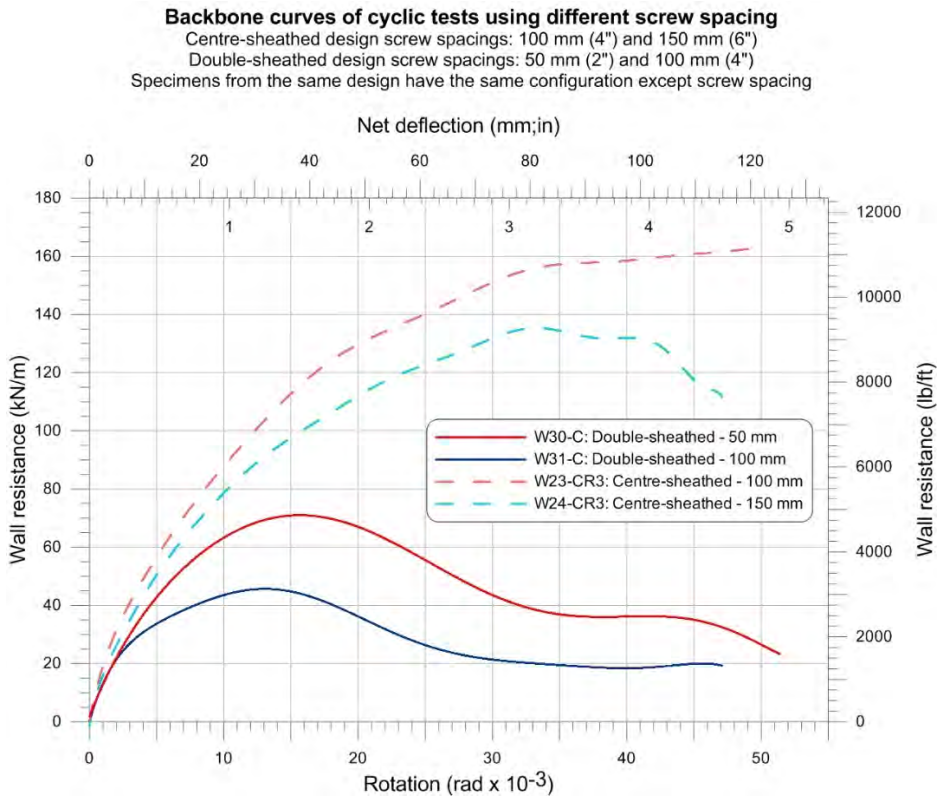

Figure 3.29 Test results from the two shear wall configurations using different sheathing screw spacing

3.5.3.3 Influence of the sheathing screw diameter

Increasing the diameter of the sheathing screws resulted in an increased ultimate shear strength of the wall, as well as a better overall ductility for both configurations (Figure 3.30). The two double-sheathed configuration specimens W28-C and W30-C present a screw spacing of 50.8 mm (2”) and the centre-sheathed configuration specimens W26-CR3 and W23B-CR3 present one of 101.6 mm (4”). Again, the bearing strength of a screw connection is directly related to the diameter of the fastener; increasing the diameter increased the bearing strength of each connector and therefore improved the ultimate shear strength of the wall.

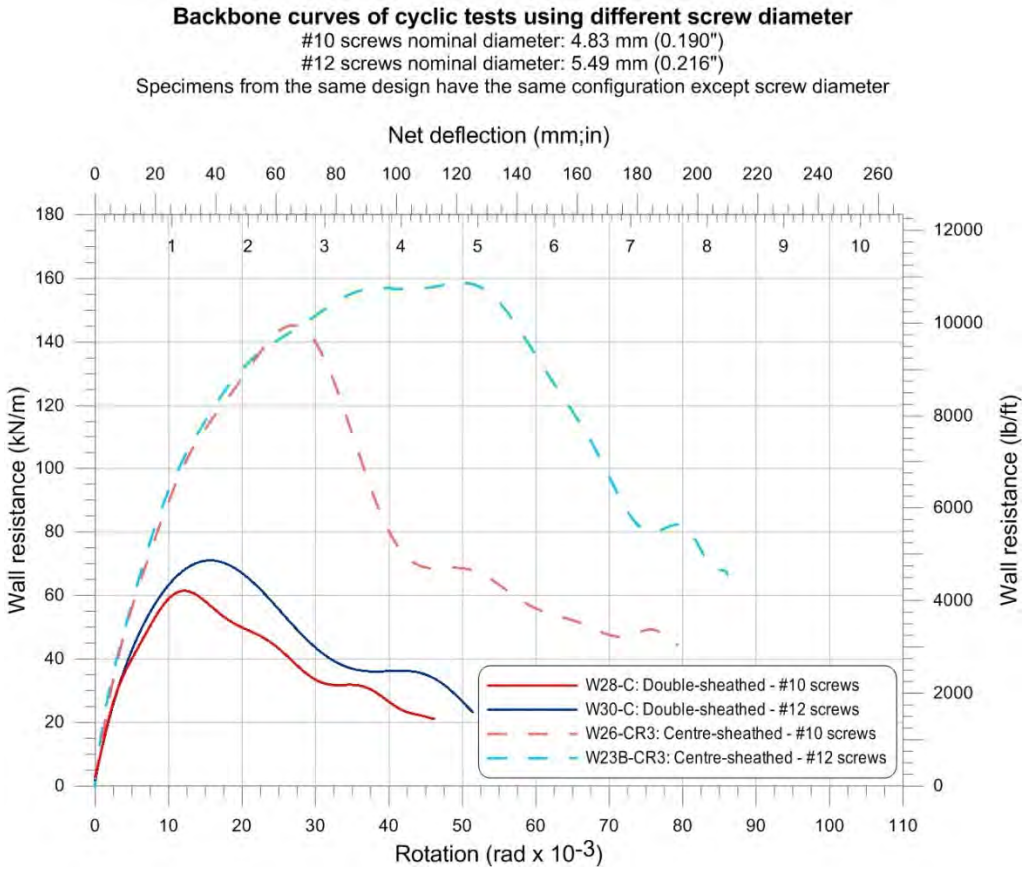

Figure 3.30 Test results from the two shear wall configurations using different screw diameter

3.5.3.4 Effect of chord stud reinforcement for centre-sheathed walls

In order to prevent the chord studs from failing due to a significant increase in shear strength for the centre-sheathed configuration specimens, and corresponding increase in moment and axial compression force, various reinforcement schemes were tried throughout the experimental test program (Section 2.2.3). Specimen W18-M was built using the original frame configuration using unreinforced chord studs; strength degradation (Figure 3.31) was observed after a 60 mm (2-3/8") lateral displacement, whereas specimen W18-MR, which was built with the first level of chord stud reinforcement, did not show strength degradation until reaching 80 mm (3-1/8") lateral displacement.

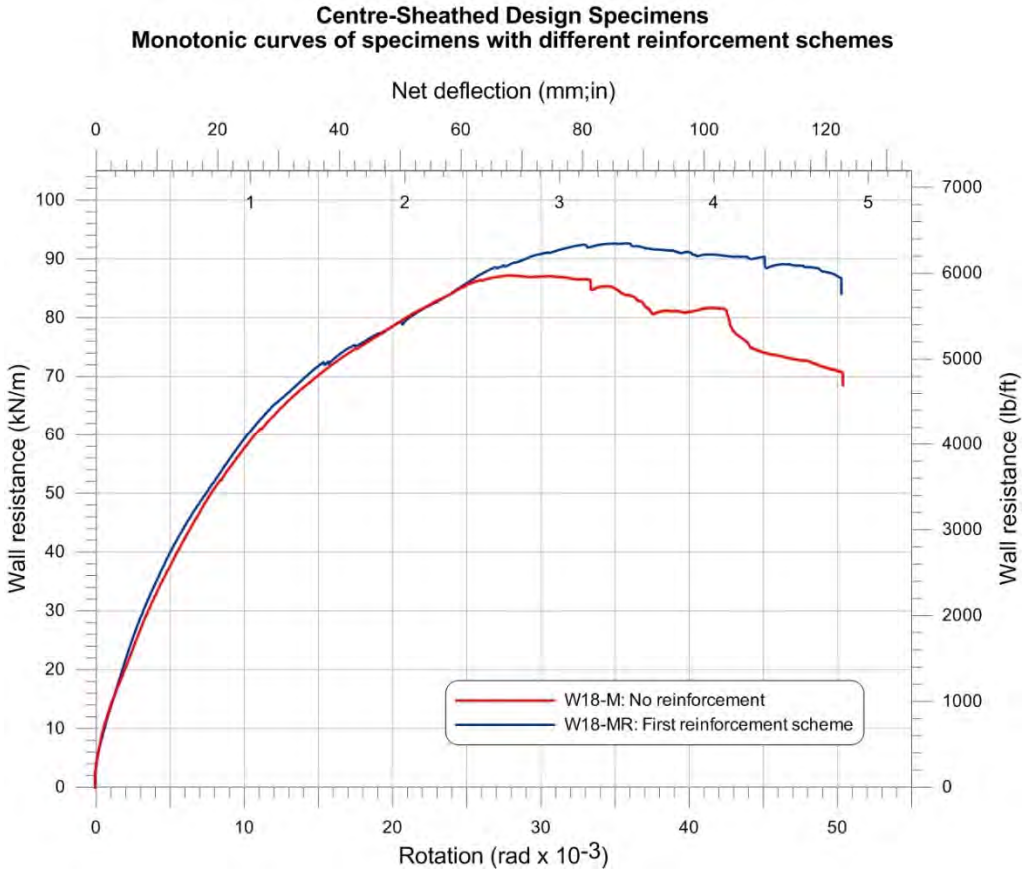

Figure 3.31 Centre-sheathed configuration monotonic test results showing behaviour of specimens with different chord stud reinforcement schemes (None & R)

When testing the first chord stud reinforcement scheme on W16-MR, using a reduced screw spacing (i.e. specimen presenting a higher shear strength as per Section 3.5.3.2), the chord stud failed due to the combination of higher compressive axial load and bending moment resulting from the higher shear strength. A similar result was observed going from wall W17-M and W17-C to wall W18-M (screw spacing of 152.4 mm (6”) for W17 test specimens and a screw spacing of 101.6 mm (4”) for W18 test specimens). Specimen W16-MR showed a shear strength up to 124.6 kN/m (8537 lb/ft) before experiencing chord stud failure on the compression side (Figure 3.32), whereas W18-MR validated the first reinforcement scheme for a limited ultimate strength of 92.7 kN/m (6349 lb/ft). The stronger chord stud allowed greater shear force to be applied to the wall, but the reinforcement was not adequate to maximize the wall’s shear resistance. Hence, a new reinforcement scheme was needed. Specimen W16-MR2 was built with the second level of reinforcement. Although it achieved a 129.6 kN/m (8880 lb/ft) shear resistance, an increase of 4% compared to the previous reinforcement scheme, the chord stud on the compression side failed once again under combined axial force and bending moment, leading to the same conclusion made after testing W16-MR. Wall W15-MR3 was then built using the third (and final) level of reinforcement (built-up box members attached on the outside of the chord studs (Section 2.5.2)). It showed a higher ultimate shear strength (149.8 kN/m (10264 lb/ft); +20.2% compared to W16-MR), no strength degradation within the lateral displacement range limited by the actuator and a better ductility.

The higher level of reinforcement had a positive side effect; although the main objective was to reinforce the chord studs to prevent them from failing under combined compressive axial force and bending moment, the reinforcement schemes also allowed for an increase in the ultimate shear resistance of the specimens. This was achieved because keeping the chord studs from failing allowed for the use of the extensive bearing resistance of the confined sheathing.

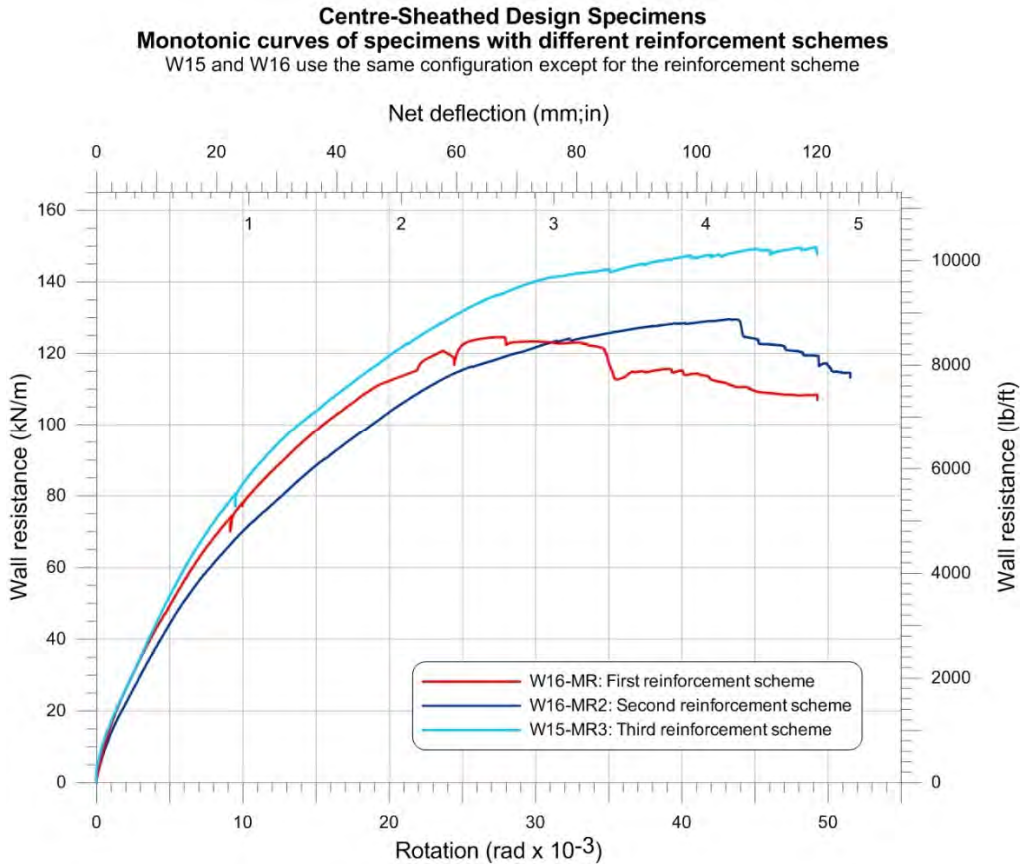

Figure 3.32 Centre-sheathed configuration monotonic test results showing behaviour of shear wall specimens with different reinforcement schemes (MR, MR2 & MR3)

3.5.4 Comparison with previous configurations

The shear wall configurations from this experimental program both showed an increase in terms of strength and ductility compared to what is currently listed in the AISI S400 Standard. Using thicker sheathing as well as thicker framing and larger screws improved the overall behaviour of the specimens, but the innovative configurations used to build them helped even more in terms of achieving the better strength and ductility exhibited by the walls.

The stronger double-sheathed configuration specimen showed an ultimate shear strength about twice the maximum listed in AISI S400, whereas the centre-sheathed configuration specimen showed an ultimate shear strength about four times that currently available. Moreover, the strongest centre sheathed specimen allowed for almost 8% drift (7.75% approximately, based on the backbone curve obtained from the cycles) before experiencing strength degradation.

El-Saloussy *(2010)* analysed US test data from Yu et al. *(2007)* and Yu and Chen *(2009)* using the same EEEP analysis approach as that used in this program. The ninety-six tested specimens comprised various building parameters, similar to those used in the calibration of the Effective Strip Method from the AISI S400 Standard. Many of the specimens analysed by El-Saloussy *(2010)* had the same aspect ratio as those included in the present experimental program, i.e. 1:2 (specimens with dimensions of 4"×8"), and can therefore be compared to one another. The observations made from this previous tests showed 95% of the monotonic tests analysed (19/20) had seen their shear strength dropping to 80% of the ultimate load before reaching 4.1% drift (100 mm (4")), when all the cyclic test specimens had seen their shear strength dropping to 80% of the ultimate load even before the 100 mm (4") lateral displacement. The highest overall shear strength reached by a specimen analysed in El-Saloussy *(2010)* was 20.41 kN/m (1398 lb/ft) (average between positive and negative cycles); the resistance of this same specimens dropped to 80% of the ultimate load post-peak at 2.6% drift, i.e. 62.45 mm (2.5").

The strongest and most ductile specimen tested in the present experimental program is the centre-sheathed configuration specimen W15B-CR3, using a 0.84 mm (0.033") thick sheathing and #10 screws at a 50.8 mm (2") spacing. It exhibited a shear strength superior to 160 kN/m (10962 lb/ft) between 5.0% and 8.3% drift, i.e. 122 mm (4.8") and 203 mm (8") lateral displacements, and the onset of strength degradation started beyond 7.75% drift. The centre-sheathed configuration allowed for a considerable gain in ductility, in addition to sustaining higher shear strengths.

To summarize, the walls analysed by El-Saloussy *(2010)* had their strength and ductility significantly lower than those exhibited by the new configurations presented in this experimental program.

3.6 Material Characterization Coupon Tests

Coupons were milled from the material used throughout this experimental program in order to check and validate the mechanical properties. As different thicknesses were used, members were formed with material coming from different zinc-coated coils (see Section 2.5 for detailed thicknesses and steel grades). Three (or two depending on the availability) samples were taken from members obtained from each coil. In the case of the sheathing members, samples were taken according to the longitudinal and transversal directions (three samples per direction), except for sheathing D which presents values for only the longitudinal direction.

The material properties were determined by completing tensile tests according to ASTM A370 *(2017)* requirements. Marks spaced at 50.8 mm (2") were punched on the coupons prior to testing in order to measure the elongation after completion of the test. The elongation of each sample was monitored during the test using a 50 mm (2") extensometer, whereas one sample from each coil was equipped with two additional strain gauges (one on each side) in the longitudinal direction to define the elastic region with a higher precision. A strain rate of 0.002 mm/s was used in the elastic range, increased to 0.01 mm/s while going through the plastic plateau region. A final rate of 0.1 mm/s was then used when entering the strain hardening region until the end of the test.

In order to measure the base metal thickness of the samples and compute the mechanical properties, the zinc coating was removed from the grip section of the coupons using a 25 % hydrochloric acid solution after completion of the tensile tests. Table 3.4 presents the results obtained for all the samples tested, in metric units. The results in imperial units can be found in Appendix F.

The tests showed greater base thicknesses than the nominal values except for the thinner sheathing specimens (sheathing B and C). All the samples exhibited higher strengths than specified by the manufacturer, except for the tensile strength of track and strip specimens which exhibited an ultimate strength equivalent to the one specified.

According to Supplement 1 of AISI S400-15, A653/A653M grades 33 and 50 have to provide a F_u/F_y ratio not less than 1.15, as well as an elongation not less than 12 % measured based on the original 50.8 mm (2") punched marks on the sample. The ratio of expected yield stress to specified minimum yield stress as well as the one of expected tensile strength to specified minimum tensile

strength are provided by Table A3.2-1 of AISI S400-15 (R_y and R_t respectively) for the existing grades of steel. These values are:

- A653/A653M grade 33 : $R_y = 1.5$ and $R_t = 1.2$
- A653/A653M grade 50 : $R_y = 1.1$ and $R_t = 1.1$

Table 3.4 shows that the sheathing B and C did not satisfy the F_u/F_y ratio since the average values between longitudinal and transversal values are inferior to the 1.15 criteria. Besides, the tests showed smaller R_y and R_t values for all the samples coming from the sheathing members as well as smaller R_t values for all the samples coming from the framing members. However, every sample satisfied the elongation criteria of 12 %.

Table 3.4 Summary of Material Properties (Metric)

Specimen	Nominal thickness, t_n (mm)	Base metal thickness, t_b (mm)	Nominal yield strength, F_{yn} (MPa)	Nominal tensile strength, F_{un} (MPa)	Measured yield strength, F_y (MPa)	Measured tensile strength, F_u (MPa)	F_u/F_y	Elongation (%)	R_y	R_t
Sheathing A Transversal dir.	0.84	0.88	230	310	302	352	1.17	40	1.3	1.1
Sheathing A Longitudinal dir.	0.84	0.87	230	310	276	358	1.30	39	1.2	1.2
Sheathing B Transversal dir.	0.48[1]	0.48	230	310	318	361	1.14	38	1.4	1.2
Sheathing B Longitudinal dir.	0.47[1]	0.47	230	310	340	368	1.08	39	1.5	1.2
Sheathing C Transversal dir.	0.36[1]	0.36	230	310	344	370	1.07	29	1.5	1.2
Sheathing C Longitudinal dir.	0.36[1]	0.36	230	310	305	358	1.18	26	1.3	1.2
Sheathing D	1.09	1.12	230	310	316	380	1.20	32	1.4	1.2
Strip	1.09	1.11	345	450	366	447	1.22	30	1.1	1.0
Stud A / Track A	1.73	1.77	345	450	386	466	1.21	34	1.1	1.0
Track B	2.46	2.54	345	450	380	451	1.19	35	1.1	1.0
Stud B	2.46	2.54	345	450	389	461	1.19	34	1.1	1.0

[1] Non standard thickness, no nominal value

CHAPTER 4 – INTERPRETATION OF THE TEST RESULTS - DISCUSSION

4.1 Introduction

Cold-formed steel sheathed shear walls have a nonlinear force / deformation behaviour; the innovative configurations tested in this program did not behave otherwise. As for the previous experimental programs on the matter realized at McGill University (e.g. Balh et al. *(2014)*, Ong-Tone *(2009)*, Balh *(2010)*, DaBreo *(2012)* and Rizk *(2017)*), the Equivalent Energy Elastic Plastic (EEEP) method (Park *(1989)*;Foliente *(1996)*) was used to describe the behaviour of the specimens with a bilinear elastic-plastic curve and evaluate design properties such as the yield force, stiffness, ductility, etc. Indeed, Branston *(2004)* showed that the EEEP model best represented the behaviour of cold-formed steel framed / wood sheathed shear walls for monotonic and any reversed cyclic loading protocol. It has then been used for cold-formed steel sheathed shear walls providing consistency in the data analysis of the different programs. The AISI S400 Standard *(2015)* contains provisions for the design of shear walls with steel sheathing; the Canadian design values were all determined from data that was analysed using the EEEP approach. This however, is not the case for the design values listed for the USA and Mexico, nor was the EEEP approach accounted for in the development of the effective strip method by Yanagi and Yu *(2014)*, where the design parameter considered is the ultimate shear resistances obtained during the test programs.

4.2 Equivalent Energy Elastic Plastic (EEEP) Method (Canada)

The main concept of this method relies on the idea that the energy dissipated during a test (monotonic or cyclic) is represented by the area under the force-displacement curve, which is also equal to the energy represented by the area under the bilinear curve obtained using the EEEP method. The energy considered here is the energy dissipated by the specimen until reaching 80 % of the ultimate load after the latter had been obtained ($0.8 \times S_u$ post-peak); once this post-peak load is reached, failure of the specimen (ultimate displacement) is considered to have occurred. Therefore, the highly nonlinear behaviour of the specimen is transformed into a perfectly elastic / plastic behaviour dissipating the same amount of energy within this definite range. The main parameters necessary to create the EEEP curve are the ultimate wall resistance, S_u, the wall

resistance at 80% of S_u post-peak, $S_{0.8u}$, the wall resistance at 40% of S_u pre-peak, $S_{0.4u}$, and their respective displacements Δ_u, $\Delta_{0.8u}$ and $\Delta_{0.4u}$ (Figure 4.1). The red and green areas on Figure 4.1 are equal, meaning the energy dissipated by the specimen within the interval [0;$\Delta_{0.8u}$] is the same than the energy dissipated by the EEEP curve on that same interval.

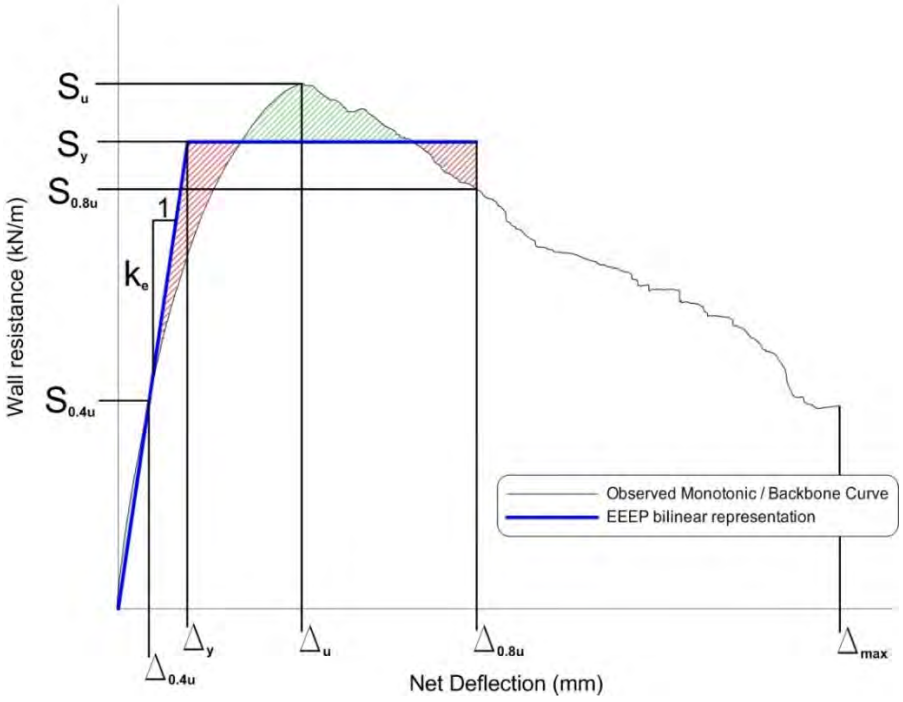

Figure 4.1 Equivalent Energy Elastic-Plastic (EEEP) bilinear model

Two cases had to be considered due to the highly resistant and ductile specimens tested during the experimental program; the 80 % ultimate load post-peak could sometimes not be reached within a realistic deflection range, or was never reached at all. Thence, the ultimate EEEP displacement is written $\Delta_{u(EEEP)}$ to differ from the displacement at 80 % of the ultimate load post-peak, $\Delta_{0.8u}$, originally considered as the ultimate displacement in the original EEEP method. In any case, the main concept of the EEEP method is satisfied as the green and red areas are equal (Figures 4.2 and 4.3).

Accordingly with the aforementioned works on the subject realized at McGill University, the different procedures were as follows:

- If $\Delta_{0.8u} < 100\ mm$ (4"), $\Delta_{u(EEEP)} = \Delta_{0.8u}$ (Figure 4.2);
- If $\Delta_{0.8u} > 100\ mm$ (4") or if $S_{0.8u}$ is never reached, $\Delta_{u(EEEP)} = 100\ mm$ (4") (Figure 4.3);

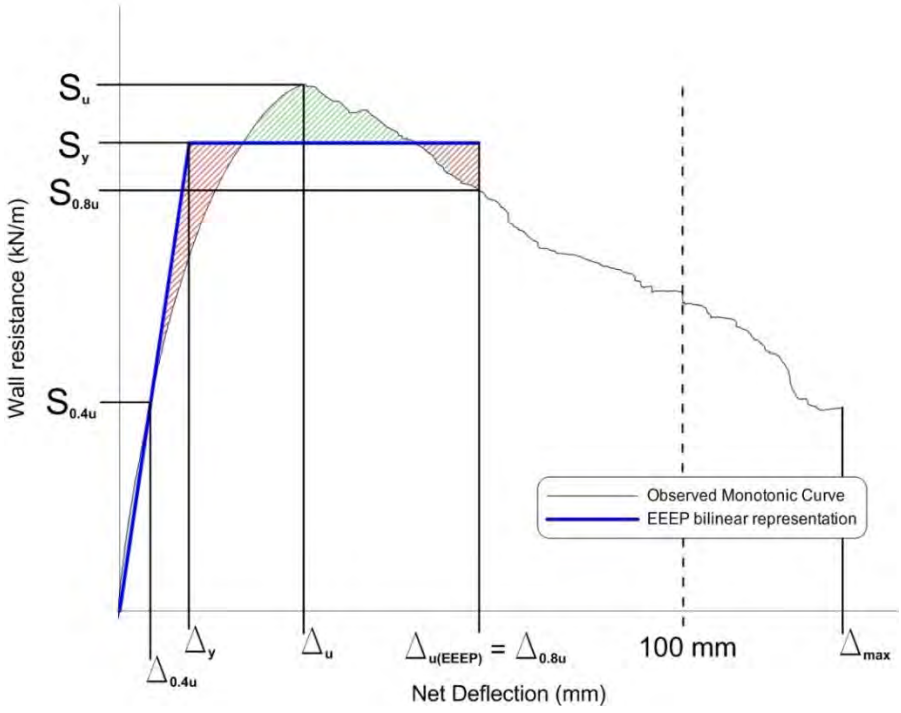

Figure 4.2 EEEP model and definition of $\Delta_{u(EEEP)}$ for case 1

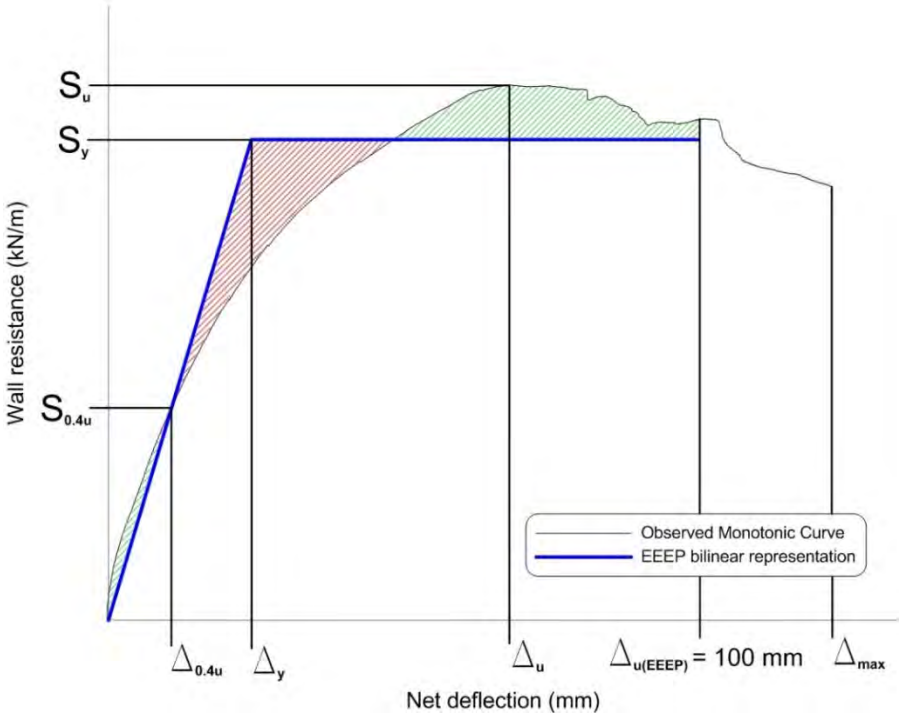

Figure 4.3 EEEP model and definition of $\Delta_{u(EEEP)}$ for case 2

The 2.5 % storey-drift limit criterion of the ASCE/SEI 7 *(2016)* and the NBCC *(2015)* was approached in Section 2.7.2 when defining the cyclic protocols. However, choosing an ultimate displacement corresponding to this limit would be too conservative; the specimens concerned either reached their ultimate resistance after that limit or had a good reserve of energy after that same limit. That is the reason why the ultimate displacement was fixed at 100 mm (4") which corresponds to a 4 % storey-drift approximately. Although some specimens did not even reach their ultimate resistance within this limit (some reaching it around an 8 % storey-drift), taking a limit greater than 4 % would not be realistic since no building is expected to exhibit such displacements during a seismic event.

The design properties used to create the EEEP curve had to be defined based on the test results. The elastic stiffness, k_e, was calculated based on the test results taken at 40 % of the ultimate load where the specimens were considered to be operating in the elastic range (Equation 4.1). Figure 4.4 shows the parameters used in the equations defining the EEEP curve. The yield wall resistance, F_y, is one of the solutions of the quadratic equation resulting from the relation of mathematical equality between the area under the observed curve and the area under the EEEP curve (hatched areas on Figure 4.4) on the interval [0;$\Delta_{u(EEEP)}$] (Equation 4.2). The slope of the triangle being k_e, it gives $F_y = k_e \times \Delta_y$, therefore the corresponding yield displacement, Δ_y, can be defined by Equation 4.3.

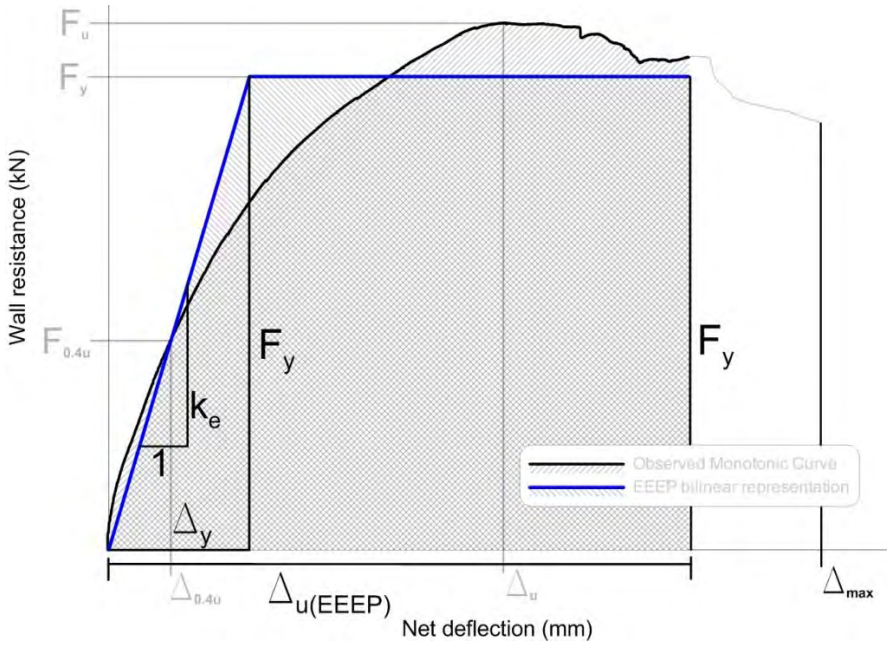

Figure 4.4 Parameters defining the EEEP curve

The ductility, μ, was calculated to characterise the ductile behaviour of the tested specimens. Its original equation compares the displacement, $\Delta_{0.8u}$, with the yield displacement, Δ_y. However, as $\Delta_{0.8u}$ could not always be reached, μ was computed following equations 4.4 and 4.5.

$$k_e = \frac{0.4 \times F_u}{\Delta_{0.4u}} \qquad \text{Eq. 4.1}$$

$$F_y = \frac{-\Delta_{u(EEEP)} \pm \sqrt{\Delta_{u(EEEP)}{}^2 - \frac{2A}{k_e}}}{-\frac{1}{k_e}} \qquad \text{Eq. 4.2}$$

If $\Delta_{u(EEEP)}{}^2 < \frac{2A}{k_e}$, it is permitted to assume $F_y = 0.85\ F_u$ (ASTM E2126, *(ASTM. 2011)*)

$$\Delta_y = \frac{F_y}{k_e} \qquad \text{Eq 4.3}$$

$$\mu = \frac{\Delta_\mu}{\Delta_y} \qquad \text{Eq 4.4}$$

$$\Delta_\mu = \begin{cases} \Delta_{0.8u}\ if\ \Delta_{0.8u} \neq \emptyset \\ \Delta_{max}\ if\ \Delta_{0.8u} = \emptyset \end{cases} \qquad \text{Eq 4.5}$$

where,

k_e = Elastic stiffness;

F_u = Ultimate wall resistance;

F_y = Yield wall resistance;

A = Area under the observed curve up to $\Delta_{u(EEEP)}$;

μ = Ductility of specimen;

$\Delta_{u(EEEP)}$ = Ultimate EEEP displacement;

Δ_{μ} = Ductility displacement;

Δ_y = Yield displacement at S_y (F_y);

$\Delta_{0.4u}$ = Displacement at $0.4S_u$ ($0.4F_u$) pre-peak;

$\Delta_{0.8u}$ = Displacement at $0.8S_u$ ($0.8F_u$) post-peak;

Δ_{max} = Ultimate displacement at the end of the test.

The EEEP curve is created based on the observed test results for the monotonic tests and on the backbone curves (positive and negative) for the cyclic tests. As explained in Section 3.3, a backbone curve can be assimilated to an equivalent monotonic curve, thus cyclic tests can then be analysed as per the monotonic tests. Figures 4.5 and 4.6 show the EEEP curves for a monotonic and a cyclic test respectively. The analysis was realised using two MATLAB scripts (one for each kind of test) and the design properties (metric units) for the configurations tested by the author are presented in Tables 4.1, 4.2 and 4.3. They provide the yield resistance of each specimen, S_y, the displacements at $0.4S_u$ and S_y as well as the corresponding chord rotations, $\Delta_{0.4u}$, Δ_y, $\theta_{0.4u}$, and θ_y, the elastic stiffness, k_e, the ductility, μ, and the energy dissipated by the EEEP curve, E_{EEEP}. The script for the cyclic tests created the backbone curves, then analysed these data to provide the EEEP results presented in Table 4.2 for the positive cycles and Table 4.3 for the negative ones. Full results in metric and imperial units as well as the representations of all EEEP and time history curves for the lateral deflection, the wall resistance developed and the cumulative energy dissipated are presented in Appendix G.

Cyclic protocols could not be completed in full for the specimens W18-CR and W23-CR3. The first experienced technical issues with the actuator while reaching 90 mm (3.54”) and had to be

stopped. Therefore, it was decided to run the larger cycle (±120 mm (±4.72")) by manually pushing then pulling the wall at a low displacement rate as is illustrated by the time history curves in Figure G-5 in Appendix G. While testing the specimen W23-CR3, built with the ultimate reinforced configuration for centre-sheathed specimens, the very high forces reached (158.7 kN (35.68 kips)) displacing the wall in the ±60 mm (±2.36") primary cycle caused the top of the wall to twist around its vertical axis as it was being pushed by the actuator. The lateral braces of the test frame were not stiff enough to sustain the lateral forces encountered, hence the stoppage of the test during the pushing phase of the following primary cycle (±90 mm (±3.54")). The larger displacement cycle (±120 mm (4.72")) was then run manually, in the positive direction only (i.e. the actuator pulling the wall, avoiding the twisting phenomenon). The unrestrained length of the braces was made shorter to avoid the problem with the next specimens to be tested, although no other specimen remaining to be tested with the symmetric reversed-cyclic protocol was expected to develop such a high shear resistance. The stronger walls were tested with the asymmetric cyclic protocol where the major displacements, demanding the highest shear resistances from the specimens, were run in the positive direction only (see Section 2.7.2), thus the protocols were run without major issues.

The approach for the USA and Mexico is rather straightforward since it concerns the ultimate strength and the corresponding displacement / rotation. Therefore, the design properties to consider for the approach available in the USA and Mexico are those tabulated in Section 3.4 for the specimens tested by the author, and are presented in full in Appendix F, using metric and imperial units.

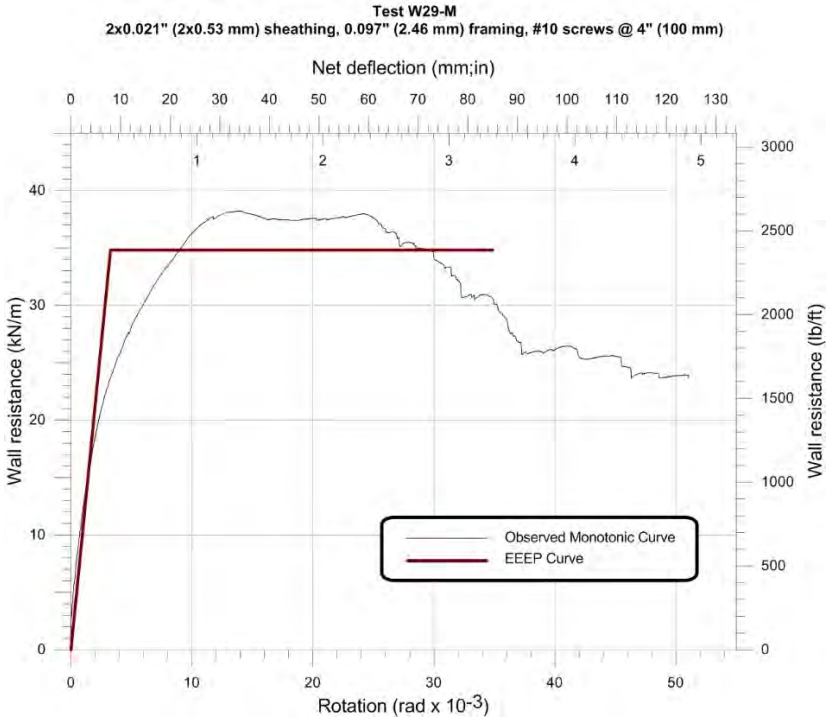

Figure 4.5 EEEP curve for the monotonic test W29-M

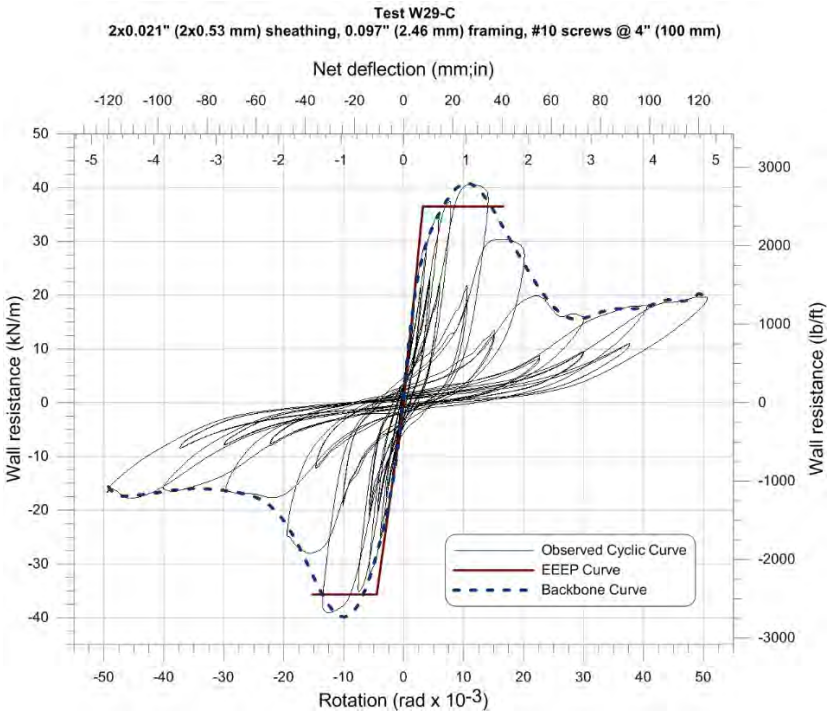

Figure 4.6 EEEP curves for the cyclic test W29-C

Table 4.1 Design Properties Summary (Metric) – Monotonic Shear Wall Tests

Test ID	Yield Resistance S_y (kN/m)	Displacement at $0.4S_u$ $\Delta_{0.4u}$ (mm)	Displacement at S_y Δ_y (mm)	Rotation at $0.4S_u$ $\theta_{0.4u}$ (rad.10^{-3})	Rotation at S_y θ_y (rad.10^{-3})	Elastic Stiffness k_e (kN/mm)	Ductility μ	Energy Dissipated E_{EEEP} (J)
Double-Sheathed Wall Configuration								
W28-M	54.21	5.41	12.01	2.22	4.93	5.51	5.15	3692
W29-M	34.81	3.51	7.97	1.44	3.27	5.33	10.66	3440
W30-M	58.79	7.16	16.12	2.94	6.61	4.45	4.26	4349
W31-M	36.28	3.21	7.43	1.32	3.05	5.96	10.26	3207
Centre-Sheathed Wall Configuration								
W18-M	78.32	10.81	24.28	4.43	9.96	3.94	5.06	8397
W18-MR	81.45	10.83	23.78	4.44	9.75	4.18	5.15	8754

Table 4.2 Design Properties Summary (Metric) – Positive Cycles of Cyclic Shear Wall Tests

Test ID	Yield Resistance S_{y+} (kN/m)	Displacement at $0.4S_u$ $\Delta_{0.4u+}$ (mm)	Displacement at S_y Δ_{y+} (mm)	Rotation at $0.4S_u$ $\theta_{0.4u+}$(rad.10^{-3})	Rotation at S_y θ_{y+} (rad.10^{-3})	Elastic Stiffness k_{e+} (kN/mm)	Ductility μ_+	Energy Dissipated E_{EEEP+} (J)
Double-Sheathed Wall Configuration								
W28-C	53.55	5.48	11.95	2.25	4.90	5.47	4.23	2909
W29-C	36.49	3.48	7.79	1.43	3.19	5.72	5.19	1627
W30-C	63.91	6.84	15.40	2.81	6.32	5.06	3.88	4063
W31-C	40.35	3.86	8.52	1.58	3.50	5.77	5.68	2173
Centre-Sheathed Wall Configuration								
W18-CR	86.02	13.03	29.57	5.34	12.13	3.55	4.02	8943
W23-CR3	138.9	15.14	32.34	6.21	13.26	5.24	3.88	14203
W23B-CR3	138.1	13.99	30.45	5.74	12.49	5.53	5.00	14281
W24-CR3	118.2	13.50	29.50	5.54	12.10	4.89	3.89	12295
W26-CR3	126.0	12.87	27.89	5.28	11.44	5.51	2.99	10693

Table 4.3 Design Properties Summary (Metric) – Negative Cycles of Cyclic Shear Wall Tests

Test ID	Yield Resistance S_{y-} (kN/m)	Displacement at $0.4S_{u-}$ $\Delta_{0.4u-}$ (mm)	Displacement at S_{y-} Δ_{y-} (mm)	Rotation at $0.4S_{u-}$ $\theta_{0.4u-}$(rad.10^{-3})	Rotation at S_{y-} θ_{y-} (rad.10^{-3})	Elastic Stiffness k_{e-} (kN/mm)	Ductility μ_-	Energy Dissipated E_{EEEP-} (J)
Double-Sheathed Wall Configuration								
W28-C	-54.49	-6.03	-13.21	-2.47	-5.42	5.03	2.88	2091
W29-C	-35.70	-4.90	-10.97	-2.01	-4.50	3.97	3.39	1381
W30-C	-60.40	-6.45	-14.21	-2.65	-5.83	5.18	3.09	2717
W31-C	-38.64	-3.86	-8.40	-1.58	-3.44	5.61	5.26	1885
Centre-Sheathed Wall Configuration								
W18-CR	-79.04	-12.72	-27.97	-5.22	-11.47	3.45	3.58	8300
W23-CR3[1]	-106.4	-11.13	-22.44	-4.56	-9.20	5.78	2.11	5074
W24-CR3	-113.4	-11.91	-26.49	-4.88	-10.86	5.22	4.12	12006

[1] Protocol stopped during test; negative cycles not completed. Maximum negative displacement reached is 50 mm (1.97")

Note: for Tables 4.1 to 4.3, 1 in = 25.4 mm, 1 ft = 0.305 m, 1 lb = 4.45 kN

4.3 Preliminary Modified Effective Strip Method for the Centre-Sheathed Configuration

The design process of the chord studs for the centre-sheathed configuration exhibited a simple fact: the Effective Strip Method from the AISI S400 Standard is not adequate for the design of these specimens and cannot be used in order to predict the maximum shear capacity of a given specimen. Therefore, it had to be adapted based on the observations that were made during the laboratory phase of the research project (Section 2.2.3). Two assumptions were made while designing the chord studs of the final centre-sheathed configuration specimens: all the screws are considered to participate in the shear resistance of the walls and each of them has its bearing resistance increased, computed considering the double shear bolt connection bearing resistance (Equation 2.11) from Section J3.3.1 of the AISI S100 *(2016)* applied to sheathing screws. Figure 4.7 shows the bearing forces at fastener locations considered in the calculation of the nominal shear resistance of the wall (predicted resistance). One can note only half of the fasteners are being attributed a bearing force in that figure; the other half of the screws represents the opposite anchors for the tension field.

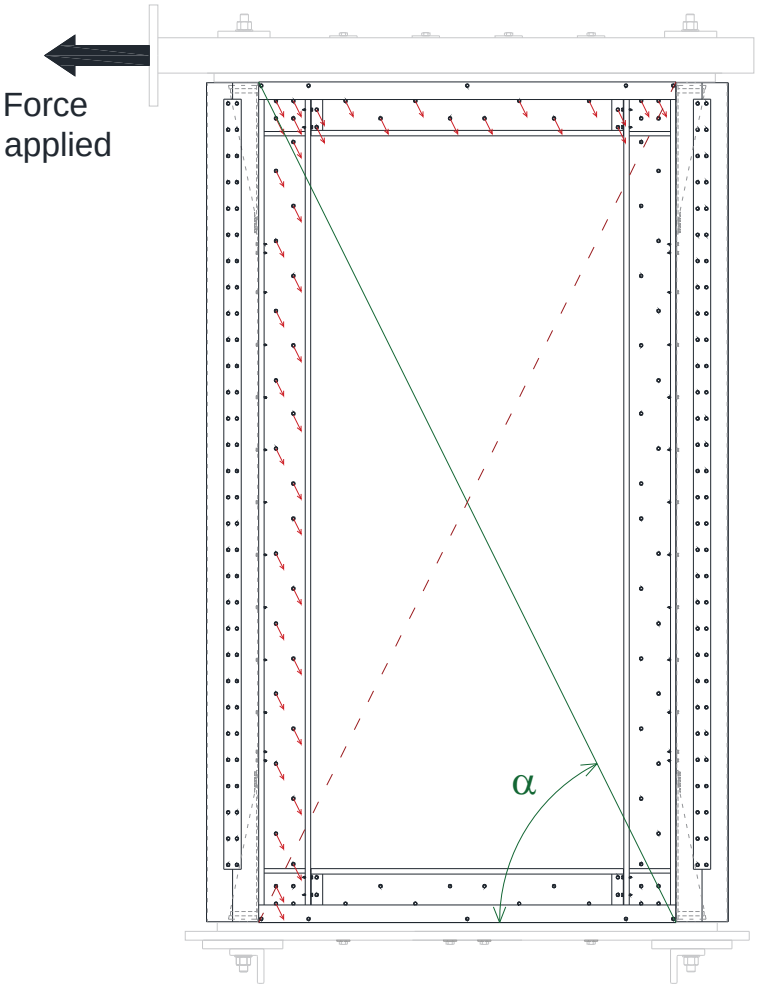

Figure 4.7 Bearing strength and screws participating for a centre-sheathed configuration specimen

The nominal shear resistance (force per unit length) predicted for a centre-sheathed configuration specimen as per the preliminary Modified Effective Strip Method, $S_{n(MESM)}$, is given by Equation 4.6:

$$S_{n(MESM)} = \left(\frac{n}{2} \times P_{nb} \times \cos\alpha\right)/w \qquad \text{Eq. 4.6}$$

where,

n = Total number of sheathing screws of the wall;

P_{nb} = Screw fastener's nominal bearing capacity as per Equation 2.11;

α = Angle given by the aspect ratio of the wall (Figure 4.7);

w = Width of the wall.

The ultimate shear resistance of the centre-sheathed configuration specimens was reached at drift ratios ranging from 2.7% (65.73 mm (2.6") for the positive cycles of W26-CR3) to 6.6% (160.0 mm (6.3") for the positive cycles of W15B-CR3); these displacements are too large to be considered in the design. As for the elaboration of the protocols in Section 2.7.2, it was decided to use the 2.5 % inelastic storey-drift limit criterion for seismic design of the ASCE/SEI 7 *(2016)* and the NBCC *(2015)*, considering the shear resistance exhibited at that displacement for the design. For comparison purposes, the ratios of test-to-predicted resistance were computed taking the average ultimate shear resistance, $S_{u,avg}$, and the average shear resistance at 2.5 % drift, $S_{2.5\%,avg}$, as the test values. They were compared with the average shear resistance obtained with the EEEP method, $S_{y,avg}$, and the shear resistance obtained with the preliminary Modified Effective Strip Method, $S_{n(MESM)}$, in order to compute the different ratios from Table 4.4.

Table 4.4 Comparison of prediction methods for centre-sheathed configuration

Test ID	Average Test Values (kN/m)		Predicted Values (kN/m)		Ratios Test/Predicted			
	$S_{u,avg}$	$S_{2.5\%,avg}$	$S_{y,avg}$ (EEEP)	$S_{n(MESM)}$	S_u/S_y	$S_u/S_{n(MESM)}$	$S_{2.5\%}/S_y$	$S_{2.5\%}/S_{n(MESM)}$
W15-R3[4]	154.3	135.2	131.2	161.8	1.18	0.95	1.03	0.84
W15B-CR3[2,4]	165.7	141.3	136.4	161.8	1.21	1.02	1.04	0.87
W23-CR3[1,3]	147.2	140.1	138.9	149.8	1.06	0.98	1.01	0.94
W23B-CR3[2]	158.6	140.8	138.1	149.8	1.15	1.06	1.02	0.94
W24-CR3[1]	131.4	121.5	115.8	115.8	1.13	1.13	1.05	1.05
W25-CR3[2,4]	116.7	106.0	102.8	95.7	1.14	1.22	1.03	1.11
W26-CR3[2]	145.3	143.3	126.0	132.1	1.15	1.10	1.14	1.09
				Avg.	1.15	1.07	1.04	0.98
				Std. Dev.	0.047	0.092	0.043	0.107
				Coeff. of Variation	4.1%	8.6%	4.1%	10.9%

[1] Average value from reversed cyclic tests only (symmetric)

[2] Positive values from asymmetric cyclic tests only

[3] Negative cycles incomplete; positive range considered

[4] Tested by Santos (2017)

The average values were considered because of the non-symmetric hysteresis plot resulting from the cyclic tests. Indeed, as explained in Section 3.5.1, strengths obtained from the negative range are slightly inferior to those from the positive range due to the wall first becoming damaged while experiencing a positive range of a cycle; hence, a reduced capacity exists while entering into the subsequent negative range of the cycle. All the successful CUREE reversed-cyclic tests realised in this program experienced the same phenomena; the ratios between the positive and negative

strengths are provided in Table 4.5, where S_{y+} and S_{y-} are the values determined applying the EEEP method to the test results, and S_{u+} and S_{u-} the ultimate shear strengths of the specimens measured during the cyclic tests.

Table 4.5 Strengths ratios from positive and negative ranges of cycles

Test ID	S_{y+}/S_{y-}	S_{u+}/S_{u-}	Average S_+/S_-
Double-Sheathed Wall Configuration			
W19-C[1]	1.08	1.09	1.08
W20-C[1]	1.00	0.98	0.99
W21-C[1]	1.07	1.06	1.06
W22-C[1]	1.00	1.00	1.00
W28-C	0.98	0.99	0.99
W29-C	1.02	1.02	1.02
W30-C	1.06	1.03	1.05
W31-C	1.04	1.03	1.04
		Avg.	1.03
		Std. Dev.	0.035
		Coeff. of Variation	3.37%
Centre-Sheathed Wall Configuration			
W15-CR3[1]	1.03	1.04	1.03
W24-CR3	1.04	1.06	1.05
[1] Tested by Santos (2017)		Avg.	1.04
		Std. Dev.	0.012
		Coeff. of Variation	1.18%

Although W23-CR3 was a successful CUREE reversed-cyclic test, the problems experienced during the test implied incomplete negative cycles, hence the absence of comparison for this test in Table 4.5.

The ratios are very consistent, with averages of 1.03 and 1.04 for the double-sheathed configuration and centre-sheathed configuration respectively, with minimal standard deviations and coefficients of variation.

Thus average test values reported in Table 4.4 are obtained following different procedures depending on the tests that were performed for the concerned configuration:

- Monotonic and reversed cyclic test performed (e.g. W15-MR3 and W15-CR3 for W15):

$$S_{avg} = \frac{S_{mono} + \frac{S_{cyclic+} - S_{cyclic-}}{2}}{2} \quad \text{Eq. 4.7}$$

- Reversed cyclic test only ([1] in Table 4.5):

$$S_{avg} = \frac{S_{cyclic+} - S_{cyclic-}}{2} \quad \text{Eq. 4.8}$$

- Asymmetric cyclic test only ([2] in Table 4.5):

$$S_{avg} = S_{cyclic+} \quad \text{Eq. 4.9}$$

Comparing the shear resistances obtained at 2.5 % drift with the values obtained applying the EEEP analysis method on the test results confirms the consistency in considering the shear resistance at 2.5 % drift for design. Although W26-CR3 presents a ratio $S_{2.5\%}/S_y$ slightly superior to the others, the mean value for this ratio is 1.04, with a standard deviation of 0.043 and a coefficient of variation of 4.1 %. The ratios considering S_u are not used since the range of displacement within which it is achieved is too large (2.7 – 6.6 % drift). However, the mean of 1.07 with a standard deviation of 0.092 and a coefficient of variation of 8.6 % for the ratio $S_u/S_{n(MESM)}$ bear out the assumptions made in the definition of the prediction method.

The ratio $S_{2.5\%}/S_{n(MESM)}$ was selected for the design method since the shear flow at that displacement was shown to be a consistent value. The mean of 0.98 is meaningful, but the standard deviation and coefficient of variation of 0.107 and 10.9 % respectively enlighten the fact that the prediction method needs to be further optimized to consider all the parameters affecting the shear resistance of a centre-sheathed configuration test specimen.

4.4 Development of a Limit States Design Procedure

A limit states design procedure for cold-formed steel framed and sheathed shear walls had been recommended by Ong-Tone *(2009)* and Balh *(2010)*, later adopted by DaBreo *(2012)*. It had been summarized by Balh et al. *(2014)*, and recently used by Rizk *(2017)*. It is also required by the AISI S100 *(2016)* / CSA S136 *(2016)* standards, stating that structural performances required to be established by tests shall be evaluated with specific performance procedure, listing the limit states design procedure as one of the options. The elaborated limit states design procedures are for Canada (LSD) and for the USA and Mexico (LRFD). This section defines the procedures for the double-sheathed configuration, associated with the EEEP method (for LSD) or the ultimate tested shear resistance (for LRFD), and the one for the centre-sheathed configuration associated with the experimental prediction method developed in Section 4.3. Because of the limited number of tests realised for both wall configurations, the test data from Santos *(2017)* are included in this section in order to work with a larger data sample to develop the limit states design procedure. In addition, the iterative design procedure for the centre-sheathed configuration (described in Section 2.2.3) resulted in failed tests that cannot be included in the present procedure. As a result, the centre-sheathed configuration specimens considered for the development of the limit states design procedure are listed in Table 4.6.

Table 4.6 Centre-sheathed configuration tests considered as successfully completed

Test ID	Sheathing Thickness mm (in)	Sheathing Screw Size (#)	Fastener Spacing mm (in)
W15-R3[1,3]	0.84 (0.033)	10	50 (2)
W15B-CR3[2,3]	0.84 (0.033)	10	50 (2)
W23-CR3	1.09 (0.043)	12	100 (4)
W23B-CR3[2]	1.09 (0.043)	12	100 (4)
W24-CR3	1.09 (0.043)	12	150 (6)
W25-CR3[2,3]	0.84 (0.033)	10	100 (4)
W26-CR3[2]	1.09 (0.043)	10	100 (4)

[1] Tested monotonically and cyclically

[2] Asymmetric cyclic test

[3] Tested by Santos (2017)

4.4.1 Calibration of the Resistance Factor

The AISI S100 Standard *(2016)* and the CSA S136 Standard *(2016)* (as well as the NBCC *(2015)*) provide the equation (Equation 4.10) that shall be satisfied by the strength of the tested elements, assemblies, connections or members, for Load and Resistance Factor Design (LRFD, the use is limited to the USA and Mexico) and Limit States Design (LSD, the use is limited to Canada):

$$\phi R_n \geq \sum \gamma_i Q_i \qquad \text{Eq. 4.10}$$

where,

ϕ = Resistance factor;

R_n = Nominal resistance;

$\sum \gamma_i Q_i$ = Required strength based on the most critical load combination. γ_i and Q_i are the load factors and load effects;

The resistance factor, ϕ, associated with a specific design method needs to be determined following the method provided in Section K2.1.1(c) of the AISI S100 Standard *(2016)*, using the following equation:

$$\phi = C_\phi (M_m F_m P_m) e^{-\beta_o \sqrt{v_M^2 + v_F^2 + c_P v_P^2 + v_Q^2}} \qquad \text{Eq. 4.11}$$

where,

C_ϕ = Calibration coefficient;

M_m = Mean value of material factor, *M*, for type of component involved;

F_m = Mean value of fabrication factor, *F*, for type of component involved;

P_m = Mean value of professional factor, *P*, for tested component;

e = Natural logarithmic base = 2.718;

β_o = Target reliability index;

V_M = Coefficient of variation of material factor for type of component involved;

V_F = Coefficient of variation of fabrication factor for type of component involved;

C_P = Correction factor;

V_P = Coefficient of variation of test results (≥ 0.065);

V_Q = Coefficient of variation of load effect (0.21 for LRFD and LSD);

Balh *(2010)* defined C_ϕ using the value determined by Branston *(2004)* based on documented wind load statistics from Ellingwood (Ellingwood et al. *(1980)*; Ellingwood and Tekie *(1999))* and Bartlett *(Bartlett et al., 2003)*. Through a conservative approach, Branston (2004) obtained a calibration coefficient of C_ϕ = 1.842 for cold-formed steel frame / wood panel shear walls subjected to wind loads. Although Balh's *(2010)* specimens utilised cold-formed steel sheathing, this value was successfully used. However, the AISI S100 Standard now provides the values of 1.52 for LRFD and 1.42 for LSD to define the calibration coefficient C_ϕ ; these values were considered for this research program.

The mean values M_m and F_m are provided in Table K2.1.1-1 of the AISI S100 Standard *(2016)*, as well as their corresponding coefficients of variation V_M and V_F (respectively); they depend on the type of component (i.e. type of members and type of connections / joints). As the chord studs of both wall configurations tested in this program are subjected to compression and flexure (see Section 2.2 for design explanations), they were considered as members under combined forces. The tracks were not considered since the tests showed they were not impacted when testing the new wall configurations. The type of connection selected was the screw connection since the principal failure mode experienced by the two tested wall configurations in this experimental program was bearing damage at screw locations. Table 4.7 provides the values for M_m,V_M, F_m and V_F with respect to the type of component they apply to.

Table 4.7 Statistical Data for the Determination of Resistance Factor (AISI S100 *(2016)*)

Type of Component	M_m	V_M	F_m	V_F
Members				
Chord Studs: Under Combined Forces	1.05	0.10	1.00	0.05
Connections and Joints				
Screw Connections	1.10	0.10	1.00	0.10

The target reliability index, β_o, is given by the AISI S100 Standard; the values are as follows:

- 2.5 for structural members and 3.5 for connections for LRFD;
- 3.0 for structural members and 4.0 for connections for LSD.

As the shear wall system under investigation is associated with a structural member, the target reliability index was set to 2.5 (LRFD) and 3.0 (LSD).

The coefficient of variation of the load effect, V_Q, is provided as well by the AISI S100 Standard and takes the value of 0.21 for LRFD and LSD.

The experimental program comprised two different shear wall configurations (double-sheathed & centre-sheathed), which are associated with different design methods. On one hand, the same design approach as found in the current AISI S400 Standard is used for the double-sheathed specimens, meaning their resistance is obtained from tabulated strengths, which were determined by applying the EEEP analysis method to the test results for Canada (LSD), or by utilizing the ultimate measured strength (USA & Mexico). By definition, this is not a prediction method based on principles of mechanics, restricting the design of the walls to the configurations and building parameters listed in Table E.2.3.1 of AISI S400 *(2015)*. On the other hand, Section 4.3 contains a prediction method to be optimized for the centre-sheathed configuration that allows for greater freedom in terms of the variety of construction parameters that can be varied. As the remaining coefficients that influence the resistance factor depend on these prediction methods, the two design methods will be treated separately.

4.4.1.1 Double-sheathed configuration

Table 4.8 provides the ratios of test-to-predicted values for the double-sheathed configuration for LSD. The only "predicted" value available for this configuration is S_y, obtained by applying the EEEP method in the analysis of the test results. The average values are obtained using Equation 4.7 as all the specimens were tested monotonically and cyclically, using the CUREE reversed cyclic protocol. As no prediction method exists to determine the ultimate shear resistance for this configuration, the resistances reached during the tests were used for the predicted values for the LRFD procedure; thus, the test-to-predicted ratio for this procedure is 1.0.

Table 4.8 Ratios of test-to-predicted values for double-sheathed configuration (LSD)

Test ID	Average Test Values $S_{u,avg}$ (kN/m)	Average Predicted Values S_y (kN/m)	S_u/S_y
W19[1]	42.1	38.0	1.11
W20[1]	28.7	25.8	1.11
W21[1]	46.0	41.6	1.11
W22[1]	29.1	26.8	1.08
W28	61.4	54.1	1.13
W29	39.3	35.5	1.11
W30	67.6	60.5	1.12
W31	42.2	37.9	1.11
		Avg. $(=P_m)$	1.11
		Std. Dev.	0.014
		Coeff. of Variation $(=V_p)$	1.3%

[1] Tested by Santos (2017)

As expected, the ratios are superior to one due to the use of the EEEP analysis method, with a mean equal to 1.11. These ratios and mean can be associated with the professional factor, *P*, which is the ratio of the test value to the predicted value (Equation 4.12), and its mean value, P_m (Equation 4.13), although they compare a ultimate strength to a yield strength. Thus, the standard deviation and coefficient of variation can be computed. A consistent behaviour of the tested specimens with respect to the EEEP method was observed, as illustrated by the values of 0.014 and 1.3 % that were obtained. Therefore, the professional factor is taken as 1.0 (more conservative than 1.11 which, in addition, cannot be used since it compares the ultimate strength to the yield strength) and the coefficient of variation, V_p, is the ratio of the standard deviation divided by the mean value of the professional factor (Equation 4.14), value with a lower bound of 6.5% imposed by the AISI S100 Standard. The same P_m and V_p values are used for the LRFD procedure since the average test-to-predicted ratio is 1.0 with a coefficient of variation null.

$$P_i = S_{test,i}/S_{predicted,i} \quad \text{Eq. 4.12}$$

$$P_m = \frac{\sum_{i=1}^{n} P_i}{n} \quad \text{Eq. 4.13}$$

$$V_p = \frac{s_c}{P_m} \geq 0.065 \quad \text{Eq. 4.14}$$

where,

$S_{test,i}$ = Tested shear resistance of wall *i*;

$S_{predicted,i}$ = Calculated nominal shear resistance of wall *i*;

n = Total number of tests;

s_c = Standard deviation of $S_{test,i}$ divided by $S_{predicted,i}$ for all of test results.

As P_m was set to 1.0, $V_p = s_c$ = 1.4 % < 6.5 %, therefore V_p is set to 6.5 %.

The correction factor, C_P, is defined by the following:

$$C_P = \frac{\left(1+\frac{1}{n}\right)m}{(m-2)} \text{ for n} \geq 4 \qquad \text{Eq. 4.15}$$

where,

n = Number of tests;

m = Degrees of freedom = $n - 1$.

Due to the limited number of tests per sets of building parameters (one or two depending if a monotonic test was realised), the number of tests, *n*, is considered for a specific configuration; thus n = 16 for the double-sheathed configuration since 8 monotonic and 8 cyclic tests had been successfully completed by the author and Santos *(2017)*; hence, the correction factor obtained is C_p = 1.23.

4.4.1.3 Centre-sheathed configuration

Table 4.9 provides the ratios of test-to-predicted values for the centre-sheathed configuration, using the preliminary Modified Effective Strip Method as the prediction method, as well as the values for P_m and V_p (superior to the 6.5% minimum value required by the AISI S100 Standard). The average shear resistance values are obtained following the Equations 4.7, 4.8 and 4.9 of Section 4.3.

Table 4.9 Ratios of test-to-predicted values for centre-sheathed configuration

Test ID	Average Test Values $S_{2.5\%,avg}$ (kN/m)	Predicted Values $S_{n(MESM)}$ (kN/m)	$S_{2.5\%}/S_{n(MESM)}$
W15-R3[4]	135.2	161.8	0.84
W15B-CR3[2,4]	141.3	161.8	0.87
W23-CR3[1,3]	140.1	149.8	0.94
W23B-CR3[2]	140.8	149.8	0.94
W24-CR3[1]	121.5	115.8	1.05
W25-CR3[2,4]	106.0	95.7	1.11
W26-CR3[2]	143.3	132.1	1.09

[1] Average value from reversed cyclic tests only (symmetric) — Avg. $(=P_m)$ 0.98

[2] Positive values from asymmetric cyclic tests only — Std. Dev. 0.107

[3] Negative cycles incomplete; positive range considered — Coeff. of Variation $(=V_p)$ 10.9%

[4] Tested by Santos (2017)

The correction factor, C_P, defined according to Equation 4.15 is equal to 1.58, considering the number of tests n = 8 since 8 tests were successfully completed with the final reinforced centre-sheathed configuration (R3) (one monotonic test and seven cyclic tests).

4.4.1.3 Summary of the results for the calibration of the resistance factor

Ultimately, several values are obtained for the resistance factor depending on the member and failure mode the resistance factor is defined for, as well as the design philosophy that is followed, i.e. LRFD or LSD. Table 4.10 presents a summary of the calibrated resistance factors with respect to the type of component and failure modes.

Table 4.11 gives the mean values of the resistance factors associated with the design method chosen. The resistance factors for the EEEP method applied to the double-sheathed configuration give mean values of 0.86 and 0.71 for LRFD and LSD, respectively. The mean values of the resistance factor for the prediction method associated with the centre-sheathed configuration are 0.79 and 0.64, respectively.

These values are slightly lower than those found by Ong-Tone *(2009)*, Balh *(2010)* and DaBreo *(2012)* for the cold-formed steel sheathed shear walls for LSD, as summarized by Balh et al.

(2014). Indeed, the recommended value of 0.7 was a conservative recommendation. The AISI S100 Standard *(2016)* provided new values for C_ϕ of 1.52 (LRFD) and 1.42 (LSD), whereas the previous calibration were all carried out using a value of 1.842 as determined by Branston *(2004)* based on wind load statistics, resulting in a higher value of C_ϕ.

As more tests need to be realised, and this for the promising centre-sheathed configuration in particular, the coefficients P_m and V_P used for the calibration of the resistance factor are expected to change. They would result in a higher value for the mean of the professional factor, P_m, with a smaller coefficient of variation, V_P, especially once the prediction method has been improved. The range in which the resistance factor would be expected using the coefficients provided by the AISI S100 Standard are as follows:

- LRFD: $\phi \in [0.8;0.9]$;
- LSD: $\phi \in [0.7;0.75]$.

Table 4.10 Summary of the resistance factor calibration for different types of components

Type of component	Type of analysis	C_ϕ	M_m	F_m	P_m	β_o	V_M	V_F	n	C_P	V_P	V_Q	ϕ
Double-Sheathed Wall Configuration													
Chord studs (under combined forces)	LRFD	1.52	1.05	1.00	1.00	2.50	0.10	0.05	16	1.23	0.065	0.21	**0.86**
	LSD	1.42	1.05	1.00	1.00	3.00	0.10	0.05	16	1.23	0.065	0.21	**0.71**
Screw connections	LRFD	1.52	1.10	1.00	1.00	2.50	0.10	0.10	16	1.23	0.065	0.21	**0.87**
	LSD	1.42	1.10	1.00	1.00	3.00	0.10	0.10	16	1.23	0.065	0.21	**0.71**
Centre-Sheathed Wall Configuration													
Chord studs (under combined forces)	LRFD	1.52	1.05	1.00	0.98	2.50	0.10	0.05	8	1.58	0.109	0.21	**0.78**
	LSD	1.42	1.05	1.00	0.98	3.00	0.10	0.05	8	1.58	0.109	0.21	**0.64**
Screw connections	LRFD	1.52	1.10	1.00	0.98	2.50	0.10	0.10	8	1.58	0.109	0.21	**0.79**
	LSD	1.42	1.10	1.00	0.98	3.00	0.10	0.10	8	1.58	0.109	0.21	**0.64**

Table 4.11 Averages of the resistance factors with respect to the design analysis

Type of analysis	Type of component	ϕ	ϕ_{avg}
Double-Sheathed Wall Configuration			
LRFD	Chord studs	0.86	**0.86**
	Screw connections	0.87	
LSD	Chord studs	0.71	**0.71**
	Screw connections	0.71	
Centre-Sheathed Wall Configuration			
LRFD	Chord studs	0.78	**0.79**
	Screw connections	0.79	
LSD	Chord studs	0.64	**0.64**
	Screw connections	0.64	

4.4.2 Factor of Safety

Considering the resistance factor, ϕ, has been determined, the factor of safety can now be computed; it is the ratio of the ultimate shear resistance reached by a given specimen during a test to the factored resistance (Figure 4.8) computed as follows for the LRFD and LSD methods:

$$Factor\ of\ Safety = \frac{S_u}{S_r} \qquad \text{Eq. 4.16}$$

where,

S_u = Ultimate shear resistance reached during test;

S_r = Factored shear resistance

$= \phi S_n$;

$S_n = S_y$ for double-sheathed configuration (LSD);

$S_n = S_u$ for double-sheathed configuration (LRFD);

$S_n = S_{n(MESM)}$ for centre-sheathed configuration (LSD and LRFD).

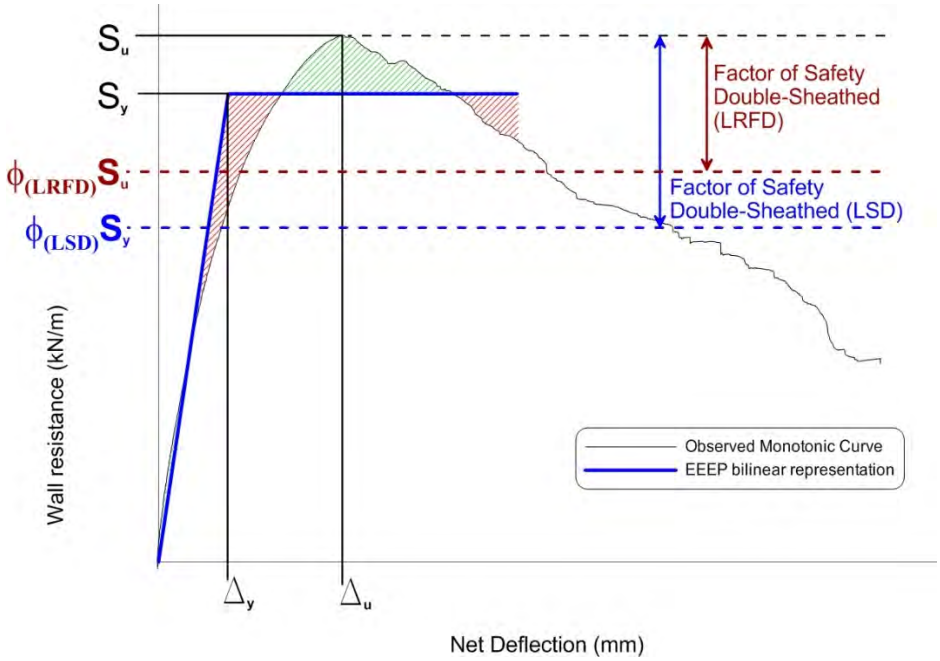

Figure 4.8 Definition of the factor of safety for double-sheathed specimens related to ultimate and factored resistances for LSD (using EEEP analysis method) and LRFD

The measured shear resistances for cyclic tests are the average shear resistances as computed in Section 4.3, taking into consideration the values from the positive and negative ranges of the cycles when available. Tables 4.12, 4.13, 4.15 and 4.16 present the factor of safety for the monotonic and cyclic tests for the double-sheathed and centre-sheathed configurations, using the lower bound of the resistance factor ranges given in Section 4.4.1. Only centre-sheathed specimens built with the final reinforcement scheme are presented in Table 4.15.

The double-sheathed specimens obtained the monotonic and cyclic average values of 1.57 and 1.60 respectively for the LSD, with coefficients of variation of 1.99 % and 1.47 % respectively. These values can be compared with the ones reported in Balh et al. *(2014)* since the analysis method is the same (i.e. the EEEP method); the average safety factor for the combined monotonic and reversed cyclic tests considered in Balh et al. *(2014)* is relatively greater since it ranged from 1.9 to 2.0. Regarding the LRFD, the coefficient of variation is 1.25 with no variation as the design value considered for the USA and Mexico for these shear walls is S_u, therefore reducing the factor of safety to the constant value of $1/\phi$.

The factor of safety for the centre-sheathed configuration specimens is even lower than the one obtained for double-sheathed configuration when comparing the cyclic tests; the cyclic average values obtained are 1.54 (LSD) and 1.35 (LRFD) with a higher coefficient of variation of 8.5 %.

These factor of safety are applicable for wind loadings applied horizontally and they do not take into consideration the potential gravity loads that could be applied on the structure. They are not relevant when designing with respect to seismic loads. Instead, another approach, developed in Section 4.4.3, has to be followed.

Table 4.12 Factor of safety for double-sheathed specimens - Monotonic tests

Test ID	Ultimate Resistance S_u (kN/m)	Nominal Resistance S_y (kN/m)[1]	ϕ (LSD)	ϕ (LRFD)	Factored Resistance ϕS_y (LSD)	Factored Resistance ϕS_u (LRFD)	Factor of Safety (LSD)	Factor of Safety (LRFD)
Double-Sheathed Wall Configuration								
W19-M[2]	39.6	35.5	0.7	0.8	24.8	31.6	1.59	1.25
W20-M[2]	27.3	25.2	0.7	0.8	17.6	21.8	1.55	1.25
W21-M[2]	45.9	41.4	0.7	0.8	29.0	36.7	1.58	1.25
W22-M[2]	28.4	26.8	0.7	0.8	18.8	22.7	1.51	1.25
W28-M	61.0	54.2	0.7	0.8	37.9	48.8	1.61	1.25
W29-M	38.2	34.8	0.7	0.8	24.4	30.6	1.57	1.25
W30-M	65.4	58.8	0.7	0.8	41.2	52.3	1.59	1.25
W31-M	39.3	36.3	0.7	0.8	25.4	31.4	1.55	1.25
						Avg.	1.57	1.25
						Std. Dev.	0.031	0.000
						Coeff. of Variation	1.99%	0.00%

[1] Nominal resistance computed using the EEEP approach (Section 4.2)

[2] Tested by Santos (2017)

Table 4.13 Factor of safety for centre-sheathed specimens - Monotonic test

Test ID	Ultimate Resistance S_u (kN/m)	Nominal Resistance $S_{n(MESM)}$ (kN/m)[1]	ϕ (LSD)	ϕ (LRFD)	Factored Resistance $\phi S_{n(MESM)}$ (LSD)	Factored Resistance $\phi S_{n(MESM)}$ (LRFD)	Factor of Safety (LSD)	Factor of Safety (LRFD)
Centre-Sheathed Wall Configuration								
W15-CR3[2]	149.8	161.8	0.7	0.8	113.3	129.4	1.32	1.16

[1] Nominal resistance computed using the peliminary Modified Effective Stip Method (Section 4.3)

[2] Tested by Santos (2017)

Table 4.14 Factor of safety for double-sheathed specimens - Cyclic tests

Test ID	Ultimate Resistance S_u (kN/m)	Nominal Resistance S_y (kN/m)[1]	ϕ (LSD)	ϕ (LRFD)	Factored Resistance ϕS_y (LSD)	Factored Resistance ϕS_u (LRFD)	Factor of Safety (LSD)	Factor of Safety (LRFD)
Double-Sheathed Wall Configuration								
W19-C[2]	44.7	40.6	0.7	0.8	28.4	35.8	1.57	1.25
W20-C[2]	30.1	26.5	0.7	0.8	18.6	24.1	1.62	1.25
W21-C[2]	46.2	41.8	0.7	0.8	29.3	36.9	1.58	1.25
W22-C[2]	29.8	26.9	0.7	0.8	18.8	23.8	1.58	1.25
W28-C	61.8	54.0	0.7	0.8	37.8	49.4	1.63	1.25
W29-C	40.3	36.1	0.7	0.8	25.3	32.3	1.60	1.25
W30-C	69.8	62.2	0.7	0.8	43.5	55.8	1.60	1.25
W31-C	45.0	39.5	0.7	0.8	27.6	36.0	1.63	1.25
						Avg.	1.60	1.25
						Std. Dev.	0.024	0.000
						Coeff. of Variation	1.47%	0.00%

[1] Nominal resistance computed using the EEEP approach (Section 4.2)

[2] Tested by Santos (2017)

Table 4.15 Factor of safety for centre-sheathed specimens - Cyclic tests

Test ID	Ultimate Resistance S_u (kN/m)	Nominal Resistance $S_{n(MESM)}$ (kN/m)[1]	ϕ (LSD)	ϕ (LRFD)	Factored Resistance $\phi S_{n(MESM)}$ (LSD)	Factored Resistance $\phi S_{n(MESM)}$ (LRFD)	Factor of Safety (LSD)	Factor of Safety (LRFD)
Centre-Sheathed Wall Configuration								
W15-CR3[4]	158.9	161.8	0.7	0.8	113.3	129.4	1.40	1.23
W15B-CR3[2,4]	165.7	161.8	0.7	0.8	113.3	129.4	1.46	1.28
W23-CR3[3]	147.2	149.8	0.7	0.8	104.9	119.8	1.40	1.23
W23B-CR3[2]	158.6	149.8	0.7	0.8	104.9	119.8	1.51	1.32
W24-CR3	135.3	115.8	0.7	0.8	81.1	92.6	1.67	1.46
W25-CR3[2,4]	116.7	95.7	0.7	0.8	67.0	76.6	1.74	1.52
W26-CR3[2]	145.3	132.1	0.7	0.8	92.5	105.7	1.57	1.37
						Avg.	1.54	1.35
						Std. Dev.	0.131	0.114
						Coeff. of Variation	8.50%	8.50%

[1] Nominal resistance computed using the peliminary Modified Effective Stip Method (Section 4.3)

[2] Positive value from asymmetric cyclic test only

[3] Negative cycles not completed; value from positive cycles only

[4] Tested by Santos (2017)

4.4.3 Capacity Based Design for Canada

In a Seismic Force Resisting System (SFRS), the energy accumulated while the system experiences extensive lateral displacement is often dissipated through a desired ductile fuse element; this is the designated energy-dissipating mechanism. In the case of cold-formed steel sheathed shear walls, the member acting as the fuse is the sheathing, dissipating energy through the inelastic bearing deformations at screw locations. The other components forming the system, such as the framing members in the case of a cold-formed steel shear wall for instance, must be designed to withstand the expected (probable) capacity that is to be developed by the fuse element itself, considering its overstrength. Thus, the fuse can undergo deformations in a ductile fashion while the other members composing the system remain elastic. In Canada, the AISI S400 Standard (*2015)* requires that for the design of such SFRS, a capacity based procedure such as follows must be followed.

As the two configurations have different approaches (EEEP for the double-sheathed configuration and the preliminary Modified Effective Strip Method for the centre-sheathed configuration), the overstrength is defined following two separate procedures. For the double-sheathed configuration, it is defined as per the approach used in the previous experimental programs involving cold-formed steel shear walls (e.g. Branston *(2004)*, Balh *(2010)*, DaBreo *(2012)*, Balh et al. *(2014)*). The overstrength of a double-sheathed specimen (Figure 4.9) is represented by the ratio of the ultimate shear resistance reached during the test to the nominal yield wall resistance obtained by applying the EEEP analysis method to the results:

$$Overstrength = {S_u}/{S_y} \qquad \text{Eq. 4.17}$$

where,

S_u = Ultimate shear resistance reached during test;

S_y = Nominal yield shear resistance from EEEP Method (Tables 4.1, 4.2 and 4.3).

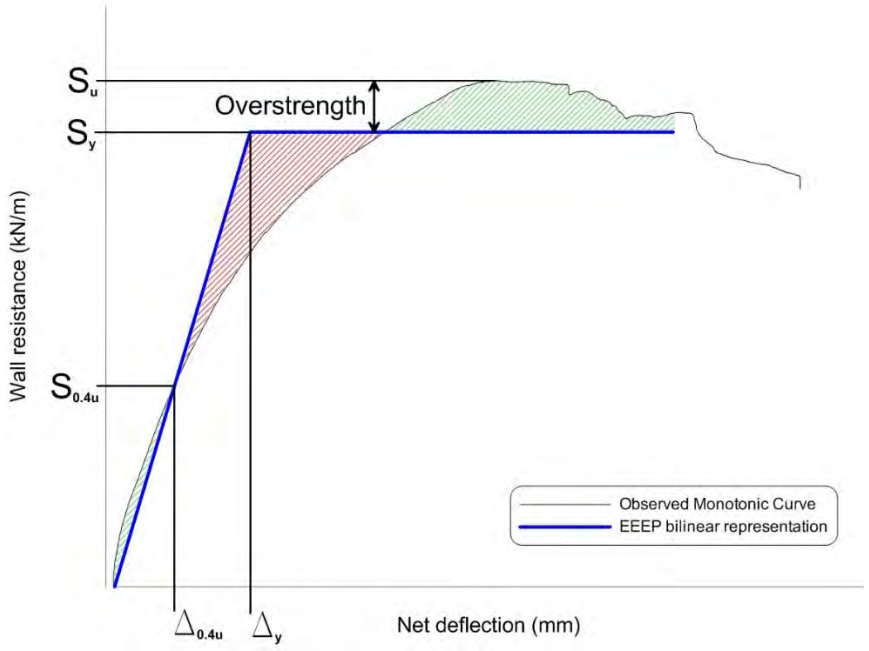

Figure 4.9 Representation of the overstrength for a double-sheathed specimen

As it is intended to develop a prediction method for the centre-sheathed configuration on the basis of the preliminary Modified Effective Strip Method (Section 4.3), the values considered for this configuration are not the same. Indeed, it has been shown that the ultimate shear strength was reached at high drift ratios that would most certainly not be reached in a regular seismic event; hence, the use of the 2.5 % inelastic storey-drift limit criterion for seismic design of the ASCE/SEI 7 *(2016)* and the NBCC*(2015)*. However, the overstrength determined at the ultimate load level, regardless of drift, was also included for comparison purposes. Figure 4.10 shows the two overstrength obtained using the ultimate shear resistance and the resistance reached at 2.5 % drift, using the following equations:

$$Design\ overstrength = {S_{2.5\%}}/{S_{n(MESM)}} \qquad \text{Eq. 4.18}$$

$$Ultimate\ overstrength = {S_u}/{S_{n(MESM)}} \qquad \text{Eq. 4.19}$$

where,

$S_{2.5\%}$ = Shear strength reached by the specimen at 2.5 % drift;

$S_{n(MESM)}$ =Nominal shear resistance predicted for centre-sheathed specimen (Eq. 4.6).

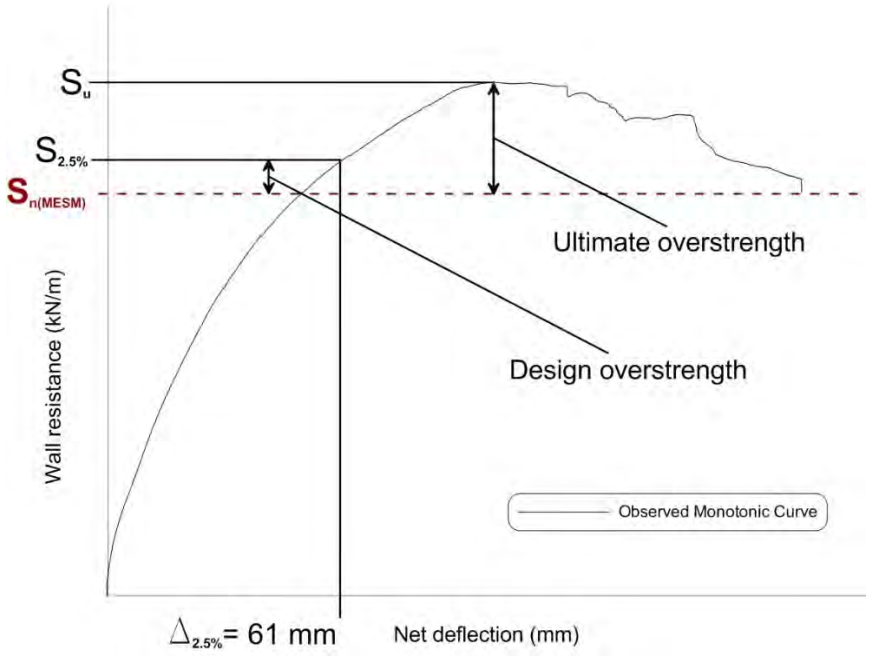

Figure 4.10 Ultimate and design overstrength for the centre-sheathed configuration

The overstrength values for both wall configurations are presented in Tables 4.16 to 4.19 considering monotonic tests and cyclic tests. The double-sheathed specimens have an overstrength value of 1.10 for the monotonic tests and 1.12 considering the cyclic tests, the two sets of data being consistent with low coefficient of variation (< 2.0 %). The centre-sheathed specimens have lower values for the overstrength due to the prediction method that was developed in Section 4.3. Considering the cyclic tests, the design overstrength has an average of 0.98 with a 10.90 % coefficient of variation and the ultimate overstrength has an average of 1.08 with an 8.50 % coefficient of variation.

Table 4.16 Overstrength design values for double-sheathed specimens – Monotonic tests

Test ID	Ultimate Resistance S_u (kN/m)	Nominal Resistance S_y (kN/m)[1]	Overstrength
Double-Sheathed Wall Configuration			
W19-M[2]	39.6	35.5	1.12
W20-M[2]	27.3	25.2	1.08
W21-M[2]	45.9	41.4	1.11
W22-M[2]	28.4	26.8	1.06
W28-M	61.0	54.2	1.12
W29-M	38.2	34.8	1.10
W30-M	65.4	58.8	1.11
W31-M	39.3	36.3	1.08
		Avg.	1.10
		Std. Dev.	0.022
		Coeff. of Variation	1.99%

[1] Nominal resistance computed using the EEEP approach (Section 4.2)

[2] Tested by Santos (2017)

Table 4.17 Overstrength design values for centre-sheathed specimens – Monotonic test

Test ID	Ultimate Resistance S_u (kN/m)	Resistance at 2.5 % drift $S_{2.5\%}$ (kN/m)	Nominal Resistance $S_{n(MESM)}$ (kN/m)[1]	Design overstrength	Ultimate overstrength
Centre-Sheathed Wall Configuration					
W15-MR3[2]	149.8	131.8	161.8	0.81	0.93

[1] Nominal resistance computed using the peliminary Modified Effective Stip Method (Section 4.3)

[2] Tested by Santos (2017)

Table 4.18 Overstrength design values for double-sheathed specimens – Cyclic tests

Test ID	Ultimate Resistance S_u (kN/m)	Nominal Resistance S_y (kN/m)[1]	Overstrength
Double-Sheathed Wall Configuration			
W19-C[2]	44.7	40.6	1.10
W20-C[2]	30.1	26.5	1.14
W21-C[2]	46.2	41.8	1.11
W22-C[2]	29.8	26.9	1.11
W28-C	61.8	54.0	1.14
W29-C	40.3	36.1	1.12
W30-C	69.8	62.2	1.12
W31-C	45.0	39.5	1.14
		Avg.	1.12
		Std. Dev.	0.016
		Coeff. of Variation	1.47%

[1] Nominal resistance computed using the EEEP approach (Section 4.2)

[2] Tested by Santos (2017)

Table 4.19 Overstrength design values for centre-sheathed specimens – Cyclic tests

Test ID	Ultimate Resistance S_u (kN/m)	Resistance at 2.5 % drift $S_{2.5\%}$ (kN/m)	Nominal Resistance $S_{n(MESM)}$ (kN/m)[1]	Design overstrength	Ultimate overstrength
Centre-Sheathed Wall Configuration					
W15-CR3[4]	158.9	135.2	161.8	0.84	0.98
W15B-CR3[2,4]	165.7	141.3	161.8	0.87	1.02
W23-CR3[3]	147.2	140.1	149.8	0.94	0.98
W23B-CR3[2]	158.6	140.8	149.8	0.94	1.06
W24-CR3	135.3	121.5	115.8	1.05	1.17
W25-CR3[2,4]	116.7	106.0	95.7	1.11	1.22
W26-CR3[2]	145.3	143.3	132.1	1.09	1.10
			Avg.	0.98	1.08
			Std. Dev.	0.106	0.092
			Coeff. of Variation	10.90%	8.50%

[1] Nominal resistance computed using the peliminary Modified Effective Stip Method (Section 4.3)

[2] Positive value from asymmetric cyclic test only

[3] Negative cycles not completed; value from positive cycles only

[4] Tested by Santos (2017)

It is anticipated that in future research programs, the preliminary Modified Effective Strip Method will undergo improvements as more is discovered about the resistance of screws in three-ply connections. There is no certainty at this time regarding the value the final overstrength would take for the centre-sheathed configuration specimen. However, it is expected to sit in the range between the two overstrength values obtained.

The overstrength values are smaller than those obtained by Balh *(2010)* and DaBreo *(2012)*. For the double-sheathed configuration, this is due to significantly stiffer walls exhibiting a more rapid strength degradation affecting the ductility (the EEEP is dependent on the displacement reached at 80 % of the ultimate resistance post-peak). Because of the relation of equality between the area under the EEEP bilinear curve and the area under the observed curve (or backbone curve for the cyclic tests) for the same displacement range, the yield shear strength has a value relatively closer to the ultimate load, hence the lower overstrength coefficient. For the centre-sheathed configuration, the lower value is simply due to the prediction method, which is still under development, and the uncertainty regarding which value it should be compared with in order to define the overstrength factor (i.e. the shear resistance obtained at 2.5 % drift or the ultimate resistance although it might be reached at drift ratios beyond 4 %).

4.4.4 Calibration of Seismic Design Parameters for Canada

The NBCC *(NRCC, 2015)* allows for the use of the static force procedure in the calculation of the seismic base shear force, *V*, as follows:

$$V = \frac{S(T_a)M_v I_e W}{R_d R_o} \qquad \text{Eq. 4.20}$$

where,

$S(T_a)$ = Design spectral acceleration;

T_a = Fundamental lateral period of vibration;

M_v = Factor to account for higher mode effects;

I_e = Importance factor for earthquake loads;

W = Dead load + 25 % snow load + 60 % storage loads;

R_d = Ductility-related force modification factor;

R_o = Overstrength-related force modification factor.

The two modification factors present in Equation 4.20 can initially be determined as "test-based" factors; this section presents the approach leading to their definition.

4.4.4.1 "Test-based" ductility-related force modification factor R_d

"The ability of a structure to undergo large amplitude cyclic deformations in the inelastic range without a substantial reduction in strength"
(Park, 1989)

According to Park *(1989)*, ductility is the ability to deform in the inelastic range, thus dissipating the energy brought into the system; the lesser the reduction in strength during the inelastic deformation the greater the energy dissipated by the system, hence the importance of the ductility in seismic design.

The ductility of the shear wall, μ, computed as per Equation 4.4 from Section 4.2, is represented in Equation 4.20 by the ductility-related force modification factor, R_d. The relation between the two was introduced by Newmark and Hall *(1982)* and depends on the natural period of the structure, T, as per the following:

$$R_d = \mu \qquad \text{for } T > 0.5 \text{ s} \qquad \text{Eq. 4.21}$$

$$R_d = \sqrt{2\mu - 1} \qquad \text{for } 0.1 \text{ s} < T < 0.5 \text{ s} \qquad \text{Eq. 4.22}$$

$$R_d = 1 \qquad \text{for } T < 0.03 \text{ s} \qquad \text{Eq. 4.23}$$

The natural periods of the specimens tested in this laboratory research program have not been determined, but Boudreault *(2005)* showed this kind of structure most likely to have a low natural period (i.e. $T < 0.5$ s). Therefore Equation 4.22 should be used in order to determine the ductility-related force modification factor, as was done in previous studies on cold-formed steel framed shear walls (e.g. Balh *(2010)*, DaBreo *(2012)* and Rizk *(2017)*). Tables 4.20 to 4.24 present the values for the ductility, μ, and the ductility-related force modification factor, R_d.

Table 4.20 presents the ductility, μ, and the R_d factor for the monotonic tests; only one monotonic test was carried out for the centre-sheathed configuration. Table 4.21 presents the average ductility values for the specimens tested with the CUREE reversed-cyclic (symmetric) protocol only. The purpose of the asymmetric protocol was to investigate the positive range, limiting the negative range to a 5 mm (0.2”) displacement. However, the specimen W23-CR3 presents the value for the positive range only, due to the stoppage of the test in the negative range (explained in Section 4.2). For the same reasons, Table 4.22, concerning the negative range of the cyclic test, does not present the values for specimen W23-CR3.

Table 4.23 presents the ductility, μ, and the R_d factor for the positive range of all the cyclic tests performed. It is important to keep in mind that 3 out of the 7 successful cyclic tests for the centre-sheathed specimens (i.e. did not experience framing failure and using the last reinforcement scheme) were performed with a symmetric cyclic protocol, limiting the displacement range and thus, preventing the specimens from experiencing a strength degradation. Therefore, the ductility, μ, and the R_d factor are negatively impacted since their computation had to be based on the ultimate

displacement achieved, which was restricted by the stroke of the actuator and not the performance of the shear wall.

For information purposes, Table 4.24 only contains data for the specimens tested with the asymmetric protocol, with the advantage of presenting values computed with data not impacted by the limited displacement range imposed by the stroke of the actuator while using the CUREE reversed-cyclic (symmetric) protocol.

Table 4.20 Ductility and R_d values for monotonic tests

Test ID	Ductility μ	Ductility-related force modification factor R_d
Double-Sheathed Wall Configuration		
W19-M[1]	5.46	3.15
W20-M[1]	9.07	4.14
W21-M[1]	5.55	3.18
W22-M[1]	9.13	4.16
W28-M	5.15	3.05
W29-M	10.66	4.51
W30-M	4.26	2.74
W31-M	10.26	4.42
	Avg.	3.67
	Std. Dev.	0.70
	Coeff. Of Variation	19.2%
Centre-Sheathed Wall Configuration		
W15-MR3[1,2]	3.87	2.60

[1] Tested by Santos (2017)

[2] Displacement limited by the stroke of the actuator

Table 4.21 Average ductility and R_d values for cyclic tests

Test ID	Ductility μ_{avg}	Ductility-related force modification factor R_d
Double-Sheathed Wall Configuration		
W19-C[1]	4.00	2.64
W20-C[1]	5.83	3.26
W21-C[1]	3.92	2.61
W22-C[1]	5.43	3.14
W28-C	3.55	2.47
W29-C	4.29	2.75
W30-C	3.49	2.44
W31-C	5.47	3.15
	Avg.	2.81
	Std. Dev.	0.33
	Coeff. of Variation	11.6%
Centre-Sheathed Wall Configuration		
W15-CR3[1,3]	3.38	2.40
W23-CR3[2,3]	3.88	2.60
W24-CR3[3]	4.01	2.65
	Avg.	2.55
	Std. Dev.	0.13
	Coeff. of Variation	5.2%

[1] Tested by Santos (2017)

[2] Negative cycles not completed; value from positive cycles only

[3] Displacement limited by the stroke of the actuator during symmetric cyclic protocol

Table 4.22 Ductility and R_d values for cyclic tests – Negative range of cycles

Test ID	Ductility μ_-	Ductility-related force modification factor R_d
Double-Sheathed Wall Configuration		
W19-C[1]	3.79	2.57
W20-C[1]	4.84	2.95
W21-C[1]	3.72	2.54
W22-C[1]	4.80	2.93
W28-C	2.88	2.18
W29-C	3.39	2.40
W30-C	3.09	2.28
W31-C	5.26	3.09
	Avg.	2.62
	Std. Dev.	0.34
	Coeff. of Variation	12.8%
Centre-Sheathed Wall Configuration		
W15-CR3[1]	3.23	2.34
W24-CR3	4.12	2.69
	Avg.	2.51
	Std. Dev.	0.25
	Coeff. of Variation	9.9%

[1] Tested by Santos (2017)

Table 4.23 Ductility and R_d values for cyclic tests – Positive range of cycles

Test ID	Ductility μ_+	Ductility-related force modification factor R_d
Double-Sheathed Wall Configuration		
W19-C[4]	4.20	2.72
W20-C[4]	6.82	3.55
W21-C[4]	4.12	2.69
W22-C[4]	6.05	3.33
W28-C	4.23	2.73
W29-C	5.19	3.06
W30-C	3.88	2.60
W31-C	5.68	3.22
	Avg.	2.99
	Std. Dev.	0.35
	Coeff. of Variation	11.8%
Centre-Sheathed Wall Configuration		
W15-CR3[2,3,4]	3.52	2.46
W15B-CR3[1,3,4]	7.62	3.77
W23-CR3[2,3]	3.88	2.60
W23B-CR3[1]	5.00	3.00
W24-CR3[2,3]	3.89	2.61
W25-CR3[1,4]	5.12	3.04
W26-CR3[1]	2.99	2.23
	Avg.	2.82
	Std. Dev.	0.51
	Coeff. of Variation	18.1%

[1] Tested with asymmetric cyclic protocol

[2] Displacement limited by the stroke of the actuator during symmetric cyclic protocol

[3] Specimen did not reach $0.8*F_u$ post-peak

[4] Tested by Santos (2017)

Table 4.24 Ductility and R_d considering the walls tested with asymmetric protocol

Test ID	Ductility μ_+	Ductility-related force modification factor R_d
Centre-Sheathed Wall Configuration		
W15B-CR3[1,2,3]	7.62	3.77
W23B-CR3[1]	5.00	3.00
W25-CR3[1,3]	5.12	3.04
W26-CR3[1]	2.99	2.23
	Avg.	3.01
	Std. Dev.	0.63
	Coeff. of Variation	20.9%

[1] Tested with asymmetric cyclic protocol

[2] Specimen did not reach $0.8*F_u$ post-peak

[3] Tested by Santos (2017)

The difference in terms of ductility for the double-sheathed configuration between the results from Table 4.20 and Table 4.21 (- 23.5 %) is explained by the strength degradation happening quickly during the cyclic tests as explained in Section 3.5.1. The values in Tables 4.20 and 4.21 for the centre-sheathed configuration are relatively similar. However, the limited data for this comparison does not allow for any conclusive statement. In addition, the values obtained do not reflect the real behaviour of the specimens due to the limited displacement range experienced. The values from Tables 4.21 and 4.22, comparing the positive and negative range of the cyclic tests, are very consistent. The slight difference observed for the double-sheathed configuration can be explained by the fact the wall first becomes damaged while experiencing a positive excursion of a cycle, hence a reduced capacity entering into the subsequent negative excursion (Section 4.3), affecting the ductility quicker than in the positive range. As the centre-sheathed configuration has the advantage of confining the sheathing between two outer studs, preventing it from escaping the contact with the screws, the difference in behaviour between positive and negative cycles is negligible.

Although it was clearly observed that the centre-sheathed configuration could extensively deform in the inelastic range experiencing very high shear forces, Table 4.23 shows a smaller average R_d value for the centre-sheathed configuration when comparing the positive range of the cyclic tests. This can be attributed once again to the limited displacement range imposed by the actuator for the centre-sheathed specimen tested with the symmetric cyclic tests. However, when considering the asymmetric test only (i.e. larger displacement not restricted by the actuator in Table 4.24), the values obtained are almost identical for both configurations.

The ductility-related force modification factor is directly related to the ratio between the displacement at 80 % of the ultimate strength reached post-peak and the displacement achieved when reaching the yield shear strength obtained applying the EEEP method, Δ_μ/Δ_y, represented by μ (Equations 4.4 and 4.5).

Due to the very stiff chord studs of the double-sheathed specimens, the yield strength is reached relatively early during the test (average of 10.4 mm (0.41”) or 0.42 % drift as per Table 4.25), whereas for the centre-sheathed specimens, although a comparable stiffness is achieved (Tables 4.25 and 4.26), the yield strength is achieved at an average displacement of 29.7 mm (1.17”) or

1.2 % drift, a value 3 times that for the double-sheathed specimens. Thus, inelastic deformations on a range three times longer need to be achieved to obtain a comparable values for $\mu = \Delta_\mu / \Delta_y$.

Figure 4.11 illustrates this behaviour when comparing the double-sheathed test specimen W29-C with the centre-sheathed test specimen W25-CR3. W29-C is stiffer (as confirmed by Table 4.25 and 4.26) than W25-CR3, and W25-CR3 exhibits inelastic deformations on a displacement range more than three times longer than that for W29-C. However, when comparing the ductility μ, W29-C has a slightly higher ductility than W25-CR3.

Although these R_d values do not seem to reflect the general superior behaviour exhibited by these shear walls, by the centre-sheathed specimens in particular, they all are superior to the value of 2.0 recommended by the AISI S400 Standard *(2015)* for steel sheet sheathed shear walls in Canada.

Table 4.25 Yield displacement and stiffness for double-sheathed design – Positive cycles

Test ID	Displacement at S_y Δ_{y+} (mm)	Elastic Stiffness k_{e+} (kN/mm)
Double-Sheathed Wall Configuration		
W19-C[1]	12.37	4.15
W20-C[1]	7.41	4.37
W21-C[1]	12.27	4.29
W22-C[1]	7.18	4.57
W28-C	11.95	5.47
W29-C	7.79	5.72
W30-C	15.40	5.06
W31-C	8.52	5.77
Avg.	10.36	4.93
Std. Dev.	3.03	0.67
Coeff. of Variation	29.3%	13.5%

[1] Tested by Santos (2017)

Table 4.26 Yield displacement and stiffness for centre-sheathed design – Positive cycles

Test ID	Displacement at S_y Δ_{y+} (mm)	Elastic Stiffness k_{e+} (kN/mm)
Centre-Sheathed Wall Configuration		
W15-CR3[1]	32.37	5.15
W15B-CR3[1]	28.42	5.85
W23-CR3	32.34	5.24
W23B-CR3	30.45	5.53
W24-CR3	29.50	4.89
W25-CR3[1]	26.80	4.68
W26-CR3	27.89	5.51
Avg.	29.68	5.26
Std. Dev.	2.16	0.40
Coeff. of Variation	7.3%	7.7%

[1] Tested by Santos (2017)

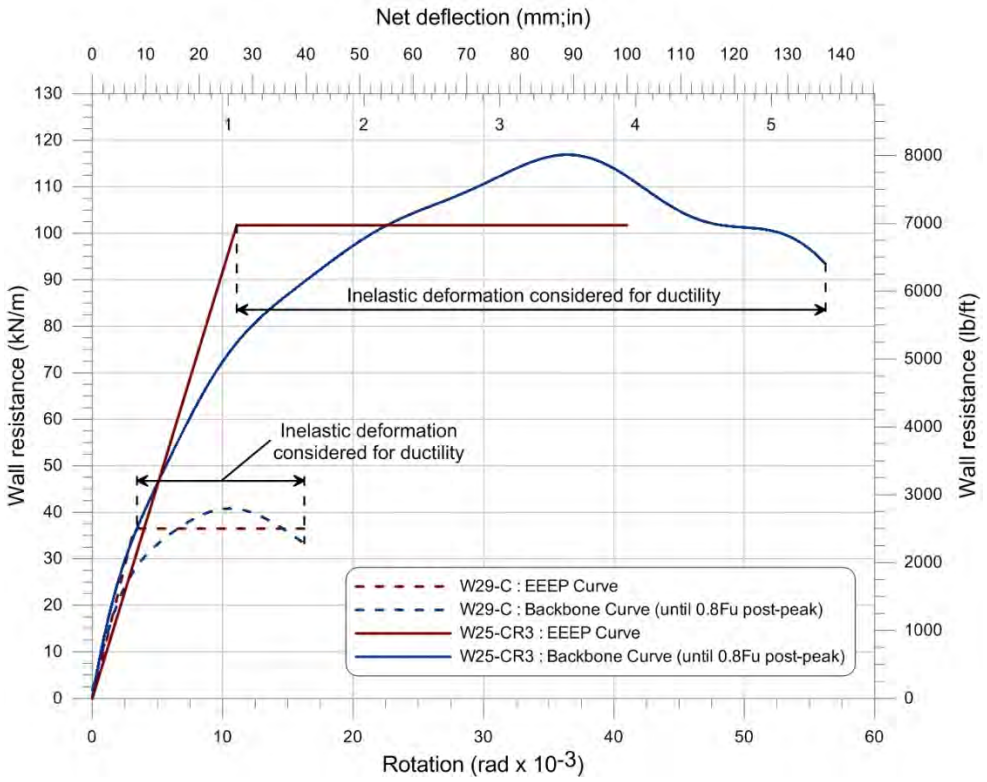

Figure 4.11 Inelastic deformations resulting in a similar R_d value for double-sheathed and centre-sheathed walls

4.4.4.2 "Test-based" overstrength-related force modification factor R_o

The resistance factors determined in Section 4.4.1 are used in limit states design to reduce (resistance factors are inferior to 1) the resistances calculated for a specific member or system, in order to account for the variability, of material for example, within the structure or member itself. The loads applied on a structure are increased using load factors in order to represent the probability of different loads occurring at the same time and the variability within a load type. In limit states design, the factored resistance has to be greater than the factored loads.

Capacity-based design relies on the fact the energy has to be dissipated within a specific part of the SFRS acting as a fuse; in the case of cold-formed steel sheathed shear walls, this fuse is the sheathing together with its connections. Through the use of resistance and load factors, the conditions to achieve the energy dissipation can often be overestimated and thus the energy dissipation may not be achieved when required. Therefore, the overstrength within the fuse

element is compensated in seismic design using the overstrength-related force modification factor, R_o, defined by the following equation proposed by Mitchell et al. *(2003)*:

$$R_o = R_{size} R_\phi R_{yield} R_{sh} R_{mech} \quad \text{Eq. 4.24}$$

where,

R_{size} = Overstrength from restricted choices for sizes and rounding of sizes;

$R_\phi = \frac{1}{\phi}$ = Accounting for the differences between nominal and factored resistances;

R_{yield} = Ratio of actual yield strength to minimum specified yield strength;

R_{sh} = Overstrength du to the development of strain hardening;

R_{mech} = Overstrength due to collapse mechanism.

R_{size} is a coefficient made to account for the fact that choices in terms of size of structural members are restricted in the industry, therefore the exact dimensions necessary to achieve a certain behaviour or strength can rarely be selected. The value selected in previous works was 1.05, it is going to be used in this program in order to stay consistent. R_ϕ is the inverse of the resistance factor, accounting for the differences between the nominal resistance and the factored resistance considered for design; as the ϕ values are different for both configurations, the following R_ϕ are obtained:

- Double-sheathed configuration: $R_\phi = {}^{1}/_{0.8} = 1.25$;
- Centre-sheathed configuration: $R_\phi = {}^{1}/_{0.7} = 1.43$.

R_{yield} accounts for the differences between the actual yield strength with the specified one, and is therefore equivalent to the overstrength factors defined in Section 4.4.3. The value attributed to R_{yield} regarding the double-sheathed configuration is 1.11 (average between the value for monotonic tests and the one for cyclic tests), whereas no overstrength will be considered for the centre-sheathed configuration; the overstrength factors obtained considering the values predicted with the preliminary Modified Effective Strip Method are very close to 1.0 and the method needs to be further optimized.

The overstrength due to strain-hardening is considered null for the cold-formed steel shear walls and R_{sh} = 1.0. In addition, R_{mech} is taken equal to 1.0 as well since the collapse mechanism has not yet been established. These same values are consistent with the previous works from Balh *(2010)* and DaBreo *(2012)*.

The double-sheathed configuration specimens obtained a R_o equal to 1.46 and the centre-sheathed walls a R_o equal to 1.50. These values are consistent with the value of 1.3 recommended in the AISI S400 *(2015)* for steel sheet sheathed shear walls in Canada.

Table 4.27 Overstrength-related force modification factor, R_o, for both configurations

	R_{size}	R_{ϕ}	R_{yield}	R_{sh}	R_{mech}	R_o
Double-sheathed configuration	1.05	1.25	1.11	1.00	1.00	**1.46**
Centre-sheathed configuration		1.43	1.00			**1.50**

4.4.5 The Use of R-Values in the Future

The analysis performed in this program in order to determine the seismic design parameters for Canada (Section 4.4.4) was based on experimental results and did not reflect the consequent improvements in terms of strength and ductile behaviour that the centre-sheathed specimens exhibited during the experimental program. Indeed, the latter configuration clearly exhibited much higher strength and ductility than the double-sheathed configuration tested throughout this same experimental program, although their R_dR_o combinations produced rather similar results.

Applying such values in design would result in overestimating the minimum seismic base shear force the Lateral Force Resisting System would have to resist. Thus, not only the number of shear walls necessary in design would be greater, all the members located within the load path used to transfer the lateral loads within the SFRS would have to be designed with respect to an overestimated load, resulting in selecting stronger members and connections than necessary. Using these “test-based” values would ultimately equate to disregard the safety reserve provided by these

shear walls through their extensive ductility and consider them as the equivalent to the CFS shear walls currently proposed for design in the CFS standards.

The FEMA P795 *(Federal Emergency Management Agency, 2011)* provides a recommended methodology (the Component Methodology), derived from the general methodology presented in FEMA P695 *(2009)* Quantification of Building Seismic Performance Factors, with the intent of ensuring that the buildings designed based on codes would have the adequate resistance to face and avoid the collapse of a building consequently to an earthquake. Following this procedure, a proposed component (such as the centre-sheathed design shear walls in the present study) can replace a reference component part of a SFRS if defined as equivalent by the Component Methodology. The reference component for this analysis would be the same as that described by Rizk *(2017)* based on all the single-sheathed configuration specimens tested in previous research programs on CFS shear walls (e.g. Yu et al. *(2007)*, Yu and Chen *(2009)*, Ong-Tone *(2009)* and Balh *(2010)*). However, the data set created during the present experimental program does not meet the requirements for this procedure, especially regarding the number of specimen per configuration to be analysed. In addition, this procedure properly completed would eventually result in authorizing the use of the centre-sheathed configuration's shear walls as an equivalent to the reference component, which would result in neglecting the superior behaviour of the centre-sheathed configuration once more.

For a thorough evaluation and selection of R-values for seismic design, along with a revised height limit, other experimental programs should be carried out in order to collect more data and obtain a broader data sample. In addition, the preliminary design method introduced in Section 4.3 should be refined following the findings obtained in this future research, the participation of the screws with respect to their position on the wall in particular. It is then imperative that a numerical analysis be carried out in line with the methodology found in FEMA P695 *(2009)*, which involves non-linear response history dynamic analyses of representative buildings constructed with the specific shear wall system in question. The dynamic models include force-deformation elements that replicate the measured hysteretic behaviour of the lateral system being investigated. All this considered, it is anticipated that a numerical investigation of this nature would demonstrate that a higher R-value, along with greater height limits, could be used in design due to the ability of the centre-sheathed configuration shear walls to carry lateral load at large drift.

CHAPTER 5 – CONCLUSIONS AND FUTURE RESEARCH

5.1 Conclusions

The construction details used for CFS framed shear walls to date have largely been restricted to a light cold-formed steel frame with thin steel sheathing installed on one side. When thick sheathing and / or a close screw spacing were used the chord studs of this configuration were prone to damage due to the eccentricity of the sheathing placement, which resulted in high torsional and axial forces. Reinforcement of the chord studs with bridging or blocking was investigated in prior studies, with mixed success.

The present experimental program allowed for the development of new configurations for cold-formed steel shear walls using steel sheet sheathing, with the intent of achieving higher strength and ductility to move towards their use in mid-rise buildings. Thicker material was used for both the sheathing and the framing, as well as larger screws to fasten the sheathing to the frame. Two innovative configurations were tested; the double-sheathed configuration and the centre-sheathed configuration, both with a common main objective of concentric placement of the sheathing and thus a reduction in the torsional forces applied to the chord studs. Overall, 31 shear walls were tested through monotonic and cyclic protocols, including 16 walls of the double-sheathed configuration (8 monotonic and 8 cyclic) and 15 wall of the centre-sheathed configuration (6 monotonic and 9 cyclic). The author was responsible for 15 of these walls, while a report on the remaining walls was written by Santos *(2017)*.

5.1.1 Double-sheathed configuration

The double-sheathed configuration comprised two steel sheets, one on the front and one the back side of the shear wall. They were fastened to built-up box chord studs made of large cold-formed steel members, capable of higher axial, moment and torsional resistances than the regular chord studs commonly specified in design. The double-sheathed specimens were tested monotonically and cyclically, using the CUREE reversed cyclic loading protocol as per the previous studies. As observed throughout the previous test programs carried out on steel sheathed shear walls, the shear

resistance of a specimen was influenced by the building parameters it was constructed with; thicker material, larger screws and smaller screw spacing all had the same impact increasing the shear strength of the specimen.

This configuration performed well in terms of increased shear strength while preserving the physical integrity of the framing; the strongest specimen achieved an ultimate shear resistance of 67.6 kN/m (4631 lb/ft), about two times what is currently available for design of a wall with sheathing on one side in AISI S400. However, it did not show improvement in terms of ductile behaviour, especially during the cyclic tests, where the screw connections pulled through the sheathing after the tear-shape holes were generated by extensive steel bearing damage. The consequences were a quick loss of shear strength resulting in ductility measurements similar to that exhibited by shear walls built using a regular construction details.

The test results were analysed using the Equivalent Energy Elastic-Plastic (EEEP) approach as per previous studies, to transform the non-linear behaviour of these shear walls into an equilvalent bilinear elastic-plastic behaviour. The Canadian design values such as the yield shear resistance, yield displacements, elastic stiffness, ductility and energy dissipation were all determined from this method for each shear wall. The design values for the USA and Mexico (i.e. ultimate shear resistance, associated displacement and chord rotations) were provided directly from the test results.

The resistance factor for use in limit states design (LSD and LRFD), ϕ, was determined based on the EEEP approach; it obtained the values of 0.71 and 0.86 respectively, both superior to the value recommended ($\phi = 0.7$) in the previous studies. Factors of safety equal to 1.57 (monotonic tests) and 1.60 (cyclic tests) for Canada (LSD) were obtained, 1.37 and 1.40 for the USA and Mexico (LRFD). These values are lower than the average factor of safety computed in Balh et al. *(2014)* (ranging from 1.9 and 2.0). This can be explained by the lower ductility exhibited; the force dropped quickly after the ultimate strength resulting in an EEEP curve behaving similarly to the monotonic / backbone curve. The overstrength design values were consistent, with an average of 1.11 and a low variability. The seismic design parameters, R_d and R_o, for use in Canada were evaluated using a “test-based” approach; the ductility-related seismic force modification factor, R_d, obtained an average value of 2.8 when considering the cyclic tests and the overstrength-related

seismic force modification factor, R_o, obtained a value of 1.46. Both these values are superior to the values of R_d = 2.0 and R_o = 1.3 recommended by the AISI S400 Standard *(2015)* for steel sheet sheathed shear walls in Canada.

Although an increase in ultimate shear strength was observed for this configuration, the behaviour did not fully lend itself to a possible use in mid-rise construction. Therefore, the focus of the present study was switched to the second innovative configuration; that is, the centre-sheathed shear wall.

5.1.2 Centre-sheathed configuration

This configuration allowed for a concentric placement of the sheathing, which was confined between the built-up vertical and horizontal framing members. The framing member design approach was developed through an iterative process due to the lack of an existing design procedure prior to launching the test program. This process was initially based on the available method used for the design of cold-formed steel shear walls with steel sheet sheathing in the USA and Mexico provisions of AISI S400 *(2015)*; that is, the Effective Strip Method by Yanagi and Yu *(2014)*. The first tests experienced failure of the compression chord stud due to the combination of high axial compression load and bending moment caused by the development of shear forces in the wall at a level substantially higher than anticipated. The Effective Strip Method was underestimating the extent of the tension field width and bearing resistance at fastener locations.

The design method of the framing was subsequently adjusted based on the observations made with respect to the width of the tension field in the sheathing and the number of fasteners that participated in carrying shear load. After a couple iterations, the final configuration was adopted, whereby the tension field was assumed to develop over the full width of the sheathing. In addition, the bearing strength prediction for the sheathing screw connections was adopted from the double shear bolt connection provision from the AISI S100 Standard *(2015)* and CSA S136 *(2012)*. Although this calculation method was not originally intended for use with screw fasteners, it was considered to be a reasonable choice given the inner ply bearing failure mechanism. As a result, the shear forces sustained by the walls were so high that the initial chord stud detail required a full

built-up box chord stud (the same as the one used for the double-sheathed configuration) on its side to act as reinforcement.

Two cyclic test protocols were used for the centre-sheathed specimens; a CUREE reversed cyclic protocol was used for the first cyclically tested specimens, whereas the last four were tested using an asymmetric cyclic protocol to capture the entire inelastic load-deformation behaviour. Indeed, the first cyclic tests of the centre-sheathed configuration using the final design of the reinforced chord studs showed a very high shear strength coupled with a high ductility, resulting in an absence of strength degradation over the ±125 mm (±4.92”) lateral displacement range imposed by the actuator. An asymmetric cyclic test protocol was created using the main principles of the CUREE reversed cyclic protocol, limiting the negative range to 5 mm (0.20”), allowing for larger lateral displacements on the positive side with a -5 mm to +225 mm considered range. Eventually, strength degradation was observed for the centre-sheathed configuration’s specimen using this protocol.

Once again, the shear resistance of a specimen was influenced by the building parameters it was constructed with (i.e. thicker material, larger screws and smaller screw provide higher shear strength). However, these parameters had to be constrained to a certain range for this configuration; the actuator capacity as well as the resistance of the chord studs facing high axial compressive force and bending moment imposed the upper limit to the shear strength of the specimens. In addition, the screw spacing had to be limited on the other end of the range as well; too large of a screw spacing would result in the separation of the built-up chord stud due to a large out-of-plane force caused by the shear buckling of the sheathing.

Performance-wise, the centre-sheathed configuration presented the advantage of keeping the sheathing working with the connections through an extensive drift range. The sheathing was confined between the framing members preventing it from escaping the screw connectors when tear-shape holes appeared as a result of large storey-drift. This allowed for full use of the extensive bearing failure mechanism. The strongest specimen from the centre-sheathed configuration achieved an ultimate shear resistance of 165.7 kN/m (11352 lb/ft), more than 4 times what is currently available for design, at a drift ratio superior to 6 %.

As per the double-sheathed configuration, the test results were analysed using the Equivalent Energy Elastic-Plastic (EEEP). However, the intent for this configuration was to define a design procedure, using a prediction method adapted to these new construction details: the preliminary Modified Effective Strip Method developed as moving along the iterative design process. Because of the high ultimate resistance developed at large drift ratios, the values considered for design were chosen differently, using the 2.5 % inelastic storey-drift limit criterion from the ASCE/SEI 7 *(2016)* and NBCC *(2015)*. Thus, the shear strength considered for the calibration of the prediction method was the shear strength achieved by the tested specimens at 2.5 % drift. The average test-to-predicted ratio was consistent, although presenting a high variability attributed to the preliminary stage of the method.

The resistance factor for use in limit states design (LSD and LRFD), ϕ, was determined based on the preliminary Modified Effective Strip Method and obtained the values of 0.64 and 0.79 respectively. The ϕ value with regard to the LSD procedure is lower than that from the previous test programs where a conservative resistance factor $\phi = 0.7$ was always considered. Nevertheless, this lower value can be attributed to the preliminary stage of the prediction method, which is in need of refinement. The bearing resistance computed used an equation available for bolts and the observed bearing damages indicated that although all of the sheathing screws participated in resisting the lateral load, they did not do so to the same extent. Taking these remarks into consideration, the anticipated ranges of 0.8 to 0.9 and 0.7 to 0.75 were considered for the ϕ factor with regard to the LRFD and LSD procedures, respectively. The factor of safety with regard to the cyclic tests gave even lower values than for the double-sheathed configuration (1.54 for LSD and 1.35 for LRFD) with a higher variability. This is attributed once again to the variability of the preliminary prediction method. The computation of the overstrength for the centre-sheathed configuration led to the conclusion that no overstrength should be considered for this configuration until further investigation and development of the prediction method. The average value for the ductility-related seismic force modification factor, R_d, was 2.8 when considering the positive range of all the cyclic tests performed, it reached 3.0 when considering the asymmetric tests only. The overstrength-related seismic force modification factor obtained a value of 1.5. Once again, the "test-based" seismic design parameters are in line with those listed in the AISI S400 Standard.

Although the tests made obvious the fact the centre-sheathed configuration can carry considerable lateral loads at large drifts, it was not reflected by the "test-based" R_d value obtained, as it was similar to that obtained for the double-sheathed configuration. A numerical investigation in line with the methodology found in FEMA P695 *(2009)* should be performed for the centre-sheathed configuration and would most likely result in R_d values better reflecting the behaviour of these shear walls.

5.2 Future Research

The centre-sheathed configuration opened a new window regarding the use of cold-formed steel shear walls using steel sheet sheathing in buildings, and looks to be promising in terms of integrating these walls into mid-rise construction. However, certain aspects still are at the primary stage and further research is needed. An important step will be to quantify the building seismic performance factors in accordance with the Federal Emergency Management Agency (FEMA) P695 *(2009)*, as indicated in Section 4.4.5.

This study highlighted the need of a new equation for the bearing strength of double shear screw connections. Laboratory tests of the connection must be realised in order to quantify its advantages and increase the level of precision of the strength prediction for this type of connection. Further, it showed all the sheathing screws impacted the shear resistance, although they did so with a different degree of participation. This aspect must be further investigated to define what are the parameters interfering with the degree of participation (screw pattern, position of the screw, etc.) and quantify their effect on the shear resistance of a specimen. The preliminary Modified Effective Strip Method introduced during this research project would be optimized integrating these new parameters. Such a design method would offer the engineers a wider choice for the construction parameters, therefore giving them the ability to choose precisely the design resistance for their shear walls and, consequently, make sure the chord studs are designed accordingly.

The centre-sheathed specimens investigated in this research project presented very high shear strengths, exceeding by far what could be experienced by a shear wall in a mid-rise building during a regular seismic event. Therefore, lower-strength walls must be designed in such a way that their capacity would range between 30 and 75 kN/m (2056-5139 lb/ft), representing more realistic

situations, while maintaining the same level of ductility. The screw spacing has to remain in a certain range to prevent the built-up chord stud members from separating because of the out-of-plane forces imposed by the shear buckling of the sheathing. This range would probably be similar to the one experienced in the present research project (i.e. 50 to 100 mm (2" to 4")) although using thinner material and / or different screw sizes. Thinner sheathing material must be evaluated in order to determine whether it will achieve the same ductility but at lower force levels.

Consequently, a numerical dynamic analysis of representative CFS framed buildings following the methodology found in FEMA P695 *(2009)* should be carried out to validate the *R*-values, height limit and other associated seismic design parameters for the centre-sheathed wall system. Eventually, numerical simulations for multi-storey shear walls subjected to seismic excitations should be realised.

Given the high loads the centre-sheathed specimens can attract, further research should be carried out with regard to the connections used to transfer the lateral forces from the diaphragm to the wall, as well as the connections transferring the forces from one wall to the other through the floor structure. Connection details must then be provided to ensure the transfer of the lateral forces from the Lateral Force Resisting System (LFRS) to the base of the structure.

In addition, a study investigating the potential use of cold-formed steel shear walls with the centre-sheathed configuration in mid-rise construction should be carried out, in comparison with the other alternatives currently available for design (such as steel plate shear walls, concrete shear walls and other comparable LFRS). This could push towards a quicker integration of such LFRS in mid-rise construction.

REFERENCES

CFS 9.0.4, RSG Software, Inc.

MATLAB R2015b (v8.6), 2015, The MathWorks, Inc.

SAP2000 v14.2.4, 2010, Computers and Structures, Inc.

AISI (2015). "North American Standard for Seismic Design of Cold-formed Steel Structural Systems." *AISI S400-15*, American Iron and Steel Institute, Washington, DC, USA.

AISI (2016). "North American Specification for the Design of Cold-Formed Steel Structural Members." *AISI S100-16*, American Iron and Steel Institute, Washington, DC, USA.

ASCE (2016). "Minimum Design Loads and Associated Criteria for Buildings and Other Structures" *ASCE/SEI 7-16*, American Society of Civil Engineers.

ASTM (2010). "Standard Test Methods and Definitions for Mechanical Testing of Steel Products." *ASTM A370-10*, ASTM International, West Conshohocken, PA, USA.

ASTM (2011). "Standard Test Methods for Cyclic (Reversed) Load Test for Shear Resistance of Vertical Elements of the Lateral Force Resisting Systems for Buildings." *ASTM E2126-11*, ASTM International, West Conshohocken, PA, USA.

Balh, N. (2010). "Development of seismic design provisions for steel sheathed shear walls." Master's Thesis, Department of Civil Engineering and Applied Mechanics, McGill University, Montreal, Québec, Canada.

Balh, N., DaBreo, J., Ong-Tone, C., El-Saloussy, K., Yu, C., and Rogers, C. (2014). "Design of Steel Sheathed Cold-Formed Steel Framed Shear Walls." *Thin Walled Structures*, Vol. 75, p. 76-86.

Boudreault, F.-A. (2005). "Seismic Analysis of Steel Frame / Wood Panel Shear Walls." Master's Thesis, Department of Civil Engineering and Applied Mechanics, McGill University, Montreal, Québec, Canada.

Boudreault, F. A., Blais, C., and Rogers, C. A. (2007). "Seismic force modification factors for light-gauge steel-frame - wood structural panel shear walls." *Canadian Journal of Civil Engineering*, Vol. 34 (No. 1), 56-65.

Branston, A. E. (2004). "Development of a Design Methodology for Steel Frame / Wood Panel Shear Walls." Master's Thesis, Department of Civil Engineering and Applied Mechanics, McGill University, Montreal, Québec, Canada.

C-CFS-15 (2015). "Connectors for Cold-Formed Steel Construction." Simpson Strong-Tie Company Inc.

CSA (2012). "North American Specification for the Design of Cold-Formed Steel Structural Members." *CSA S136-12*, Canadian Standards Association, Mississauga, ON, Canada.

DaBreo, J. (2012). "Impact of Gravity Loads on the Lateral Performance of Cold-Formed Steel Frame / Steel Sheathed Shear Walls." Master's Thesis, Department of Civil Engineering and Applied Mechanics, McGill University, Montreal, Québec, Canada.

DaBreo, J., Balh, N., Ong-Tone, C., and Rogers, C. (2014). "Steel Sheathed Cold-Formed Steel Framed Shear Walls Subjected to Lateral and Gravity Loading." *Thin Walled Structures*, Vol. 74, p. 232-245.

El-Saloussy, K. (2010). "Additional Cold-formed Steel Frame/steel Sheathed Shear Wall Design Values for Canada." Project Report, Department of Civil Engineering & Applied Mechanics, McGill University, Montreal, Québec, Canada.

FEMA (2009). "Quantification of Building Seismic Performance Factors." *FEMA P695*, Federal Emergency Management Agency, Washington, DC, USA.

FEMA (2011). "Quantification of Building Seismic Performance Factors: Component Equivalency Methodology." *FEMA P795*, Federal Emergency Management Agency, Washington, DC, USA.

Foliente, G. C. (1996). "Issues in Seismic Performance Testing and Evaluation of Timber Structural Systems." *International Wood Engineering Conference*, October 28-31, 1996, New Orleans, USA.

Krawinkler, H., Parisi, F., Ibarra, L., Ayoub, A., and Medina, R. (2000). "Development of a Testing Protocol for Woodframe Structures." *CUREE Publication No. W-02*, Consortium of Universities for Research in Earthquake Engineering (CUREE), Richmond, CA, USA.

Lu, S. (2015). "Influence of gypsum panels on the response of cold-formed steel framed shear walls." Master's Thesis, Department of Civil Engineering and Applied Mechanics, McGill University, Montreal, Québec, Canada.

Mitchell, D., Tremblay, R., Karacabeyli, E., Paultre, P., Saatcioglu, M., and Anderson, D. L. (2003). "Seismic force modification factors for the proposed 2005 edition of the National Building Code of Canada." *Canadian Journal of Civil Engineering*, Vol. 30 (No. 2), 308-327.

Morello, D. (2009). "Seismic Performance of multi-Storey Structures with Cold-Formed Steel Wood Sheathed Shear Walls." Master's Thesis, Department of Civil Engineering and Applied Mechanics, McGill University, Montreal, Québec, Canada.

NRC (2015). "National Building Code of Canada 2015." *NBC 2015*, National Research Council Canada, Ottawa, ON, Canada.

Ong-Tone, C. (2009). "Tests and Evaluation of Cold-Formed Steel Frame / Steel Sheathed Shear Walls." Project Report, Department of Civil Engineering & Applied Mechanics, McGill University, Montreal, Québec, Canada.

Park, R. (1989). "Evaluation of Ductility of Structures and Structural Assemblages from Laboratory Testing." *Bulletin of the New Zealand National Society for Earthquake Engineering*, Vol. 22 (No. 3), 155-166.

Rizk, R. (2017). "Cold-Formed Steel Frame - Steel Sheathed Shear Walls: Improved Range of Shear Strength Values Accounting for Effect of Full Frame Blocking and Thick Sheathing / Framing Members." Master's Thesis, Department of Civil Engineering and Applied Mechanics, McGill University, Montreal, Québec, Canada.

Santos, V. (2017). "Higher Capacity Cold-Formed Steel Sheathed and Framed Shear Walls for Mid-rise Buildings : Part 1." Master's Thesis, Department of Civil Engineering and Applied Mechanics, McGill University, Montreal, Québec, Canada.

Serrette, R., Encalada, J., Hall, G., Matchen, B., Nguygen, H., and Williams, A. (1997). "Additional Shear Wall Values for Light Weight Steel Framing." *AISI-Specifications for the Design of Cold-Formed Steel Structural Members. 118,* Santa Clara, California (USA) - [Report No. LGSRG-1-97].

Shamim, I. (2012). "Seismic Design of Lateral Force Resisting Cold-Formed Steel Framed (CFS) Structures." Master's Thesis, Department of Civil Engineering and Applied Mechanics, McGill University, Montreal, Québec, Canada.

Shamim, I., DaBreo, J., and Rogers, C. (2013). "Dynamic Testing of Single- and Double-Story Steel-Sheathed Cold-Formed Steel-Framed Shear Walls." *Journal of Structural Engineering*, Vol. 139 (No. 5), p. 807-817.

Shamim, I., and Rogers, C. (2013). "Steel sheathed/CFS framed shear walls under dynamic loading: numerical modelling and calibration." *Thin-Walled Structures*, Vol. 71, p. 57-71.

Shamim, I., and Rogers, C. (2015). "Numerical evaluation: AISI S400 steel-sheathed CFS framed shear wall seismic design method." *Thin-Walled Structures*, Vol. 95, p. 48-59.

SMDI (2010). "Cold-Formed Steel in Buildings Construction." Steel Market Development Institute.

Yanagi, N., and Yu, C. (2014). "Effective Strip Method for the Design of Cold-Formed Steel Framed Shear Wall with Steel Sheet Sheathing." *Journal of Structural Engineering*, Vol. 140 (No. 4).

Yu, C. (2010). "Shear resistance of cold-formed steel framed shear walls with 0.686 mm, 0.762 mm, and 0.838 mm steel sheet sheathing." *Engineering Structures*, Vol. 32 (No. 6), 1522-1529.

Yu, C., and Chen, Y. (2009). "Steel Sheet Sheathing Options for Cold-Formed Steel Framed Shear Wall Assemblies Providing Shear Resistance - Phase 2." Department of Engineering Technology, University of North Texas, Denton, Texas (USA) - [Report No. UNT-G70752].

Yu, C., and Chen, Y. (2011). "Detailing recommendations for 1.83 m wide cold-formed steel shear walls with steel sheathing." *Journal of Constructional Steel Research*, Vol. 67 (No. 1), 93-101.

Yu, C., Vora, H., Dainard, t., Tucker, J., and Veetvkuri, P. (2007). "Steel Sheet Sheathing Options for Cold-Formed Steel Framed Shear Wall Assemblies Providing Shear Resistance." Department of Engineering Technology, University of North Texas, Denton, Texas (USA) - [Report No. UNT-G76234].

APPENDIX A. DETAILS FOR TEST CONFIGURATIONS

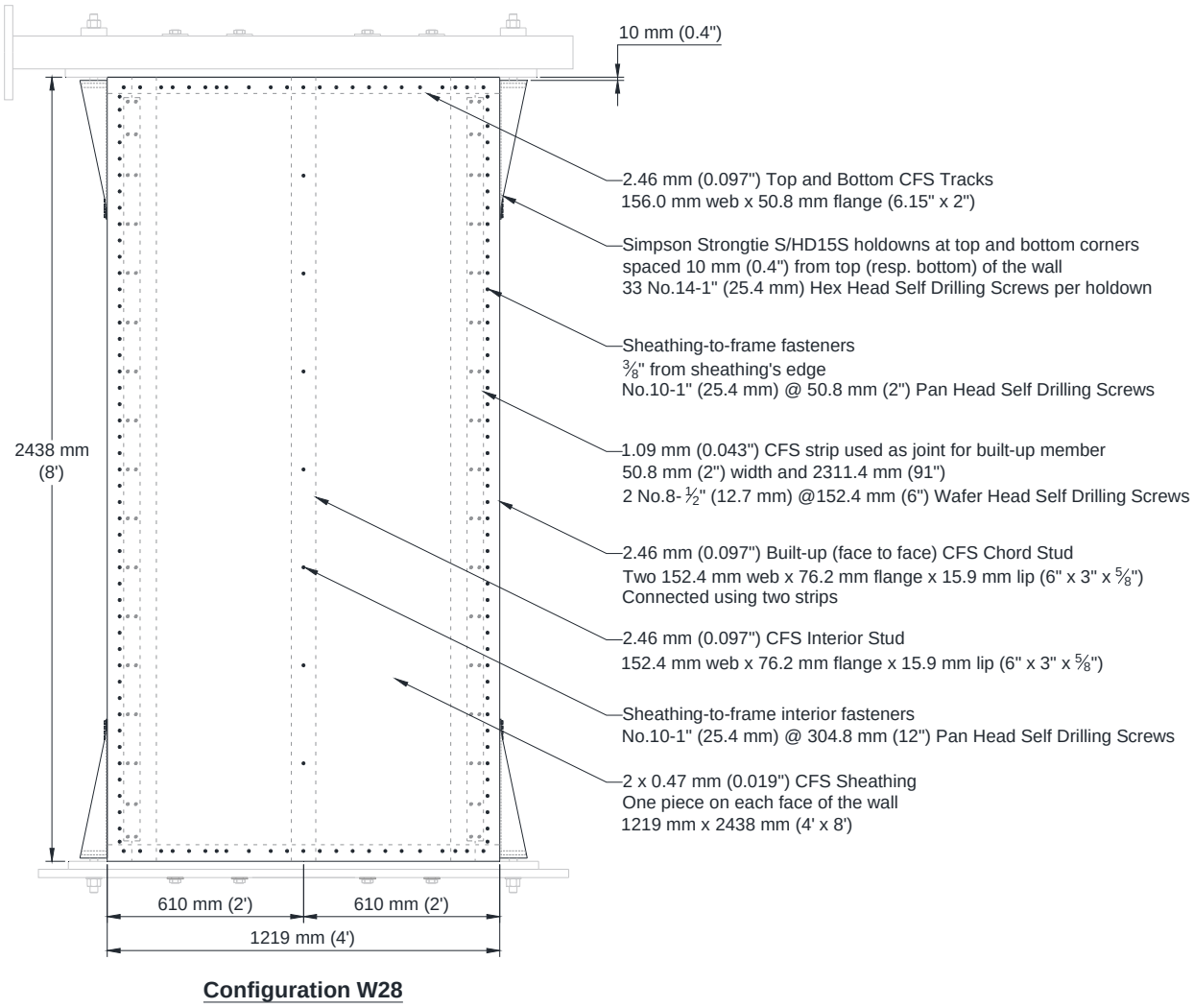

Figure A-1 Double-sheathed configuration: dimensions and specifications for walls W28

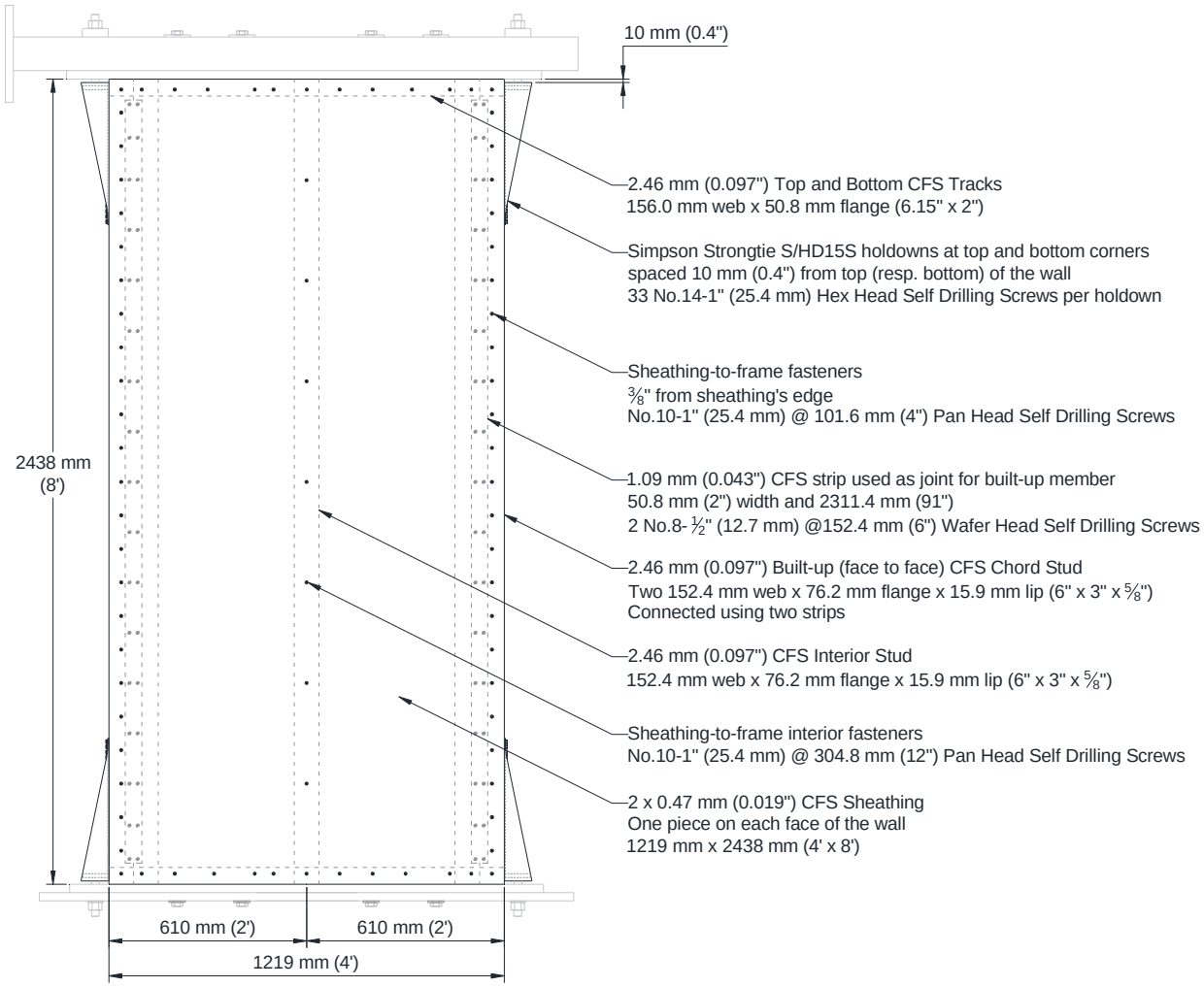

Configuration W29

Figure A-2 Double-sheathed configuration: dimensions and specifications for walls W29

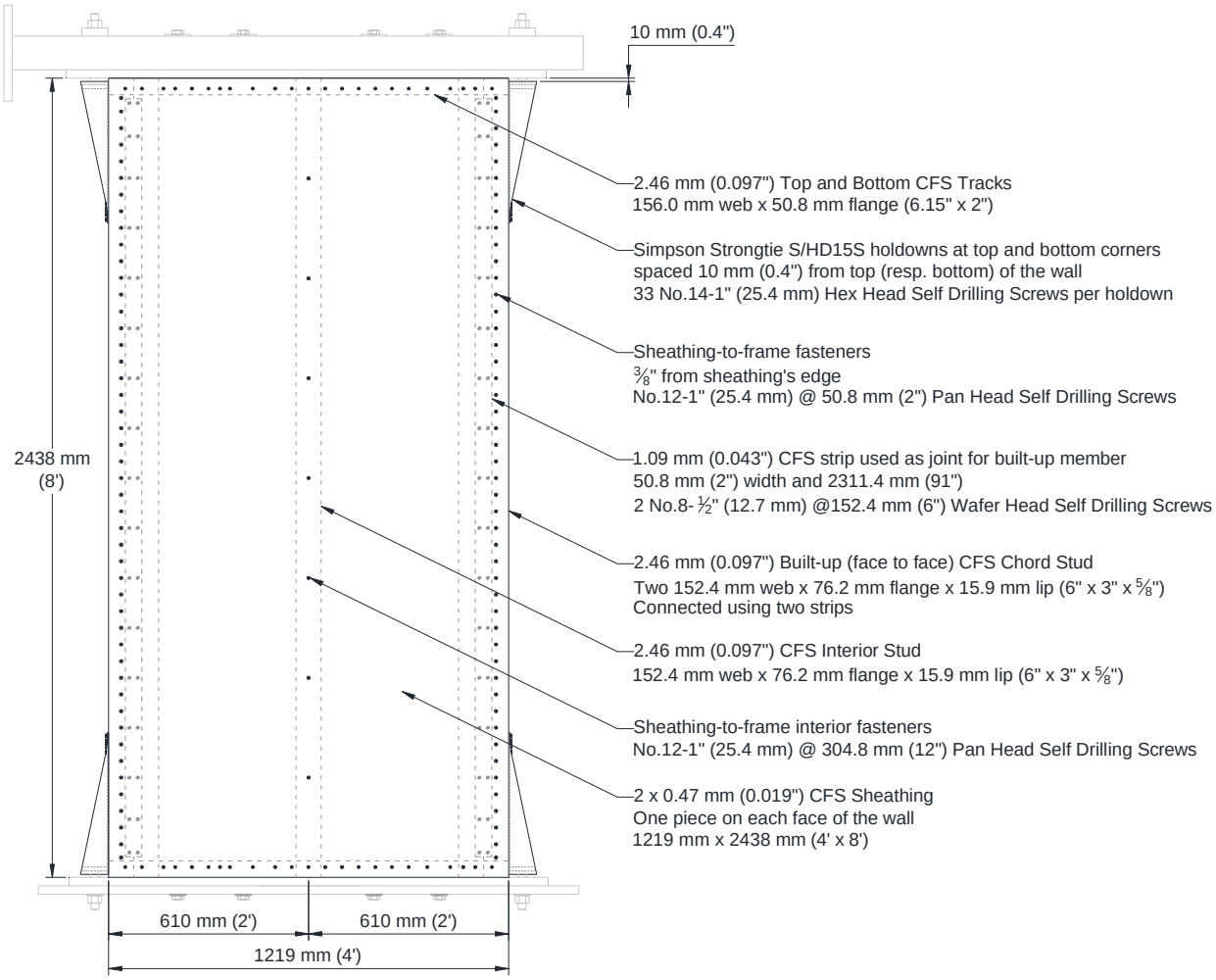

Figure A-3 Double-sheathed configuration: dimensions and specifications for walls W30

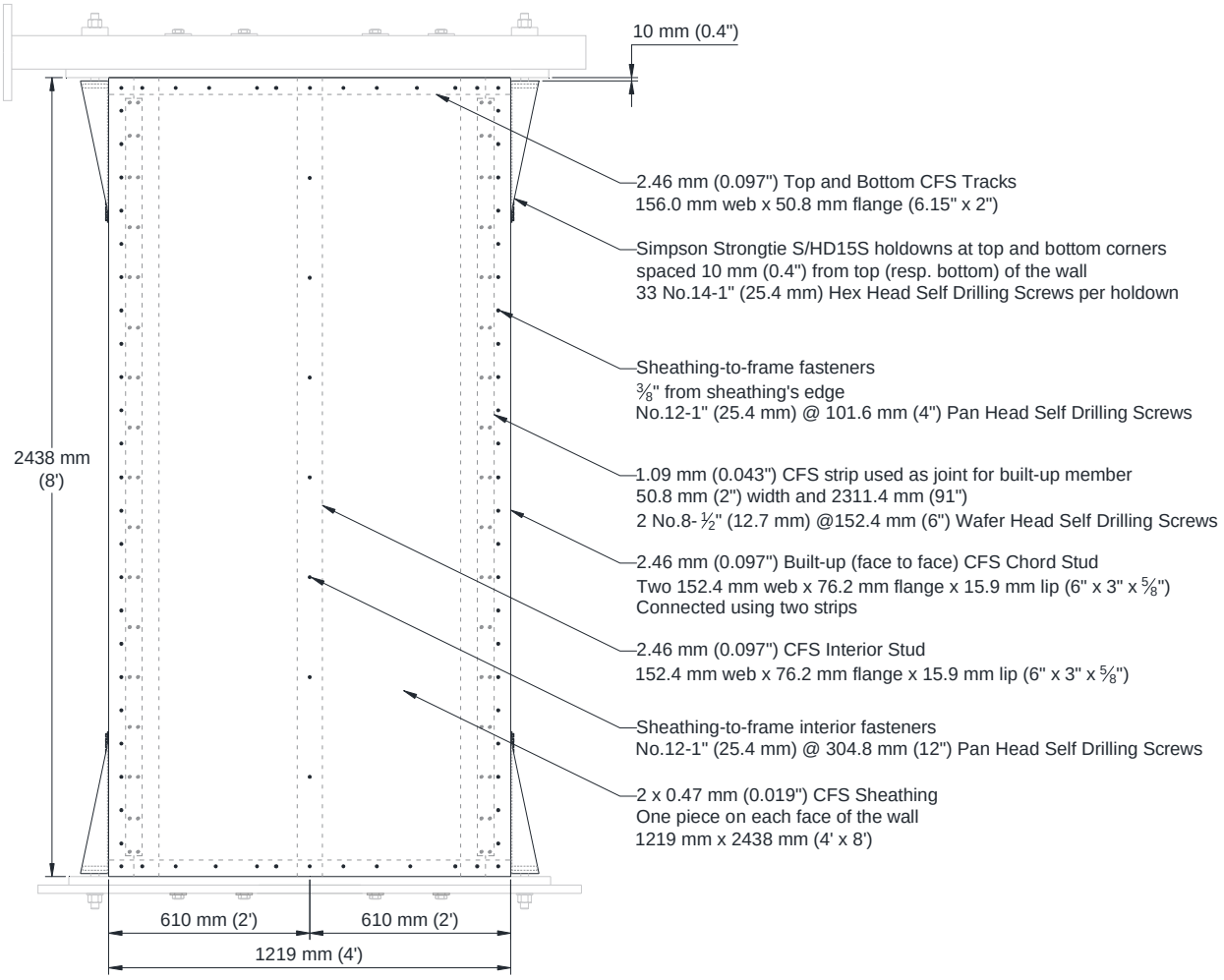

Figure A-4 Double-sheathed configuration: dimensions and specifications for walls W31

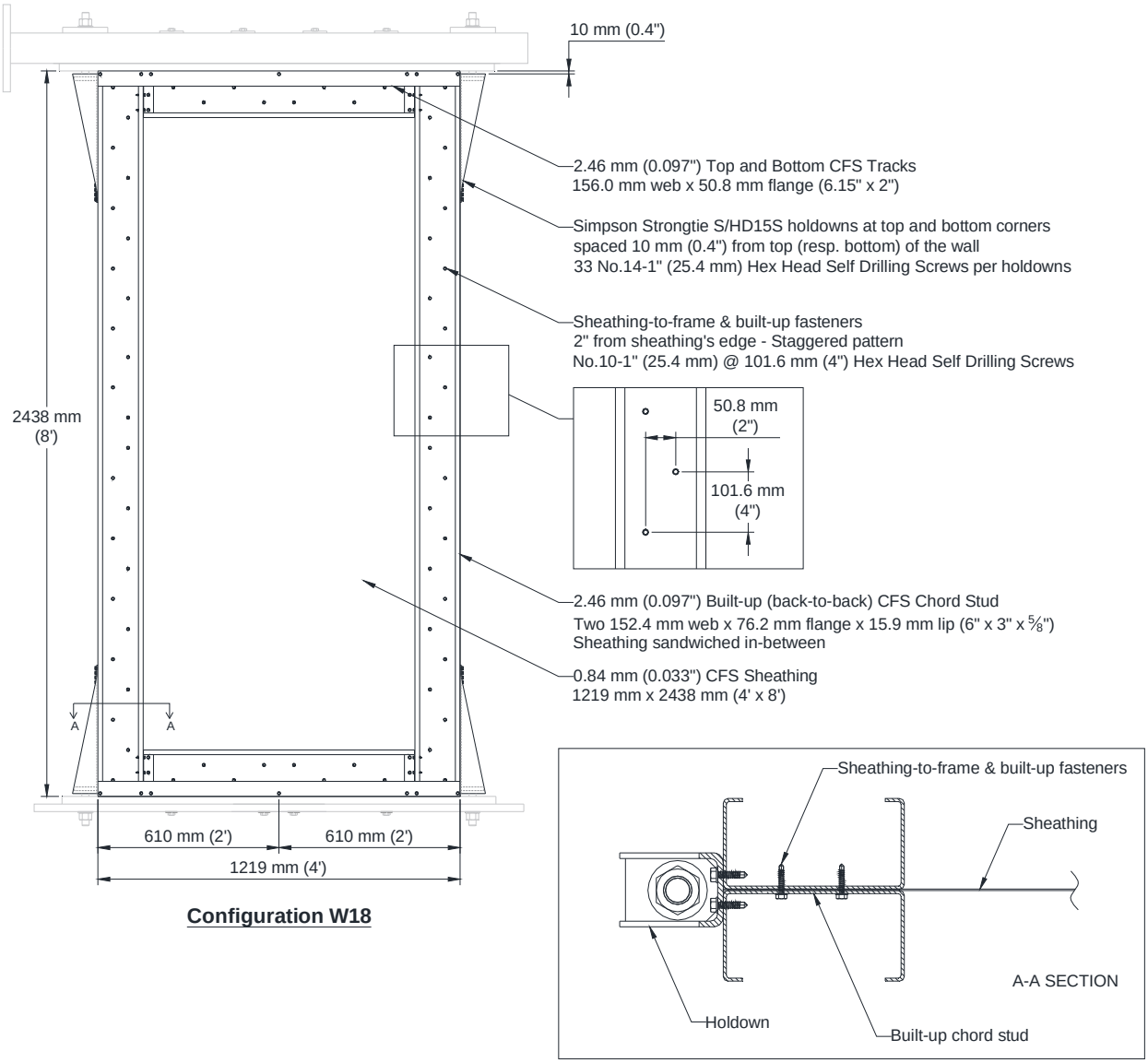

Configuration W18

Figure A-5 Centre-sheathed configuration: dimensions and specifications for wall W18

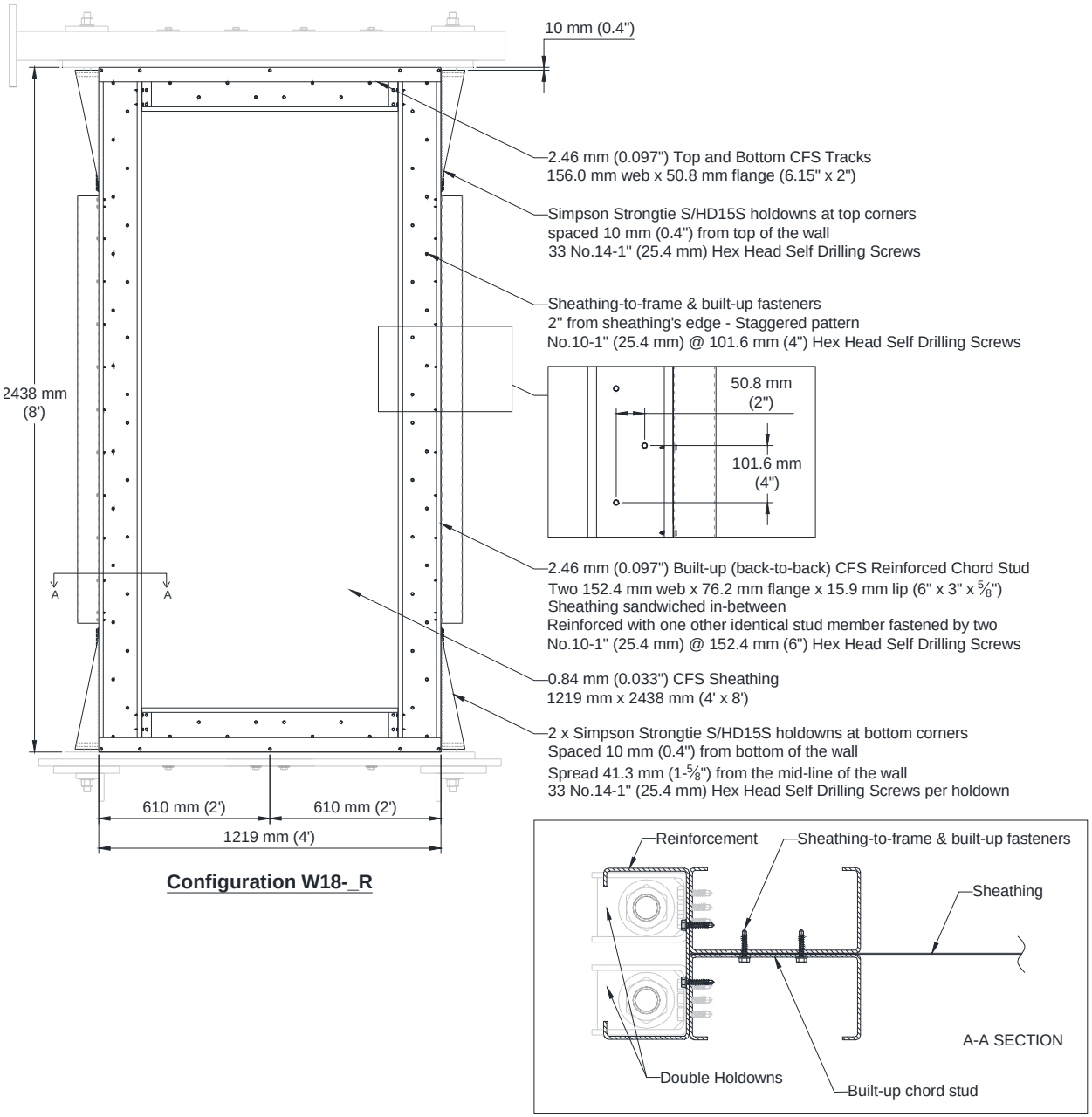

Configuration W18-_R

Figure A-6 Centre-sheathed configuration: dimensions and specifications for walls W18-_R

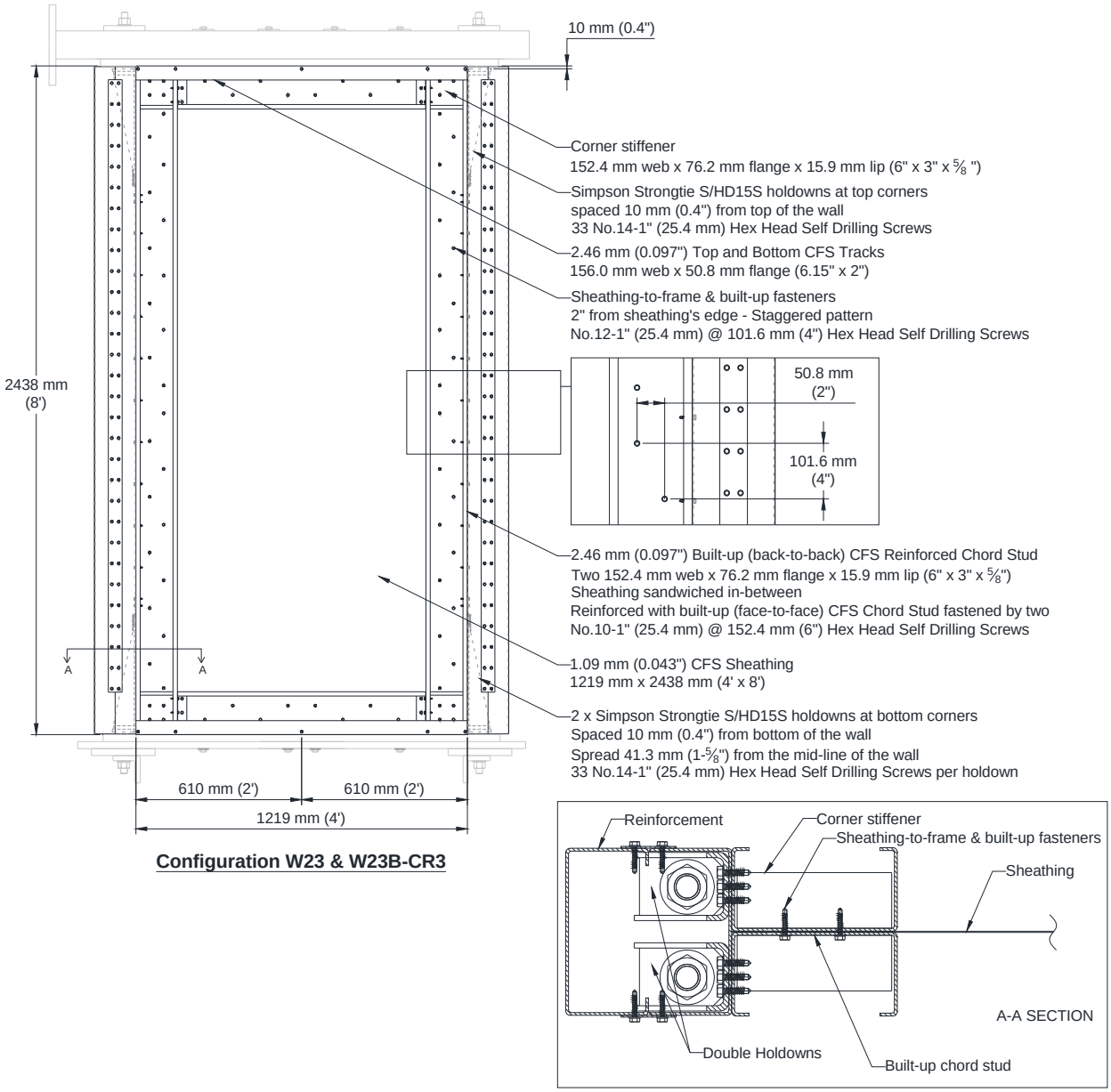

Configuration W23 & W23B-CR3

Figure A-7 Centre-sheathed configuration: dimensions and specifications for walls W23 & W23B-CR3

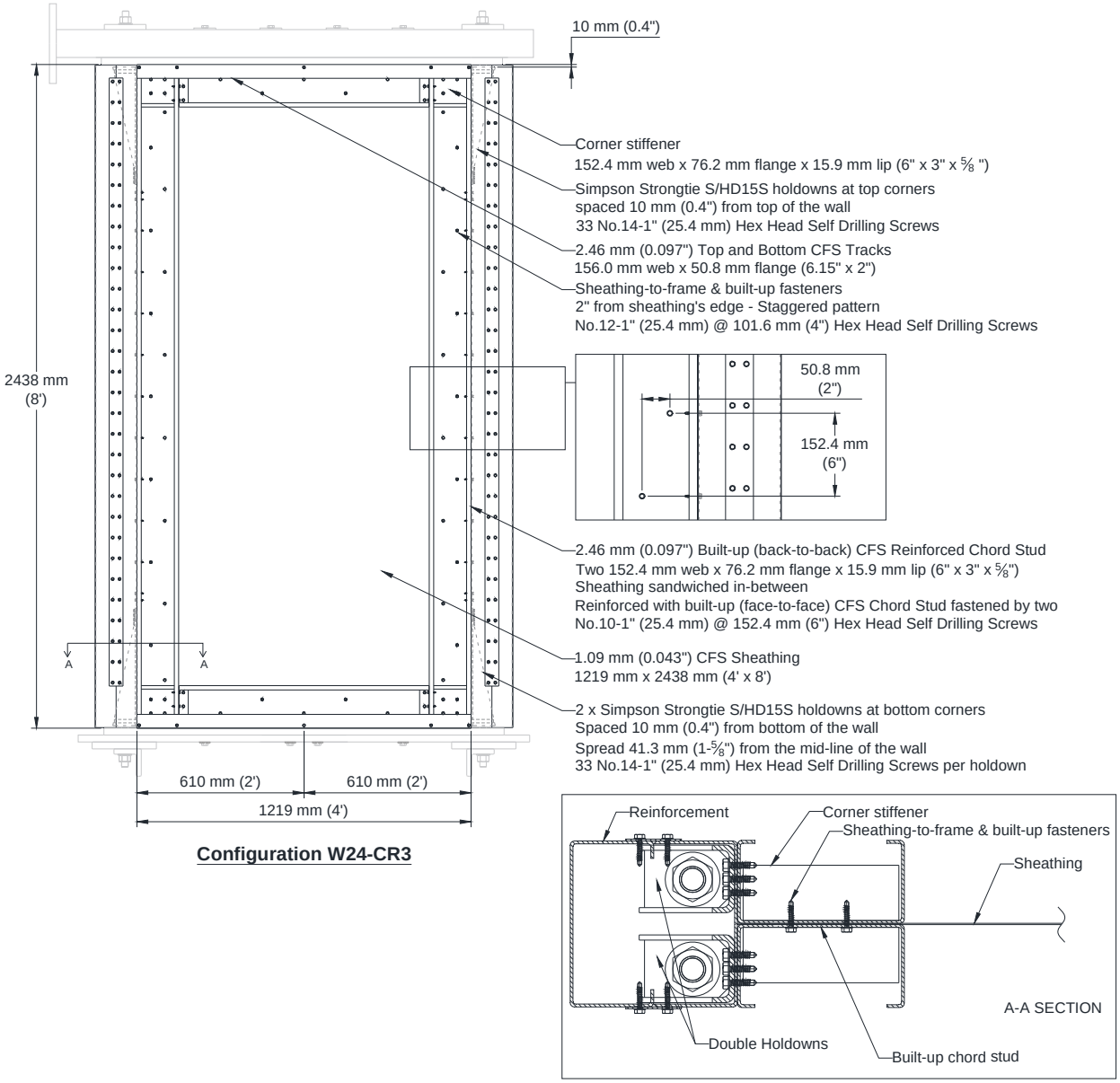

Configuration W24-CR3

Figure A-8 Centre-sheathed configuration: dimensions and specifications for wall W24-CR3

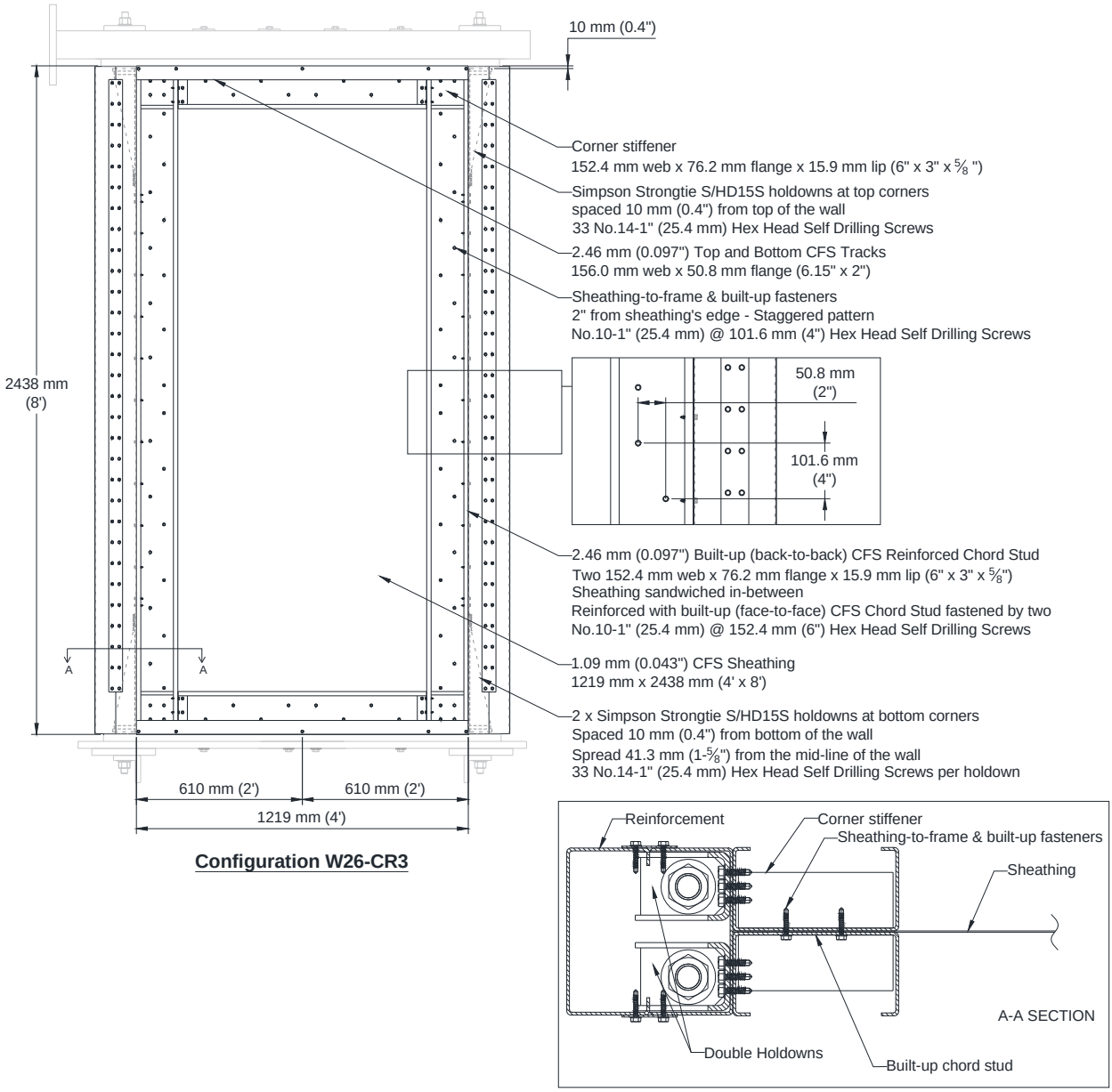

Configuration W26-CR3

Figure A-9 Centre-sheathed configuration: dimensions and specifications for configuration W26-CR3

APPENDIX B. FABRICATION OF THE SPECIMENS – DRAWINGS AND DETAILS

Figure B-1 Loading beam under preparation after welding

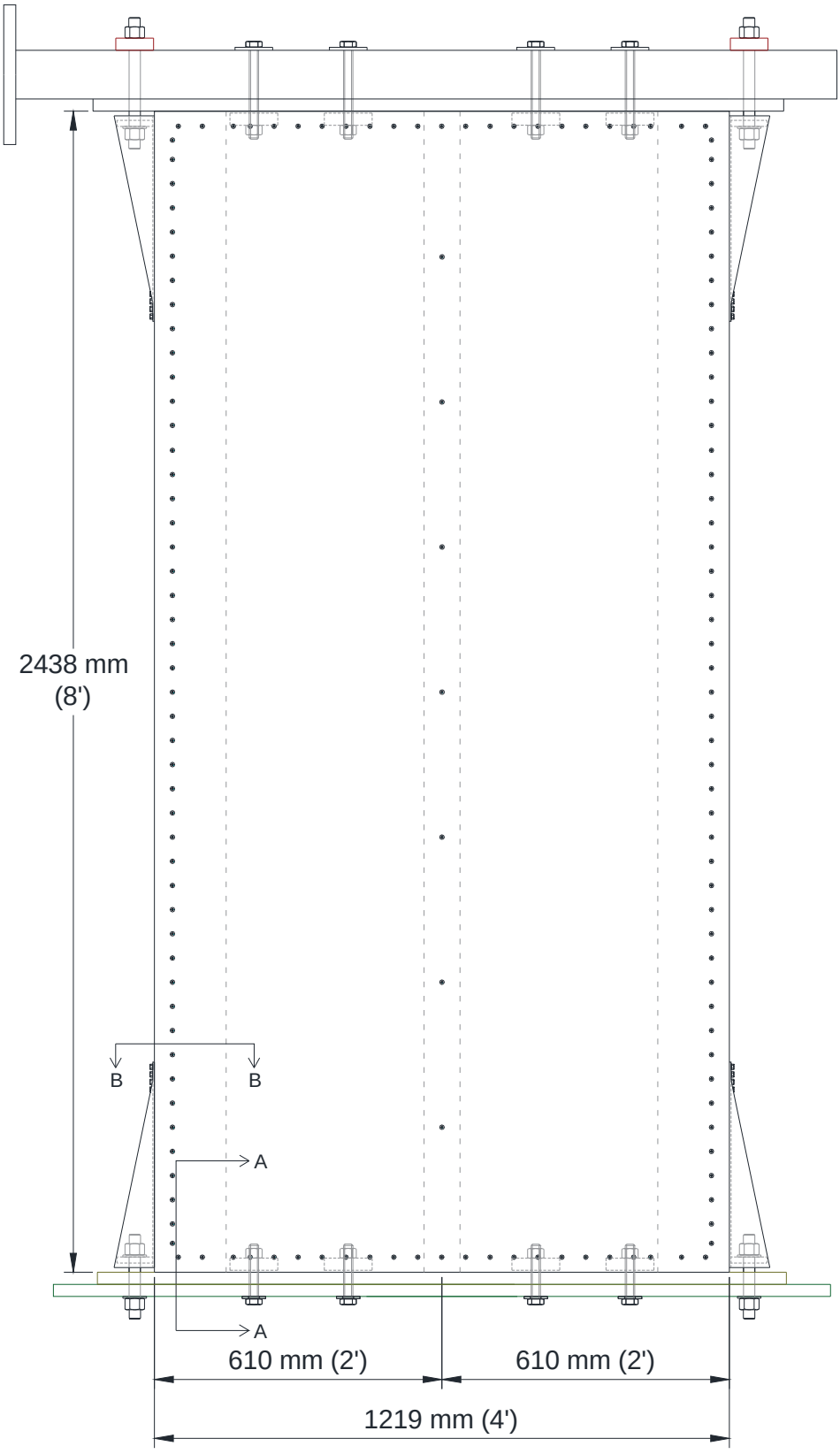

Figure B-2 Double-sheathed configuration: elevation view

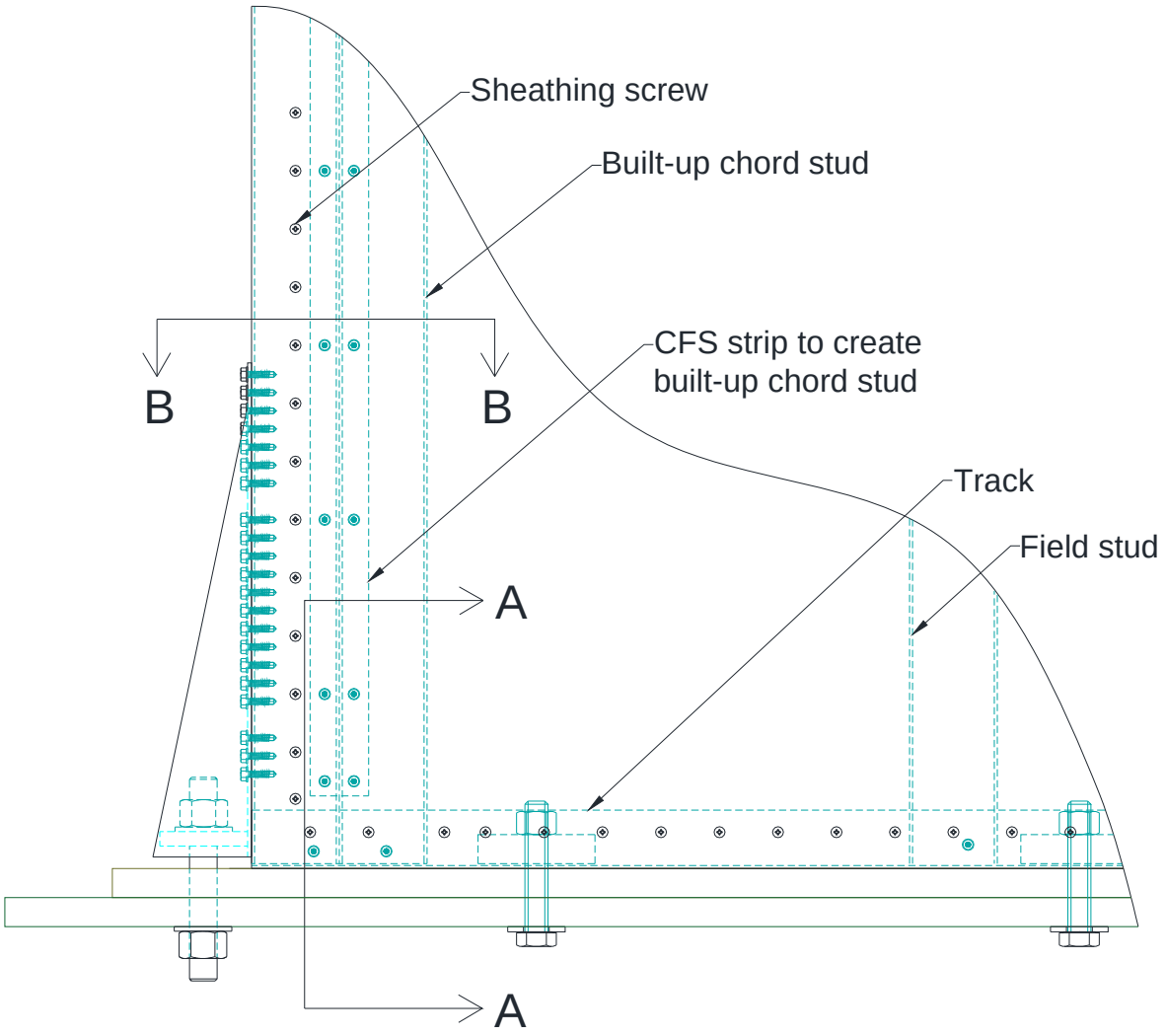

Figure B-3 Double-sheathed configuration: detailing of the screw pattern in the corner (hidden parts in blue)

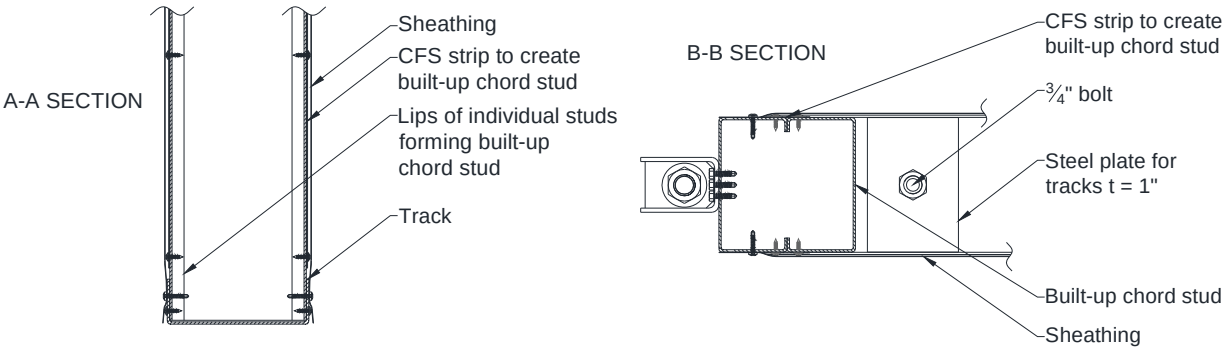

Figure B-4 Double-sheathed configuration: cross-sections

Figure B-5 Double-sheathed configuration: steel plates at shear anchors position (photo taken prior to installation of second sheathing member)

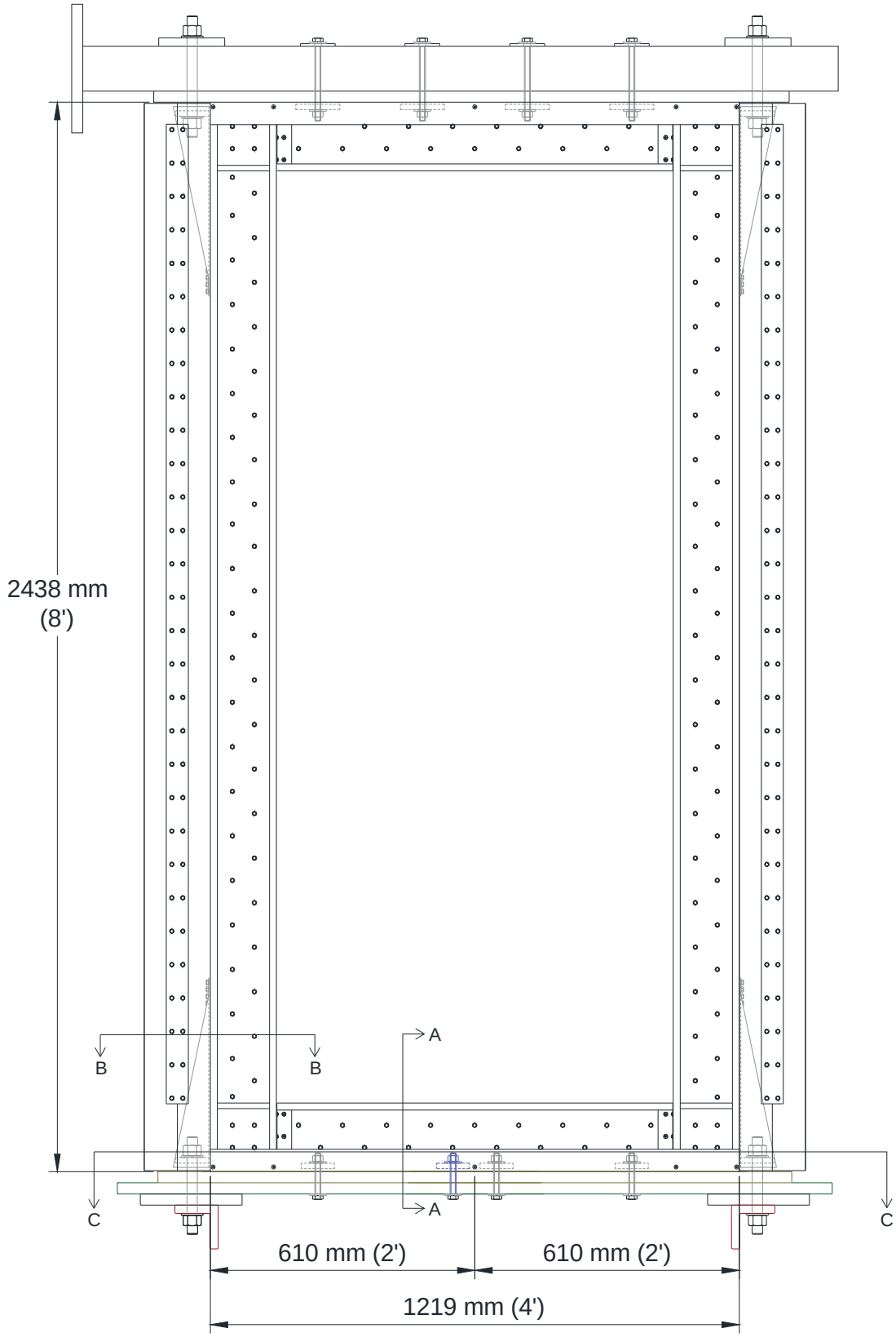

Figure B-6 Centre-sheathed configuration: final level of reinforcement (R3) – elevation view

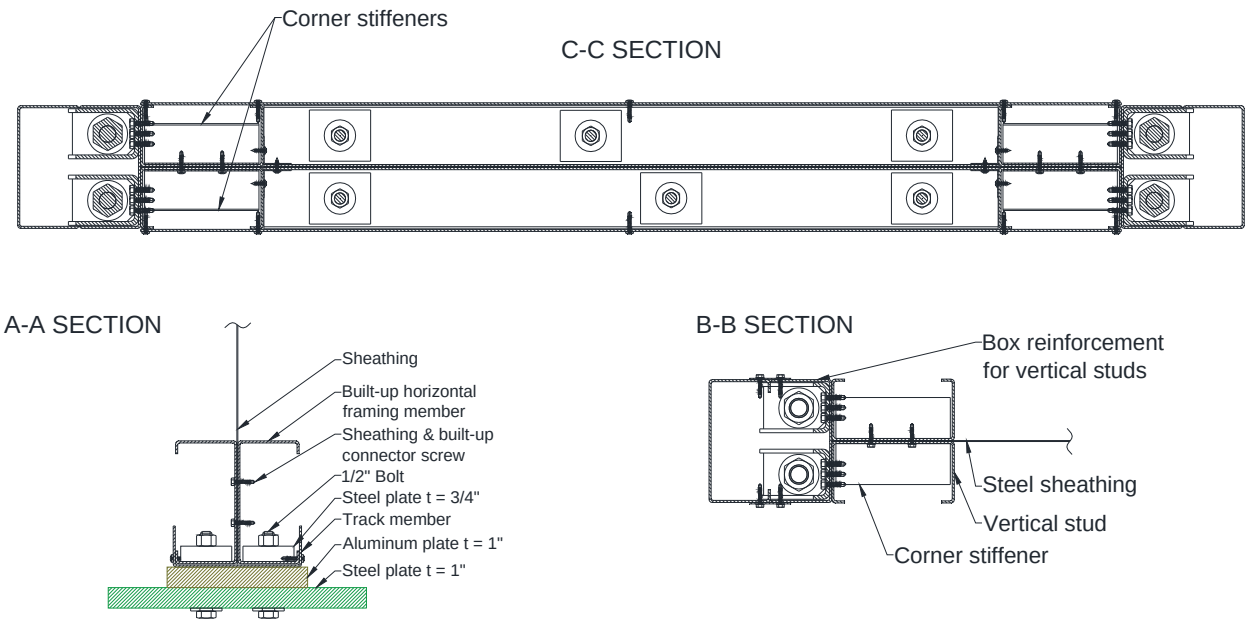

Figure B-7 Centre-sheathed configuration: final level of reinforcement (R3) – cross-sections

Figure B-8 Centre-sheathed configuration: steel plates at shear anchor positions

Figure B-9 Centre-sheathed configuration: W18 (unreinforced)

a. b.

Figure B-10 Centre-sheathed configuration: a. holdown and b. corner of W18

Figure B-11 Centre-sheathed configuration: W18-R

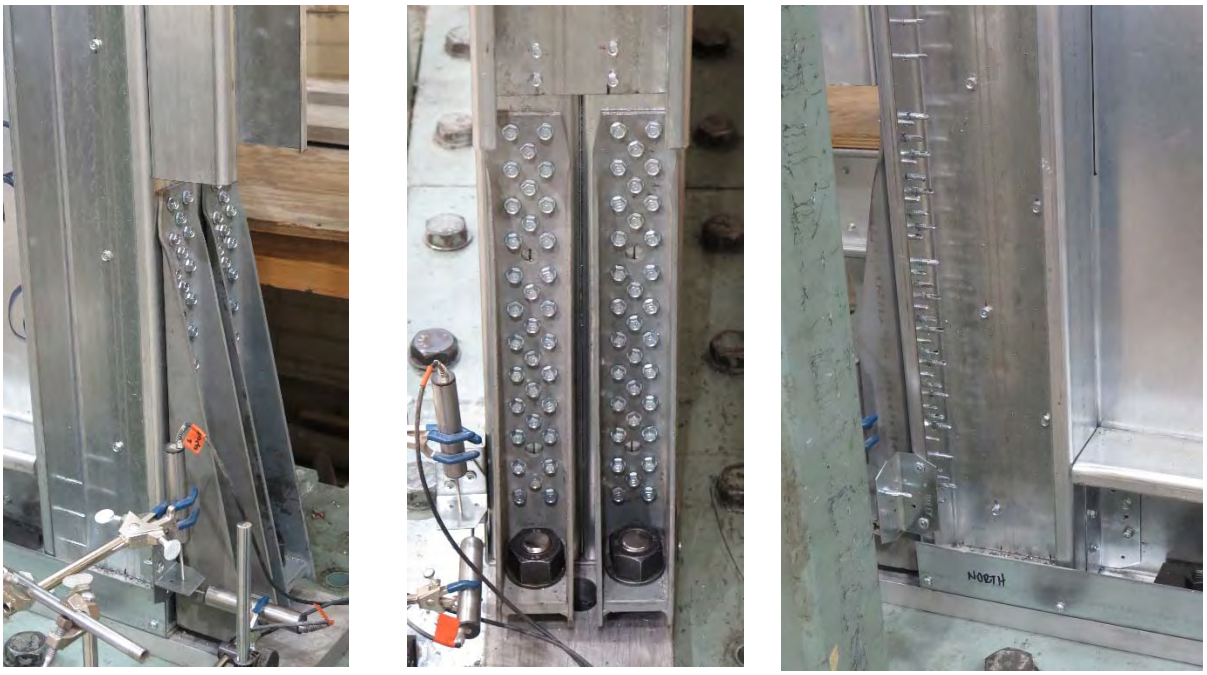

a. b. c.

Figure B-12 Centre-sheathed configuration: bottom holdowns (a. & b.) and c. corner of W18-R

Figure B-13 Centre-sheathed configuration: W16-R2

a. b.

Figure B-14 Centre-sheathed configuration: a. bottom holdowns and b. reinforced corner of W16-R2

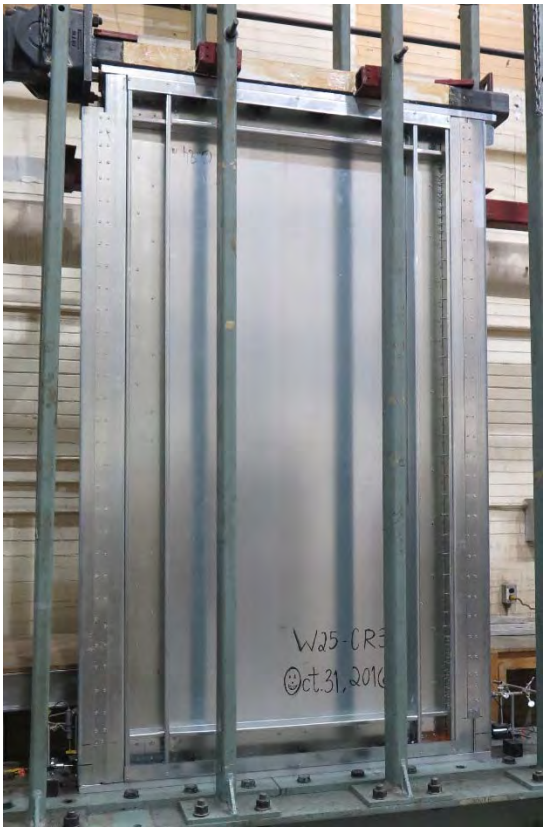

Figure B-15 Centre-sheathed configuration: W25-R3

a. b.

Figure B-16 Centre-sheathed configuration: a. holdowns before completion of reinforcement and b. reinforced corner with completed reinforcement of W25-R3

APPENDIX C. NUMERICAL MODEL AND SAMPLE RESULTS OF THE NUMERICAL ANALYSIS

Full Section Properties

Area	1672.3	mm^2	Wt.	0.12862	kN/m	Width	647.38 mm
Ix	6335602	mm^4	rx	61.551	mm	Ixy	-1 mm^4
Sx(t)	83144	mm^3	y(t)	76.200	mm	α	0.000 deg
Sx(b)	83144	mm^3	y(b)	76.200	mm		
			Height	152.400	mm		
Iy	5729048	mm^4	ry	58.531	mm	Xo	0.000 mm
Sy(l)	75362	mm^3	x(l)	76.020	mm	Yo	0.000 mm
Sy(r)	75362	mm^3	x(r)	76.020	mm	jx	0.000 mm
			Width	152.040	mm	jy	0.000 mm
I1	6335602	mm^4	r1	61.551	mm		
I2	5729048	mm^4	r2	58.531	mm		
Ic	12064650	mm^4	rc	84.938	mm	Cw	2.3368e04 mm^6
Io	12064650	mm^4	ro	84.938	mm	J	8655036 mm^4

Member Check - 2012 North American Specification - Canada (LSD)

Material Type: A653 SS Grade 50/1, Fy=344.74 MPa
Design Parameters:

Lx	2.4400 m	Ly	2.4400 m	Lt	2.4400 m
Kx	1.0000	Ky	1.0000	Kt	1.0000
Cbx	1.0000	Cby	1.0000	ex	0.0000 mm
Cmx	1.0000	Cmy	1.0000	ey	0.0000 mm
Braced Flange: None		kϕ	0 kN		
Red. Factor, R: 0		Lm	6.0960 m		

Loads:	P (kN)	Mx (kN-m)	Vy (kN)	My (kN-m)	Vx (kN)
Entered	72.23	3.785	0.00	0.000	16.90
Applied	72.23	3.785	0.00	0.000	16.90
Strength	320.62	21.441	123.96	18.619	121.15

Effective section properties at applied loads:

Ae	1672.3	mm^2	Ixe	6335602	mm^4	Iye	5729048 mm^4
			Sxe(t)	83144	mm^3	Sye(l)	75362 mm^3
			Sxe(b)	83144	mm^3	Sye(r)	75362 mm^3

Interaction Equations

NAS Eq. C5.2.2-1	(P, Mx, My)	0.225 + 0.183 + 0.000 = 0.408	<= 1.0
NAS Eq. C5.2.2-2	(P, Mx, My)	0.211 + 0.177 + 0.000 = 0.387	<= 1.0
NAS Eq. C3.3.2-1	(Mx, Vy)	Sqrt(0.027 + 0.000)= 0.165	<= 1.0
NAS Eq. C3.3.2-1	(My, Vx)	Sqrt(0.000 + 0.019)= 0.140	<= 1.0

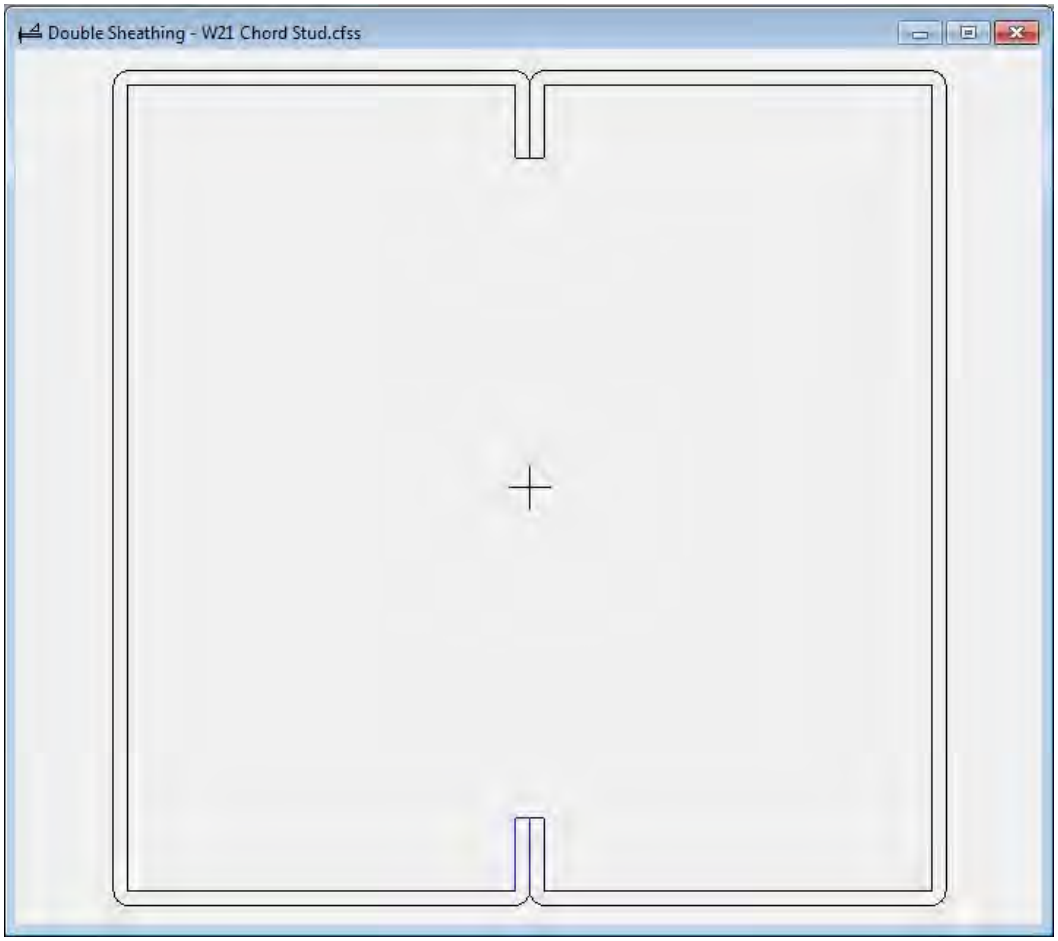

Figure C-1 Chord stud for double-sheathed configuration wall W21 on CFS Software associated to the preceding results

CFS Version 9.0.4
Section: Quad Chord Stud.cfss
Double Channel 152.4x76.2x15.9-12 Gage

Full Section Properties

Area	3279.6 mm^2	Wt.	0.25223 kN/m	Width	1269.6 mm
Ix	30851700 mm^4	rx	96.99 mm	Ixy	-2 mm^4
Sx(t)	202439 mm^3	y(t)	152.40 mm	α	0.000 deg
Sx(b)	202439 mm^3	y(b)	152.40 mm		
		Height	304.80 mm		
Iy	8313747 mm^4	ry	50.35 mm	Xo	0.00 mm
Sy(l)	109104 mm^3	x(l)	76.20 mm	Yo	51.10 mm
Sy(r)	109104 mm^3	x(r)	76.20 mm	jx	0.00 mm
		Width	152.40 mm	jy	-47.98 mm
I1	30851700 mm^4	r1	96.99 mm		
I2	8313748 mm^4	r2	50.35 mm		
Ic	39165450 mm^4	rc	109.28 mm	Cw	1.2154e10 mm^6
Io	47727860 mm^4	ro	120.64 mm	J	7294.7 mm^4

Fully Braced Strength - 2012 North American Specification - Canada (LSD)

Material Type: A653 SS Grade 50/1, Fy=344.74 MPa

Compression		Positive Moment		Positive Moment	
ϕPno	710.1 kN	ϕMnxo	54.186 kN-m	ϕMnyo	30.411 kN-m
Ae	2574.7 mm^2	Ixe	27816650 mm^4	Iye	7720245 mm^4
		Sxe(t)	174645 mm^3	Sye(l)	104846 mm^3
Tension		Sxe(b)	191147 mm^3	Sye(r)	98015 mm^3
ϕTn	1017.5 kN				
		Negative Moment		Negative Moment	
		ϕMnxo	56.121 kN-m	ϕMnyo	30.411 kN-m
Shear		Ixe	28595030 mm^4	Iye	7720245 mm^4
ϕVny	227.5 kN	Sxe(t)	194905 mm^3	Sye(l)	98015 mm^3
ϕVnx	227.5 kN	Sxe(b)	180882 mm^3	Sye(r)	104846 mm^3

Member Check - 2012 North American Specification - Canada (LSD)

Material Type: A653 SS Grade 50/1, Fy=344.74 MPa
Design Parameters:

Lx	2.4400 m	Ly	0.0000 m	Lt	0.0000 m
Kx	1.0000	Ky	1.0000	Kt	1.0000
Cbx	1.0000	Cby	1.0000	ex	0.0000 mm
Cmx	1.0000	Cmy	1.0000	ey	0.0000 mm
Braced Flange: None		kϕ	0 kN		
Red. Factor, R: 0		Lm	6.0960 m		

Loads:	P (kN)	Mx (kN-m)	Vy (kN)	My (kN-m)	Vx (kN)
Entered	276.00	36.900	76.00	0.000	0.00
Applied	276.00	15.869	76.00	0.000	0.00
Strength	656.59	53.377	227.45	28.215	227.45

Effective section properties at applied loads:

Ae	3243.2 mm^2	Ixe	30010380 mm^4	Iye	8313143 mm^4
		Sxe(t)	194749 mm^3	Sye(l)	109096 mm^3
		Sxe(b)	199137 mm^3	Sye(r)	109096 mm^3

```
Interaction Equations
NAS Eq. C5.2.2-1  (P, Mx, My)  0.420 + 0.305 + 0.000 = 0.726 <= 1.0
NAS Eq. C5.2.2-2  (P, Mx, My)  0.389 + 0.297 + 0.000 = 0.686 <= 1.0
NAS Eq. C3.3.2-1     (Mx, Vy)     Sqrt(0.086 + 0.112)= 0.444 <= 1.0
NAS Eq. C3.3.2-1     (My, Vx)     Sqrt(0.000 + 0.000)= 0.000 <= 1.0
```

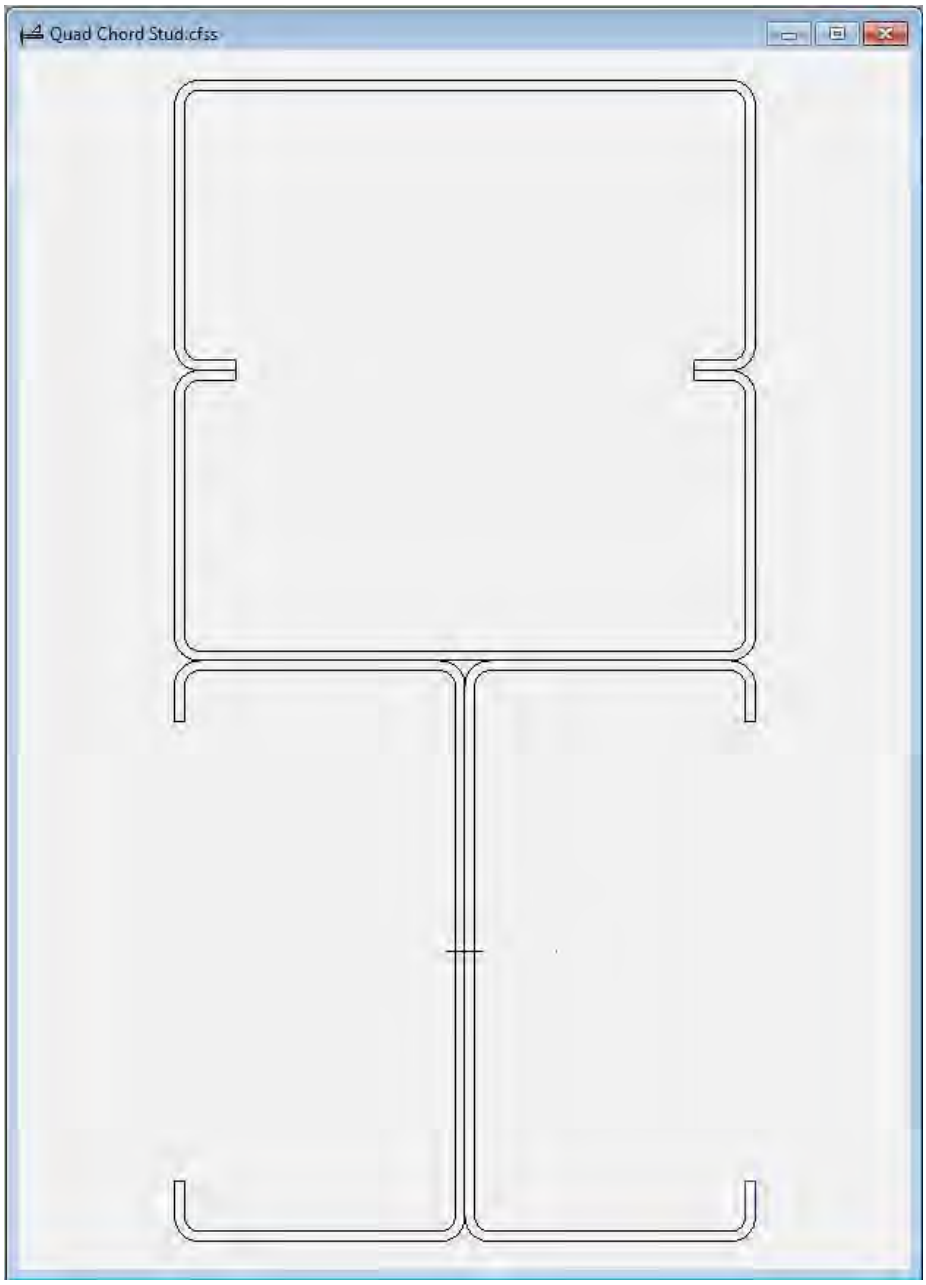

Figure C-2 Chord stud for centre-sheathed configuration W15 on CFS Software associated to the preceding results

APPENDIX D. EFFECTIVE STRIP METHOD BY YANAGI AND YU *(2014)* – CALCULATION DETAILS

The nominal shear force of a given wall configuration (V_n) was calculated using the Effective Strip Method (Yanagi and Yu *(2014)*). This method takes in consideration all the parameters given by the building parameters of the wall (thicknesses, spacing, etc.). Below is the list of the equations and the variables used throughout this method.

Effective Width Calculation

$$\boldsymbol{W_e} = \begin{cases} \boldsymbol{W_{max,}} & \boldsymbol{if\ \lambda \leq 0.0819} \\ \boldsymbol{\rho W_{max,}} & \boldsymbol{if\ \lambda > 0.0819} \end{cases}$$ (Figure D-1)

$$W_{max} = W/sin\alpha$$

$$\alpha = tan^{-1}(a)$$

$$\rho = \frac{1 - 0.55(\lambda - 0.08)^{0.12}}{\lambda^{0.12}}$$

$$\lambda = 1.736\frac{\alpha_1\alpha_2}{\beta_1\beta_2\beta_3^2 a}$$

$$\alpha_1 = \frac{F_{e,ush}}{310.3\ MPa}, \qquad \alpha_2 = \frac{F_{e,uf}}{310.3\ MPa}$$

$$F_{e,ush} = R_t F_{ush}, \qquad F_{e,uf} = R_t F_{uf}$$

$$\beta_1 = \frac{t_{sh}}{0.457}, \qquad \beta_2 = \frac{t_f}{0.457}, \qquad \beta_3 = \frac{s}{152.4}$$

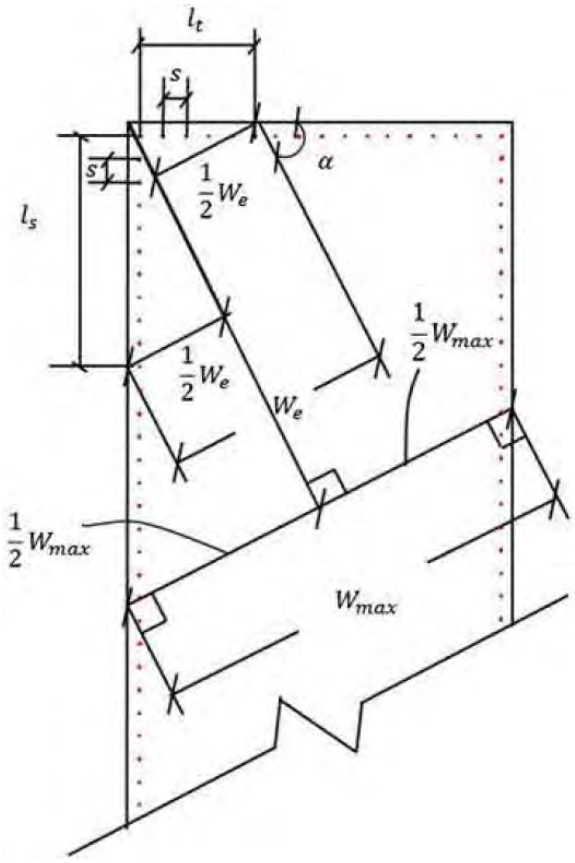

Figure D-1 Sheathing-to-framing fastener connection layout and maximum width of the effective strip by Yanagi and Yu *(2014)*

where,

W_e = Effective strip width;

W_{max} = Maximum width of effective strip;

a = Shear wall's aspect ratio (height/width);

$F_{e,ush}$ = Expected tensile strength of steel sheet sheathing;

$F_{e,uf}$ = Expected controlling tensile strength of framing materials (track or stud);

R_t = Ratio of expected and specified minimum tensile strengths (AISI S400 *(2015)*);

F_{ush} = Tensile strength of steel sheet sheathing;

F_{uf} = Controlling tensile strength of framing materials (smaller of track and stud);

t_{sh} = Thickness of sheathing;

t_f = Smaller of thickness of track and stud;

s = Fastener spacing on the sheathing panel edges.

Nominal Capacity of Individual Fasteners

$$\boldsymbol{P_{ns} = \min(P_{ns,a}, P_{ns,b}, P_{ns,c})}$$

$$for\ {}^{t_2}/_{t_1} \le 1.0 \qquad P_{ns,a} = min\begin{cases} 4.2(t_2^3 d)^{1/2} F_{e,u2} \\ 2.7 t_1 d F_{e,u1} \\ 2.7 t_2 d F_{e,u2} \end{cases}$$

$$for\ {}^{t_2}/_{t_1} \ge 2.5 \qquad P_{ns,a} = min\begin{cases} 2.7 t_1 d F_{e,u1} \\ 2.7 t_2 d F_{e,u2} \end{cases}$$

$$* \textit{Use linear interpolation between the previous cases if } \ 1.0 < {}^{t_2}/_{t_1} \ge 2.5$$

$$F_{e,u1} = R_t F_{u1}, \qquad F_{e,u2} = R_t F_{u2}$$

$$P_{ns,b} = teF_{e,ush}$$

$e = \frac{w_f}{2cos\alpha}$ (Figure D-2)

$$P_{ns\,c} = fastener\ shear\ strength\ provided\ by\ manufacturer$$

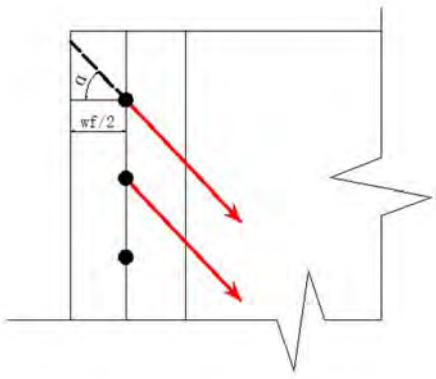

Figure D-2 Illustration of geometry to calculate distance e.

where,

t_1 = Thickness of member with contact with screw head or washer;

t_2 = Thickness of member not in contact with screw head or washer;

d = Nominal screw diameter;

F_{u1} = Tensile strength of member in contact with screw head or washer;

F_{u2} = Tensile strength of member not in contact with screw head or washer;

$F_{e,u1}$ = Expected tensile strength of member in contact with screw head or washer;

$F_{e,u2}$ = Expected tensile strength of member not in contact with screw head or washer;

P_{ns} = Nominal capacity of individual fasteners;

$P_{ns,a}$ = Connection capacity based on tilting and bearing;

$P_{ns,b}$ = Connection capacity based on end distance shear;

$P_{ns,c}$ = Connection capacity based on manufacturer's shear strength;

t = Thickness of part in which the end distance is measured;

e = Distance measured in line of force from centre of a standard hole to nearest end of connection;

w_f = Width of stud flange.

Nominal Shear Strength of the Shear Wall

$$\boldsymbol{V_n = min\left\{\left[\left(\frac{W_e}{2s\ sin\alpha}P_{ns,t} + \frac{W_e}{2s\ cos\alpha}\ P_{ns,s} + P_{ns,s\&t}\right)cos\alpha\right], W_e t_{sh} F_{e,ysh}\ cos\alpha\right\}} \quad \text{(Figure D-3)}$$

$$F_{e,ysh} = R_y F_{ysh}$$

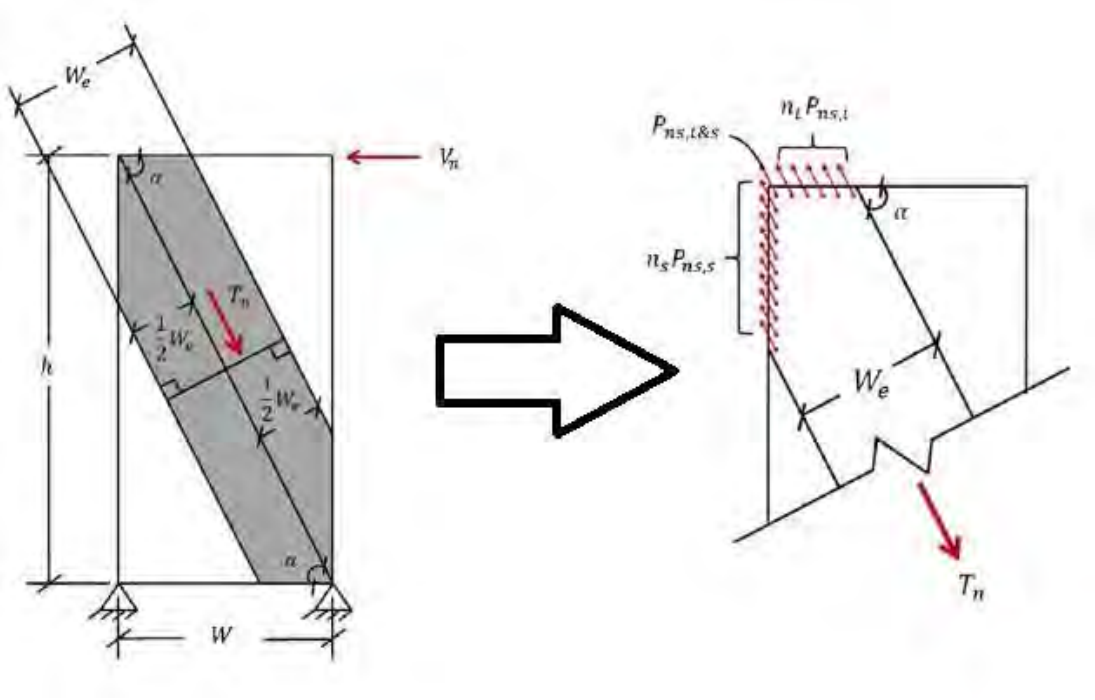

Figure D-3 Shear force applied and equivalent tension force in the sheathing (Yanagi and Yu *(2014)*)

where,

V_n = Nominal shear strength of the shear wall;

$P_{ns,s}$ = Nominal capacity of individual fasteners in sheathing to stud connection;

$P_{ns,t}$ = Nominal capacity of individual fasteners in track connection;

$P_{ns,s\&t}$ = Nominal capacity of individual fasteners in stud to track connection;

F_{ysh} = Nominal yield stress of sheathing;

R_y = Ratio of expected to specified minimum yield stresses (AISI S400 *(2015)*);

$F_{e,ysh}$ = Expected yield stress of sheathing.

APPENDIX E. TEST OBSERVATION SHEETS

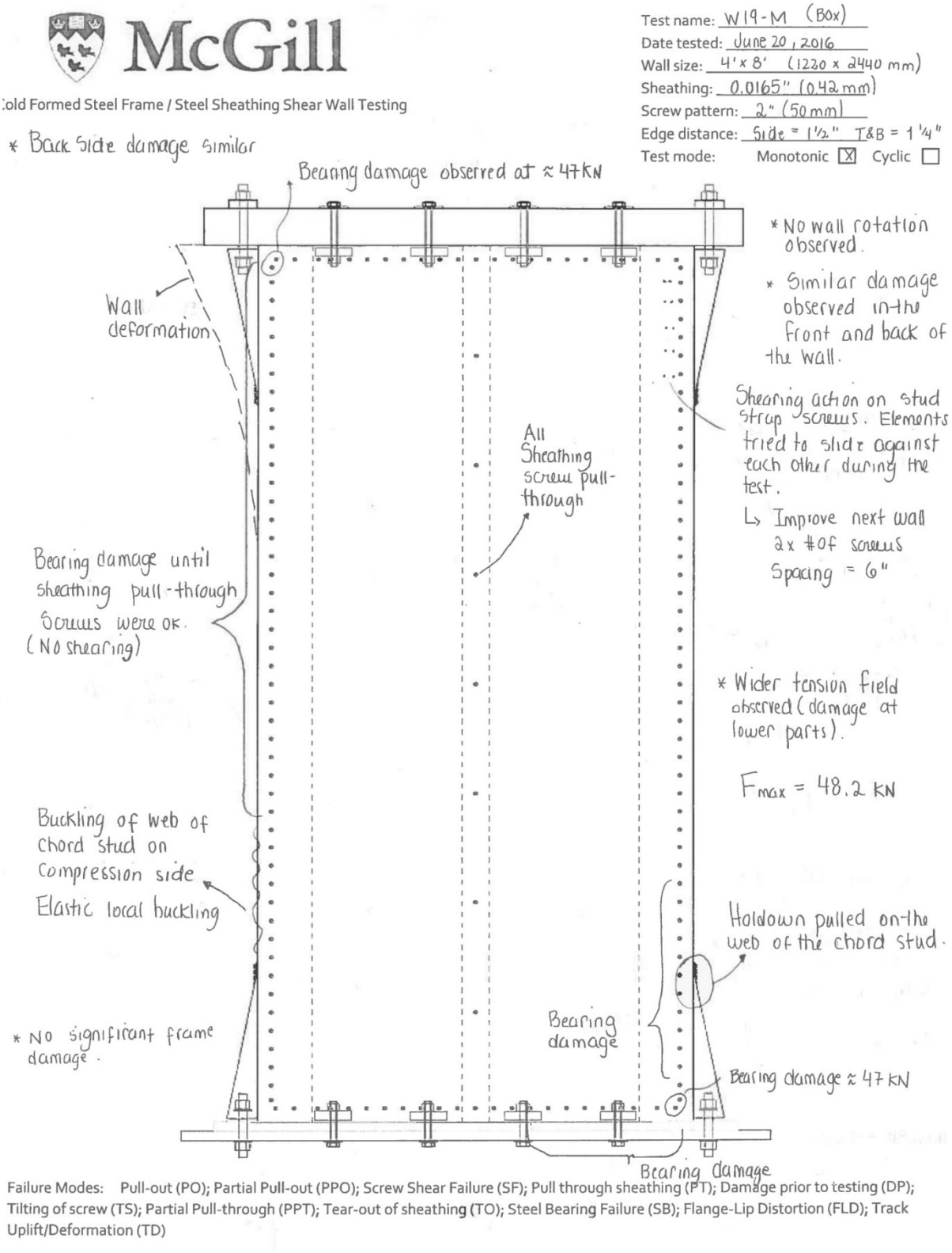

Figure E-1 Test observations for test W19-M

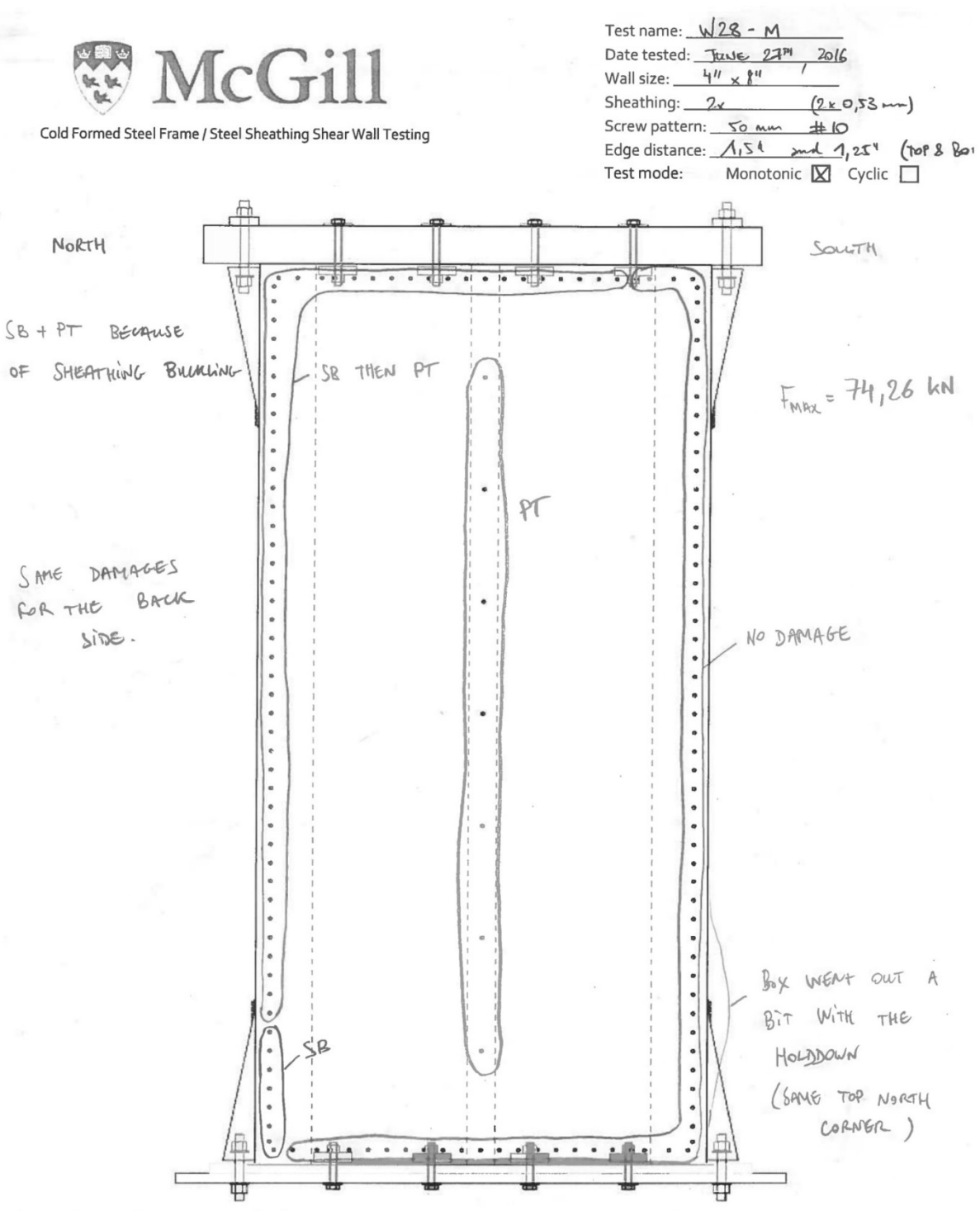

Figure E-2 Test observations for test W28-M

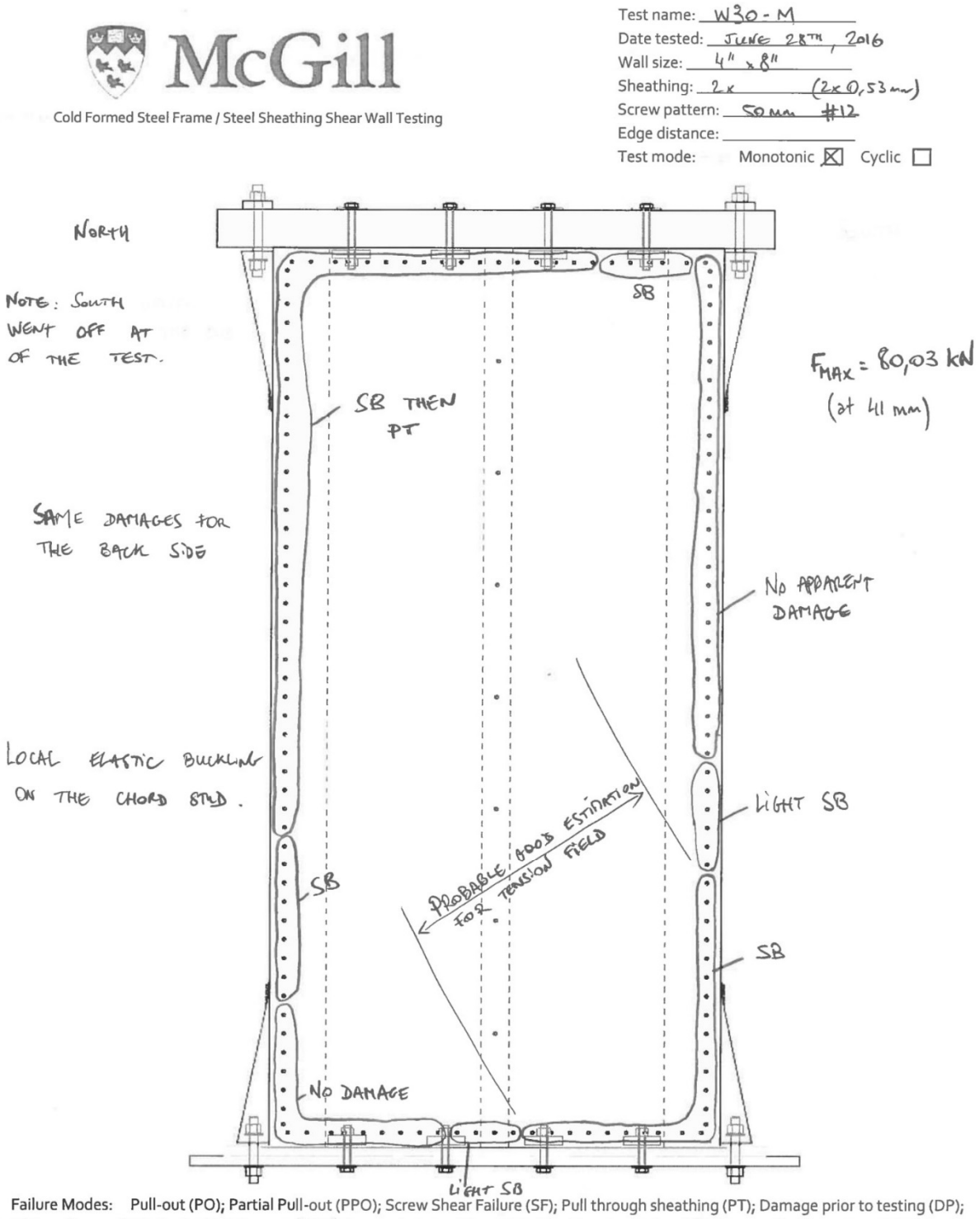

Figure E-3 Test observations for test W30-M

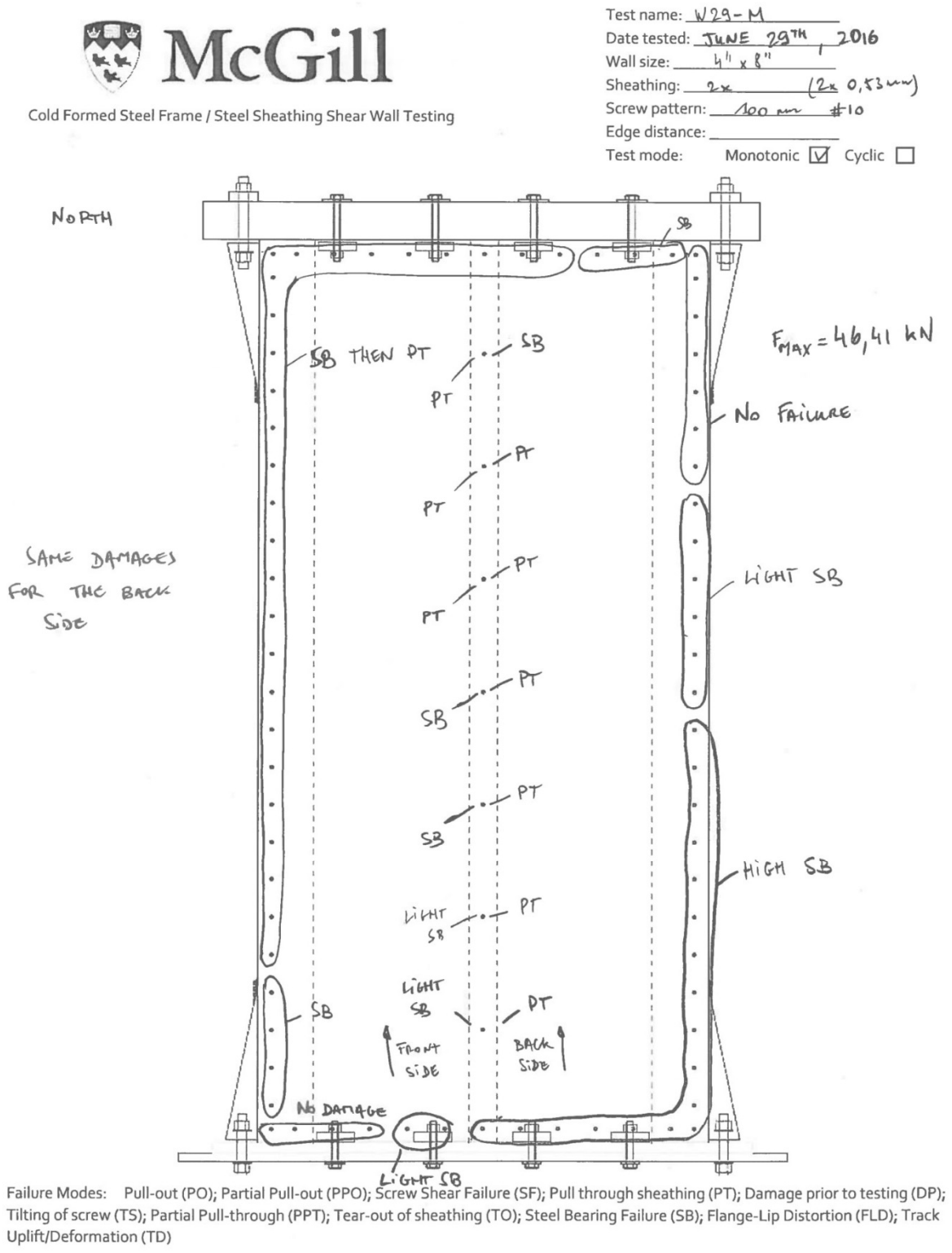

Figure E-4 Test observations for test W29-M

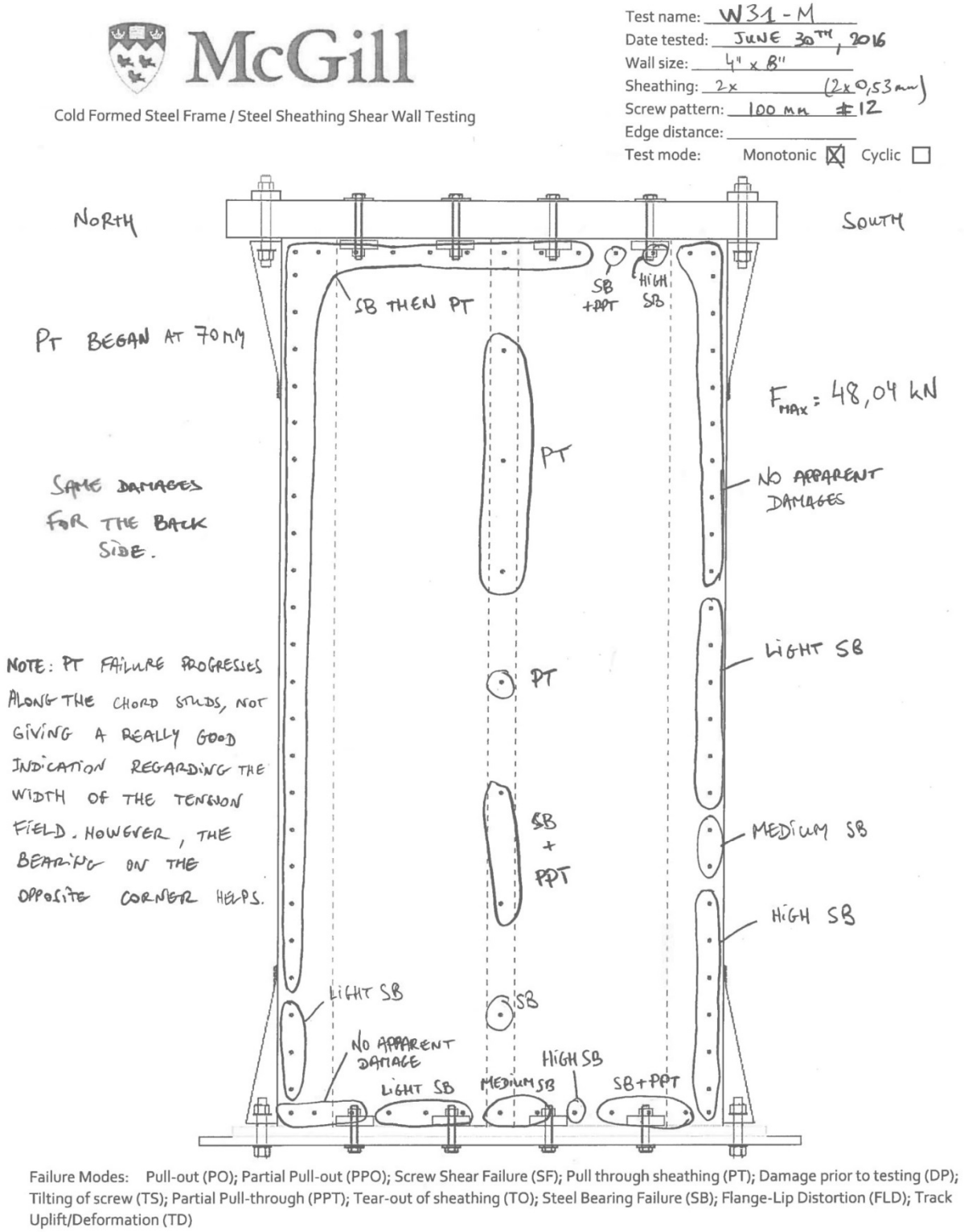

Figure E-5 Test observations for test W31-M

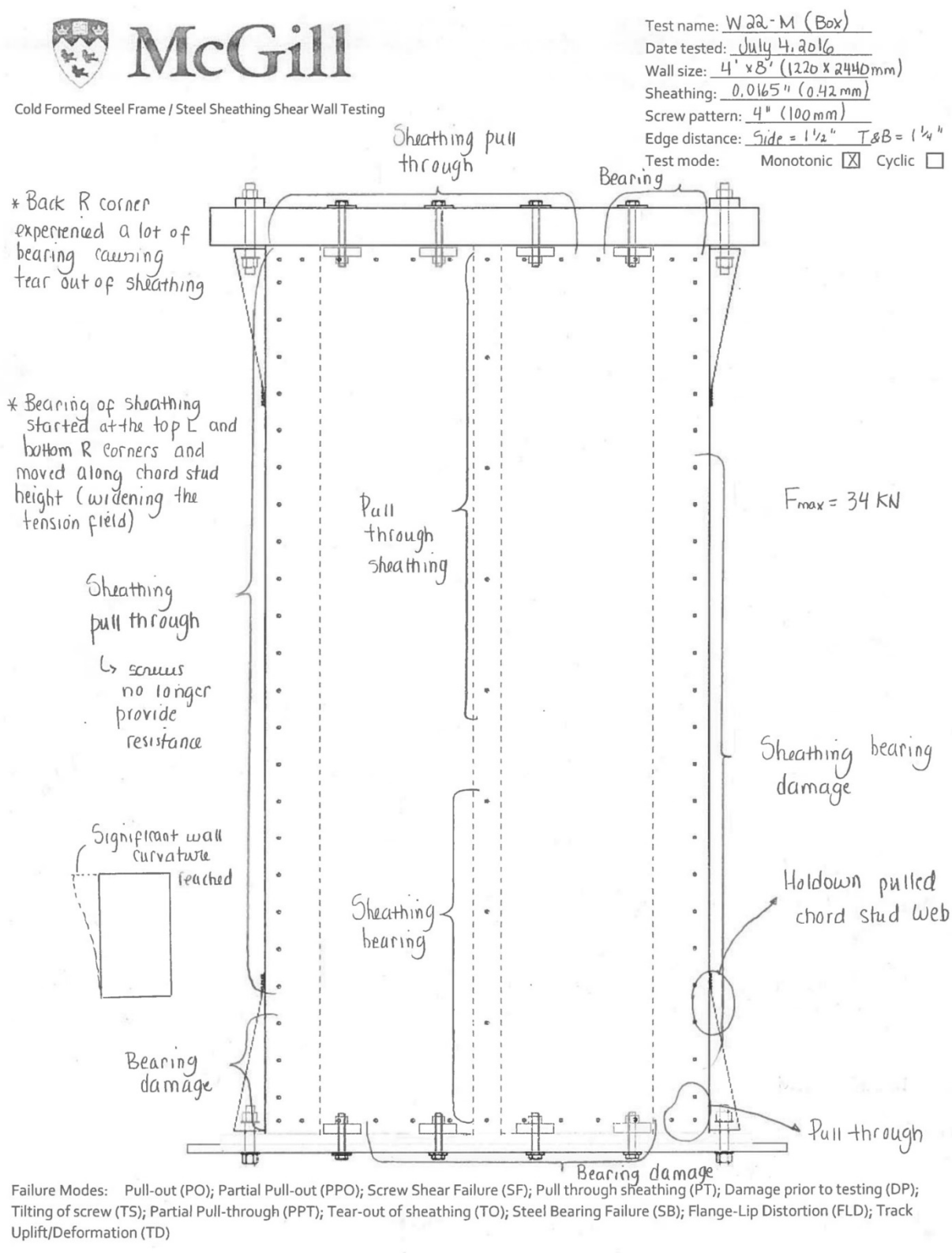

Figure E-6 Test observations for test W22-M

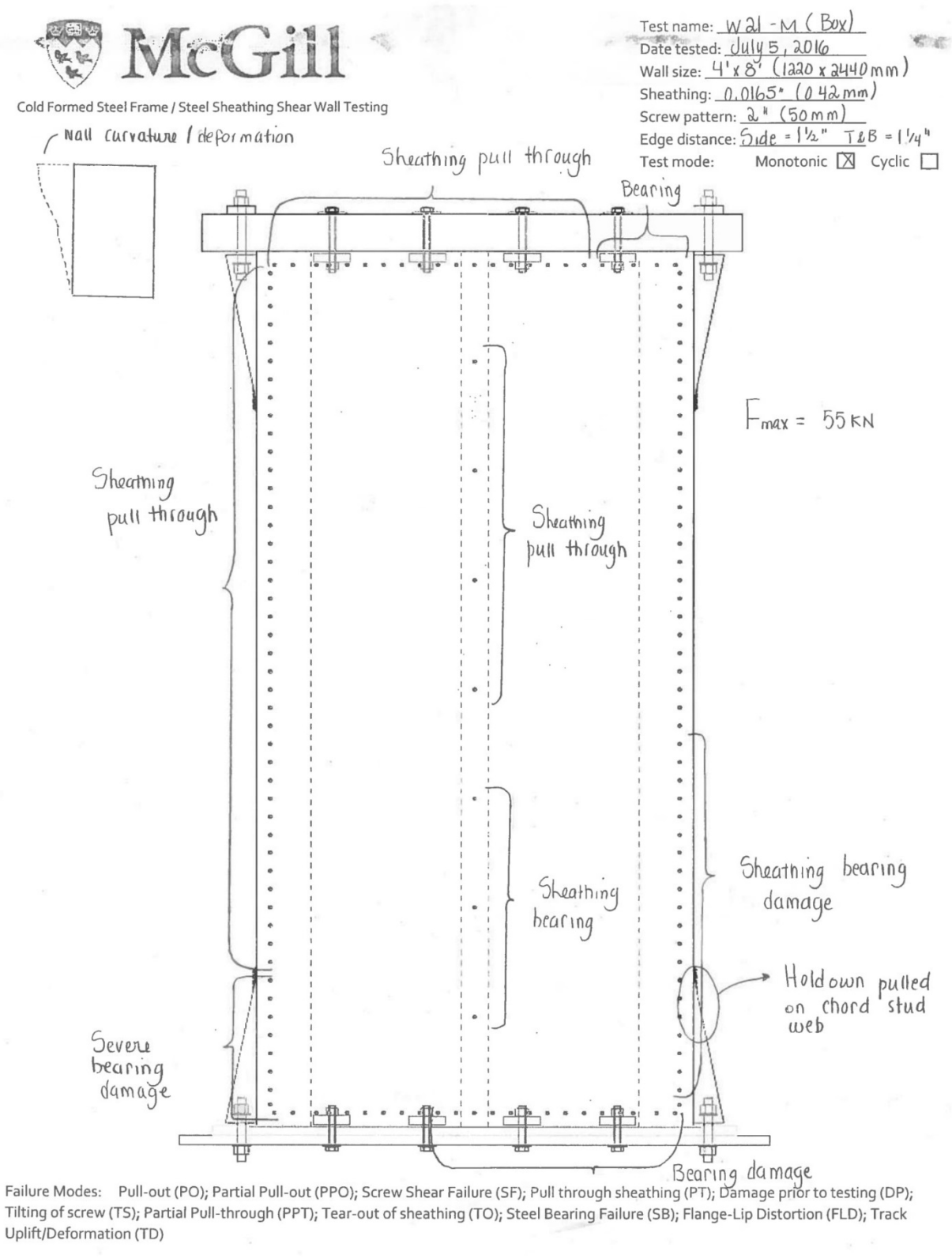

Figure E-7 Test observations for test W21-M

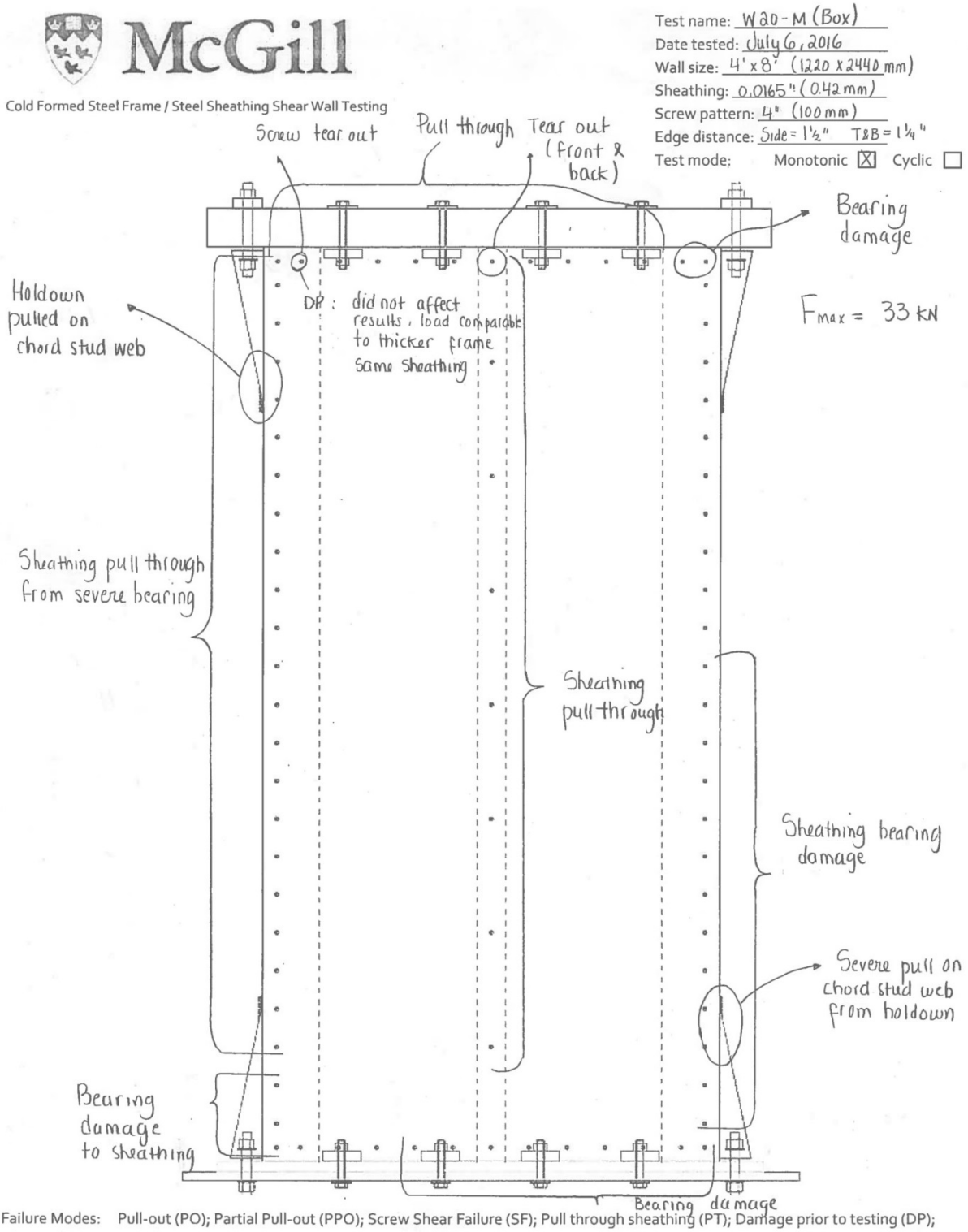

Figure E-8 Test observations for test W20-M

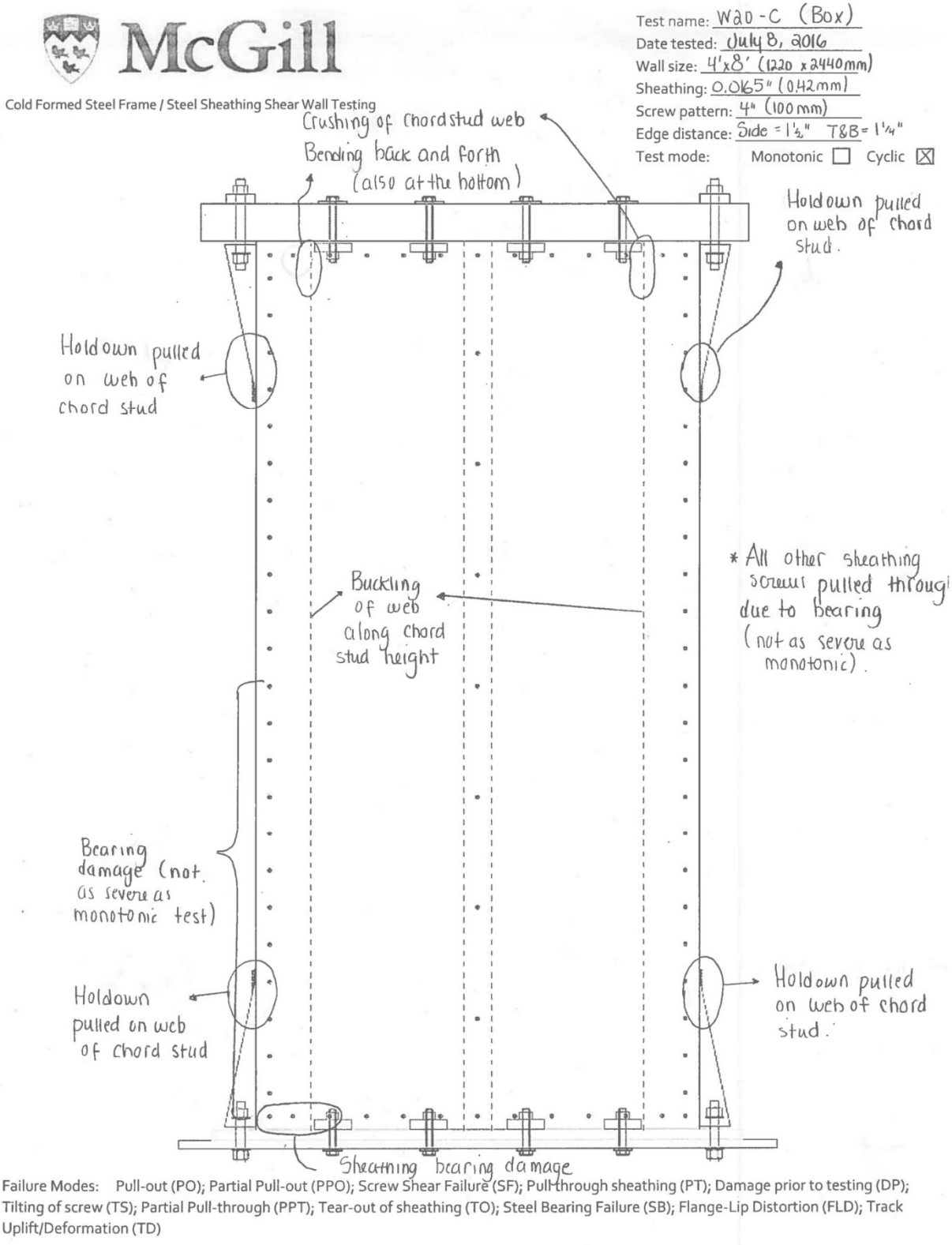

Figure E-9 Test observations for test W20-C

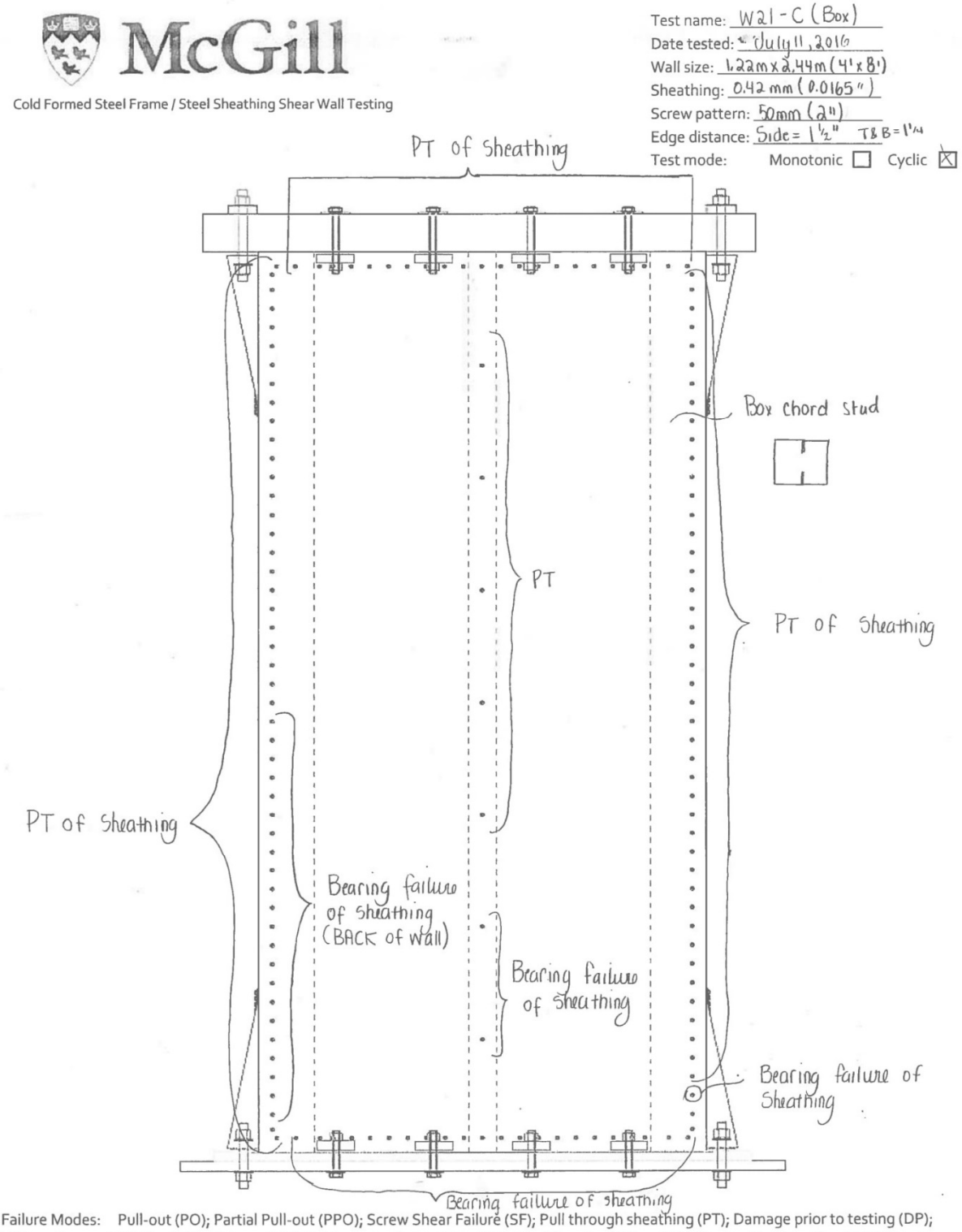

Figure E-10 Test observations for test W21-C

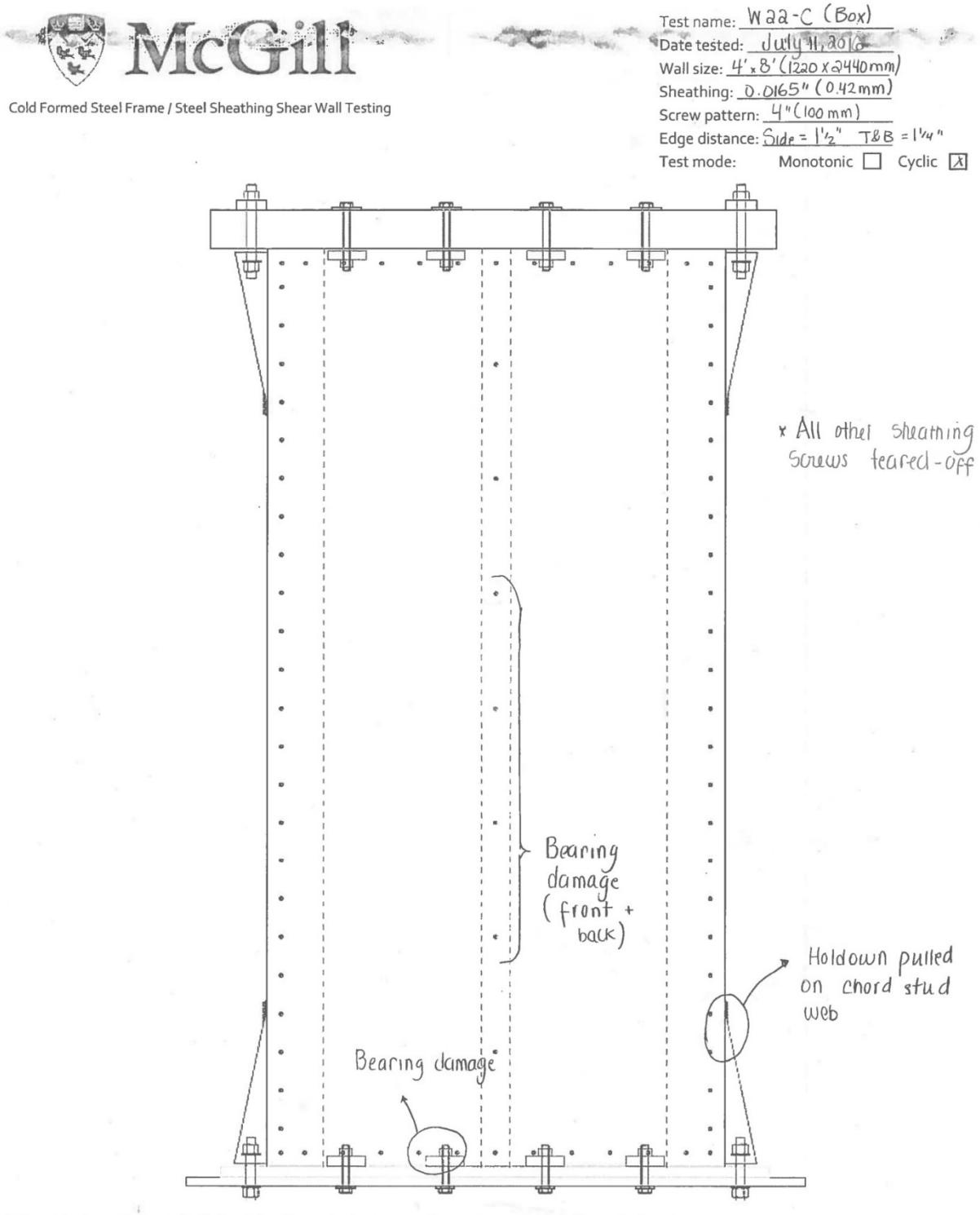

Figure E-11 Test observations for test W22-C

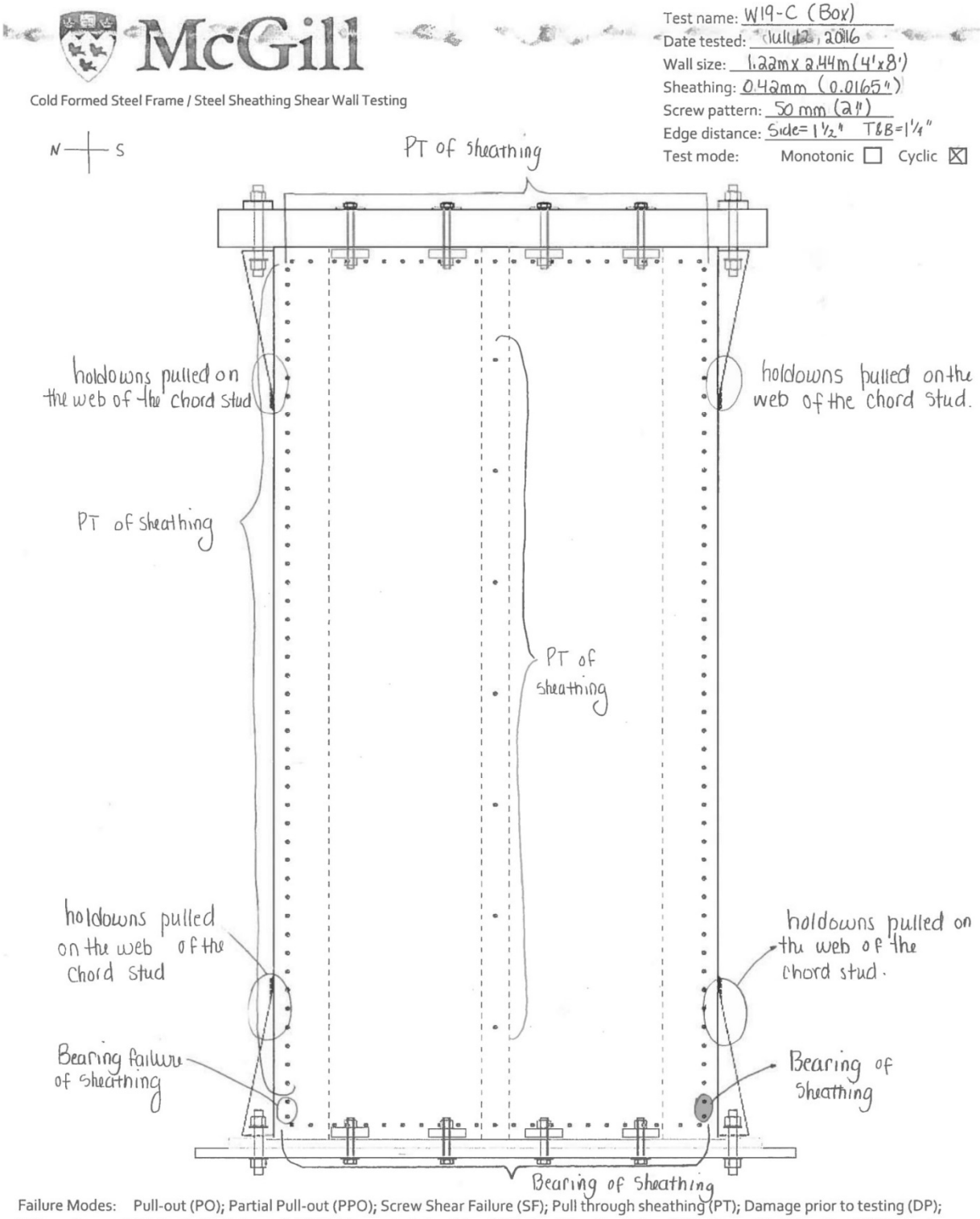

Figure E-12 Test observations for test W19-C

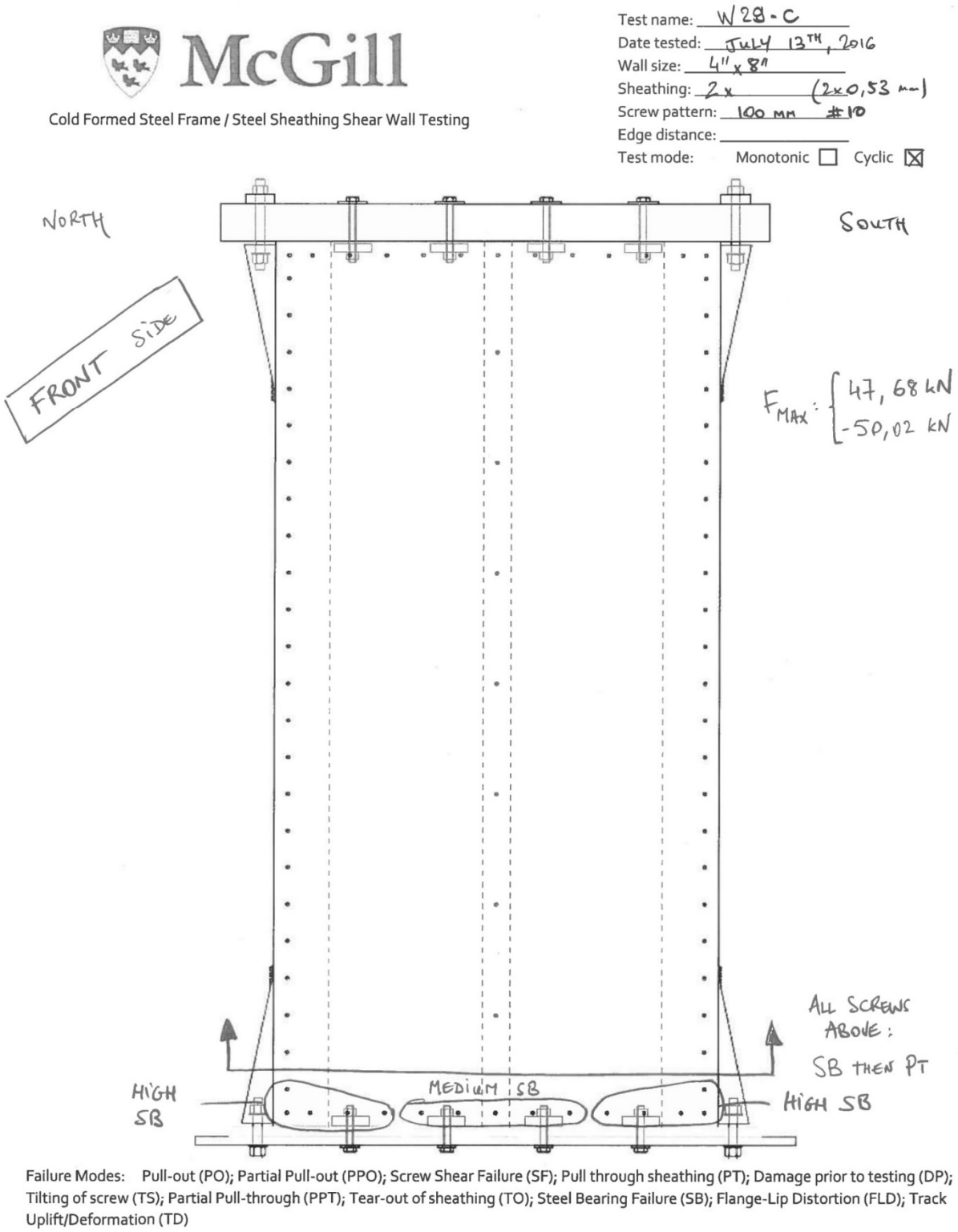

Figure E-13.a Test observations for test W29-C (front side)

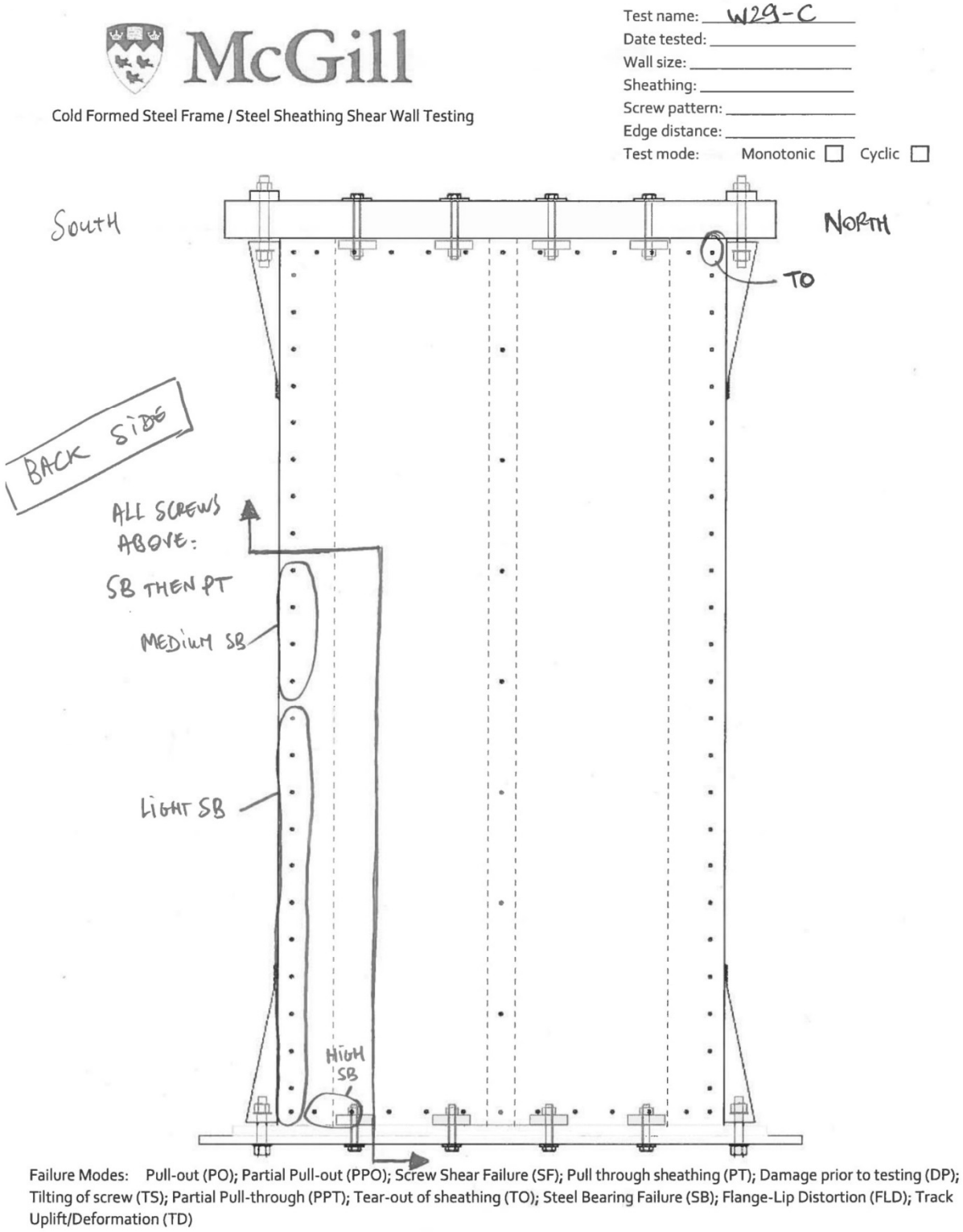

Figure E-13.b Test observations for test W29-C (back side)

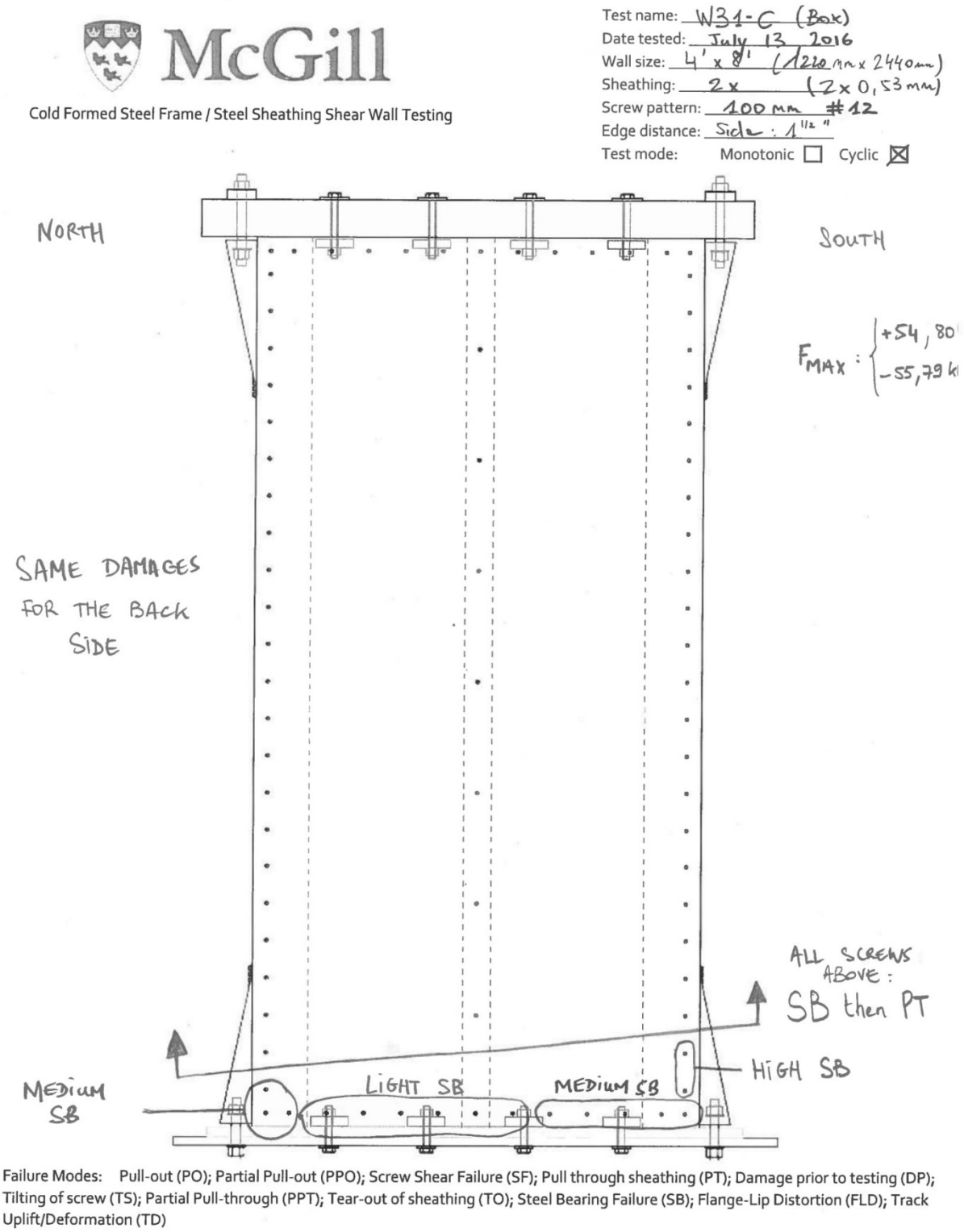

Figure E-14 Test observations for test W31-C

McGill

Cold Formed Steel Frame / Steel Sheathing Shear Wall Testing

Test name: _W28-C_____
Date tested: _July 14th,2016_____
Wall size: __4"x8"_____
Sheathing: _2x0.53 mm_____
Screw pattern: __50 mm #10_____
Edge distance: _____
Test mode: Monotonic ☐ Cyclic ■

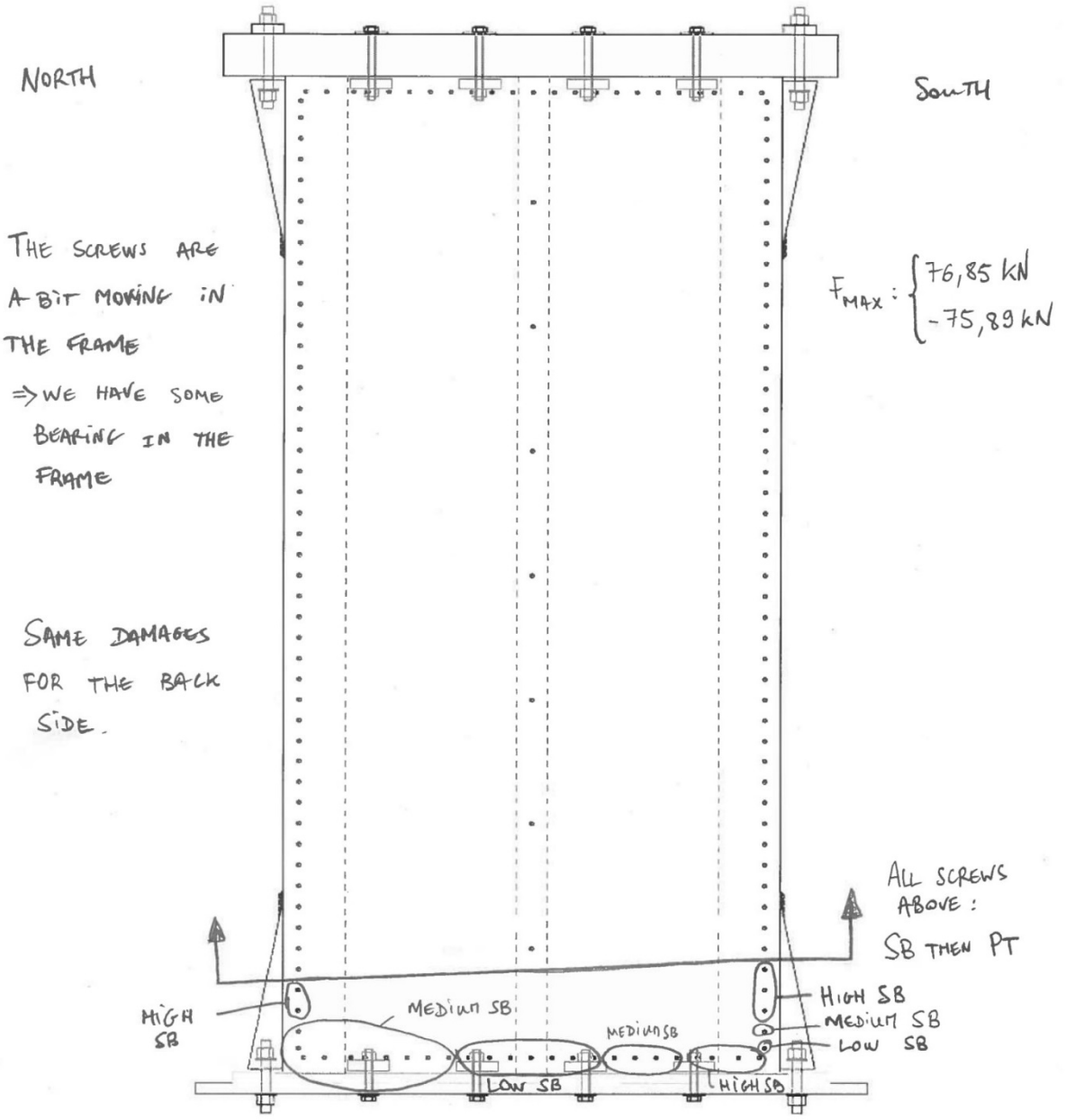

Failure Modes: Pull-out (PO); Partial Pull-out (PPO); Screw Shear Failure (SF); Pull through sheathing (PT); Damage prior to testing (DP); Tilting of screw (TS); Partial Pull-through (PPT); Tear-out of sheathing (TO); Steel Bearing Failure (SB); Flange-Lip Distortion (FLD); Track Uplift/Deformation (TD)

Figure E-15 Test observations for test W28-C

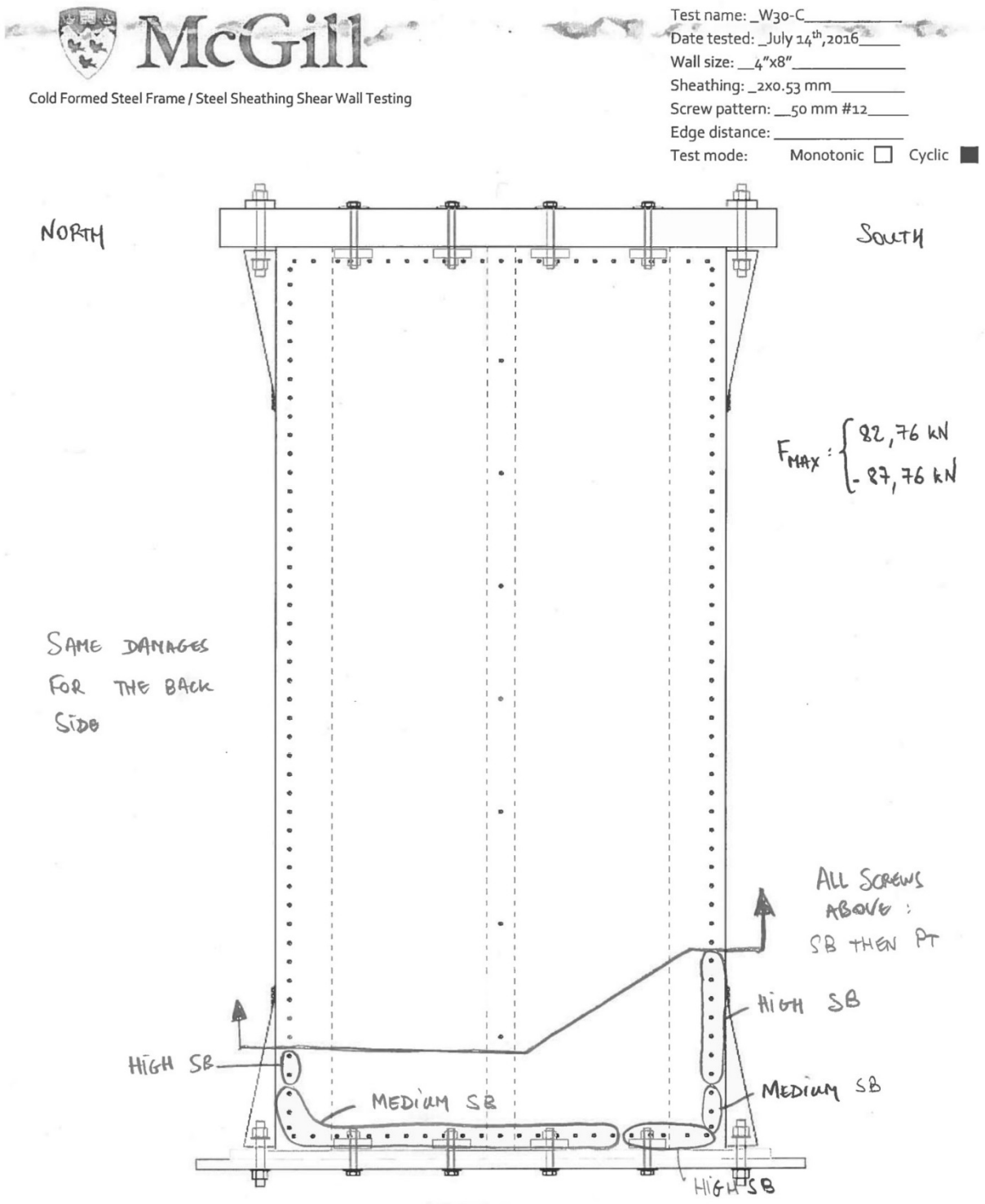

Figure E-16 Test observations for test W30-C

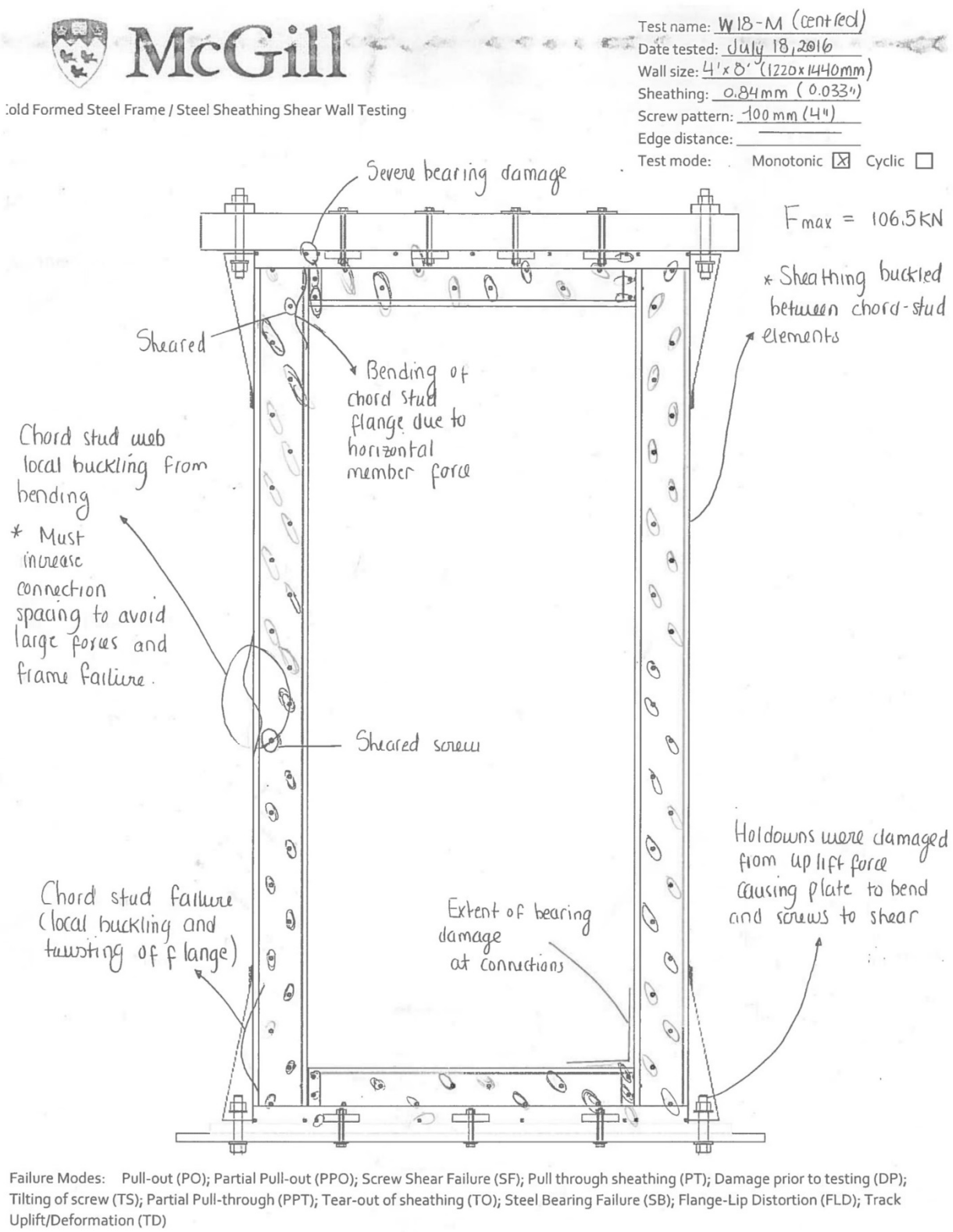

Figure E-17 Test observations for test W18-M

McGill

Cold Formed Steel Frame / Steel Sheathing Shear Wall Testing

Test name: W17-M (centred)
Date tested: July 20, 2016
Wall size: 1.22m x 2.44m (4'x8')
Sheathing: 0.84mm (0.033")
Screw pattern: 150mm (6")
Edge distance: ———
Test mode: Monotonic ☒ Cyclic ☐

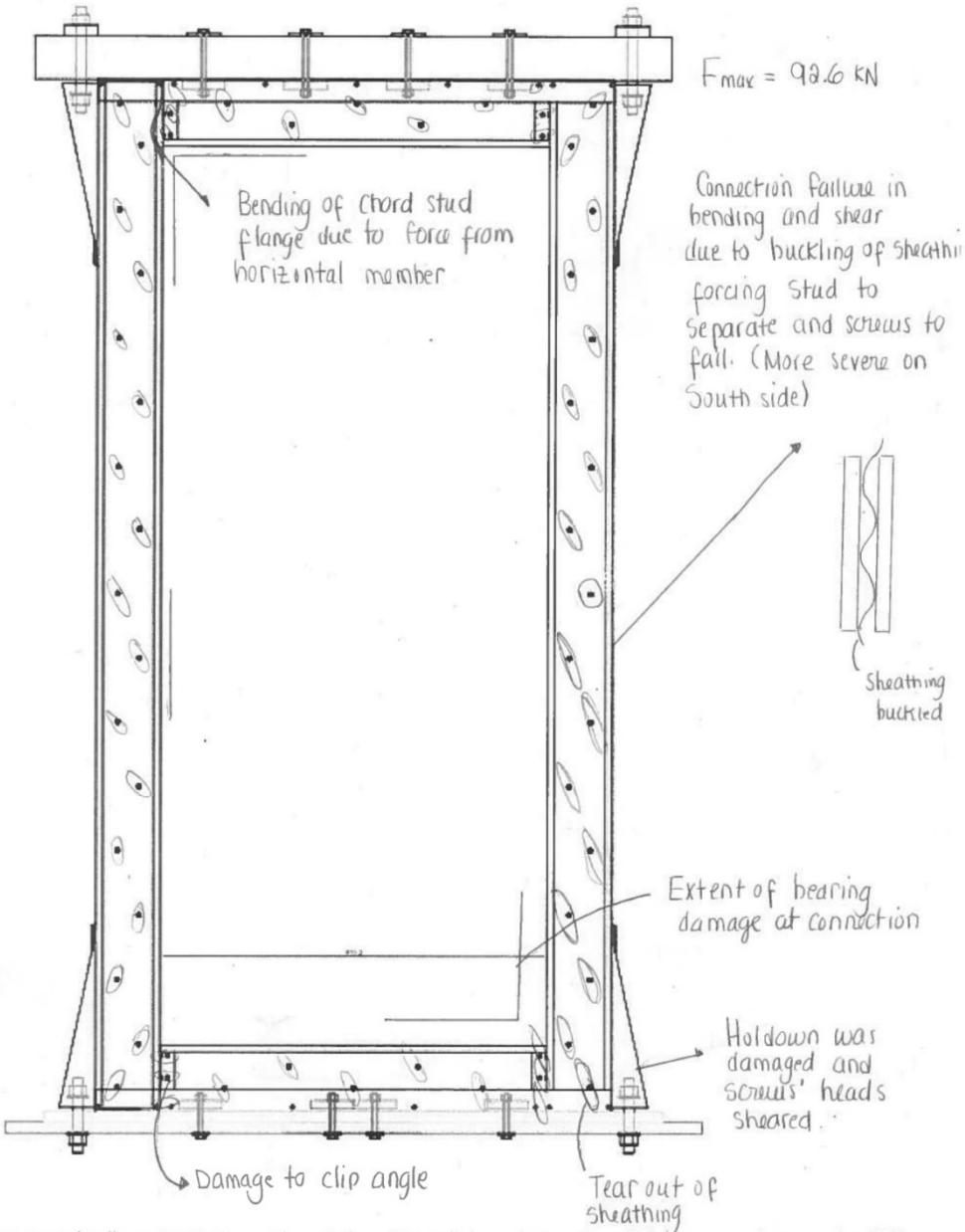

Failure Modes: Pull-out (PO); Partial Pull-out (PPO); Screw Shear Failure (SF); Pull through sheathing (PT); Damage prior to testing (DP); Tilting of screw (TS); Partial Pull-through (PPT); Tear-out of sheathing (TO); Steel Bearing Failure (SB); Flange-Lip Distortion (FLD); Track Uplift/Deformation (TD)

Figure E-18 Test observations for test W17-M

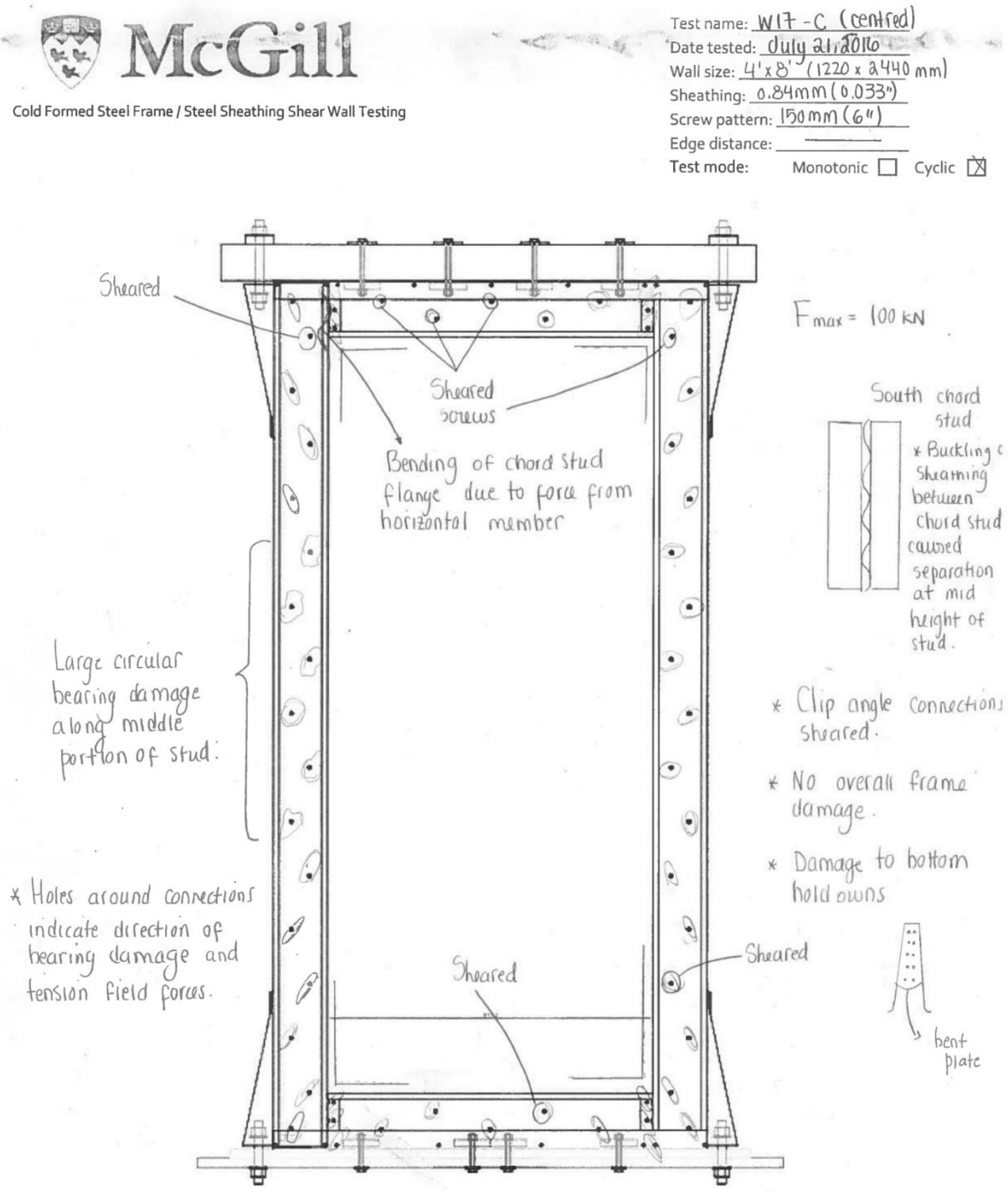

Failure Modes: Pull-out (PO); Partial Pull-out (PPO); Screw Shear Failure (SF); Pull through sheathing (PT); Damage prior to testing (DP); Tilting of screw (TS); Partial Pull-through (PPT); Tear-out of sheathing (TO); Steel Bearing Failure (SB); Flange-Lip Distortion (FLD); Track Uplift/Deformation (TD)

Figure E-19 Test observations for test W17-C

McGill

Cold Formed Steel Frame / Steel Sheathing Shear Wall Testing

Test name: W18-MR (centred - reinforce
Date tested: July 27, 2016
Wall size: 1.22m x 2.44m (4' x 8')
Sheathing: 0.84mm (0.033")
Screw pattern: 100mm (4")
Edge distance: ——
Test mode: Monotonic ☒ Cyclic ☐

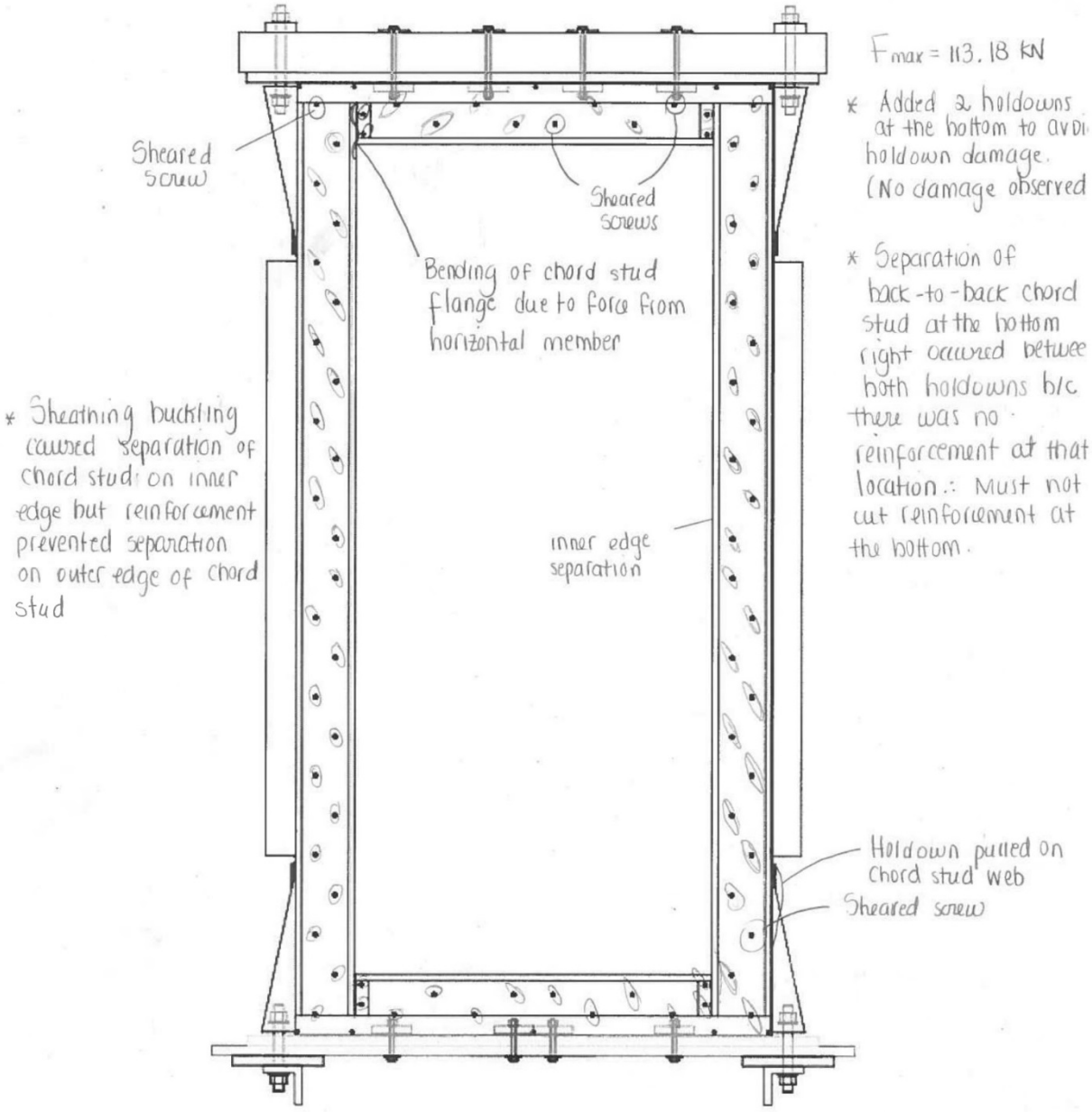

F_{max} = 113.18 kN

* Added 2 holdowns at the bottom to avoi holdown damage. (No damage observed

* Separation of back-to-back chord stud at the bottom right occured betwee both holdowns b/c there was no reinforcement at that location.: Must not cut reinforcement at the bottom.

* Sheathing buckling caused separation of chord stud on inner edge but reinforcement prevented separation on outer edge of chord stud

Failure Modes: Pull-out (PO); Partial Pull-out (PPO); Screw Shear Failure (SF); Pull through sheathing (PT); Damage prior to testing (DP); Tilting of screw (TS); Partial Pull-through (PPT); Tear-out of sheathing (TO); Steel Bearing Failure (SB); Flange-Lip Distortion (FLD); Track Uplift/Deformation (TD)

Figure E-20 Test observations for test W18-MR

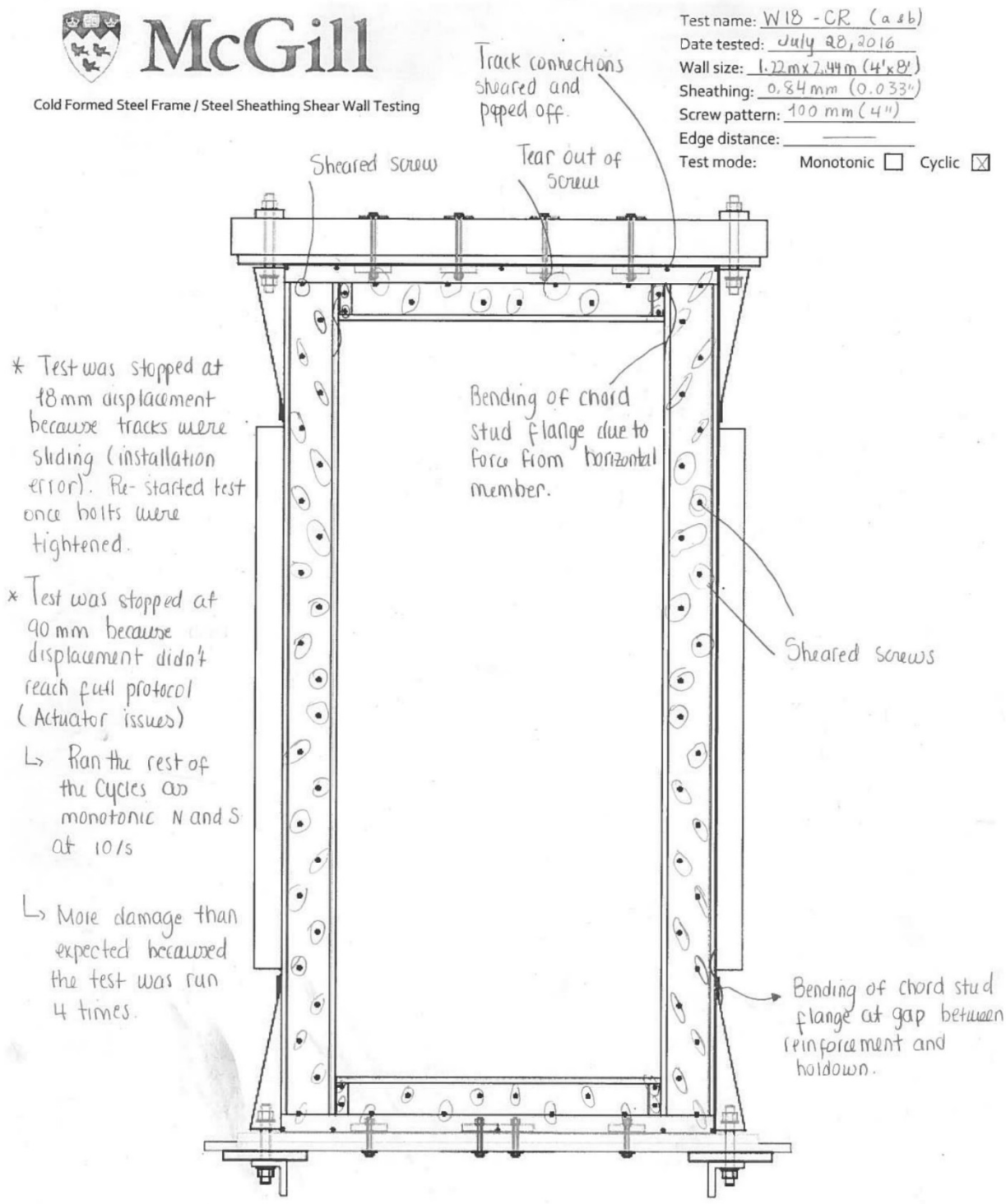

Failure Modes: Pull-out (PO); Partial Pull-out (PPO); Screw Shear Failure (SF); Pull through sheathing (PT); Damage prior to testing (DP); Tilting of screw (TS); Partial Pull-through (PPT); Tear-out of sheathing (TO); Steel Bearing Failure (SB); Flange-Lip Distortion (FLD); Track Uplift/Deformation (TD)

Figure E-21 Test observations for test W18-CR

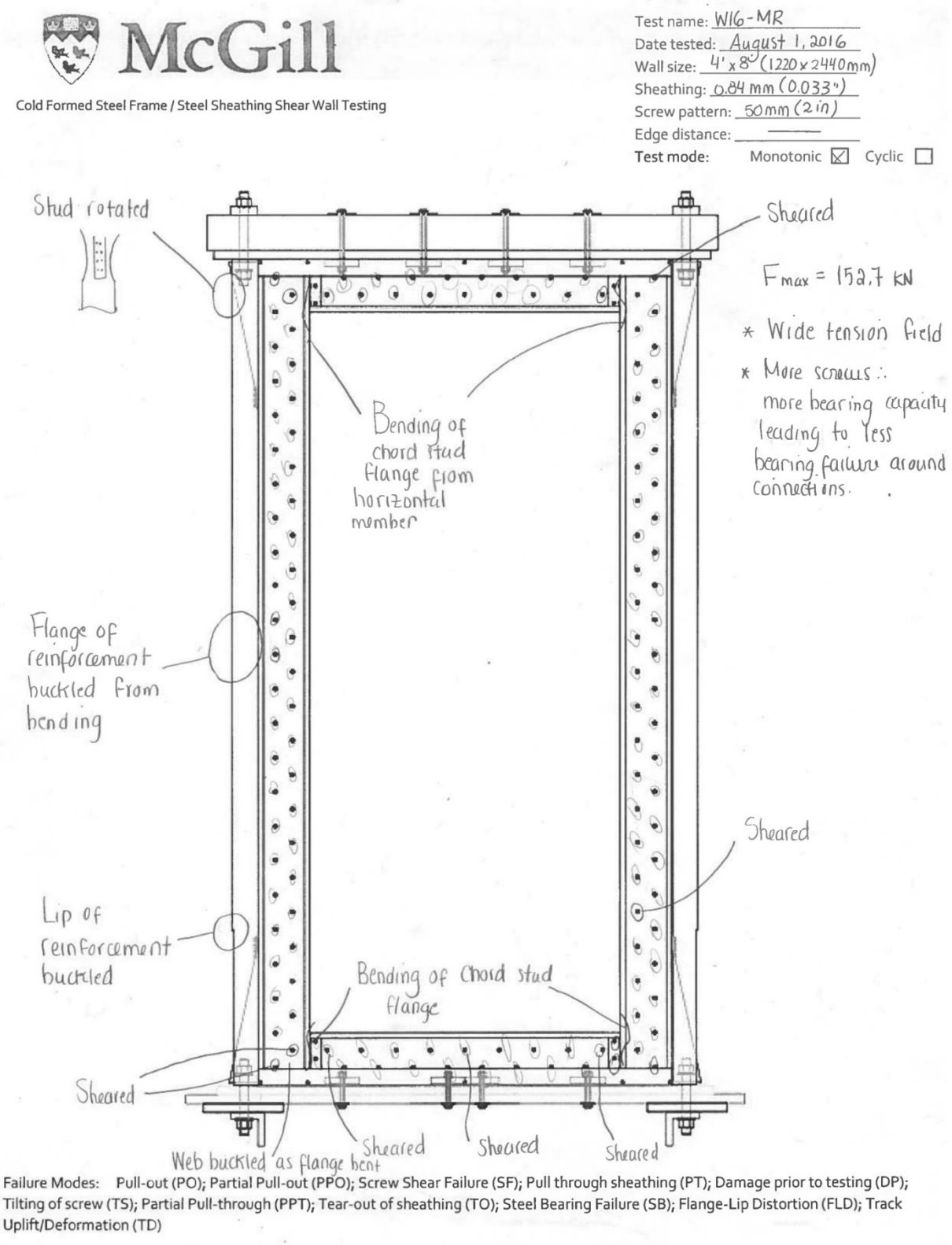

Figure E-22 Test observations for test W16-MR

McGill

Cold Formed Steel Frame / Steel Sheathing Shear Wall Testing

Test name: W16 - MR2
Date tested: Aug 4, 2016
Wall size: 4' x 8' (1220 x 2440 mm)
Sheathing: 0.84 mm (0.033")
Screw pattern: 50 mm (2 in)
Test mode: Monotonic ☒ Cyclic ☐

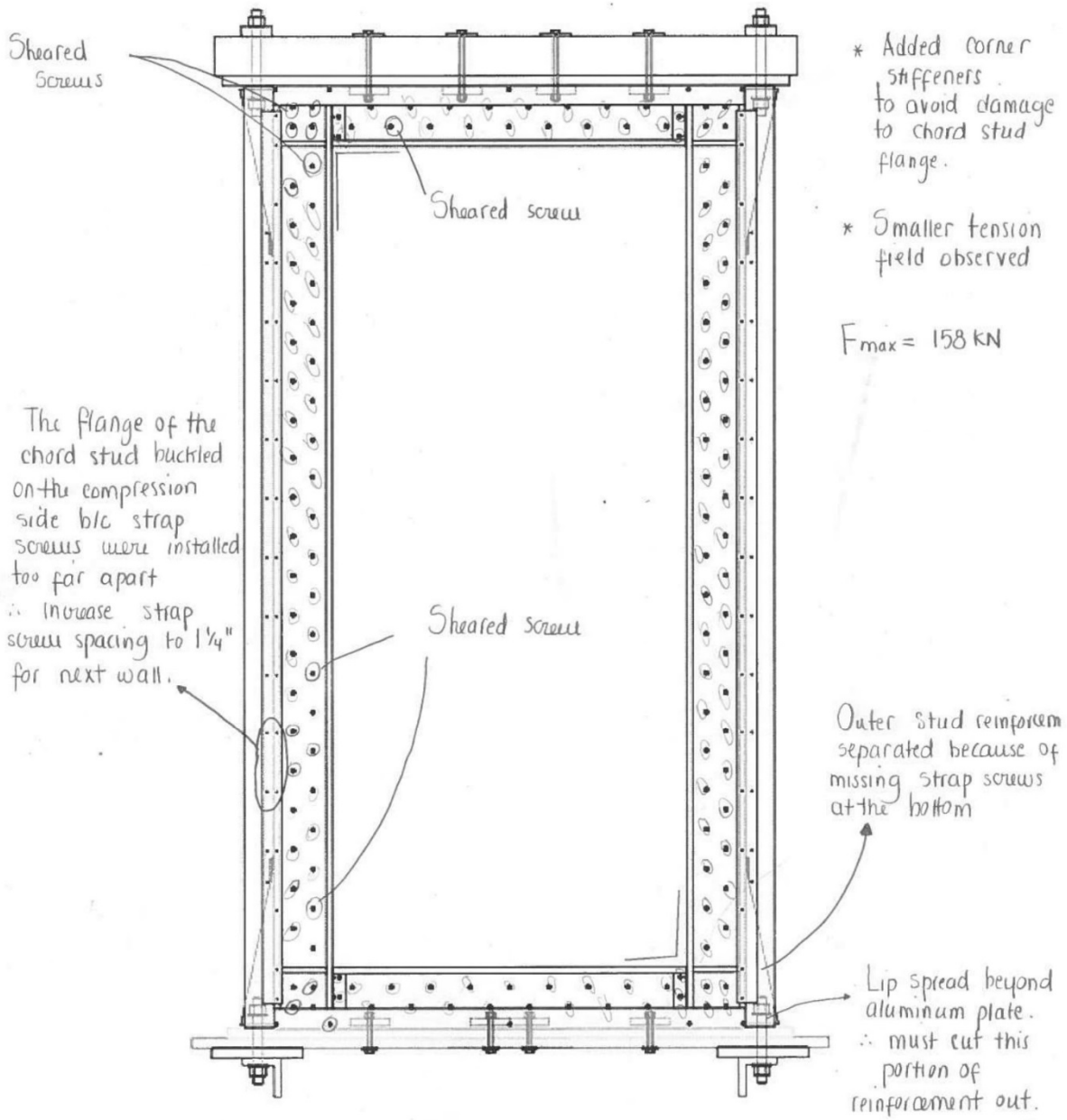

Failure Modes: Pull-out (PO); Partial Pull-out (PPO); Screw Shear Failure (SF); Pull through sheathing (PT); Damage prior to testing (DP); Tilting of screw (TS); Partial Pull-through (PPT); Tear-out of sheathing (TO); Steel Bearing Failure (SB); Flange-Lip Distortion (FLD); Track Uplift/Deformation (TD)

Figure E-23 Test observations for test W16-MR2

McGill

Cold Formed Steel Frame / Steel Sheathing Shear Wall Testing

Test name: W15 - MR3
Date tested: Aug 12, 2016
Wall size: 1.22m x 2.44m (4'x8')
Sheathing: 0.84mm (0.033")
Screw pattern: 50mm (2")
Test mode: Monotonic [X] Cyclic [ ]

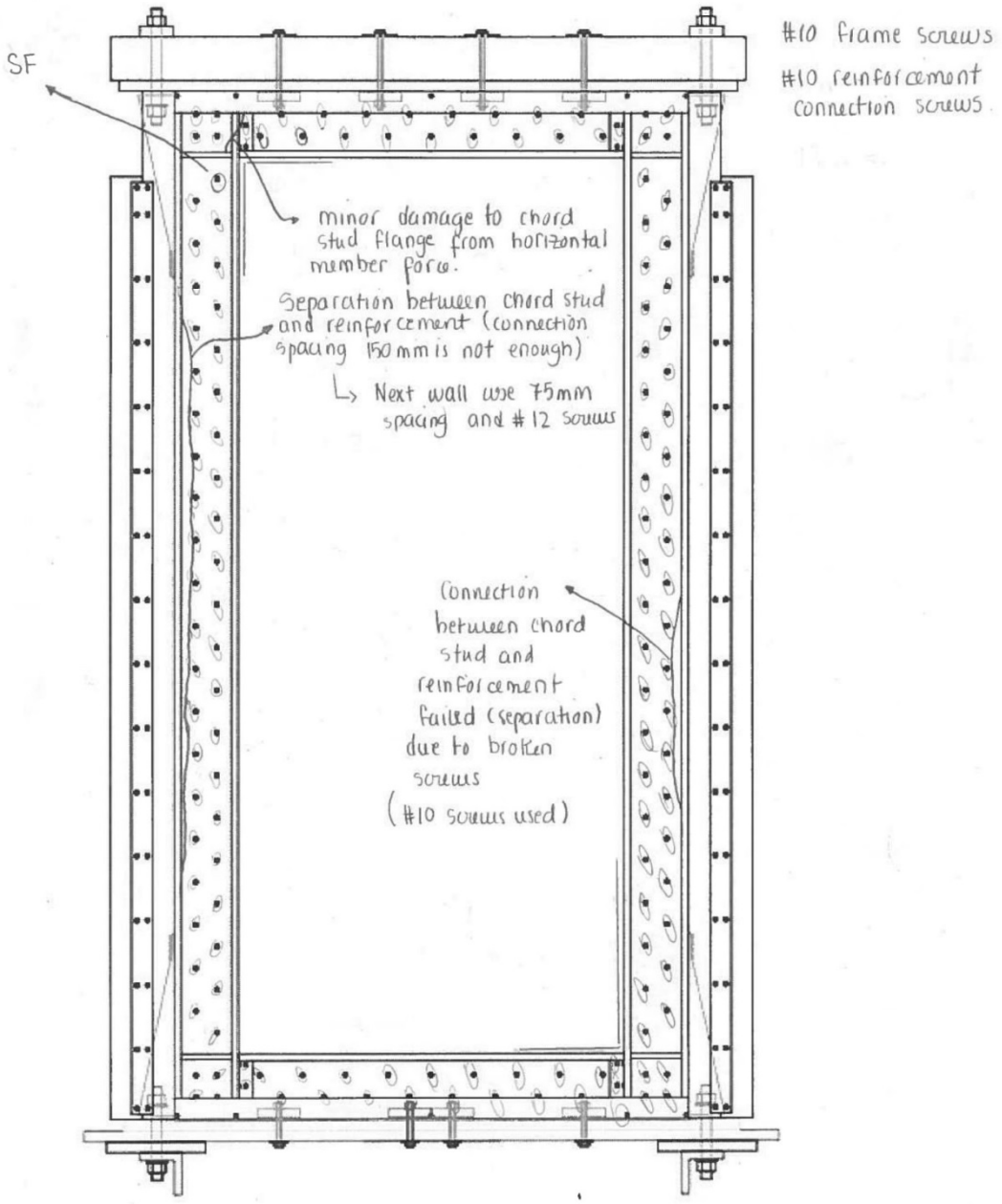

Failure Modes: Pull-out (PO); Partial Pull-out (PPO); Screw Shear Failure (SF); Pull through sheathing (PT); Damage prior to testing (DP); Tilting of screw (TS); Partial Pull-through (PPT); Tear-out of sheathing (TO); Steel Bearing Failure (SB); Flange-Lip Distortion (FLD); Track Uplift/Deformation (TD)

Figure E-24 Test observations for test W15-MR3

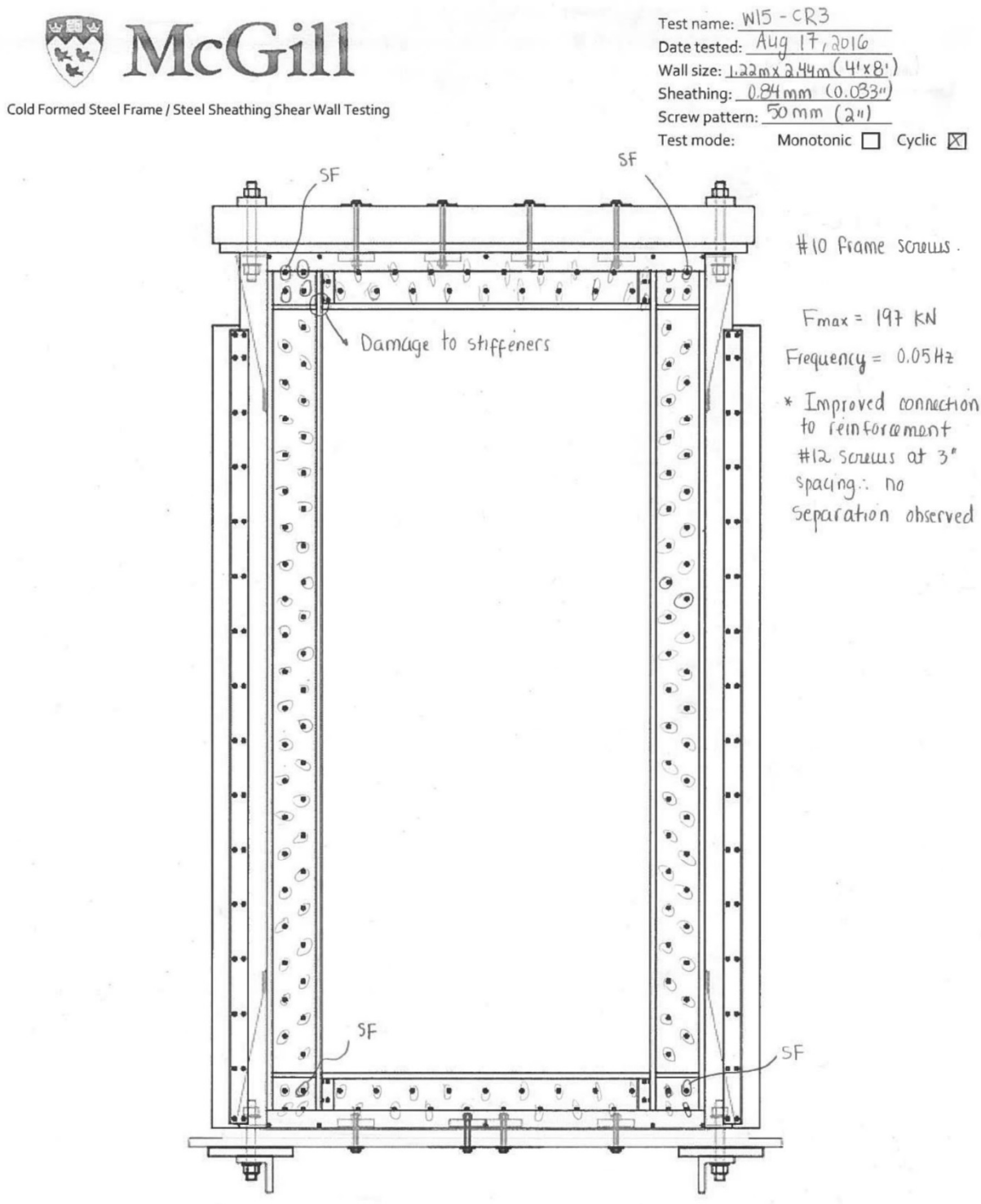

Figure E-25 Test observations for test W15-CR3

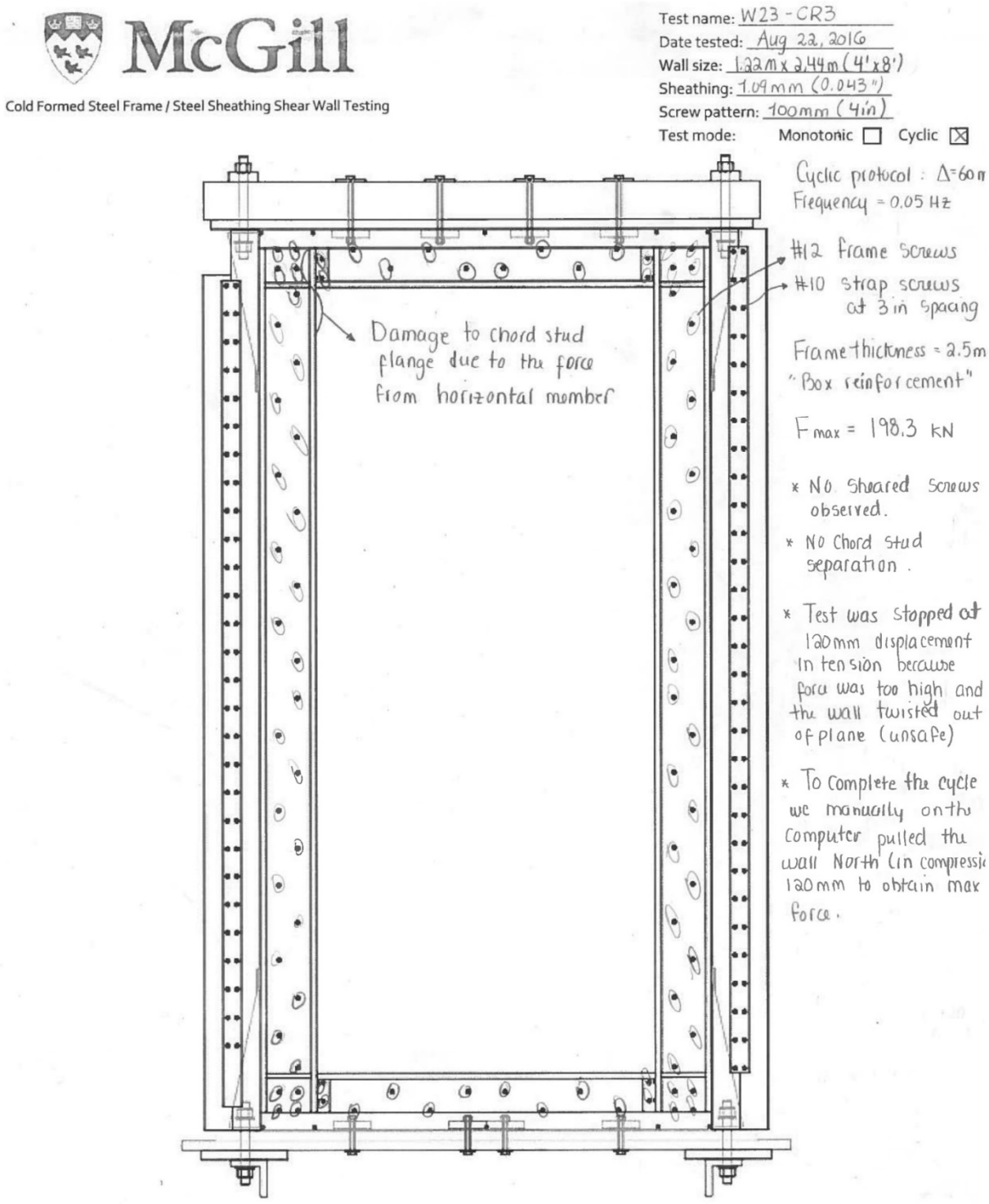

Figure E-26 Test observations for test W23-CR3

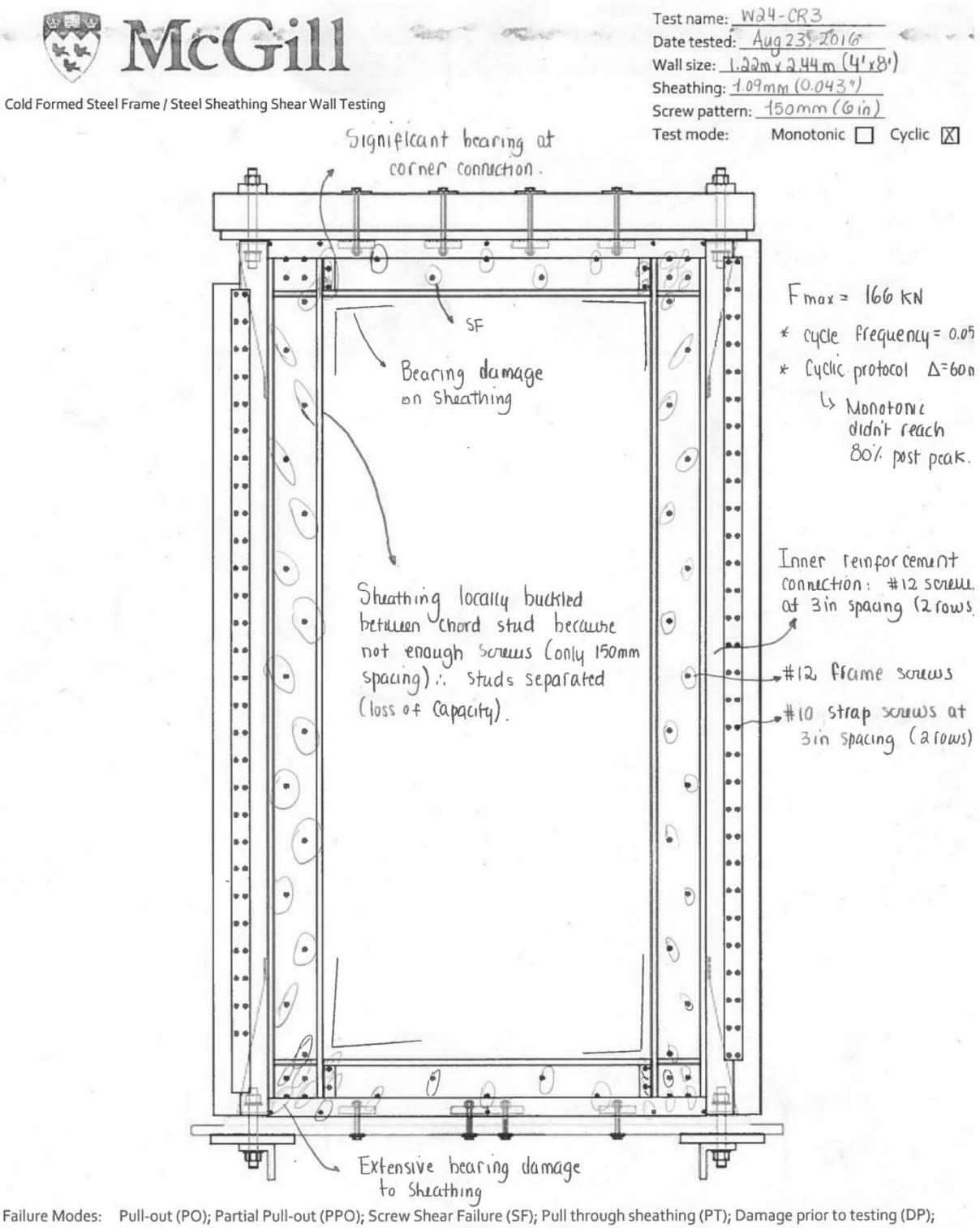

Figure E-27 Test observations for test W24-CR3

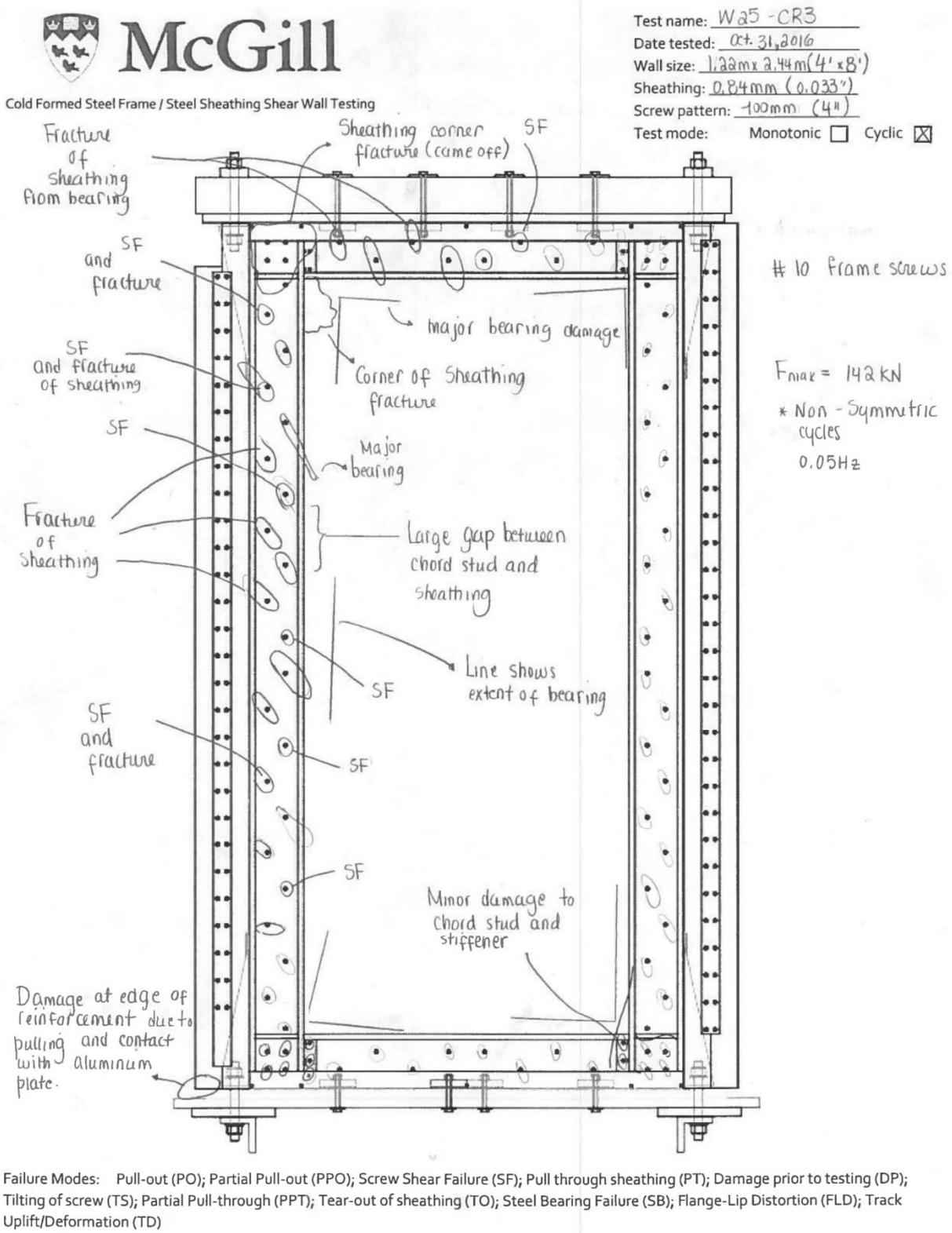

Figure E-28 Test observations for test W25-CR3

McGill

Cold Formed Steel Frame / Steel Sheathing Shear Wall Testing

Test name: W15B-CR3
Date tested: Nov 7, 2016
Wall size: 1.22m x 2.44m (4'x8')
Sheathing: 0.84mm (0.033")
Screw pattern: 50mm (2")
Test mode: Monotonic ☐ Cyclic ☒

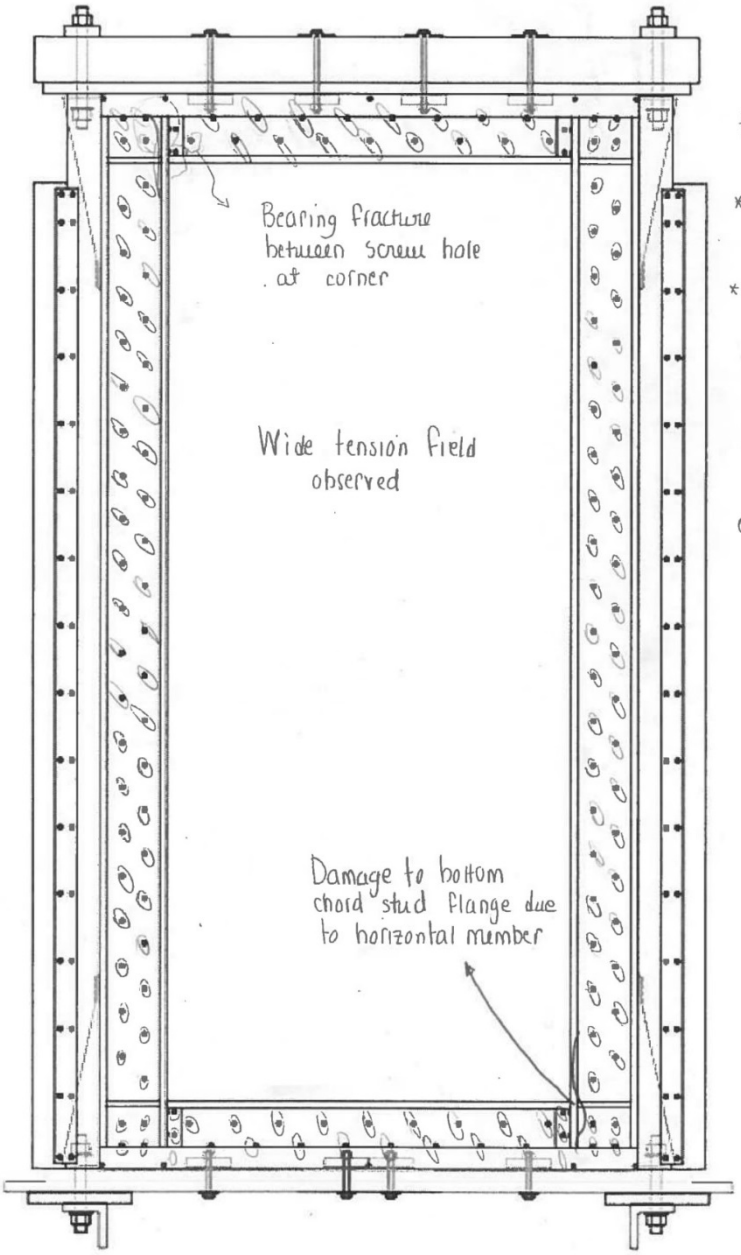

F_{max} = -200.5 kN @ 195mm displacement

#10 frame screws

* Actuator didn't run last cycle.
* Manually reduced cycle speed to 0.025Hz and ran last cycle to 215mm displac. and another cycle to 220 mm to obtain curve degradation

Failure Modes: Pull-out (PO); Partial Pull-out (PPO); Screw Shear Failure (SF); Pull through sheathing (PT); Damage prior to testing (DP); Tilting of screw (TS); Partial Pull-through (PPT); Tear-out of sheathing (TO); Steel Bearing Failure (SB); Flange-Lip Distortion (FLD); Track Uplift/Deformation (TD)

Figure E-29 Test observations for test W15B-CR3

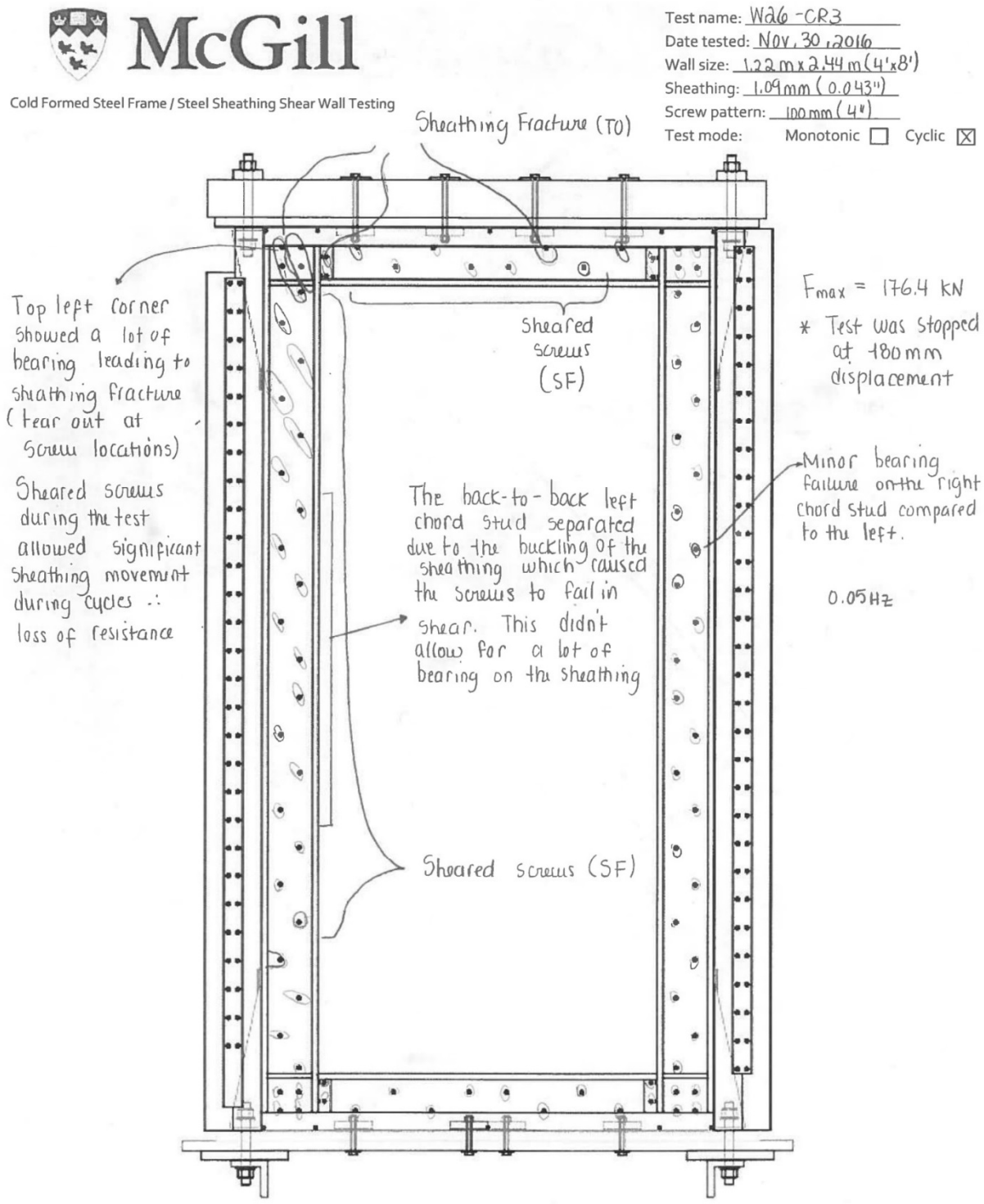

Figure E-30 Test observations for test W26-CR3

McGill

Cold Formed Steel Frame / Steel Sheathing Shear Wall Testing

Test name: W23B - CR3
Date tested: Dec. 8, 2016
Wall size: 1.22m x 2.44m (4'x8')
Sheathing: 1.09 mm (0.043")
Screw pattern: 100mm (4")
Test mode: Monotonic ☐ Cyclic ☒

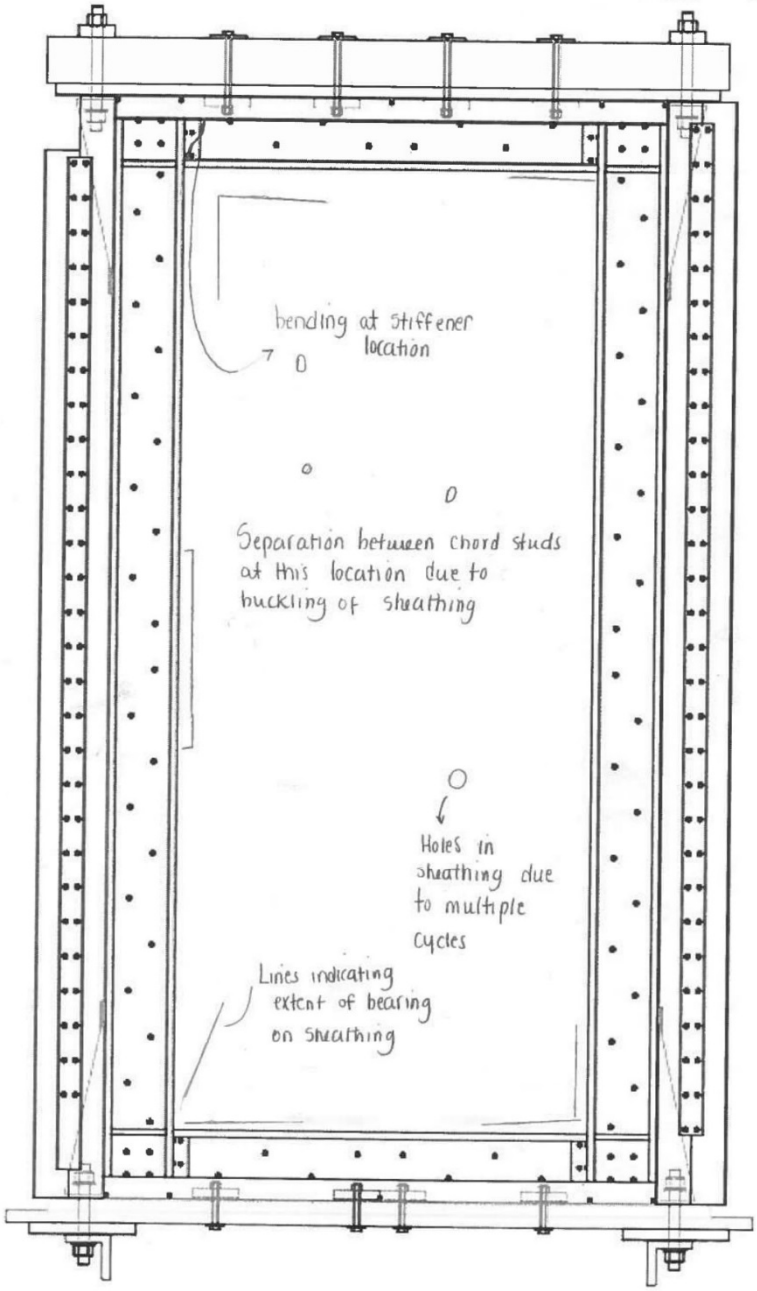

Failure Modes: Pull-out (PO); Partial Pull-out (PPO); Screw Shear Failure (SF); Pull through sheathing (PT); Damage prior to testing (DP); Tilting of screw (TS); Partial Pull-through (PPT); Tear-out of sheathing (TO); Steel Bearing Failure (SB); Flange-Lip Distortion (FLD); Track Uplift/Deformation (TD)

Figure E-31 Test observations for test W23B-CR3

APPENDIX F. COMPLETE TEST RESULTS

Table F-1a Full test results summary (metric) – Monotonic tests

Test ID	Ultimate Resistance S_u (kN/m)	Displacement at S_u Δ_u (mm)	Displacement at $0.4S_u$ $\Delta_{0.4u}$ (mm)	Displacement at $0.8S_u$ $\Delta_{0.8u}$ (mm)	Rotation at S_u θ_u (rad.10^{-3})	Rotation at $0.4S_u$ $\theta_{0.4u}$ (rad.10^{-3})	Rotation at $0.8S_u$ $\theta_{0.8u}$ (rad.10^{-3})	Total Energy Dissipated E_{TOT} (J)
Double-Sheathed Wall Configuration								
W19-M[2]	39.56	28.06	4.65	57.05	11.51	1.91	23.40	4230
W20-M[2]	27.28	39.33	3.18	66.72	16.13	1.31	27.36	3158
W21-M[2]	45.87	26.98	4.47	56.13	11.06	1.83	23.02	4980
W22-M[2]	28.36	41.19	3.45	74.47	16.89	1.41	30.54	3606
W28-M[1]	60.99	31.71	5.41	61.82	13.01	2.22	25.35	6463
W29-M[1]	38.22	34.29	3.51	85.01	14.06	1.44	34.86	4674
W30-M[1]	65.42	38.99	7.16	68.70	15.99	2.94	28.17	7248
W31-M[1]	39.29	29.94	3.21	76.18	12.28	1.32	31.24	4783
Centre-Sheathed Wall Configuration								
W15-MR3[2]	149.8	119.9	14.71	100.0	49.19	6.03	41.01	16788
W16-MR[2]	124.6	67.48	12.33	99.99	27.67	5.06	41.01	14479
W16-MR2[2]	129.6	105.5	15.14	99.99	43.25	6.21	41.01	15207
W17-M[2]	75.71	99.41	10.86	99.98	40.77	4.45	41.00	9221
W18-M[1]	87.22	68.22	10.81	100.0	27.98	4.43	41.02	10481
W18-MR[1]	92.65	87.28	10.83	99.99	35.79	4.44	41.01	11211

[1] Tested by the author

[2] Tested by Santos (2017)

Table F-1b Full test results summary (imperial) – Monotonic tests

Test ID	Ultimate Resistance S_u (lb/ft)	Displacement at S_u Δ_u (in)	Displacement at $0.4S_u$ $\Delta_{0.4u}$ (in)	Displacement at $0.8S_u$ $\Delta_{0.8u}$ (in)	Rotation at S_u θ_u (rad.10^{-3})	Rotation at $0.4S_u$ $\theta_{0.4u}$ (rad.10^{-3})	Rotation at $0.8S_u$ $\theta_{0.8u}$ (rad.10^{-3})	Total Energy Dissipated E_{TOT} (ft.lb)
Double-Sheathed Wall Configuration								
W19-M[2]	2710.7	1.10	0.18	2.25	11.51	1.91	23.40	3120
W20-M[2]	1869.3	1.55	0.13	2.63	16.13	1.31	27.36	2329
W21-M[2]	3143.1	1.06	0.18	2.21	11.06	1.83	23.02	3673
W22-M[2]	1943.3	1.62	0.14	2.93	16.89	1.41	30.54	2660
W28-M[1]	4178.8	1.25	0.21	2.43	13.01	2.22	25.35	4767
W29-M[1]	2618.9	1.35	0.14	3.35	14.06	1.44	34.86	3447
W30-M[1]	4482.7	1.54	0.28	2.70	15.99	2.94	28.17	5346
W31-M[1]	2692.2	1.18	0.13	3.00	12.28	1.32	31.24	3528
Centre-Sheathed Wall Configuration								
W15-MR3[2]	10264.4	4.72	0.58	3.94	49.19	6.03	41.01	12382
W16-MR[2]	8537.7	2.66	0.49	3.94	27.67	5.06	41.01	10679
W16-MR2[2]	8880.3	4.15	0.60	3.94	43.25	6.21	41.01	11216
W17-M[2]	5187.7	3.91	0.43	3.94	40.77	4.45	41.00	6801
W18-M[1]	5976.2	2.69	0.43	3.94	27.98	4.43	41.02	7730
W18-MR[1]	6348.6	3.44	0.43	3.94	35.79	4.44	41.01	8269

[1] Tested by the author

[2] Tested by Santos (2017)

Table F-2a Full test results summary (metric) – Positive cycles of cyclic tests

Test ID	Ultimate Resistance S_{u+} (kN/m)	Displacement at S_u Δ_{u+} (mm)	Displacement at $0.4S_u$ $\Delta_{0.4u+}$ (mm)	Displacement at $0.8S_u$ $\Delta_{0.8u+}$ (mm)	Rotation at S_u θ_{u+} (rad.10^{-3})	Rotation at $0.4S_u$ $\theta_{0.4u+}$ (rad.10^{-3})	Rotation at $0.8S_u$ $\theta_{0.8u+}$ (rad.10^{-3})	Total Energy Dissipated E_{TOT} (J)
Double-Sheathed Wall Configuration								
W19-C[2]	46.52	34.00	6.36	51.95	13.94	2.61	21.30	15062
W20-C[2]	29.85	28.00	3.51	50.50	11.48	1.44	20.71	10508
W21-C[2]	47.58	29.05	6.04	50.57	11.91	2.48	20.74	13970
W22-C[2]	29.80	26.17	3.17	43.43	10.73	1.30	17.81	9493
W28-C[1]	61.40	29.54	5.48	50.50	12.12	2.25	20.71	18482
W29-C[1]	40.80	25.71	3.48	40.44	10.55	1.43	16.58	12611
W30-C[1]	70.96	38.20	6.84	59.82	15.66	2.81	24.53	24628
W31-C[1]	45.65	31.86	3.86	48.40	13.07	1.58	19.85	14282
Centre-Sheathed Wall Configuration								
W15-CR3[2]	162.0	111.9	15.00	100.0	45.91	6.15	41.01	75743
W15B-CR3[2,3]	165.7	160.0	13.32	100.4	65.62	5.46	41.19	109013
W17-C[2]	81.75	74.27	12.40	100.6	30.46	5.09	41.27	56432
W18-CR[1]	94.75	89.03	13.03	100.0	36.51	5.34	41.01	64012
W23-CR3[1]	162.5	120.4	15.14	100.0	49.40	6.21	41.01	48419
W23B-CR3[1,3]	158.6	121.6	13.99	100.0	49.87	5.74	41.01	98377
W24-CR3[1]	135.3	81.20	13.50	100.0	33.30	5.54	41.01	76112
W25-CR3[2,3]	116.7	86.00	12.67	100.0	35.27	5.20	41.01	70483
W26-CR3[1,3]	145.3	65.73	12.87	83.53	26.96	5.28	34.25	61059

[1] Tested by the author

[2] Tested by Santos (2017)

[3] Asymmetric cyclic test to reach a higher maximum chord rotation

Table F-2b Full test results summary (imperial) – Positive cycles of cyclic tests

Test ID	Ultimate Resistance S_{u+} (lb/ft)	Displacement at S_u Δ_{u+} (in)	Displacement at $0.4S_u$ $\Delta_{0.4u+}$ (in)	Displacement at $0.8S_u$ $\Delta_{0.8u+}$ (in)	Rotation at S_u θ_{u+} (rad.10^{-3})	Rotation at $0.4S_u$ $\theta_{0.4u+}$(rad.10^{-3})	Rotation at $0.8S_u$ $\theta_{0.8u+}$(rad.10^{-3})	Total Energy Dissipated E_{TOT} (ft.lb)
Double-Sheathed Wall Configuration								
W19-C[2]	3187.6	1.34	0.25	2.05	13.94	2.61	21.30	11109
W20-C[2]	2045.4	1.10	0.14	1.99	11.48	1.44	20.71	7750
W21-C[2]	3260.2	1.14	0.24	1.99	11.91	2.48	20.74	10304
W22-C[2]	2041.9	1.03	0.12	1.71	10.73	1.30	17.81	7002
W28-C[1]	4207.2	1.16	0.22	1.99	12.12	2.25	20.71	13632
W29-C[1]	2795.4	1.01	0.14	1.59	10.55	1.43	16.58	9302
W30-C[1]	4862.5	1.50	0.27	2.36	15.66	2.81	24.53	18165
W31-C[1]	3127.9	1.25	0.15	1.91	13.07	1.58	19.85	10534
Centre-Sheathed Wall Configuration								
W15-CR3[2]	11100.4	4.41	0.59	3.94	45.91	6.15	41.01	55865
W15B-CR3[2]	11353.9	6.30	0.52	3.95	65.62	5.46	41.19	80404
W17-C[2]	5601.6	2.92	0.49	3.96	30.46	5.09	41.27	41622
W18-CR[1]	6492.4	3.51	0.51	3.94	36.51	5.34	41.01	47213
W23-CR3[1]	11136.6	4.74	0.60	3.94	49.40	6.21	41.01	35712
W23B-CR3[1,3]	10866.0	4.79	0.55	3.94	49.87	5.74	41.01	72560
W24-CR3[1]	9269.5	3.20	0.53	3.94	33.30	5.54	41.01	56138
W25-CR3[2,3]	7996.4	3.39	0.50	3.94	35.27	5.20	41.01	51986
W26-CR3[1,3]	9952.9	2.59	0.51	3.29	26.96	5.28	34.25	45035

[1] Tested by the author

[2] Tested by Santos (2017)

[3] Asymmetric cyclic test to reach a higher maximum chord rotation

Table F-3a Full test results summary (metric) – Negative cycles of cyclic tests

Test ID	Ultimate Resistance S_{u-} (kN/m)	Displacement at S_u Δ_{u-} (mm)	Displacement at $0.4S_u$ $\Delta_{0.4u-}$ (mm)	Displacement at $0.8S_u$ $\Delta_{0.8u-}$ (mm)	Rotation at S_u θ_{u-} (rad.10^{-3})	Rotation at $0.4S_u$ $\theta_{0.4u-}$ (rad.10^{-3})	Rotation at $0.8S_u$ $\theta_{0.8u-}$ (rad.10^{-3})	Total Energy Dissipated E_{TOT} (J)
Double-Sheathed Wall Configuration								
W19-C[2]	-42.87	-25.00	-6.43	-45.48	-10.25	-2.64	-18.65	15062
W20-C[2]	-30.31	-24.48	-3.69	-36.00	-10.04	-1.51	-14.76	10508
W21-C[2]	-44.78	-21.54	-4.80	-40.96	-8.83	-1.97	-16.80	13970
W22-C[2]	-29.81	-23.98	-3.41	-39.25	-9.83	-1.40	-16.10	9493
W28-C[1]	-62.14	-26.43	-6.03	-38.05	-10.84	-2.47	-15.61	18482
W29-C[1]	-39.86	-24.30	-4.90	-37.19	-9.97	-2.01	-15.25	12611
W30-C[1]	-68.59	-31.21	-6.45	-43.97	-12.80	-2.65	-18.03	24628
W31-C[1]	-44.42	-26.53	-3.86	-44.18	-10.88	-1.58	-18.12	14282
Centre-Sheathed Wall Configuration								
W15-CR3[2]	-155.7	-103.1	-15.48	-100.0	-42.29	-6.35	-41.01	75743
W17-C[2]	-79.76	-78.89	-10.90	-99.63	-32.35	-4.47	-40.86	56432
W18-CR[1]	-89.91	-70.72	-12.72	-100.1	-29.00	-5.22	-41.03	64012
W23-CR3[1,3]	-131.8	-50.32	-11.13	-50.32	-20.64	-4.56	-20.64	48419
W24-CR3[1]	-127.5	-77.97	-11.91	-100.0	-31.97	-4.88	-41.01	76112

[1] Tested by the author

[2] Tested by Santos (2017)

[3] Protocol stopped during test; negative cycles not completed. Maximum negative displacement reached is 50 mm (1.97")

Table F-3b Full test results summary (imperial) – Negative cycles of cyclic tests

Test ID	Ultimate Resistance S_{u-} (lb/ft)	Displacement at S_u Δ_{u-} (in)	Displacement at $0.4S_u$ $\Delta_{0.4u-}$ (in)	Displacement at $0.8S_u$ $\Delta_{0.8u-}$ (in)	Rotation at S_u θ_{u-} (rad.10^{-3})	Rotation at $0.4S_u$ $\theta_{0.4u-}$ (rad.10^{-}	Rotation at $0.8S_u$ $\theta_{0.8u-}$ (rad.10^{-}	Total Energy Dissipated E_{TOT} (ft.lb)
Double-Sheathed Wall Configuration								
W19-C[2]	-2937.5	-0.98	-0.25	-1.79	-10.25	-2.64	-18.65	11109
W20-C[2]	-2076.9	-0.96	-0.15	-1.42	-10.04	-1.51	-14.76	7750
W21-C[2]	-3068.4	-0.85	-0.19	-1.61	-8.83	-1.97	-16.80	10304
W22-C[2]	-2042.6	-0.94	-0.13	-1.55	-9.83	-1.40	-16.10	7002
W28-C[1]	-4257.9	-1.04	-0.24	-1.50	-10.84	-2.47	-15.61	13632
W29-C[1]	-2731.1	-0.96	-0.19	-1.46	-9.97	-2.01	-15.25	9302
W30-C[1]	-4699.9	-1.23	-0.25	-1.73	-12.80	-2.65	-18.03	18165
W31-C[1]	-3043.4	-1.04	-0.15	-1.74	-10.88	-1.58	-18.12	10534
Centre-Sheathed Wall Configuration								
W15-CR3[2]	-10668.7	-4.06	-0.61	-3.94	-42.29	-6.35	-41.01	55865
W17-C[2]	-5465.2	-3.11	-0.43	-3.92	-32.35	-4.47	-40.86	41622
W18-CR[1]	-6160.7	-2.78	-0.50	-3.94	-29.00	-5.22	-41.03	47213
W23-CR3[1,3]	-9033.7	-1.98	-0.44	-1.98	-20.64	-4.56	-20.64	35712
W24-CR3[1]	-8735.7	-3.07	-0.47	-3.94	-31.97	-4.88	-41.01	56138

[1] Tested by the author

[2] Tested by Santos (2017)

[3] Protocol stopped during test; negative cycles not completed. Maximum negative displacement reached is 50 mm (1.97")

Table F-4a Summary of Material Properties (Metric)

Specimen	Nominal thickness, t_n (mm)	Base metal thickness, t_b (mm)	Nominal yield strength, F_{yn} (MPa)	Nominal tensile strength, F_{un} (MPa)	Measured yield strength, F_y (MPa)	Measured tensile strength, F_u (MPa)	F_u/F_y	Elongation (%)	R_y	R_t
Sheathing A Transversal dir.	0.84	0.88	230	310	302	352	1.17	40	1.3	1.1
Sheathing A Longitudinal dir.	0.84	0.87	230	310	276	358	1.30	39	1.2	1.2
Sheathing B Transversal dir.	0.48[1]	0.48	230	310	318	361	1.14	38	1.4	1.2
Sheathing B Longitudinal dir.	0.47[1]	0.47	230	310	340	368	1.08	39	1.5	1.2
Sheathing C Transversal dir.	0.36[1]	0.36	230	310	344	370	1.07	29	1.5	1.2
Sheathing C Longitudinal dir.	0.36[1]	0.36	230	310	305	358	1.18	26	1.3	1.2
Sheathing D	1.09	1.12	230	310	316	380	1.20	32	1.4	1.2
Strip	1.09	1.11	345	450	366	447	1.22	30	1.1	1.0
Stud A / Track A	1.73	1.77	345	450	386	466	1.21	34	1.1	1.0
Track B	2.46	2.54	345	450	380	451	1.19	35	1.1	1.0
Stud B	2.46	2.54	345	450	389	461	1.19	34	1.1	1.0

[1] Non standard thickness, no nominal value

Table F-4b Summary of Material Properties (Imperial)

Specimen	Nominal thickness, t_n (in)	Base metal thickness, t_b (in)	Nominal yield strength, F_{yn} (ksi)	Nominal tensile strength, F_{un} (ksi)	Measured yield strength, F_y (ksi)	Measured tensile strength, F_u (ksi)	F_u/F_y	Elongation (%)	R_y	R_t
Sheathing A Transversal dir.	0.033	0.035	33	45	44	51	1.17	40	1.3	1.1
Sheathing A Longitudinal dir.	0.033	0.034	33	45	40	52	1.30	39	1.2	1.2
Sheathing B Transversal dir.	0.019[1]	0.019	33	45	46	52	1.14	38	1.4	1.2
Sheathing B Longitudinal dir.	0.019[1]	0.019	33	45	49	53	1.08	39	1.5	1.2
Sheathing C Transversal dir.	0.014[1]	0.014	33	45	50	54	1.07	29	1.5	1.2
Sheathing C Longitudinal dir.	0.014[1]	0.014	33	45	44	52	1.18	26	1.3	1.2
Sheathing D	0.043	0.044	33	45	46	55	1.20	32	1.4	1.2
Strip	0.043	0.044	50	65	53	65	1.22	30	1.1	1.0
Stud A / Track A	0.068	0.070	50	65	56	68	1.21	34	1.1	1.0
Track B	0.097	0.100	50	65	55	65	1.19	35	1.1	1.0
Stud B	0.097	0.100	50	65	56	67	1.19	34	1.1	1.0

[1] Non standard thickness, no nominal value

APPENDIX G. ANALYSIS OF THE TEST RESULTS

Table G-1a Full Design Properties Summary (Metric) – Monotonic Shear Wall Tests

Test ID	Yield Resistance S_y (kN/m)	Displacement at $0.4S_u$ $\Delta_{0.4u}$ (mm)	Displacement at S_y Δ_y (mm)	Rotation at $0.4S_u$ $\theta_{0.4u}$ (rad.10^{-3})	Rotation at S_y θ_y (rad.10^{-3})	Elastic Stiffness k_e (kN/mm)	Ductility μ	Energy Dissipated E_{EEEP} (J)
Double-Sheathed Wall Configuration								
W19-M[2]	35.46	4.65	10.45	1.91	4.29	4.14	5.46	2242
W20-M[2]	25.18	3.18	7.36	1.31	3.02	4.17	9.07	1937
W21-M[2]	41.43	4.47	10.12	1.83	4.15	5.00	5.55	2581
W22-M[2]	26.79	3.45	8.15	1.41	3.34	4.01	9.13	2301
W28-M[1]	54.21	5.41	12.01	2.22	4.93	5.51	5.15	3692
W29-M[1]	34.81	3.51	7.97	1.44	3.27	5.33	10.66	3440
W30-M[1]	58.79	7.16	16.12	2.94	6.61	4.45	4.26	4349
W31-M[1]	36.28	3.21	7.43	1.32	3.05	5.96	10.26	3207
Centre-Sheathed Wall Configuration								
W15-MR3[2]	127.6	14.25	31.02	5.85	12.72	5.02	3.87	13158
W16-MR[2]	112.0	12.33	27.68	5.06	11.35	4.94	4.34	11774
W16-MR2[2]	111.2	14.95	32.34	6.13	13.26	4.20	3.88	11377
W17-M[2]	66.62	10.86	23.90	4.45	9.80	3.40	5.16	7154
W18-M[1]	78.32	10.81	24.28	4.43	9.96	3.94	5.06	8397
W18-MR[1]	81.45	10.83	23.78	4.44	9.75	4.18	5.15	8754

[1] Tested by the author

[2] Tested by Santos (2017)

Table G-1b Full Design Properties Summary (Imperial) – Monotonic Shear Wall Tests

Test ID	Yield Resistance S_y (lb/ft)	Displacement at $0.4S_u$ $\Delta_{0.4u}$ (in)	Displacement at S_y Δ_y (in)	Rotation at $0.4S_u$ $\theta_{0.4u}$ (rad.10^{-3})	Rotation at S_y θ_y (rad.10^{-3})	Elastic Stiffness k_e (kips/in)	Ductility μ	Energy Dissipated E_{EEEP} (lb.ft)
Double-Sheathed Wall Configuration								
W19-M[2]	2429.8	0.18	0.41	1.91	4.29	23.64	5.46	1654
W20-M[2]	1725.4	0.13	0.29	1.31	3.02	23.84	9.07	1429
W21-M[2]	2838.8	0.18	0.40	1.83	4.15	28.53	5.55	1904
W22-M[2]	1835.7	0.14	0.32	1.41	3.34	22.89	9.13	1697
W28-M[1]	3714.5	0.21	0.47	2.22	4.93	31.46	5.15	2723
W29-M[1]	2385.0	0.14	0.31	1.44	3.27	30.41	10.66	2538
W30-M[1]	4028.1	0.28	0.63	2.94	6.61	25.40	4.26	3208
W31-M[1]	2485.7	0.13	0.29	1.32	3.05	34.03	10.26	2365
Centre-Sheathed Wall Configuration								
W15-MR3[2]	8743.3	0.56	1.22	5.85	12.72	28.67	3.87	9705
W16-MR[2]	7674.4	0.49	1.09	5.06	11.35	28.19	4.34	8684
W16-MR2[2]	7619.5	0.59	1.27	6.13	13.26	23.96	3.88	8391
W17-M[2]	4564.9	0.43	0.94	4.45	9.80	19.42	5.16	5277
W18-M[1]	5366.8	0.43	0.96	4.43	9.96	22.47	5.06	6194
W18-MR[1]	5580.8	0.43	0.94	4.44	9.75	23.86	5.15	6457

[1] Tested by the author

[2] Tested by Santos (2017)

Table G-2a Full Design Properties Summary (Metric) – Positive Range of Cyclic Shear Wall Tests

Test ID	Yield Resistance S_{y+} (kN/m)	Displacement at $0.4S_u$ $\Delta_{0.4u+}$ (mm)	Displacement at S_y Δ_{y+} (mm)	Rotation at $0.4S_u$ $\theta_{0.4u+}$(rad.10^{-3})	Rotation at S_y θ_{y+} (rad.10^{-3})	Elastic Stiffness k_{e+} (kN/mm)	Ductility μ_+	Energy Dissipated E_{EEEP+} (J)
Double-Sheathed Wall Configuration								
W19-C[2]	42.12	6.36	12.37	2.61	5.07	4.15	4.20	2352
W20-C[2]	26.53	3.51	7.41	1.44	3.04	4.37	6.82	1515
W21-C[2]	43.15	6.04	12.27	2.48	5.03	4.29	4.12	2339
W22-C[2]	26.90	3.17	7.18	1.30	2.95	4.57	6.05	1307
W28-C[1]	53.55	5.48	11.95	2.25	4.90	5.47	4.23	2909
W29-C[1]	36.49	3.48	7.79	1.43	3.19	5.72	5.19	1627
W30-C[1]	63.91	6.84	15.40	2.81	6.32	5.06	3.88	4063
W31-C[1]	40.35	3.86	8.52	1.58	3.50	5.77	5.68	2173
Centre-Sheathed Wall Configuration								
W15-CR3[2]	136.6	15.00	32.37	6.15	13.28	5.15	3.52	13970
W15B-CR3[2]	136.4	13.32	28.42	5.46	11.66	5.85	7.62	14347
W17-C[2]	73.99	12.40	28.20	5.09	11.56	3.20	3.61	7812
W18-CR[1]	86.02	13.03	29.57	5.34	12.13	3.55	4.02	8943
W23-CR3[1]	138.9	15.14	32.34	6.21	13.26	5.24	3.88	14203
W23B-CR3[1]	138.1	13.99	30.45	5.74	12.49	5.53	5.00	14281
W24-CR3[1]	118.2	13.50	29.50	5.54	12.10	4.89	3.89	12295
W25-CR3[2]	102.8	12.67	26.80	5.20	10.99	4.68	5.12	10866
W26-CR3[1]	126.0	12.87	27.89	5.28	11.44	5.51	2.99	10693

[1] Tested by the author

[2] Tested by Santos (2017)

Table G-2b Full Design Properties Summary (Imperial) – Positive Range of Cyclic Shear Wall Tests

Test ID	Yield Resistance S_{y+} (lb/ft)	Displacement at $0.4S_u$ $\Delta_{0.4u+}$ (in)	Displacement at S_y Δ_{y+} (in)	Rotation at $0.4S_u$ $\theta_{0.4u+}$(rad.10^{-3})	Rotation at S_y θ_{y+} (rad.10^{-3})	Elastic Stiffness k_{e+} (kips/in)	Ductility μ_+	Energy Dissipated E_{EEEP+} (lb.ft)
Double-Sheathed Wall Configuration								
W19-C[2]	2886.1	0.25	0.49	2.61	5.07	23.71	4.20	1735
W20-C[2]	1817.9	0.14	0.29	1.44	3.04	24.95	6.82	1117
W21-C[2]	2956.7	0.24	0.48	2.48	5.03	24.49	4.12	1725
W22-C[2]	1843.2	0.12	0.28	1.30	2.95	26.10	6.05	964
W28-C[1]	3669.2	0.22	0.47	2.25	4.90	31.22	4.23	2145
W29-C[1]	2500.6	0.14	0.31	1.43	3.19	32.64	5.19	1200
W30-C[1]	4379.1	0.27	0.61	2.81	6.32	28.91	3.88	2997
W31-C[1]	2764.7	0.15	0.34	1.58	3.50	32.97	5.68	1602
Centre-Sheathed Wall Configuration								
W15-CR3[2]	9360.0	0.59	1.27	6.15	13.28	29.40	3.52	10304
W15B-CR3[2]	9346.3	0.52	1.12	5.46	11.66	33.43	7.62	10582
W17-C[2]	5069.9	0.49	1.11	5.09	11.56	18.28	3.61	5762
W18-CR[1]	5894.2	0.51	1.16	5.34	12.13	20.27	4.02	6596
W23-CR3[1]	9516.0	0.60	1.27	6.21	13.26	29.91	3.88	10476
W23B-CR3[1]	9461.5	0.55	1.20	5.74	12.49	31.59	5.00	10533
W24-CR3[1]	8099.6	0.53	1.16	5.54	12.10	27.92	3.89	9068
W25-CR3[2]	7044.0	0.50	1.06	5.20	10.99	26.73	5.12	8014
W26-CR3[1]	8631.0	0.51	1.10	5.28	11.44	31.46	2.99	7887

[1] Tested by the author

[2] Tested by Santos (2017)

Table G-3a Full Design Properties Summary (Metric) – Negative Range of Cyclic Shear Wall Tests

Test ID	Yield Resistance S_{y-} (kN/m)	Displacement at $0.4S_{u-}$ $\Delta_{0.4u-}$ (mm)	Displacement at S_{y-} Δ_{y-} (mm)	Rotation at $0.4S_{u-}$ $\theta_{0.4u-}$(rad.10^{-3})	Rotation at S_{y-} θ_{y-} (rad.10^{-3})	Elastic Stiffness k_{e-} (kN/mm)	Ductility μ-	Energy Dissipated E_{EEEP-} (J)
Double-Sheathed Wall Configuration								
W19-C[2]	-39.07	-6.43	-11.99	-2.64	-4.92	3.97	3.79	1882
W20-C[2]	-26.47	-3.69	-7.43	-1.52	-3.05	4.34	4.84	1043
W21-C[2]	-40.43	-4.80	-11.02	-1.97	-4.52	4.48	3.72	1748
W22-C[2]	-26.89	-3.41	-8.17	-1.40	-3.35	4.02	4.80	1154
W28-C[1]	-54.49	-6.03	-13.21	-2.47	-5.42	5.03	2.88	2091
W29-C[1]	-35.70	-4.90	-10.97	-2.01	-4.50	3.97	3.39	1381
W30-C[1]	-60.40	-6.45	-14.21	-2.65	-5.83	5.18	3.09	2717
W31-C[1]	-38.64	-3.86	-8.40	-1.58	-3.44	5.61	5.26	1885
Centre-Sheathed Wall Configuration								
W15-CR3[2]	-132.9	-14.50	-31.89	-5.95	-13.08	5.08	3.23	13629
W17-C[2]	-71.28	-10.90	-23.60	-4.47	-9.68	3.68	4.31	7638
W18-CR[1]	-79.04	-12.72	-27.97	-5.22	-11.47	3.45	3.58	8300
W23-CR3[1,3]	-106.4	-11.13	-22.44	-4.56	-9.20	5.78	2.11	5074
W24-CR3[1]	-113.4	-11.91	-26.49	-4.88	-10.86	5.22	4.12	12006

[1] Tested by the author

[2] Tested by Santos (2017)

[3] Protocol stopped during test; negative cycles not completed. Maximum negative displacement reached is 50 mm (1.97")

Table G-3b Full Design Properties Summary (Imperial) – Negative Range of Cyclic Shear Wall Tests

Test ID	Yield Resistance S_{y-} (lb/ft)	Displacement at $0.4S_{u-}$ $\Delta_{0.4u-}$ (in)	Displacement at S_{y-} Δ_{y-} (in)	Rotation at $0.4S_{u-}$ $\theta_{0.4u-}$(rad.10^{-3})	Rotation at S_{y-} θ_{y-} (rad.10^{-3})	Elastic Stiffness k_{e-} (kips/in)	Ductility μ-	Energy Dissipated E_{EEEP-} (lb.ft)
Double-Sheathed Wall Configuration								
W19-C[2]	-2677.1	-0.25	-0.47	-2.64	-4.92	22.70	3.79	1388
W20-C[2]	-1813.8	-0.15	-0.29	-1.52	-3.05	24.81	4.84	769
W21-C[2]	-2770.3	-0.19	-0.43	-1.97	-4.52	25.56	3.72	1289
W22-C[2]	-1842.5	-0.13	-0.32	-1.40	-3.35	22.93	4.80	851
W28-C[1]	-3733.7	-0.24	-0.52	-2.47	-5.42	28.73	2.88	1542
W29-C[1]	-2445.9	-0.19	-0.43	-2.01	-4.50	22.67	3.39	1018
W30-C[1]	-4138.4	-0.25	-0.56	-2.65	-5.83	29.61	3.09	2004
W31-C[1]	-2647.7	-0.15	-0.33	-1.58	-3.44	32.05	5.26	1390
Centre-Sheathed Wall Configuration								
W15-CR3[2]	-9106.4	-0.57	-1.26	-5.95	-13.08	29.04	3.23	10052
W17-C[2]	-4884.2	-0.43	-0.93	-4.47	-9.68	21.04	4.31	5634
W18-CR[1]	-5415.8	-0.50	-1.10	-5.22	-11.47	19.70	3.58	6122
W23-CR3[1,3]	-7289.2	-0.44	-0.88	-4.56	-9.20	33.02	2.11	3743
W24-CR3[1]	-7772.5	-0.47	-1.04	-4.88	-10.86	29.83	4.12	8855

[1] Tested by the author

[2] Tested by Santos (2017)

[3] Protocol stopped during test; negative cycles not completed. Maximum negative displacement reached is 50 mm (1.97")

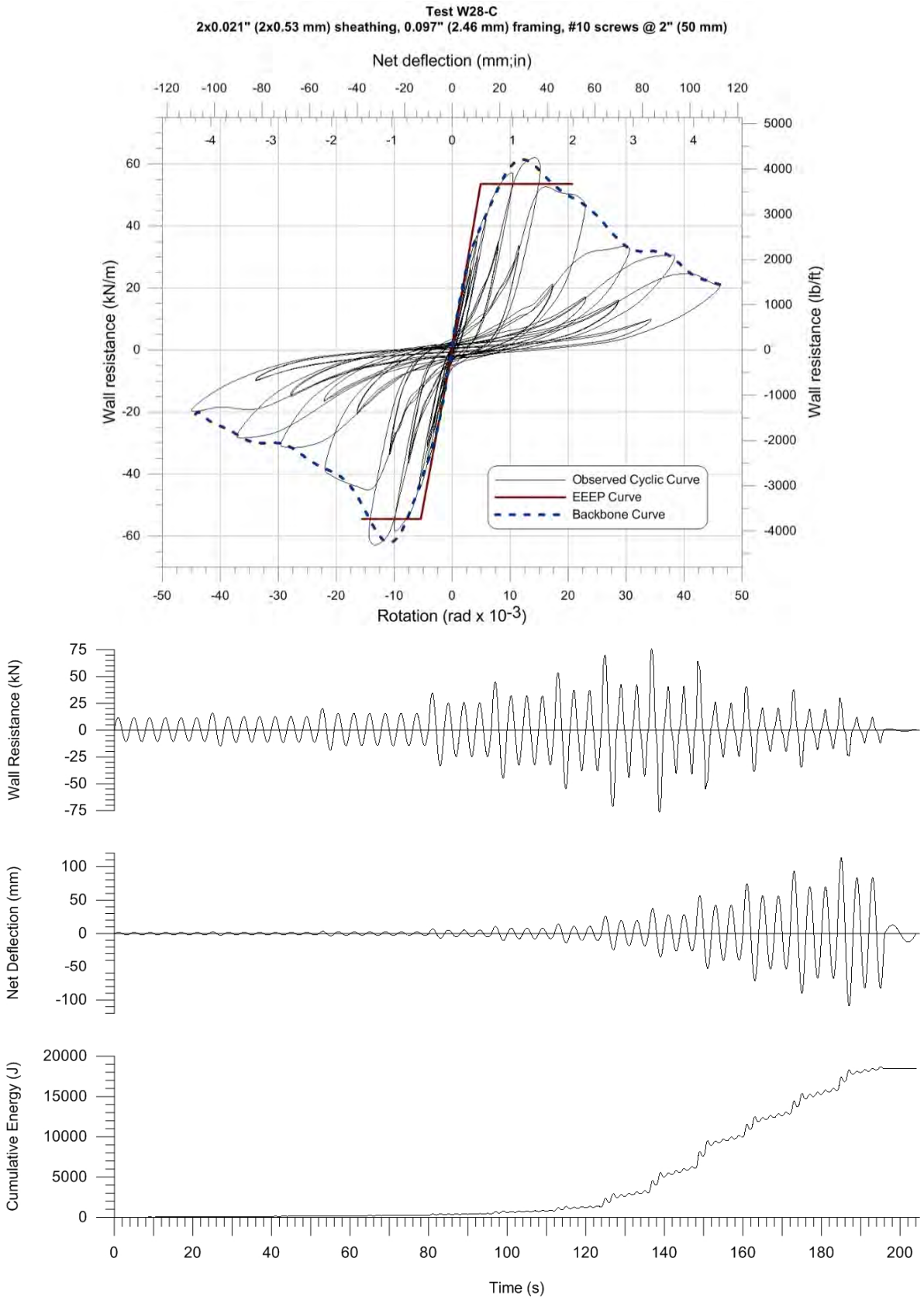

Figure G-1 Observed / EEEP curves and time history for cyclic test W28-C

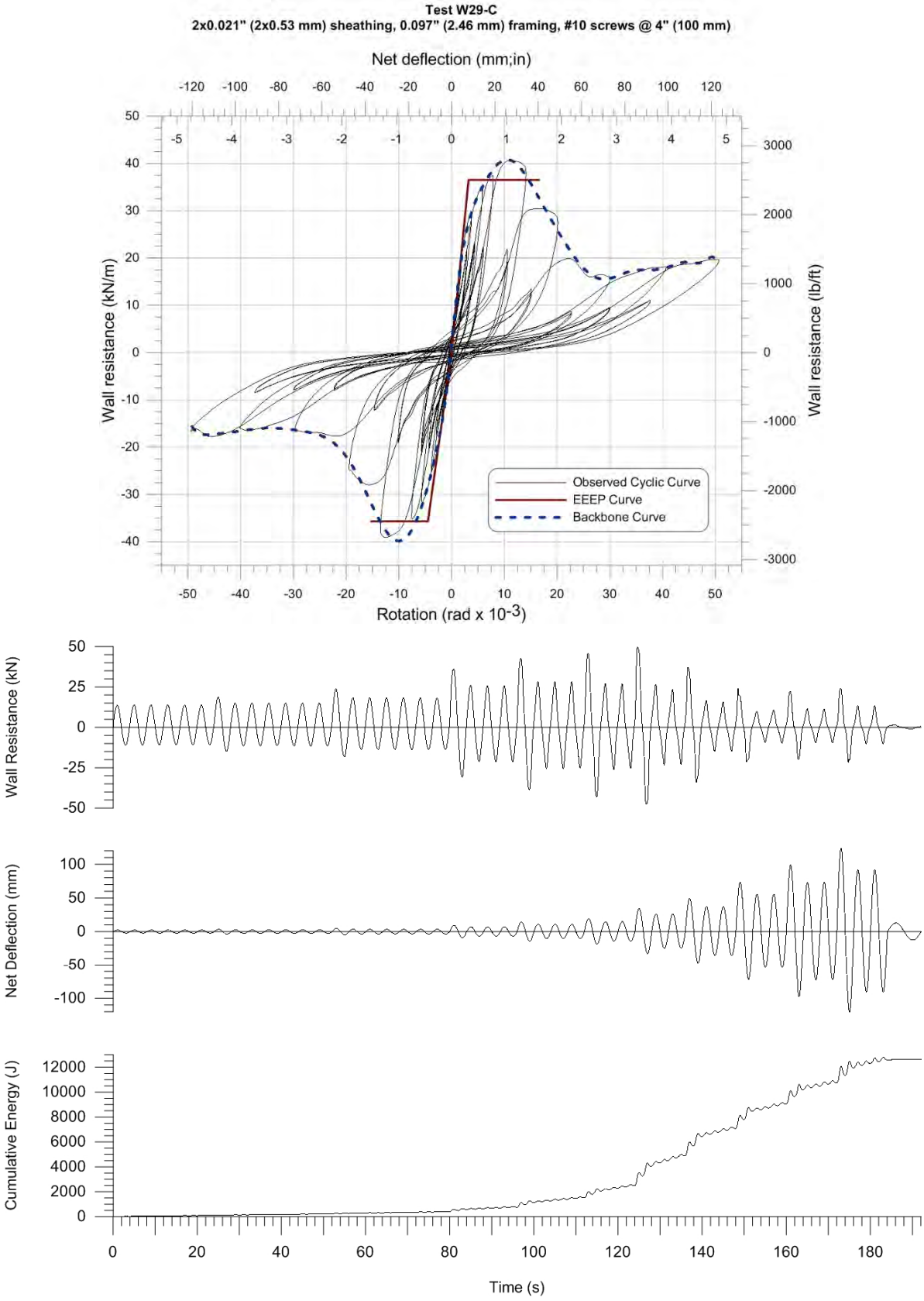

Figure G-2 Observed / EEEP curves and time history for cyclic test W29-C

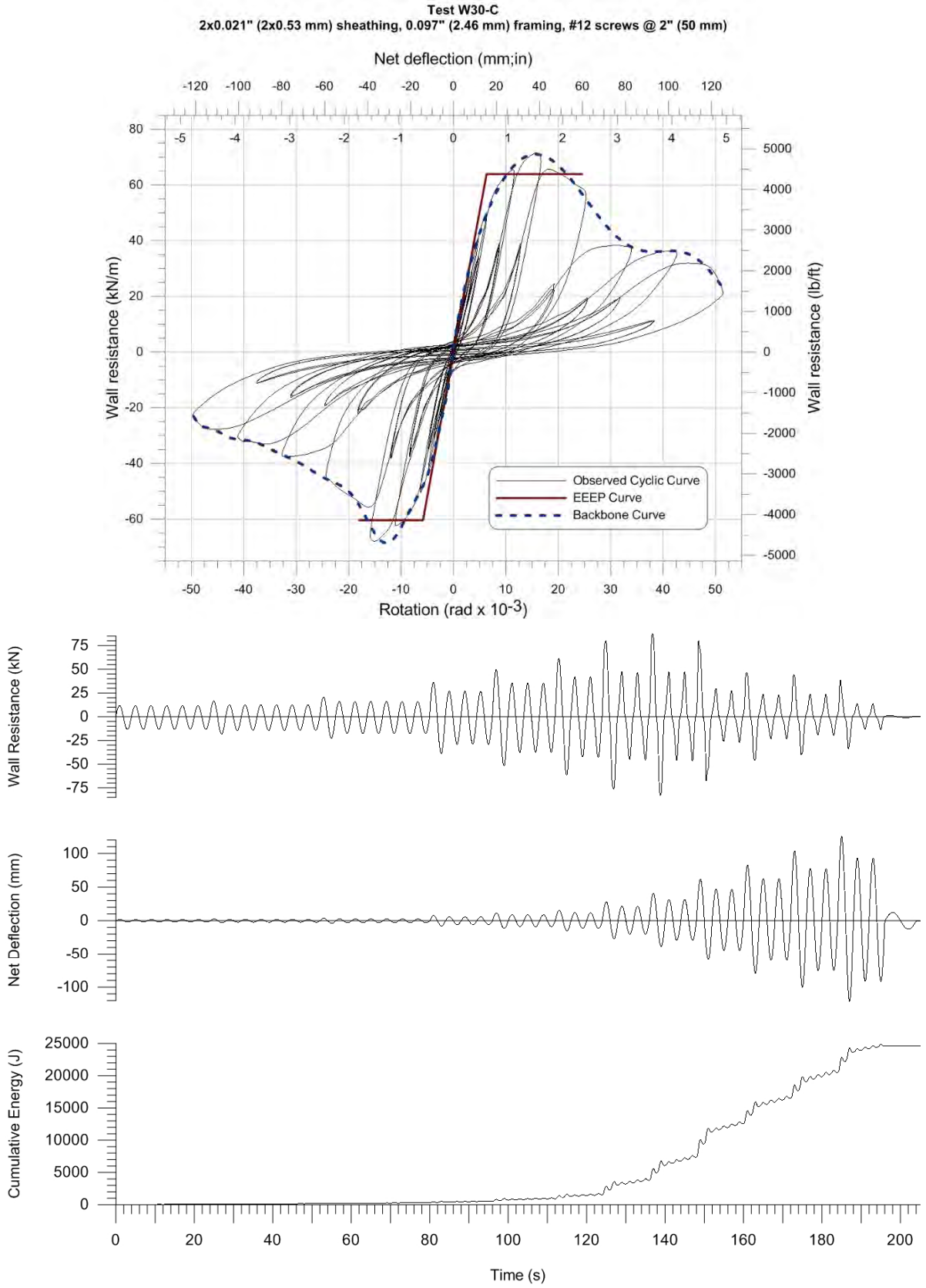

Figure G-3 Observed / EEEP curves and time history for cyclic test W30-C

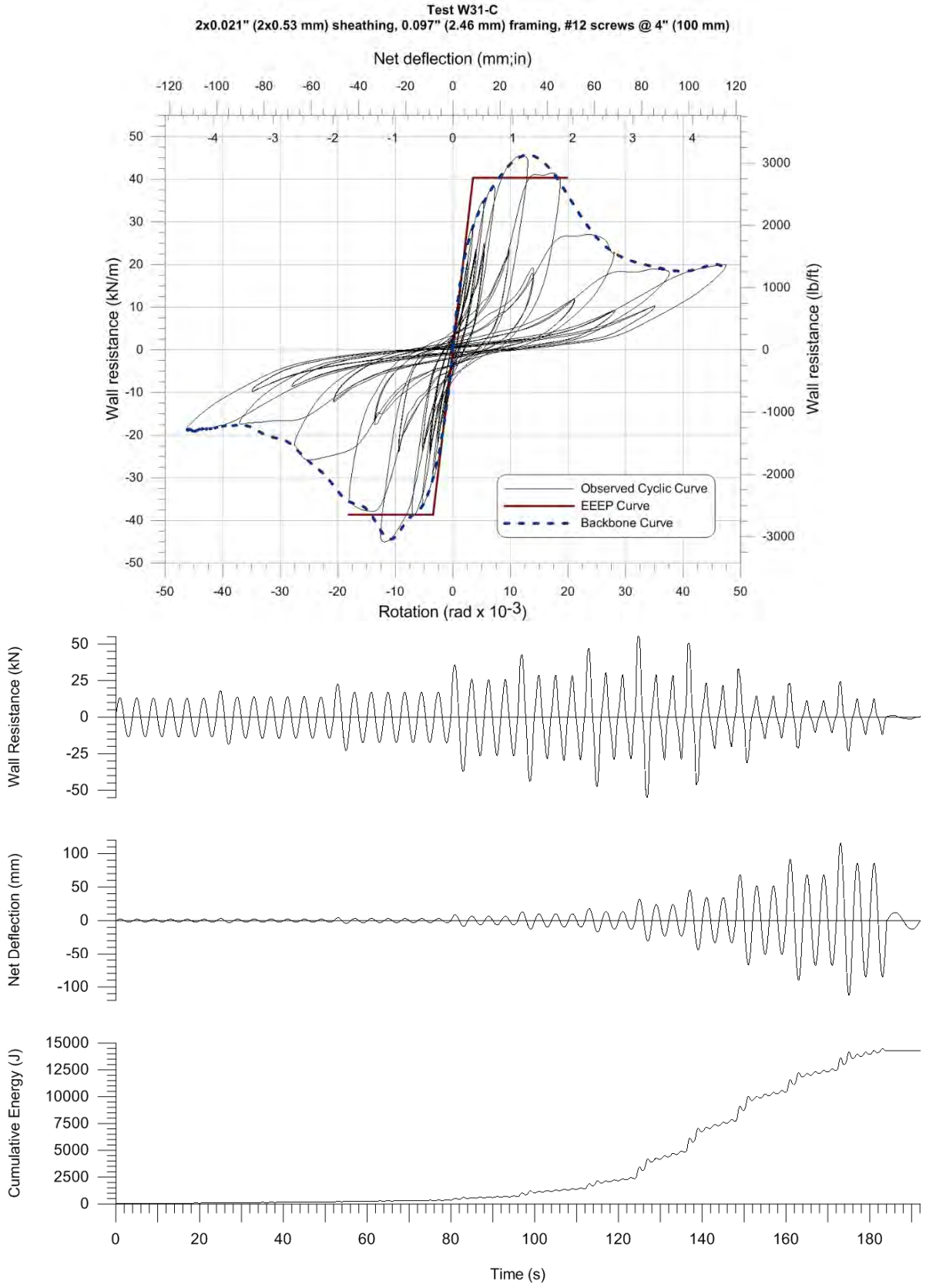

Figure G-4 Observed / EEEP curves and time history for cyclic test W31-C

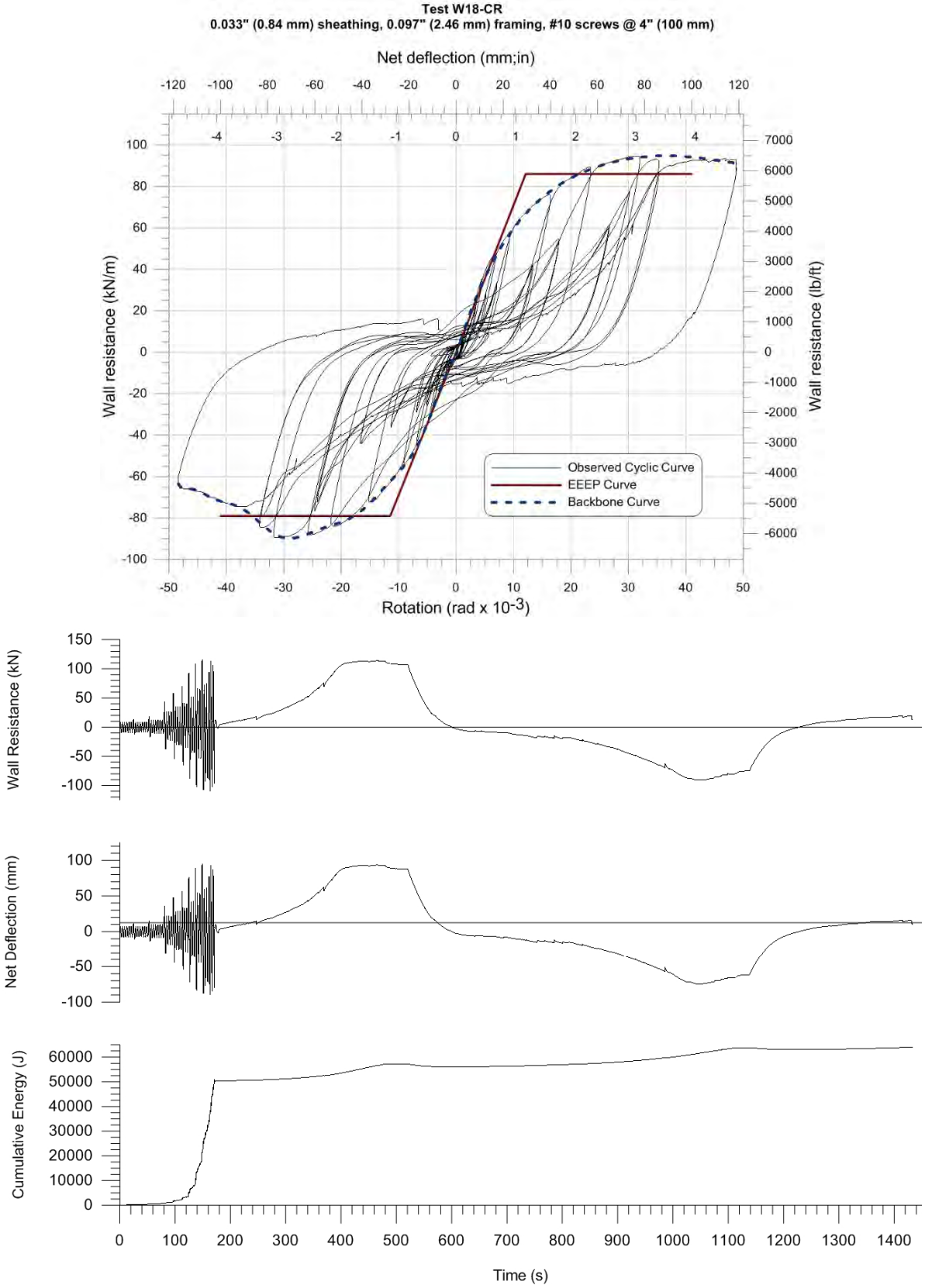

Figure G-5 Observed / EEEP curves and time history for cyclic test W18-CR

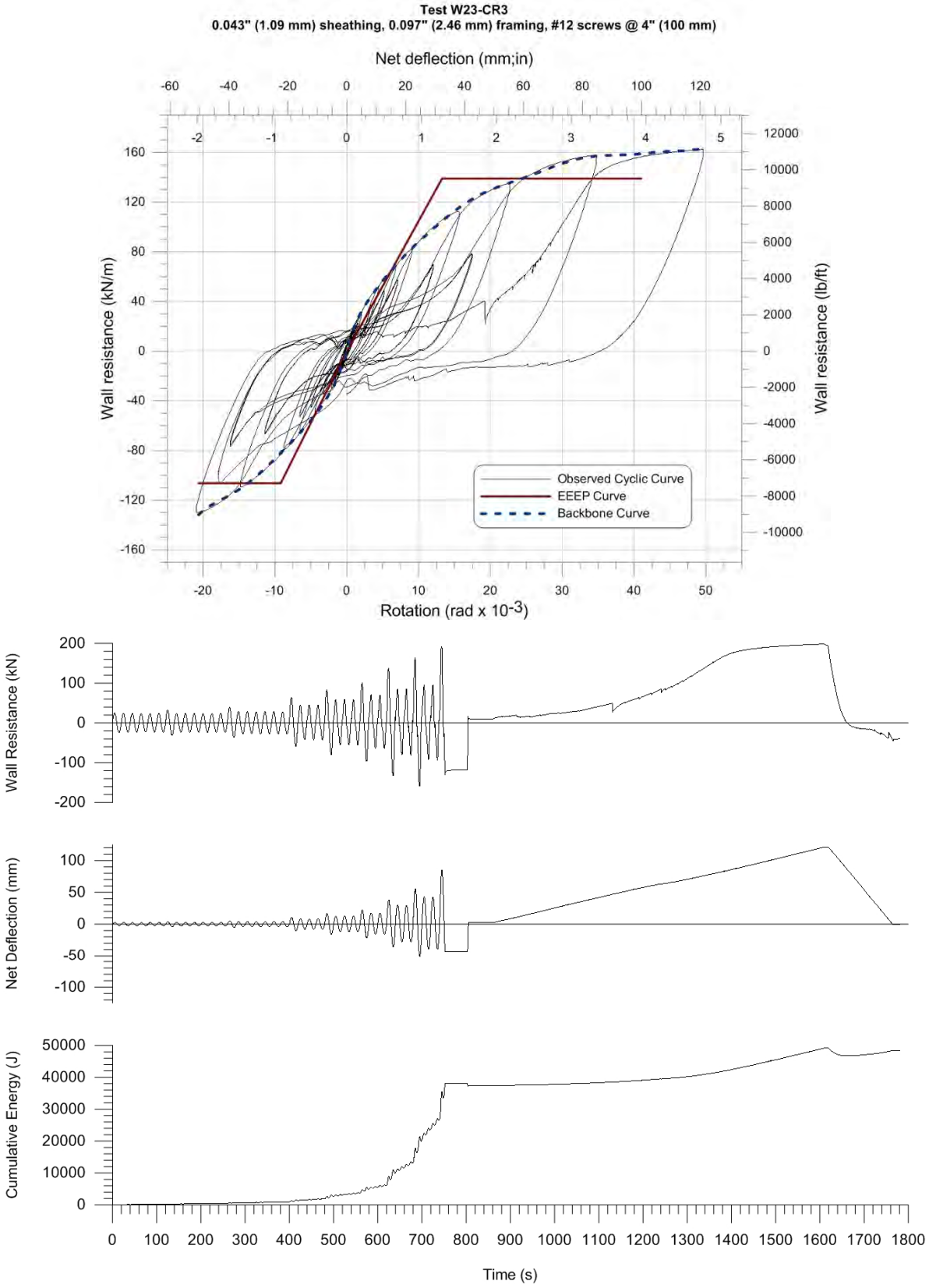

Figure G-6 Observed / EEEP curves and time history for cyclic test W23-CR3

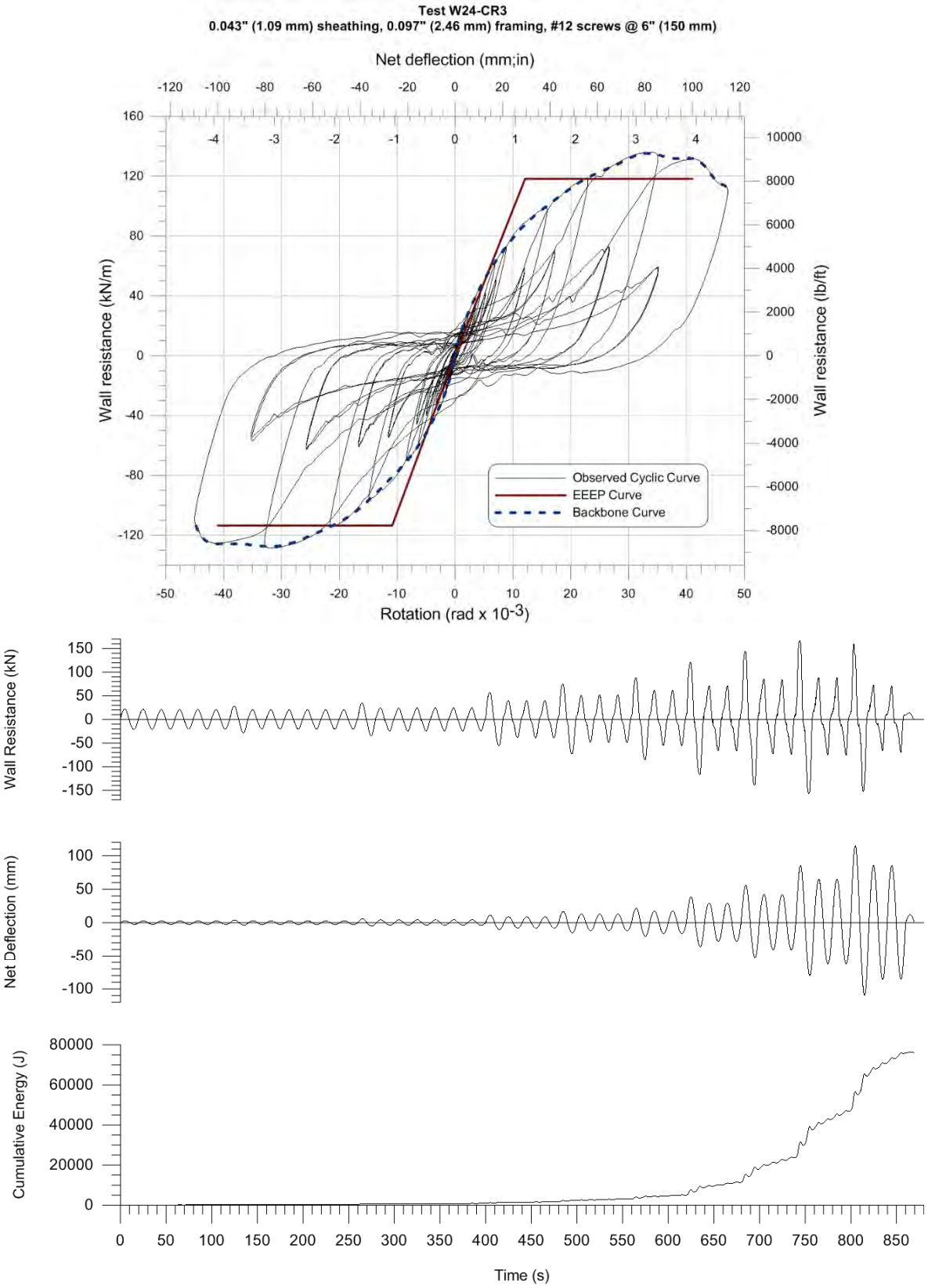

Figure G-7 Observed / EEEP curves and time history for cyclic test W24-CR3

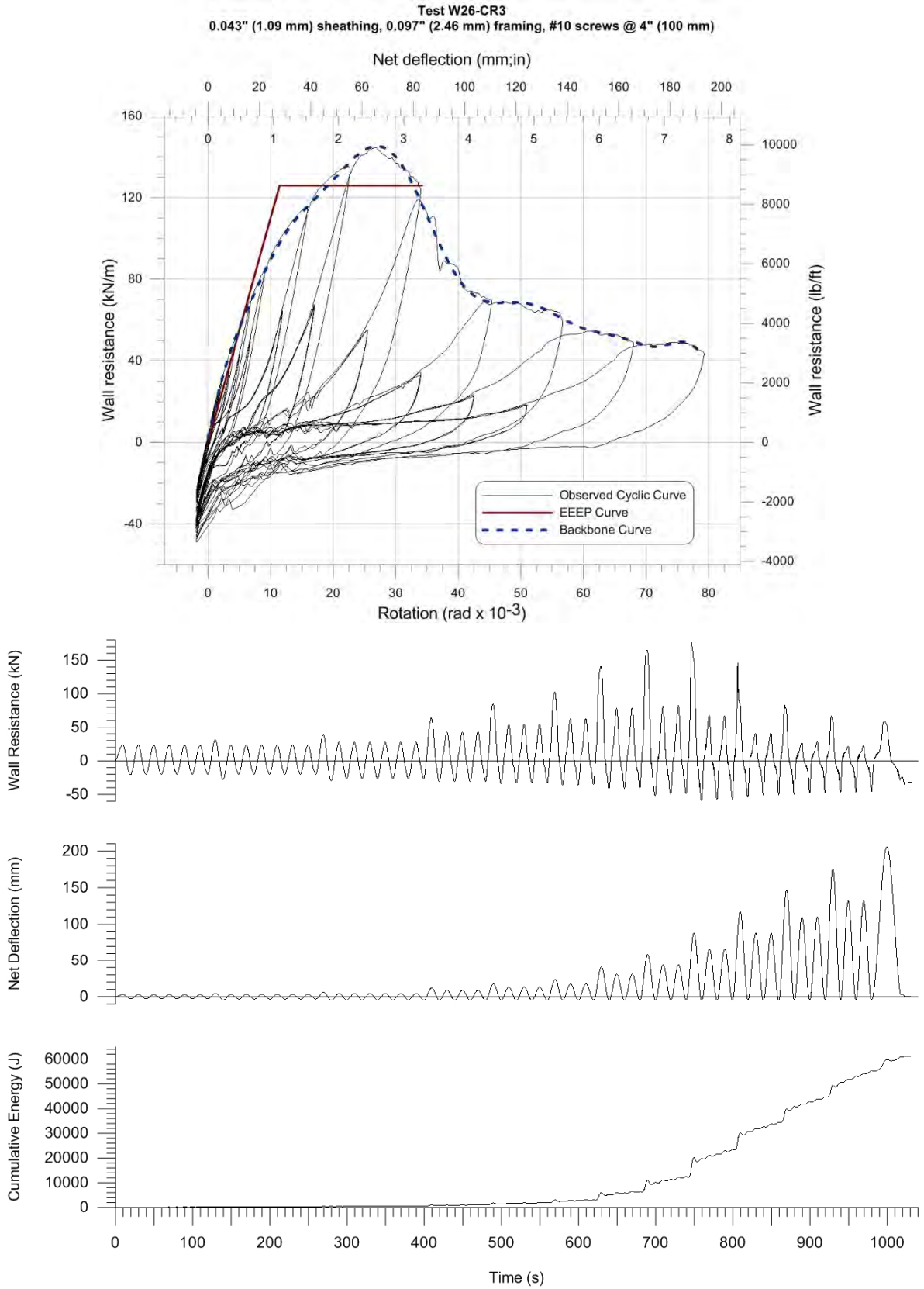

Figure G-8 Observed / EEEP curves and time history for cyclic test W26-CR3

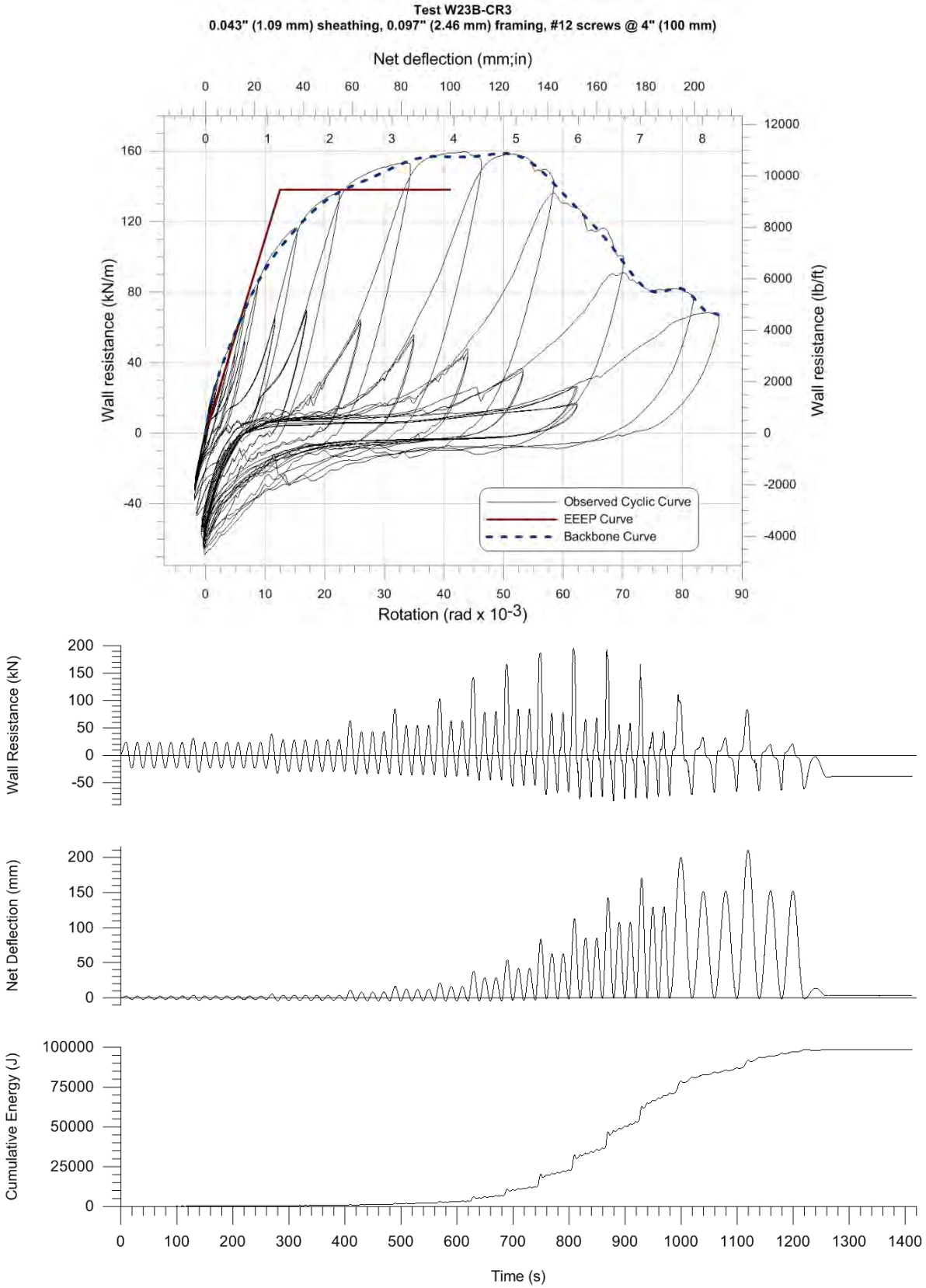

Figure G-9 Observed / EEEP curves and time history for cyclic test W23B-CR3

American Iron and Steel Institute

25 Massachusetts Avenue, NW
Suite 800
Washington, DC 20001

www.steel.org

Research Report RP-17-6